EPA-600/3-76-101
September 1976

Ecological Research Series

AN EXPERIMENTAL/ANALYTICAL INVESTIGATION OF DEEP SUBMERGED MULTIPLE BUOYANT JETS

Environmental Research Laboratory
Office of Research and Development
U.S. Environmental Protection Agency
Corvallis, Oregon 97330

RESEARCH REPORTING SERIES

Research reports of the Office of Research and Development, U.S. Environmental Protection Agency, have been grouped into five series. These five broad categories were established to facilitate further development and application of environmental technology. Elimination of traditional grouping was consciously planned to foster technology transfer and a maximum interface in related fields. The five series are:

1. Environmental Health Effects Research
2. Environmental Protection Technology
3. Ecological Research
4. Environmental Monitoring
5. Socioeconomic Environmental Studies

This report has been assigned to the ECOLOGICAL RESEARCH series. This series describes research on the effects of pollution on humans, plant and animal species, and materials. Problems are assessed for their long- and short-term influences. Investigations include formation, transport, and pathway studies to determine the fate of pollutants and their effects. This work provides the technical basis for setting standards to minimize undesirable changes in living organisms in the aquatic, terrestrial, and atmospheric environments.

This document is available to the public through the National Technical Information Service, Springfield, Virginia 22161.

EPA 600/3-76-101
September 1976

AN EXPERIMENTAL/ANALYTICAL INVESTIGATION OF DEEP SUBMERGED MULTIPLE BUOYANT JETS

by

L. D. Kannberg
L. R. Davis
Oregon State University
Corvallis, Oregon 97330

Grant No. R-800818

Project Officer

M. A. Shirazi
Assessment and Criteria Development Division
Corvallis Environmental Research Laboratory
Corvallis, Oregon 97330

U.S. ENVIRONMENTAL PROTECTION AGENCY
OFFICE OF RESEARCH AND DEVELOPMENT
CORVALLIS ENVIRONMENTAL RESEARCH LABORATORY
CORVALLIS, OREGON 97330

DISCLAIMER

This report has been reviewed by the Corvallis Environmental Research Laboratory, U. S. Environmental Protection Agency, and approved for publication. Approval does not signify that the contents necessarily reflect the views and policies of the U. S. Environmental Protection Agency, nor does mention of trade names or commercial products constitute endorsement or recommendation for use.

CONTENTS

FIGURES

LIST OF NOMENCLATURE AND SYMBOLS

A - Area

A_{entr} - Entrainment surface area

a - Entrainment coefficient

$a_{0,1,2,\ldots}$ - Entrainment coefficients, also regression fit coefficients

a'_{41} - Entrainment coefficient

a'_{4} - Entrainment coefficient

a_{ij} - (i,j - 1-5) Zone of flow establishment simultaneous equation coefficients

B - Slot plume discharge point width

b - 3/2 power profile plume half width = $.53b_1$

C - Species concentration

C_o - Concentration at port discharge

C_∞ - Ambient concentration

C_D - Drag coefficient

c_v - Specific heat

$c_{1,2,3,4}$ - Entrainment coefficients for Davis model, zone of flow establishment

D - Port diameter

D_c - Species diffusion coefficient

d_{1-8} - Coefficients defined for the zone of flow establishment

E - Entrainment

E_r - Round jet entrainment

E_s - Slot jet entrainment

e_s - Slot jet entrainment coefficient

F - Froude Number = $U_o / \left(\frac{\Delta\rho}{\rho_o} gD \right)^{1/2}$

F_L - Plume local Froude Number = $u_c / \left(\frac{\Delta\rho}{\rho_o} gb \right)^{1/2}$

F_D - Drag force

$\overline{f}$ - Time averaged quantity

f' - Fluctuating quantity

$f_{1,2,\ldots}$ - Defined quantities for the solution of simultaneous equations in the zone of flow establishment

$G_{1,2,3,4}$ - Flux quantities in the zone of single plume flow

$\overline{g}$ - Gravitational force (without bar - it is the gravitational constant

$H_{1,2,3,4}$ - Flux quantities in the merging zone

$h_{1,2,3}$ - Incomplete integrals defined in the merging zone

$i_{51,52}$ - Coefficients defined for the zone of flow establishment

k - Thermal conductivity

L - Distance between ports

$N_{,1,2,3}$ - Normal terms, employed in the drag force relation

P - Pressure

P^+ - Motion pressure $(P-P_\infty)$

$\overline{q}$ - Defined by equation (39)

R - Towing ratio = U_∞ / U_o

r - Plume radius and radial coordinate

r_c - Species core radius for the zone of flow establishment

r_t - Temperature core radius

r_u - Velocity core radius

r_o - Port radius = D/2

S,s - Distance along centerline and centerline coordinate

S_e - Starting length

T - Temperature

T_a, T_∞ - Ambient temperature

T_c - Centerline temperature

ΔT_c - $(T_c - T_\infty)$

T_o - Port discharge temperature

ΔT_o - $(T_o - T_\infty)$

t - Time

t_2 - An arbitrary point in time

U_o - Port discharge velocity

U_∞ - Ambient velocity

u - Velocity in the S direction

u_c - Centerline velocity in the S direction

Δu_c - $(u_c - U_\infty \cos \theta_2 \sin \theta_1)$

$\overline{V}$ - Vector velocity

v - Velocity in radial, r, direction

W - Plume width, vertical or X-sectional

X - Horizontal downstream distance and coordinate

x - Dummy variable

Y - Vertical coordinate and height above ports

Z - Transverse coordinate along line of ports

α - Measure of merging = L/b

β - Coefficient of thermal expansion

Γ - A variable

γ - Coefficient of species concentration expansion

ε - General eddy diffusivity

ε_c - Species eddy diffusivity

ε_h - Thermal eddy diffusivity

ε_m - Momentum eddy diffusivity

ζ - Merging coordinate along line of jet centerlines

η - Merging coordinate perpendicular to the - S plane

θ_2 and θ - Angle of plume centerline to the X - Z plane

θ_1 - Angle of projection of the plume centerline on the X - Z plane from the Z-axis

θ_{1o} - θ_1 at the discharge point

θ_{2o} - θ_2 at the discharge point

κ_1 and κ_2 - Curvatures of the plume centerline with respect to θ_1 and θ_2

λ - Schmidt Number

ν - Kinematic viscosity

ρ - Density

$\Delta\rho$ - $(\rho - \rho_\infty)$

$\Delta\rho_c$ - $(\rho_c - \rho_\infty)$

ρ_c - Plume centerline density

ρ_o - Discharge density

ρ_∞ - Ambient density

σ - Standard deviation

Φ - Various quantities

ϕ - Circumferential plume coordinate

ACKNOWLEDGMENTS

The authors are indebted to several people for the efforts they extended in helping to reach a successful conclusion to this study. Of particular mention is Dr. Mostafa Shirazi, whose comments, criticisms, and encouragements were most helpful. We are also indebted to Jim Shew, Jim Carr, G. Kranick, N. Kunz, Barbara Gniewosz and Mary Holland for their assistance in the experimental program. We are grateful for the assistance of the staff at the U. S. Environmental Protection Agency's Corvallis Environmental Research Laboratory, Corvallis, Oregon. And finally, our thanks are extended to Chris Snow for her enthusiasm while typing this work, and to the Environmental Protection Agency whose financial support made this study possible.

SECTION I

INTRODUCTION

Energy consumption in this country is doubling at a rate of once every 15 years. As it now appears, fossil and nuclear electric generating plants will produce nearly all of the electricity required to meet these demands. Thermodynamically, these plants are 30 to 40% efficient meaning that 70 to 60% of the energy developed must be rejected. Considering the magnitude of this energy release, the "waste" heat (or thermal) discharge emerges as a legitimate environmental concern. Increased awareness of the ecological effects of these waste heat discharges has resulted in stringent state and federal regulation controlling it.

While several methods are available to discharge waste heat, including the use of cooling devices and cooling ponds, the least expensive method is once through cooling. There is naturally a strong demand and competition for such use, which is consequently regulated by local and federal guidelines. Since many state regulations specify the maximum allowable temperature regime in the neighborhood of an outfall, knowledge of the dilution characteristics of various discharge systems is required before issuing of a permit. Deep submerged thermal discharge has been recognized as one that provides rapid dilution, thus causing small surface temperature in the water body. While in some cases a simple single port outfall may provide adequate dilution, many others require multiple port or slot diffusers to comply with the required regulations.

This report is concerned primarily with multiple discharges and the effects on dilution of neighboring plumes interfering with one another. In an effort to obtain quantitative information concerning the dilution characteristics of merging thermal discharges and in order to isolate these effects from others such as surface and bottom interactions, deep submerged discharges were experimentally and analytically investigated. The results of this investigation are presented in two parts. The first part is concerned with the experimental program. The second part details a recently advanced multiple port analysis[17][1] and presents the results of its application to the discharge conditions considered in the experiment.

[1] Footnotes shall be indicated by a number in square brackets, superscript numbers without brackets indicate References.

SECTION II

SUMMARY

The results of an experimental and analytical study of deep submerged multiple-port thermal discharges are presented. The experimental results include the measured downstream thermal dilution, width, and centerline trajectory of the buoyant thermal plume from multiport jets. Independent parameters for which measurements were obtained include port spacing, discharge Froude Number, discharge angle, and discharge to ambient velocity ratio. Results indicate that decreasing port spacing greatly decreases thermal dilution. Changing port spacing will also affect trajectory to a small extent while only slightly changing plume width. Altering the Froude Number appears to have little effect on downstream dilution, width, or trajectory when an ambient current is present. By increasing discharge angle from the horizontal, greater initial dilution may be obtained as well as greater widths and higher trajectories. The effect of ambient current on dilution depends on the angle of discharge. For crossflow discharges the thermal dilution at any point downstream decreased with increasing ambient current, while for co-flow the reverse was observed. The jets were bent over rapidly for crossflow discharges particularly when large ambient currents were present.

The analytical portion of this report employs the lumped differential model of Hirst[6] as modified for merging multiple jets by Davis.[17] The essential features of the analysis are: 1) the gradual transition of the profiles from simple axisymmetric pro-

files to merging profiles and finally to fully merged, pseudo-slot, two-dimensional profiles, and 2) an entrainment based on the available entrainment surface.

Results indicate that the overprediction of plume characteristics associated with "transition" or "equivalent slot" models may be overcome using such an analysis and that suitable prediction may be obtained.

SECTION III

CONCLUSIONS

The experimental program provided results that offer important information on the dilution, width, and trajectory of deep submerged multiport discharges. This information may be summarized as follows:

1) Increasing the velocity ratio, R, increased dilution with downstream distance, x, except at steep discharge angles (>60°). The trajectories were dramatically affected by the towing rate even for very small angles.
2) Froude No. had little if any effect on dilution, width, or trajectory for cases with ambient current with the possible exception of close spacing and low R's where slightly lower dilution for higher Froude No's. was observed.
3) Increasing the angle of discharge from the horizontal up to about 60° increased the dilution; from 60° on, the general trajectories and dilution remained about the same for cases with current.
4) Increasing the L/D decreased the thermal dilution dramatically, especially near a towing ratio of R = 0.10. The trajectory appeared to rise with decreased port spacing. However, the widths showed little change with L/D variation.

A model has been analyzed and implemented which attempts to simulate multiple port thermal discharges. Agreement between the model and experiment was generally quite good. The thermal dilutions and trajectories were predicted accurately for buoyant single port jets of varying Froude Number, however, plume widths and possibly centerline velocities were not predicted well for high Froude Number discharges. Buoyant discharges into a co-flowing stream were briefly considered. For co-flow it was found that inclusion of the turbulence terms of the equations allowed for prediction of dilution trends but the dilution could not be accurately predicted. The field is in need of a more involved and thorough examination of co-flow discharge.

Thermal dilution and trajectory for discharge into a cross-flow were predicted reasonably well by the model. While the results deviate slightly for experiments for high or low ambient to discharge velocity ratios, the prediction is quite good for moderate velocity ratios. Evidence seems to support the need for an additional entrainment term based on the drag induced curvature of the jet.

The model advanced handled the merging of adjacent jets in a manner that was more physically reasonable than any of the other models thus far advanced for multiple port merging discharges. By allowing the profiles of temperature, species, and velocity to adjust naturally from the axisymmetric single plume profiles to those approaching a two-dimensional slot profile, the model avoided the arbitrary transition from one solution to

another. Since the change in profiles was geared to the growth of the jet, the transition was smooth and continuous. Davis[17] suggested an entrainment function which depends on the available entrainment area of the jet. This function was found to approach a limit considerably less than the appropriate slot entrainment value. Despite this, use of the "entrainment area" entrainment function in the model provided predictions which agreed well with the limited experimental data available.

When considering multiple-port crossflow discharge it was found necessary to include the drag force on the plume. Unfortunately, good agreement could not be obtained unless the drag coefficient varied inversely with the ambient to discharge velocity ratio.

The model predicted that changing port spacing would have a significant effect upon dilution and trajectory.

When the multiple port discharges have merged to form a pseudo slot jet, the entrainment remains between 50% and 70% less than the normal slot entrainment value. This is true for at least the first 10 or 15 port spacings along the plume centerline and perhaps considerably further.

SECTION IV

HISTORICAL BACKGROUND

It has only been in the last ten years that in-depth investigations of multiport diffusers have been performed, although investigations of single port thermal plumes were carried out as early as the 1930's. In that decade the study of wakes led to treatments of free turbulence. An interesting paper by Reichardt[1] treated the diffusion of heat and momentum and provided one of the first quantitative evaluations of the two diffusion processes. Schmidt[2] also considered the problem and employed the mixing length theory to arrive at a solution for a point and line plume that agreed quite well with his experimental results. In 1949 a paper appeared by Albertson, et. al.,[3] which along with a later paper by Morton, et. al.,[4] extensively documented the experimental and theoretical treatments of those early years. Forstall and Shapiro[38] also provide excellent references for pre-1950 treatments of slot and round discharges. Investigations by prominent authors of the late 1950's and 1960's are summarized in Trent and Welty[5] and Hirst[6].

The bulk of the work on multiport discharges has been investigations of discharges into confined environments. The primary aim has been to model a specific diffuser and site.

Jirka and Harleman[7] published an extensive work concerning multiport discharges into stagnant and flowing shallow ambients. Argue[8] conducted a laboratory investigation of shallow multiport discharges into a flowing ambient at an angle of 20° from the

horizontal. Larsen and Hecker[9] performed experiments on multiple port discharges into shallow ambients with the primary interest on the free surface concentrations. All of the above were restricted to discharges into confined environments. Such discharges yield little information concerning the merging and mixing of adjacent jets since in most cases boundary effects dominated the hydraulics of the jet and necessarily influenced heavily the mixing phenomenon.

Koh, et. al,[10] investigated various diffuser configurations (several staggered multiport diffuser manifolds) for discharge into stagnant and flowing ambients (this was a basin model study which included a specific geometry and site restrictions). Liseth[11] performed an experimental investigation of multiport discharge into stagnant ambients from a diffuser with ports on both sides of the manifold.

Iwasa and Yatsuzuka[12] proposed a model (similar to the Hirst[6] single port treatment) and compared it with near surface concentrations taken from a system employing 8 radially discharging ports from a vertical tube, each at a 45° circumferential displacement. Acceptable success appeared to be obtained from this technique, however, no attempt was made to account for merging of the plumes which would occur in other geometries or closer spacings. Essentially, little experimental work has been done that focuses on the merging of adjacent jets or the effects of spacing on dilution and trajectory.

Several analytical attempts have been made to account for the merging of adjacent jets of a multiport thermal discharge.

Koh and Fan[13] formulated a mathematical model for analyzing a multiport thermal discharge by matching single round port and slot jet solutions at a desired transition point. The advantage of this technique was its simplicity. However, the accuracy of this model is questionable. A recent publication by Kannberg and Davis[14] compared data obtained for a multiple port discharge with that predicted by the transition model. That comparison showed the transition model overpredicting the dilution found experimentally.

A slightly modified version of the Koh and Fan model was employed by Shirazi and Davis[15]; however their work would be subject to the same restrictions as the Koh and Fan work. Harleman and Jirka[7] cited an "equivalent slot" method for calculating dilution and trajectory. For the equivalent slot, the same discharge per unit diffusion length and the same momentum flux per unit length as the multiport discharge is required. This results in a theoretical slot of width, $B = D^3\pi/4L$ when D and L are the actual port diameter and spacing respectively. This technique was also found by Kannberg and Davis to overpredict the dilution observed experimentally. To date, no theory has been advanced which adequately handles merging multiport thermal discharges.

SECTION V

EXPERIMENTAL WORK

MODELING PARAMETERS

In order to legitimately model the multiport thermal discharge experimentally and theoretically, the laws of geometric and dynamic similitude must be followed. Relations for similitude may be obtained from a dimensional analysis. Such an analysis yields the following independent parameters: 1) the densimetric Froude No., $F = U_o / \left(\frac{\Delta\rho}{\rho} gD\right)^{1/2}$, which is the ratio of inertial to buoyant forces; 2) the current to jet discharge velocity ratio, $R = U_o/U_\infty$; 3) discharge port spacing, L/D; and 4) discharge angle relative to the current, θ. Since the plume is usually turbulent, Reynolds Number (R_e) effects are negligible (R_e varied, 2100 to 6300).

The dependent variables are: 1) the ratio of local excess temperature to the excess temperature at discharge, $\left(T_c - T_a\right)/\left(T_o - T_a\right) = \Delta T_c/\Delta T_o$; 2) dimensionless plume width, W/D (for a very long diffuser and effects are small and the length of the plume is ignored), and 3) plume centerline coordinates, X/D and Y/D.

In this investigation wide ranges of the independent variables were considered. They were

L/D = 10,5,2.5

F = 10,30,58

θ = 0,15,30,45,60,90° from the horizontal

R = 0,0.05,0.10,0.25,0.50.

Due to equipment limitations and lack of time, all combinations of

these variables could not be considered. A parameter matrix showing cases for which data was gathered is given in Table 1.

The data collection yielded excess plume centerline temperature, cross sectional width and position of maximum temperature (trajectory).

APPARATUS AND DATA ACQUISITION

The experiments were conducted at the Hydraulics Laboratory of the U. S. Environmental Protection Agency's Corvallis Environmental Research Laboratory. Warm water was discharged into a towing channel (40' x 2' x 3') containing cool tap water. The diffusers consisted of 2.54 cm. (1") O.D. thin wall tapered acrylic manifolds with .635 cm. (1/4") I.D. round acrylic ports of approximately 10 cm. to 13 cm. length. There were 4 ports for the L/D = 10 diffuser; 6 ports for the L/D = 5 diffuser; and 8 ports for the L/D = 2.5 diffuser. In each case the mass discharge rate from any single port deviated less than 3.3% from the average of all ports and generally the deviation was much less. Figure 1 shows the diffusers used in the study.

The flow rate tests were run at the nominal flow rates used for the actual data. Very little deviation occurred with changes in bulk flow rate. The measured deviation in temperature of the various ports varied less than .7% from port to neighboring port.[2] The L/D = 10 diffuser ports had a 45° bend in them to allow for measurements at an angle of 0° from the horizontal which were free

[2] Based on L/D = 10 where this deviation would be the greatest.

TABLE 1 INDEPENDENT PARAMETER MATRIX OF EXPERIMENTAL CASES

Numbers in matrix indicate L/D's of experiments for indicated F, R, and θ.

F = 11

θ \ R	0	0.05	0.10	0.25	0.50
0		10	10	10	10
15			10	10	10
45			2.5,5,10		10
90			2.5,5,10		2.5,5,10

F = 30

θ \ R	0	0.05	0.10	0.25	0.50
0	10	10	10	10	10
15	10	10	10	10	10
30	10			10	
45	10	10	10	10	
60	10			10	
90		10	10	10	10

F = 58

θ \ R	0	0.05	0.10	0.25	0.50
0	10	10	10	10	10
15		10	10	10	10
45		5,10	5,10		
90		2.5,5,10	2.5,5,10	10	2.5,5,10

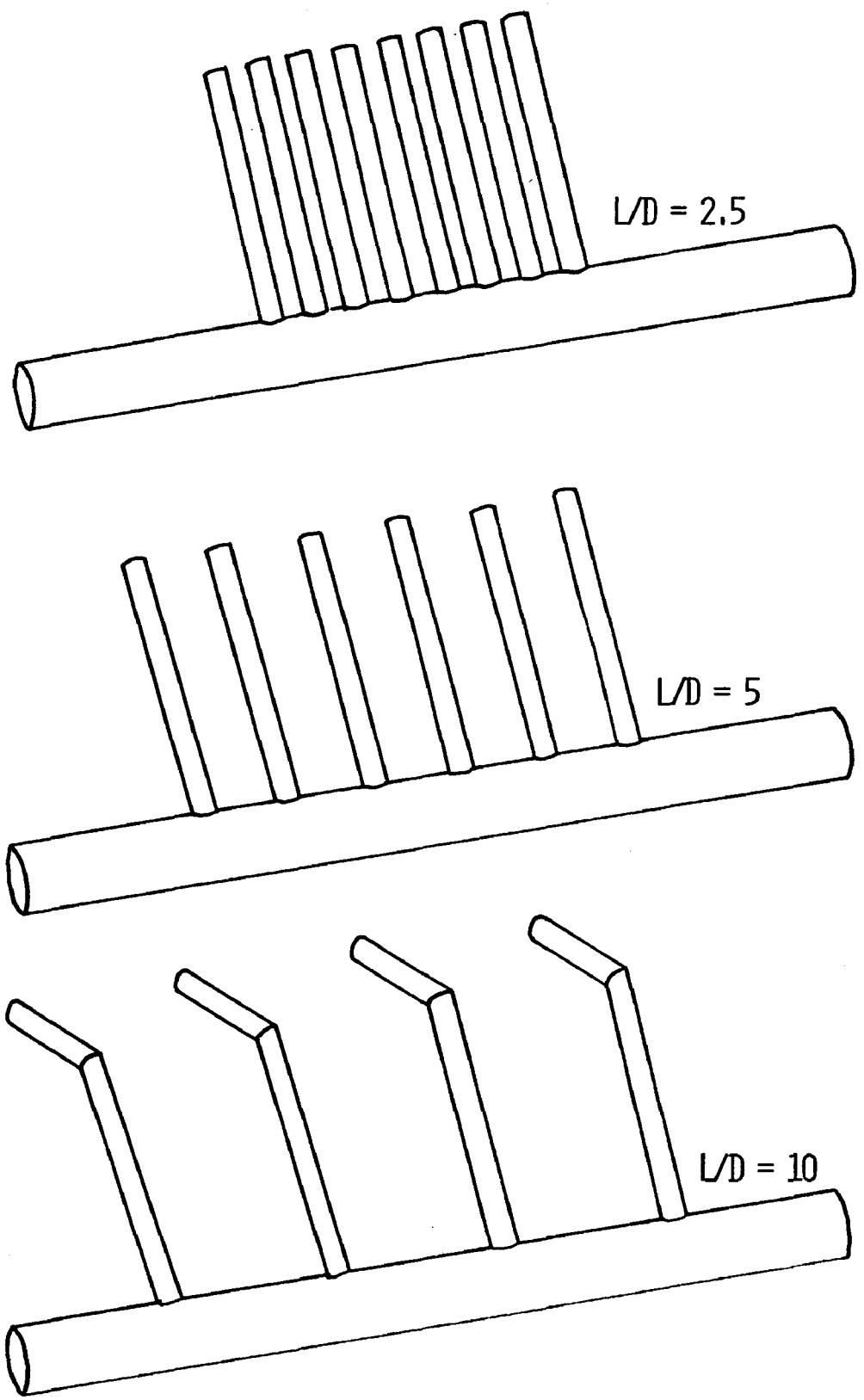

Figure 1. Diffusers used in the experimental work, L/D's = 10, 5, 2.5.

from manifold wake effects. Each of the other two had only straight ports and did not allow measurements at small angles. The manifold was connected to a warm water reservoir by supply lines at both ends. The diffuser was mounted across the channel's width and towed the length of the channel.

In order to hydraulically simulate an infinite string of ports, image walls (one 1/16" Aluminum and one 1/8" plexiglass plate) were placed at a distance L/2D outside the end ports of the diffuser. These extended 15 cm. (23.6D) ahead of the line of discharge and 125 cm. (198D) behind it. For the experimental program employed, the maximum boundary layer thickness and displacement thicknesses developed on the image walls were 4.8D and 1.6D, respectively as calculated from flat plate boundary layer theory[35]. The effect of the image walls on the dilution was found to be negligible for the port spacing, L/D of 10; consequently, for many of the runs performed at this spacing the image walls were not used. However, the presence of the walls were shown to decrease dilution by about 20% (compared to cases without image walls) for a L/D of 5. Hence, they were incorporated for L/D = 5 and L/D = 2.5.

The warm water reservoir was kept at constant head by bubbling in air as the water was discharged. Figure 2 is a diagram of the warm water reservoir.[3] As water is released from the reservoir, air pressure pushes the water from the bubbling tubes until the air escapes from the tubes into the reservoir. In this manner the

[3] The use of this tank was originally suggested by Ken Loose, formerly of EPA.

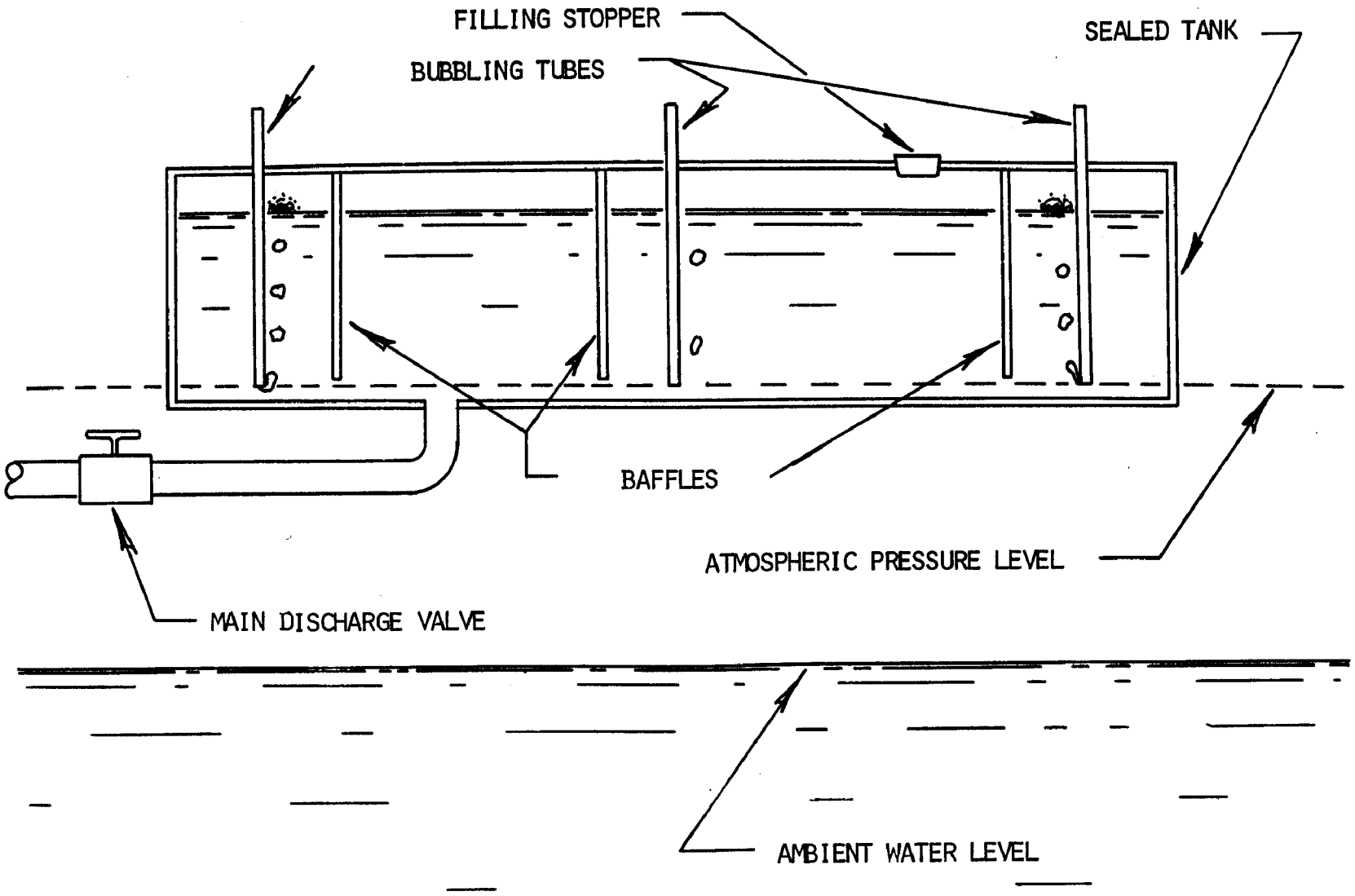

Figure 2. Warm water constant head reservoir.

level of ambient air pressure is kept at the level of the bottom of the bubbling tubes. Baffles were included in the construction of the reservoir for the purpose of damping out waves that would appear when the reservoir was being towed. The baffles proved to be quite successful. The warm water reservoir was filled with hot tap water from a conventional water heater of the desired temperature prior to each run.

A main discharge valve was located at the outlet of the warm water reservoir and acted as an on-off valve for the reservoir. Discharge water flowing from this main discharge valve divided into the two manifold supply lines (1/2" acrylic flexible tubing). A control valve on each supply line was adjusted to give control of both bulk flow rate and individual supply line flow rate. The flow rate out of the port in whose wake the temperatures were monitored was assumed to be the average of all the ports and was computed by measuring the bulk flow out of the reservoir during a given time and dividing by the number of ports. This was done for each run.

For F = 10 the nominal discharge velocity, U_o, was 25 cm./sec. and the nominal difference between discharge temperature and ambient water temperature was about 33°C (depending on ambient temperature). Cases at F = 30 had a nominal U_o of 50 cm./sec. and had a nominal difference between discharge temperature and ambient temperature of about 18°C (depending on ambient temperature). The F = 58 runs maintained a nominal discharge velocity of 75 cm./sec.[4] and nominal difference between discharge temperature and

ambient temperature of about 14°C[4] (depending on ambient temperature). Ambient temperatures varied from a low of 11.30°C to a high of 24.44°C with the seasons.

The temperature of the discharge was measured at the point where the warm water was discharged into the cooler channel water. A Hewlett-Packard Quartz Thermometer was used to measure all reference temperatures (ambient and discharge temperatures were measured to 0.01°C).

A conical hot film sensor (TSI, model 12-30W) with a Thermal Systems, Inc. constant temperature anemometer was used to record the excess temperatures in the field of the jet. The sensor was mounted on a rod that traversed vertically through the plume. The vertical motion was motorized and its direction and speed controlled remotely. The sensor was fixed at some downstream position X/D relative to the line of discharge for each run.[5] During each run the sensor would be moved up and down through the plume several times. In this manner the vertical temperature profile could be obtained at a single downstream distance. The temperature signal of the anemometer and a potentiometric position signal were recorded on a Honeywell Visicorder. The experimental apparatus is illustrated in Figure 3.

At a later date the signals were examined and a value placed on the maximum mean temperature in the vertical profile and its position. The points where the bottom and top of the jet were encountered were also determined. During many runs more than one

[4] For L/D = 5 and L/D = 2.5 these values were about 60 cm./sec. and 11°C, respectively.
[5] Runs were made with different X/D positions of the probe.

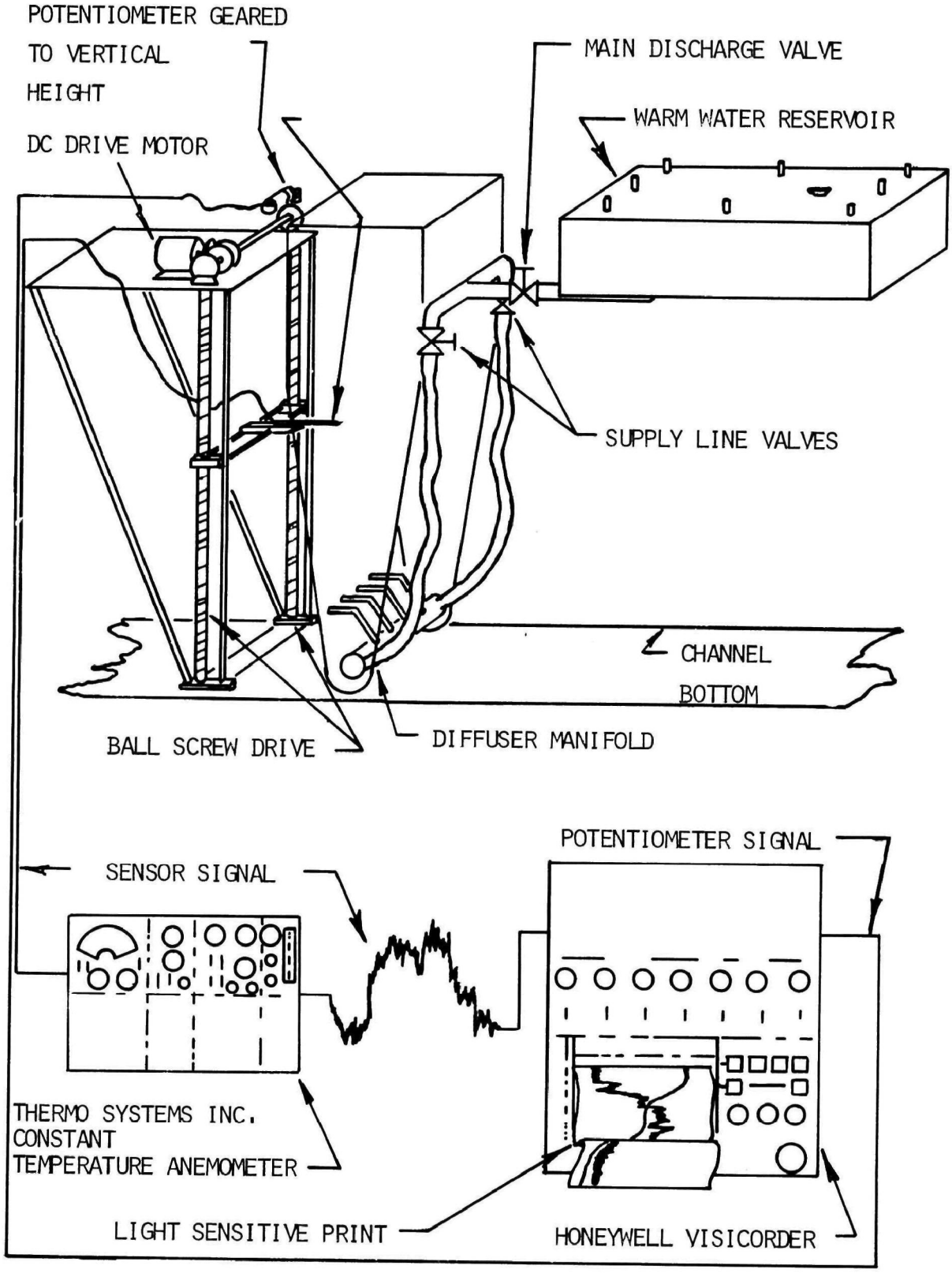

Figure 3. Experimental apparatus and electronic instrumentation.

traverse was performed (1 to 12). This provided more information since each traverse was evaluated for the above items and plotted. In order to have reasonable confidence in the final curves multiple points were obtained at each downstream position. In some cases this required additional runs. Due to the multitude of runs taken, duplication of conditions was impossible without enormous loss of time. The standard deviation from the desired values was about 8% on Froude Number and R, the towing ratio. The L/D and angle of discharge were reasonably exact.

Considerable noise in the electronics due to the proximity of large power equipment and use of flourescent lights was noted. Contamination of the sensor also offered some trouble. Occasionally, high gains were necessary for small temperature differences which amplified the noise and the normally slight drift of the signal.

These factors compound the analysis of the signal to noise ratio. The predominant noise element, the AC 60 Hz. noise, was appreciable in some cases. While generally the 60 Hz. noise was on the order of 12% of the signal, it reached 30% for some cases requiring high gain. The random noise, however, was at most 6% of the signal. The measurements requiring high gains were ordinarily in regions where the jet turbulence was on the order of 2 Hz. or 3 Hz. Near the discharge point lower gains were needed and higher signal to 60 Hz. noise ratios were evident. Often in this region the 60 Hz. noise was only about 6% of the signal amplitude. Near the discharge the jet turbulence was on the order of 50 Hz. Hence, where the noise was the greatest it was most easily

recognized. It should be mentioned that the jet turbulence near the centerline was such that the signal contained turbulent oscillations about the mean of anywhere from 25% to 100% (generally about 70% of the mean signal). In general one may say that while the occasionally large 60 Hz. noise impaired the precision of the measurements it did not detract from the accuracy.

The mechanism to move the sensor vertically for traversing the plume employed a double ball screw drive powered by a remotely controlled D.C. motor (see Figure 3). The sensor was positioned laterally on a rod such that it followed the vertical centerplane of the jet chosen for measurements, as shown in Figure 4. Once in position the sensor was fixed so that only vertical motion occurred. The sequence of events, called a run, which formed the basic experimental test is enumerated as follows:

1) Calibrate the T.S.I. anemometer using an overheat ratio of 1.075 and obtain a temperature versus voltage line (always linear but of slightly varying slope).
2) Prepare and align the traversing mechanism for the particular downstream distance, X/D, then align and position image walls as necessary.
3) Fill reservoir with warm water for the desired temperature.
4) Check for ambient stratification (if stratified then mix; an ambient stratification of 0.05°C was the maximum allowed. Generally it was about $\pm$ 0.02°C).
5) Obtain ambient temperature in the channel water.

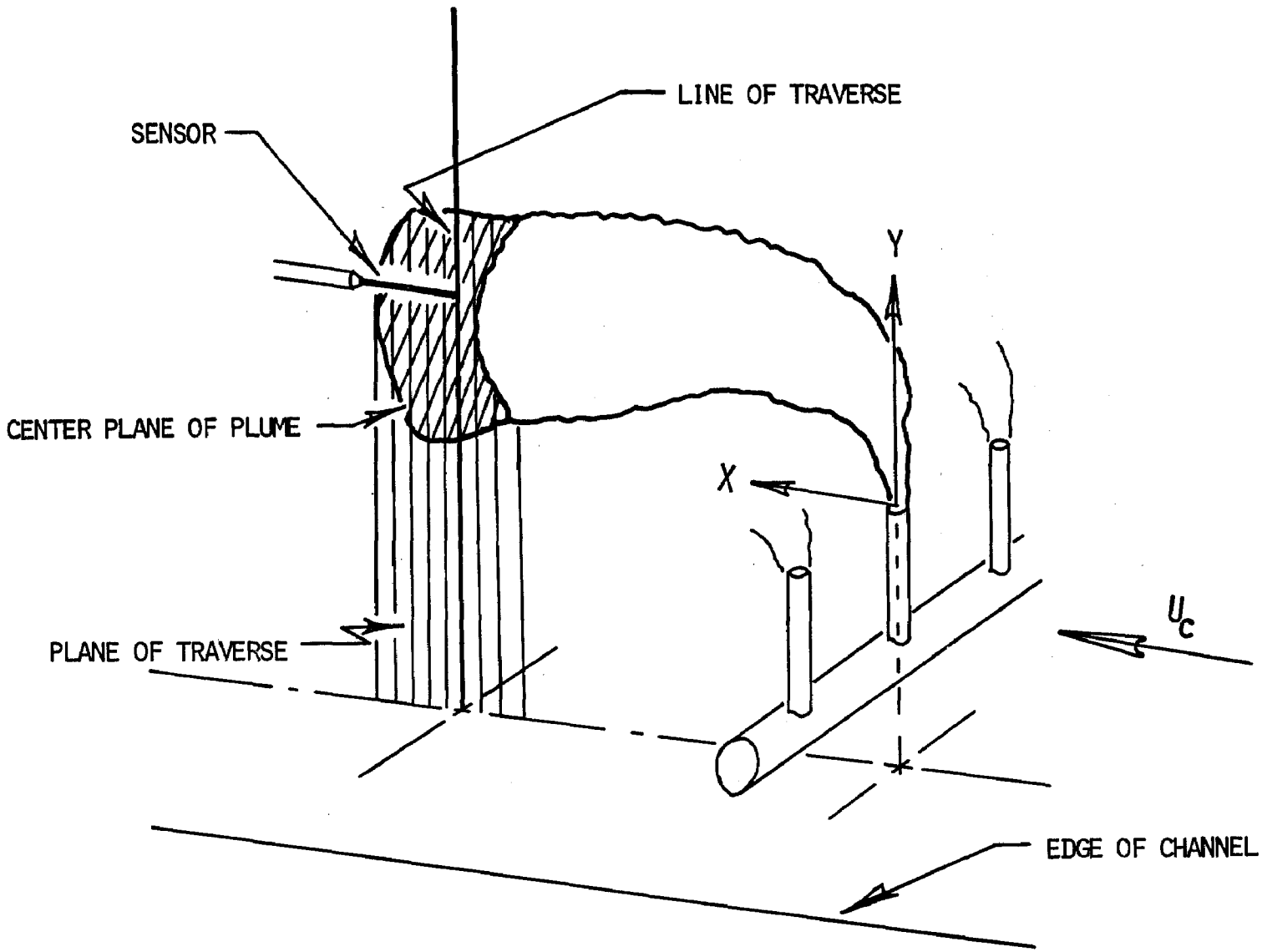

Figure 4. Plane of traverse of the sensor.

6) Measure initial probe height.

7) Open the main valve and allow the water to issue from the ports. (Prior to this the supply line control valves will have been adjusted to give a balanced flow rate near the desired value.)

8) Allow the discharge temperature to reach equilibrium and record this value.

9) Initiate tow (if required) and begin traversing the jet with the sensor. Particular emphasis was placed on the region of maximum temperature during the traverse. The traverse was often stopped in and near the point of maximum temperature so that an accurate record of the temperature there was obtained. (The frequency response of the sensor was well above the 50 to 60 Hz. maximum fluctuation rate of the turbulent eddying jet. The eddy structure was certainly evident in the Visicorder print, however, no attempt was made to analyze this.)

10) After passing through the plume several times or at the conclusion of the tow, the final sensor height was determined and the port discharge temperature again measured. (The reservoir water cooled slightly during the run and as such the average of the before and after port discharge temperatures were used. The difference between these two temperatures never exceeded 2.5% and was generally less than 1.5%.) It is conceivable that the discharge temperatures were depressed

during the towing due to the forced convection on the supply lines. However, since the supply lines were made of thick wall acrylic tubing the depression would not be inordinate and would be compensated for by the "after" port discharge temperature measurement.

11) The volumetric flow rate for the discharge was measured by timing the change in water level in the reservoir, from this the average port discharge velocity was calculated.

12) The main valve was shut off and the test ended. If a tow was made, the average speed of two was computed. (Care was taken to use only that portion of the towing channel that was uniform in its towing speed.)

A typical visicorder plot of the temperature and position signals is shown in Figure 5. The temperature plots obtained on the visicorder were examined and values ascribed for the maximum mean temperature, its vertical position and the top and bottom of the vertically traversed plume.

These values were estimated by visual scrutiny of the visicorder plots. Little can be said to describe this process except that runs were eliminated where the position and quantity of the mean temperature were indistinguishable from the rest of the record. The determination of these values thus was somewhat subjective. Visual scrutiny was also employed when estimating curves through log-log plots of the data values obtained as described above.

These values were normalized and reduced with the aid of the computer to the forms $\Delta T_c/\Delta T_o$, Y/D, and W/D. Figure 6 shows the

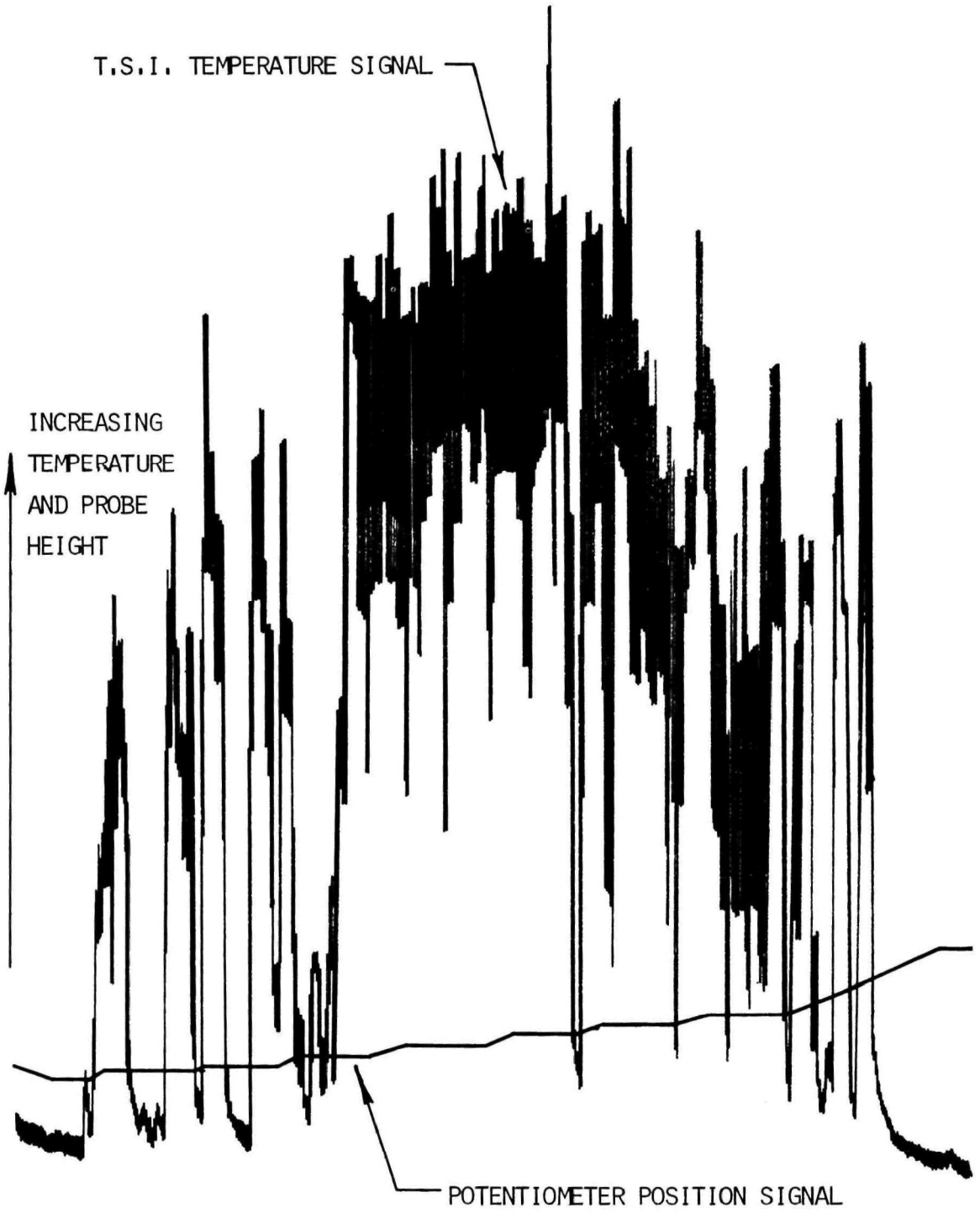

Figure 5. Typical Visicorder print of temperature and position

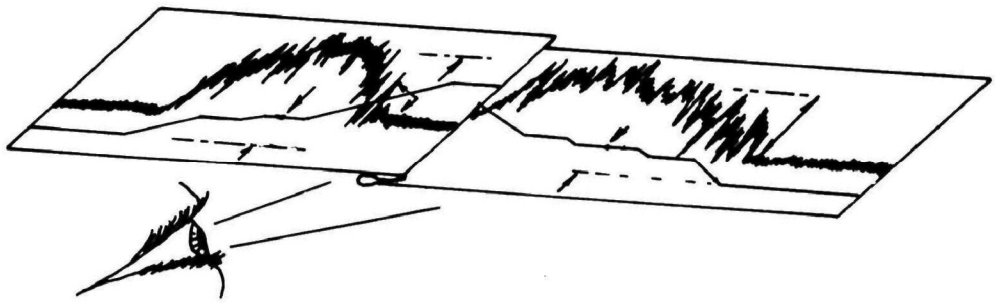

ESTIMATE THE MEAN VALUE OF THE MAXIMUM PROFILE TEMPERATURE AND THE POSITIONS OF 'BOTTOM' AND 'TOP' OF PLUME BY EYE.

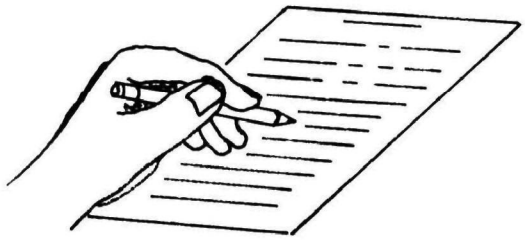

RECORD THE VALUES AS WELL AS OTHER IMPORTANT INFORMATION.

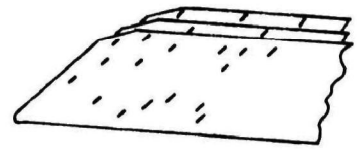

ENTER THE INFORMATION ON DATA CARDS FOR REDUCTION.

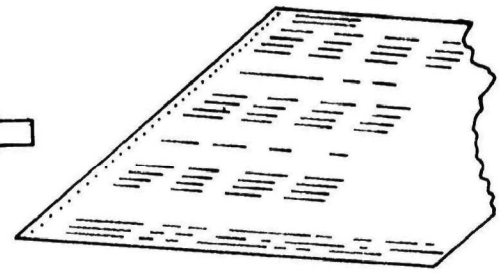

THE DATA IS NORMALIZED BY COMPUTER AND DIMENSIONLESS PARAMETERS COMPUTED. THE NORMALIZED DATA IS GIVEN IN APPENDIX A, WITH VERTICAL WIDTHS.

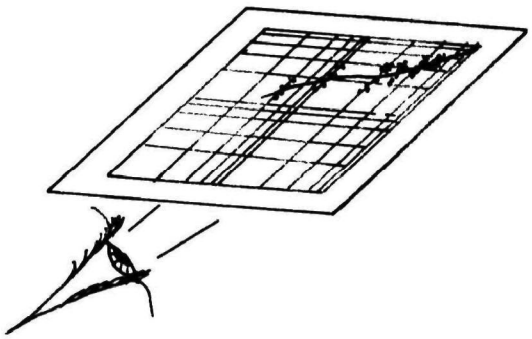

THE NORMALIZED DATA IS PLOTTED ON LOG-LOG GRAPH AND A LINE DRAWN BY EYE THROUGH THE APPROXIMATE MEAN OF ALL THE DATA GROUPS.

Figure 6. Data treatment process.

stages of processing the data. The edges of the plume were specified as those points where the mean temperature began to deviate from the ambient. These points were usually obvious because one generally encountered "eddying balls" of warm fluid rather than an indistinct merging of the plume temperature into that of the ambient and were observed both at the top and bottom of the plume. The position values were used to determine the vertical width and then with the trajectory the cross section widths.

In general the apparatus operated as desired and had acceptable error. The channel was well suited for the type of work performed, however, its potential for offering an ambient free of turbulence was not used to the full extent. The major drawback of the towing channel was its short length. Indeed some of the fastest towing speeds allowed for only about 17 seconds of run time thus requiring numerous runs. The instrumentation was good although microthermocouples might have offered a more noise free response than the T.S.I., had it been feasible to employ them.

Sensor residence time at or near the centerline was about 4 sec. although residence times ranged from 2 sec. to 15 sec. The measured time constant associated with the signal was $\sigma = 7.675$. Thus the signal would go from 0 to .67 of the step change value in .14 sec. and .9 of the step value in .3 sec. The sensor residence times were sufficient to allow for reasonable approach to the true mean signal. The longer residence times were necessary for slower towing speeds where the scale of turbulence was larger.

Implicit in the discussion and in the measurements have been several concepts. First, it was assumed that the jet possesses a

single maximum mean temperature and that this maximum may be measured as the mean of the signal; i.e., a single maximum mean temperature exists (at least vertically) and is measurable. Second, it has been assumed that all processes affecting the measurements and their treatment may be considered random. With the exception of the 60 Hz. noise, no examinations were made to verify either of these statements or that the values reported here are anything but true mean values.

THE DATA AND ITS TREATMENT

The experimental plan called for measurements of jet excess temperature ratio, trajectory, and width downstream from the points of discharge for various values of port spacing (L/D), discharge angle (θ), Froude No. (F), and velocity ratio (R). These measurements were performed as cited in the previous section. At each downstream distance (X/D) several values for each of the above measurements were obtained. These were then tabulated and plotted for all the downstream distances. An example of the plots and several data points for temperature, width and trajectory are shown on Figures 7, 8, and 9. Some of the data points have been shifted off the true X/D value in order to clarify the plot. The lines drawn through the data are intended to be the average values. An attempt to fit the data with a least square curve fit was found to be undesirable in some cases and at best not significantly different from the "eye" fits shown in the figures. Had there been measurements taken at more downstream positions, the least squares method would have worked better.[16]

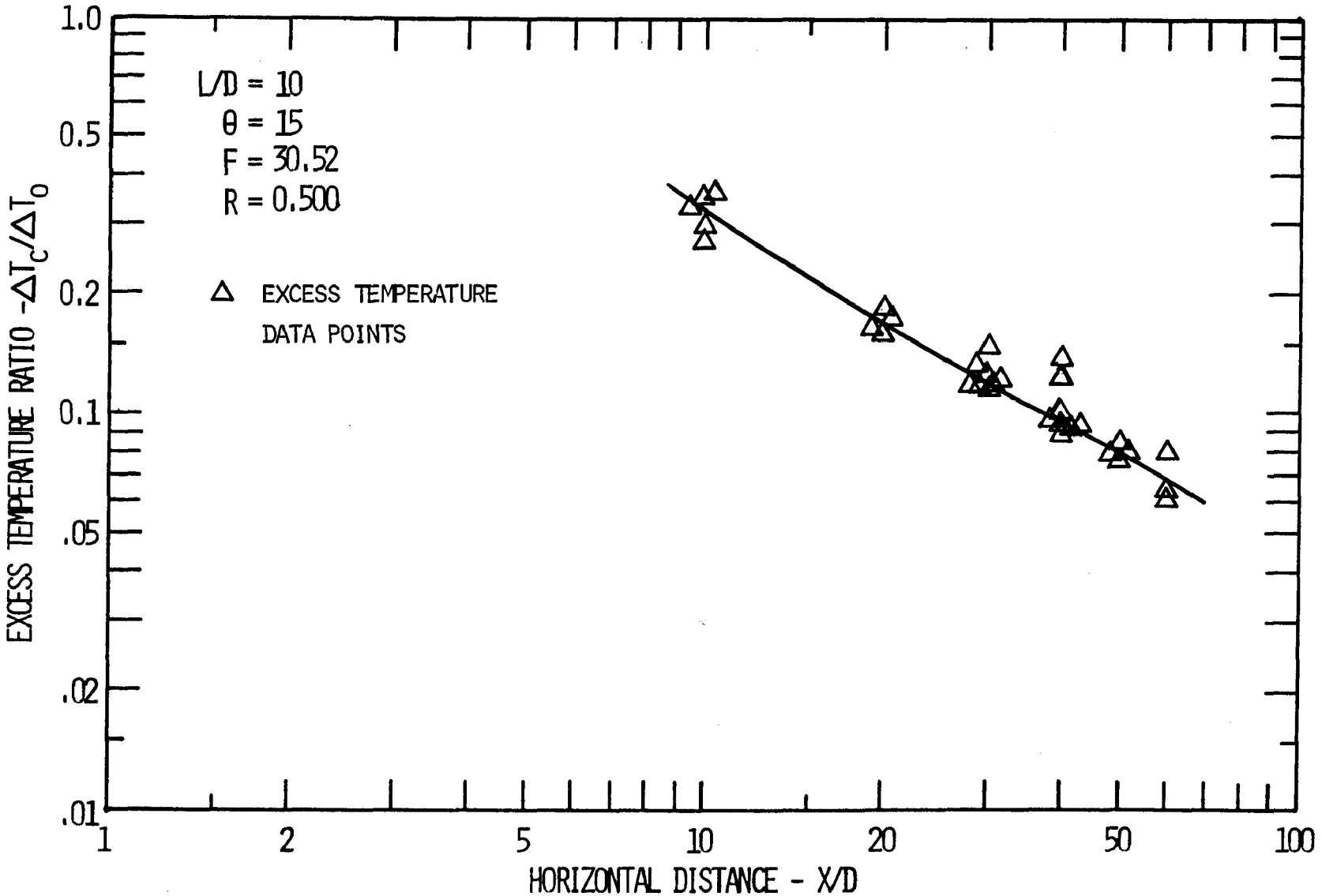

Figure 7. Example of typical excess temperature data and its' representative curve.

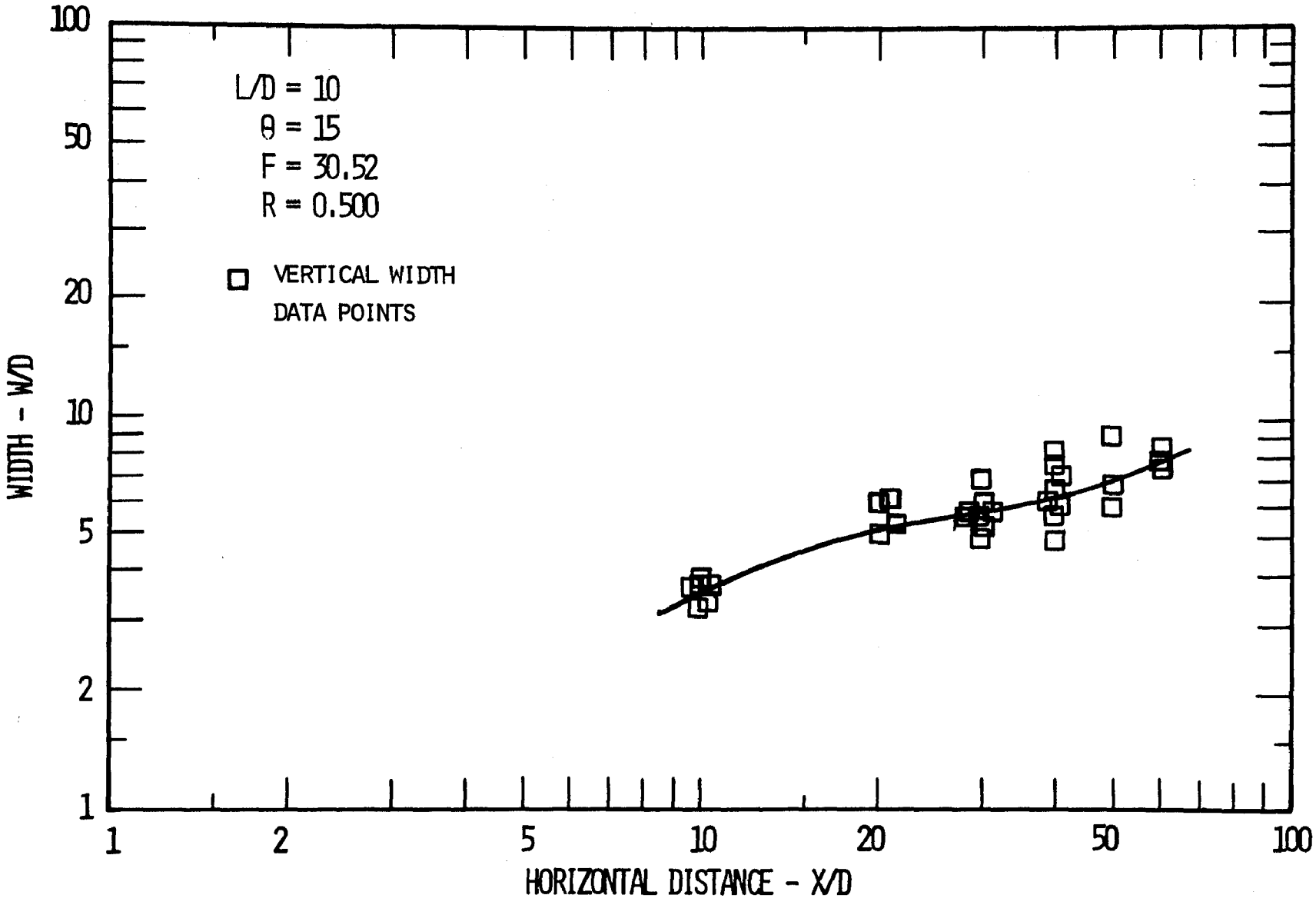

Figure 8. Example of typical vertical width data and its' representative curve.

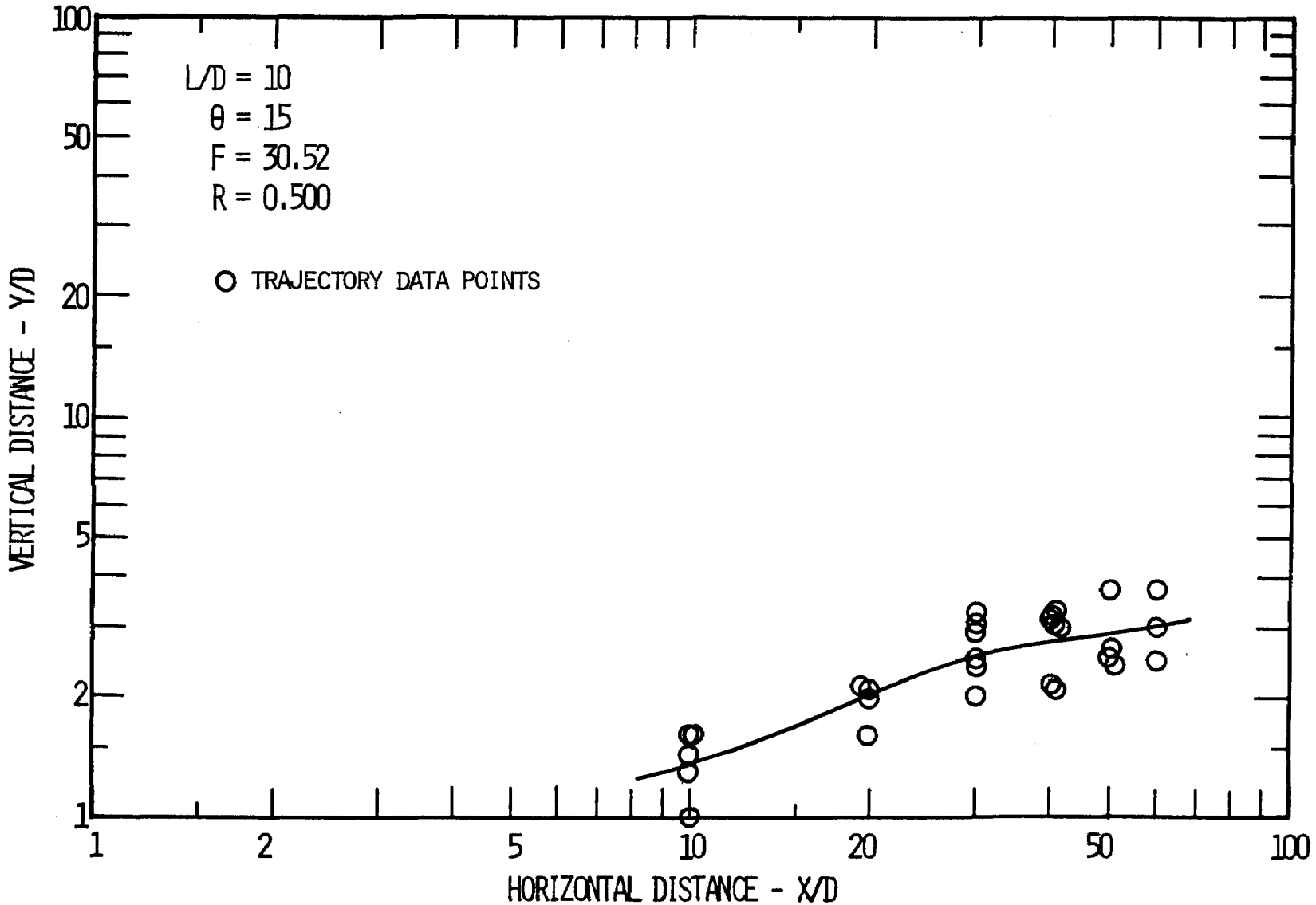

Figure 9. Example of typical trajectory data and its' representative curve.

The data gathered in this study is detailed in Appendix A. The information given in that appendix includes the measured plume information and the experimental discharge conditions. While the vertical widths measured in the experiments are given in Appendix A, the discussion here is restricted to the plume widths in a plane perpendicular to the centerline trajectory, i.e., the cross-sectional widths. The cross-section widths were generated by plotting the experimental centerline and plume edge data and measuring the widths at various points downstream on a line estimated to be perpendicular to the local centerline trajectory. Curves are presented in Reference 41, for all of the information presented in Appendix A.

EXPERIMENTAL ERROR ANALYSIS

An error analysis for the data was undertaken. Using a method for small sample data groups outlined by Benedict,[16] for obtaining the estimated 95% probability confidence interval. Employing that technique on the typical data curves offered earlier (Figures 7, 8, and 9) the confidence interval may be drawn to illustrate the quality of the data. Figures 10, 11 and 12 shows graphically the results of such an illustration.

As a general rule when considering all of the data, the 95% probability confidence intervals may be said to be of the following dimensions:

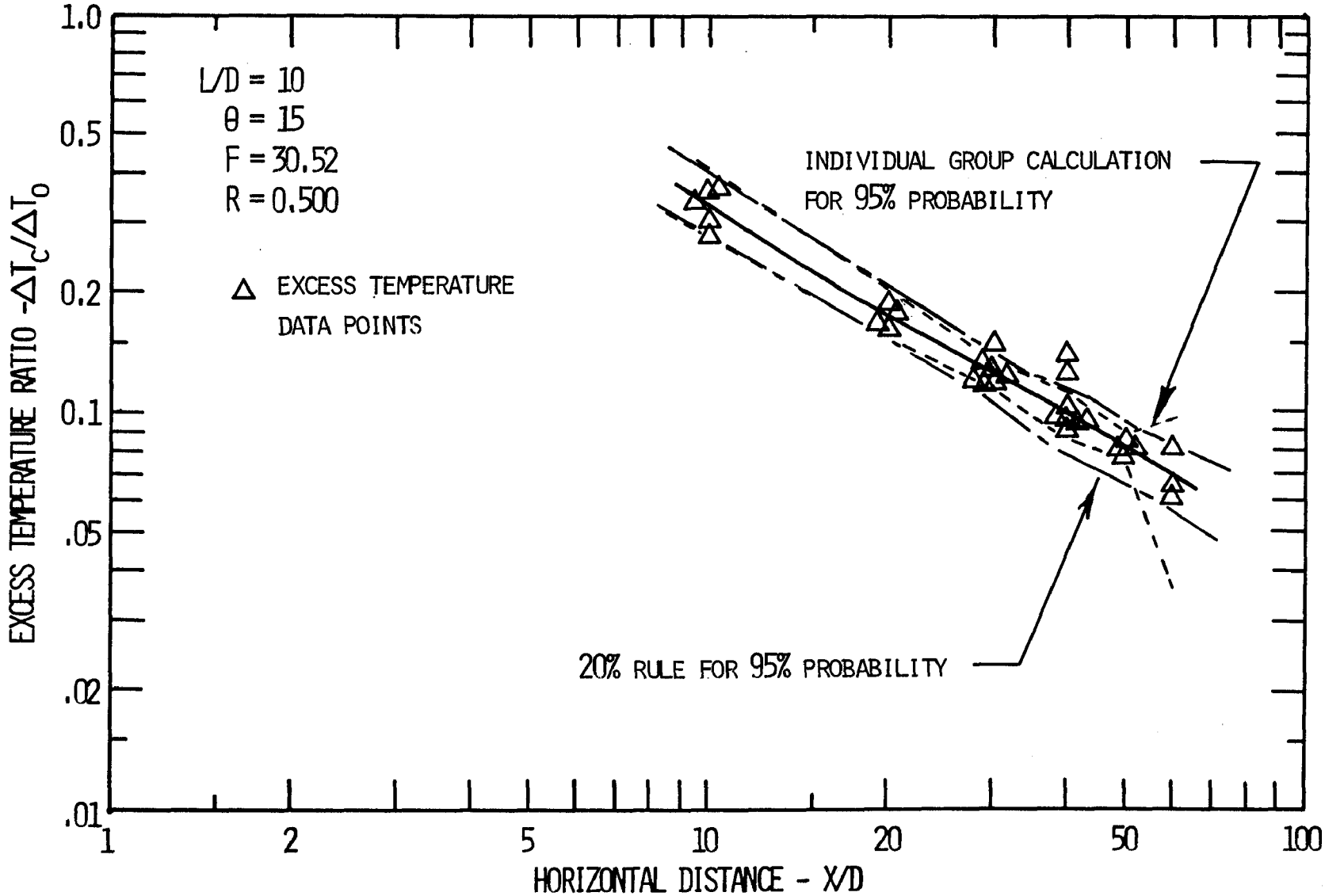

Figure 10. Confidence interval for typical excess temperature data.

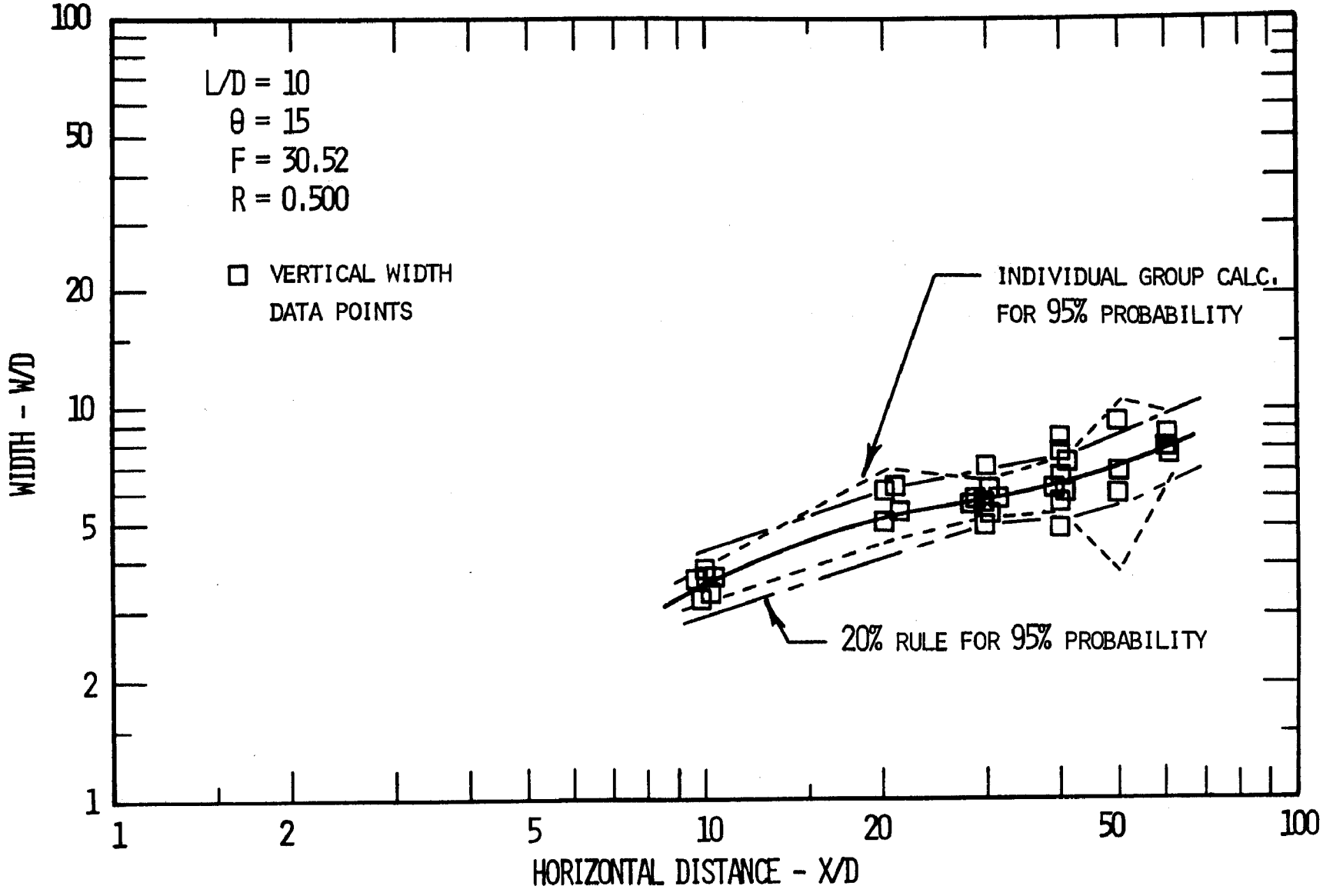

Figure 11. Confidence interval for typical vertical width data.

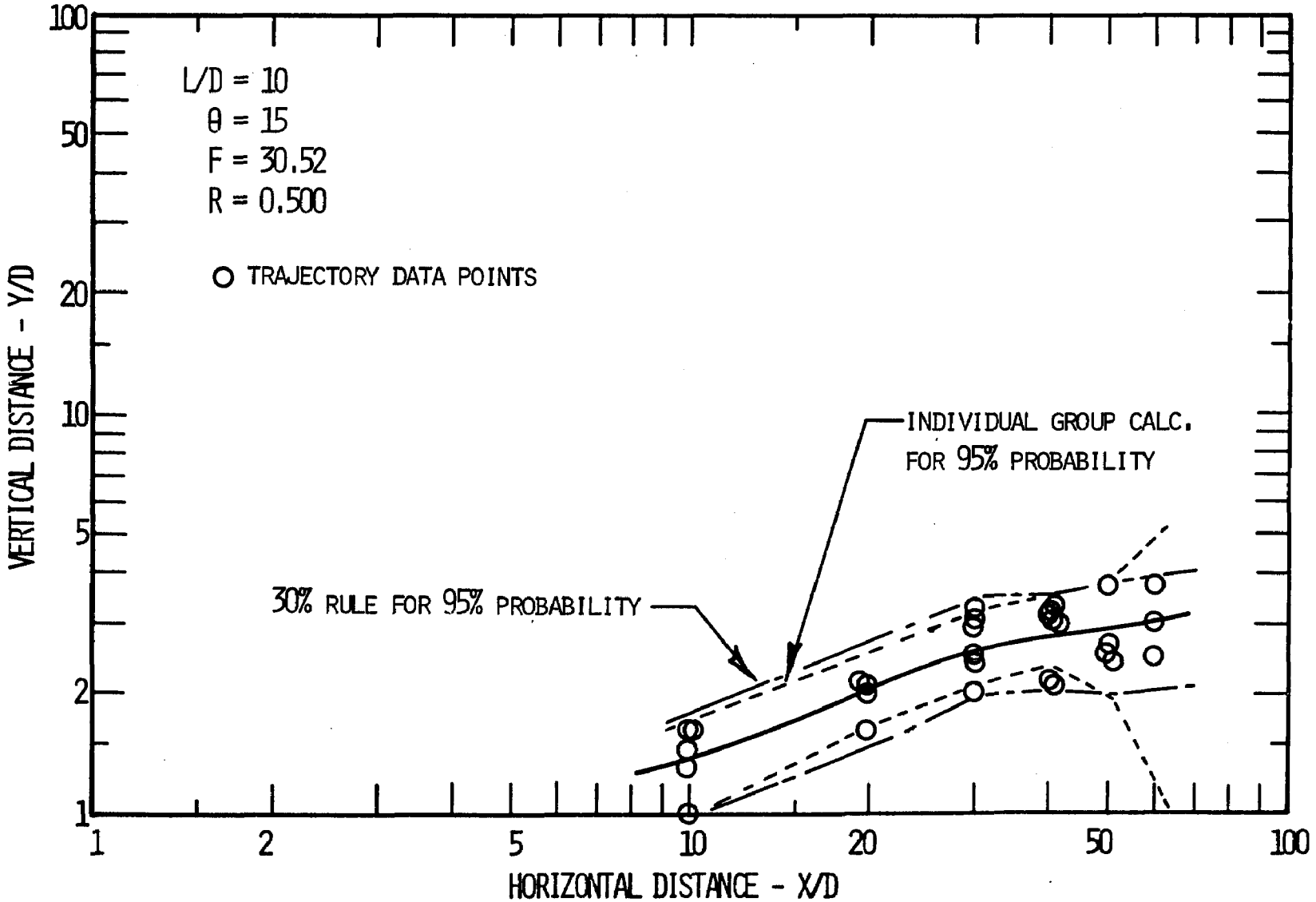

Figure 12. Confidence interval for typical trajectory data.

For Excess Temperature Ratio:		95% C.I. encloses approximately 20% of the value of the Excess Temperature Ratio.
For Cross-Section Width	:	95% C.I. encloses approximately 20% of the value of the X-Sec. Width.
For Vertical Height (Trajectory)	:	95% C.I. encloses approximately 30% of the value of the Vertical Height.

As is obvious from the general statement above, the quality of the trajectory data appears to be slightly less accurate than the excess temperature ratio and the cross-section width data. This should be kept in mind when examining the data presented and when considering the discussion of the results in the next session.

Another measure of the quality of the data is given by the correlation coefficient of a least squares curve fit. While this basically relates a proposed curve equation to the data, it also implies qualitatively how much of the data variation follows legitimate trends and how much is really random scatter. At the close of the next section curve fits are offered which include correlation coefficients.

THE RESULTS

The effects of F, R, θ, and L/D on dilution, plume width and trajectory are of major concern. The results are best demonstrated by the plots of $\Delta T_c/\Delta T_o$, W/D, and Y/D plotted against X/D for the various combinations of F, R, θ, and L/D as given in Appendix A.

The effect of the R at low discharge angles is similar to that reported in Reference 14 for co-flow. The dilution was greater for increased towing speed. This observation is supported by both the excess temperature ratio and the width as shown in Figures 13, 14, and 15 for $\theta = 15°$. However, for $\theta = 90°$ the trends are distinctly different. Figures 16, 17, and 18 illustrate that in this case the dilution is greater for slower towing rates, when compared for various distances downstream. The trajectories are dramatically affected by towing rates even for very small angles as seen in Figures 15 and 18. The results quoted are typical of the results for other conditions examined including other L/D's.

The effect of Froude Number is very minor. The information offered in Reference 14 indicated that the dilution increased with decreasing Froude Number. The data presented there to support that conclusion indicated a very minor effect. Figures 19-24 show Froude Number effects on temperature, width, and trajectory for two different combinations of θ and R for L/D = 10. It can be seen that there is little if any change in dilution, widths, and trajectory for current cases at an L/D of 10. The same trends were observable for other conditions tested with the exception of low R's for L/D = 5 and L/D = 2.5 where there was slightly lower dilution for higher Froude Numbers. In general, it may be stated that Froude Number variation has very little effect on discharges into an ambient current.

The effect of angle of discharge on dilution, widths, and trajectory for the cases with current for an L/D of ten, F = 30 and

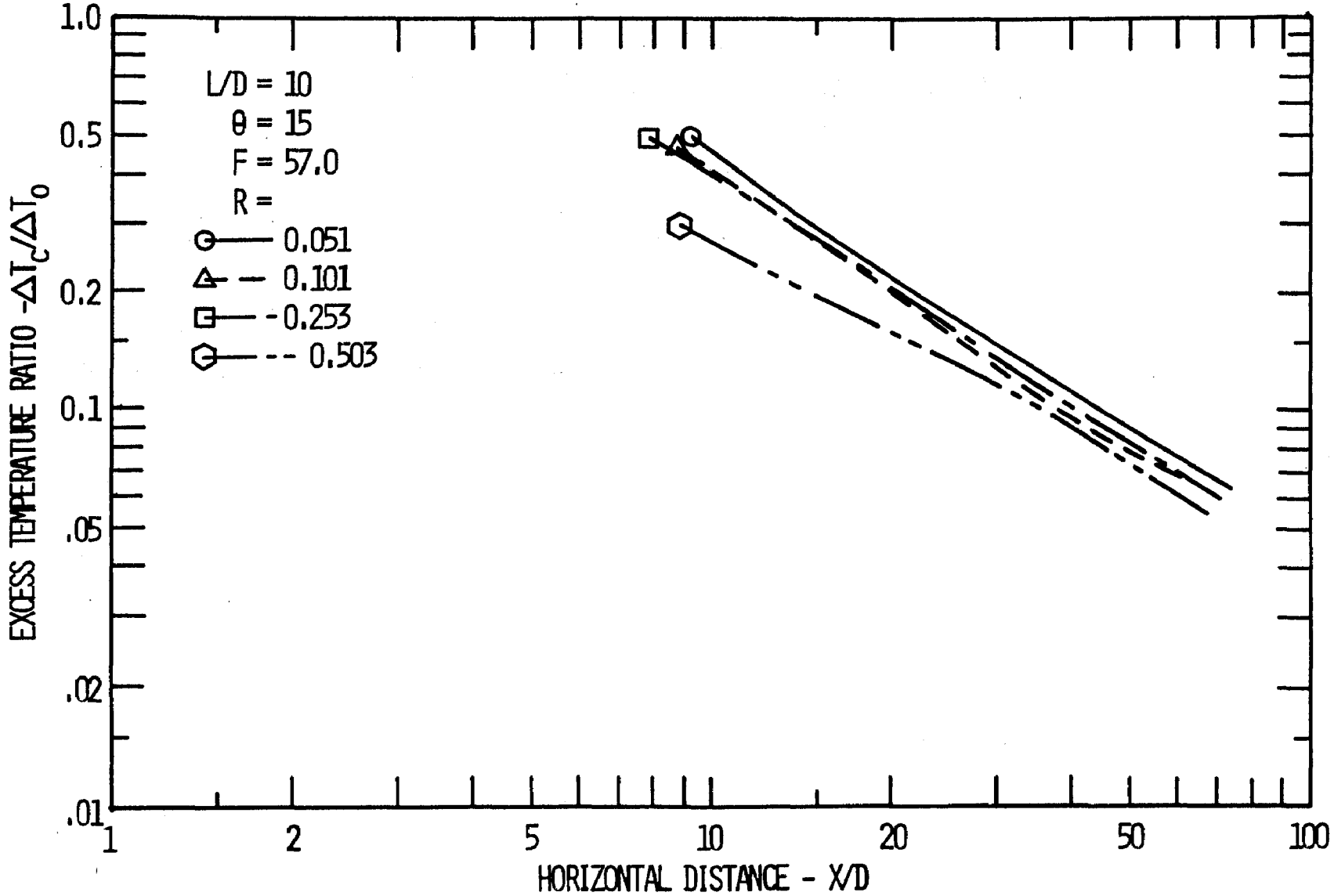

Figure 13. Effect of varying R on excess temperature ratio for L/D=10., θ=15, F=57.0.

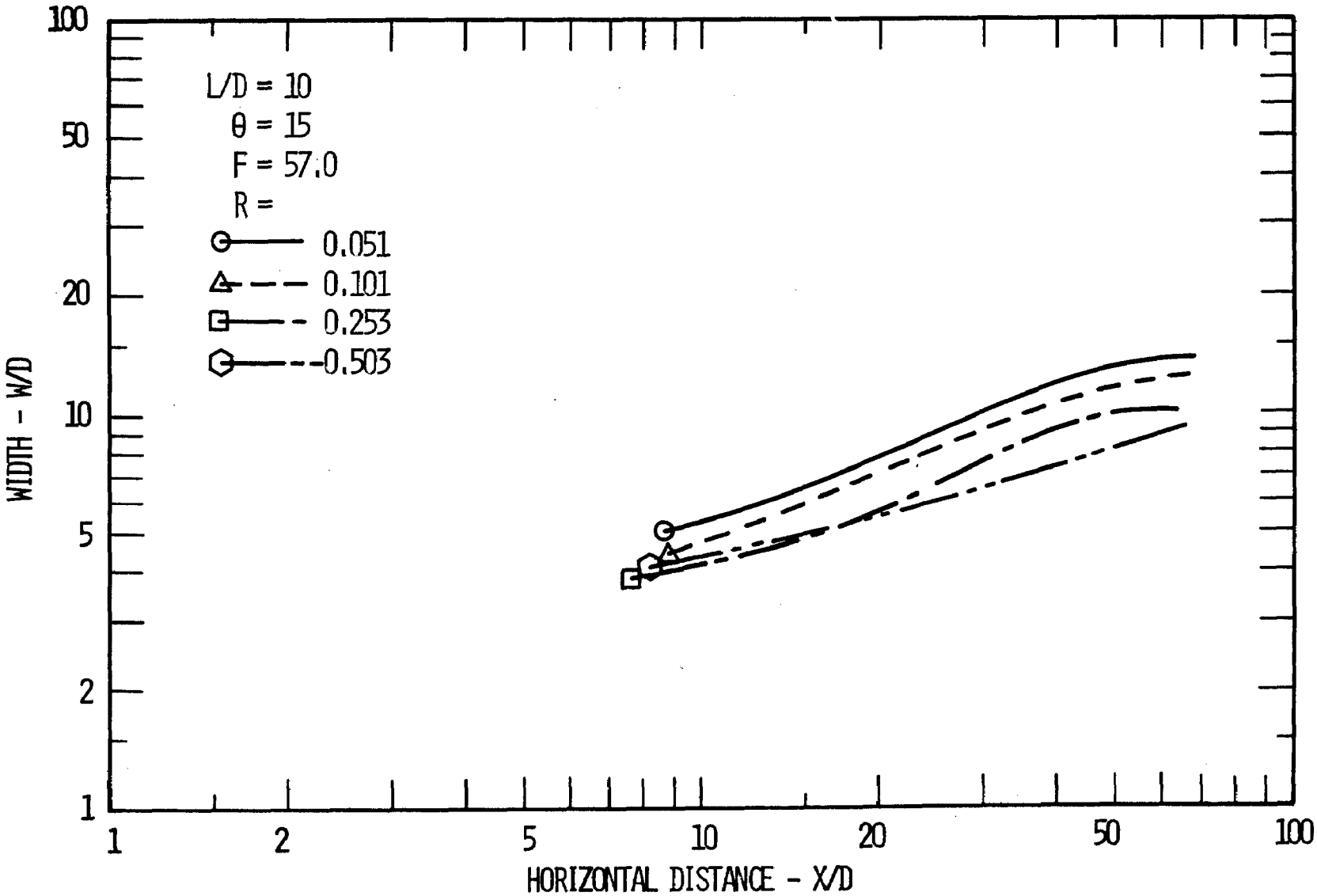

Figure 14. Effect of varying R on width for L/D=10., θ=15, F=57.0.

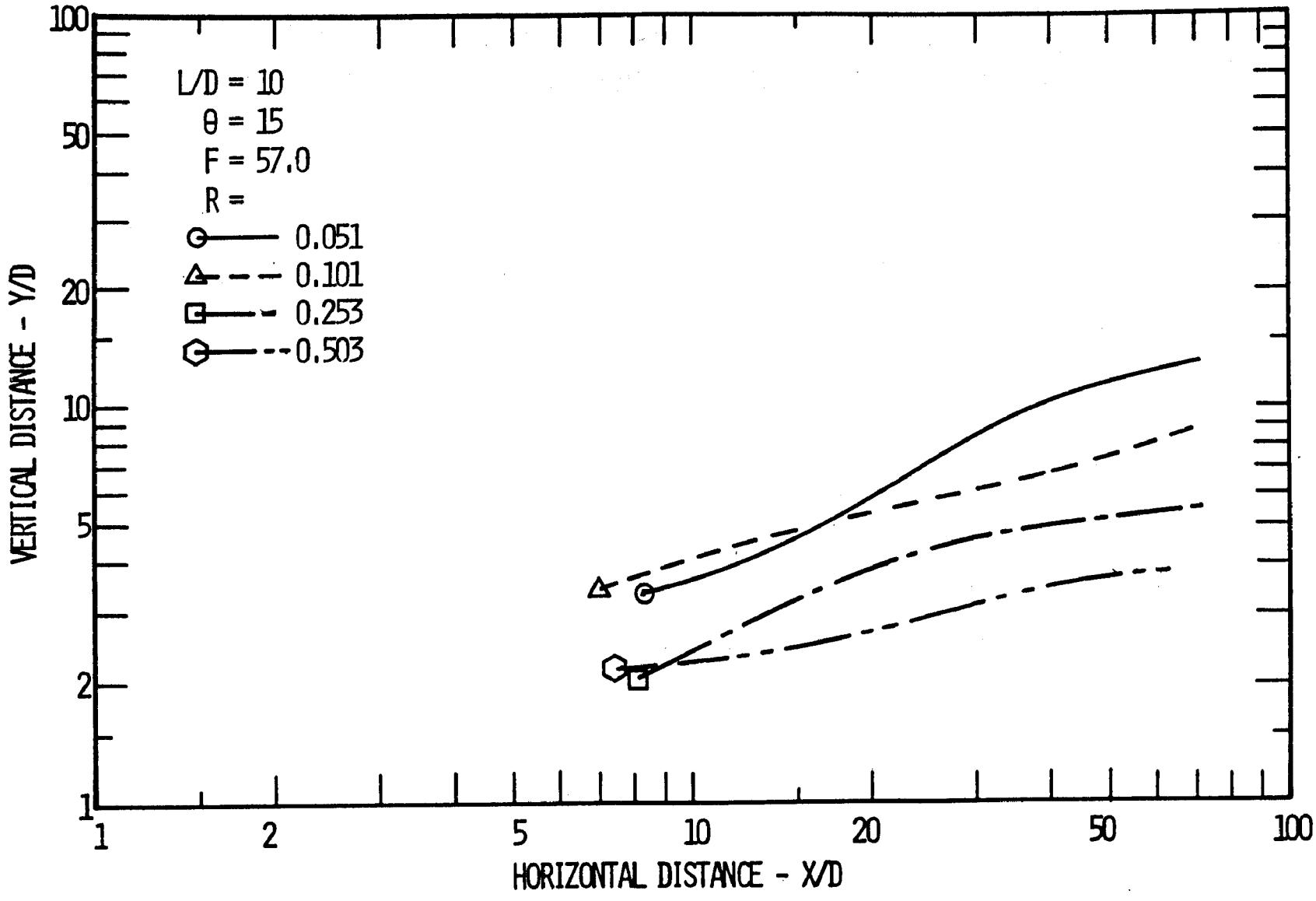

Figure 15. Effect of varying R on trajectory for L/D=10., θ=15, F=57.0.

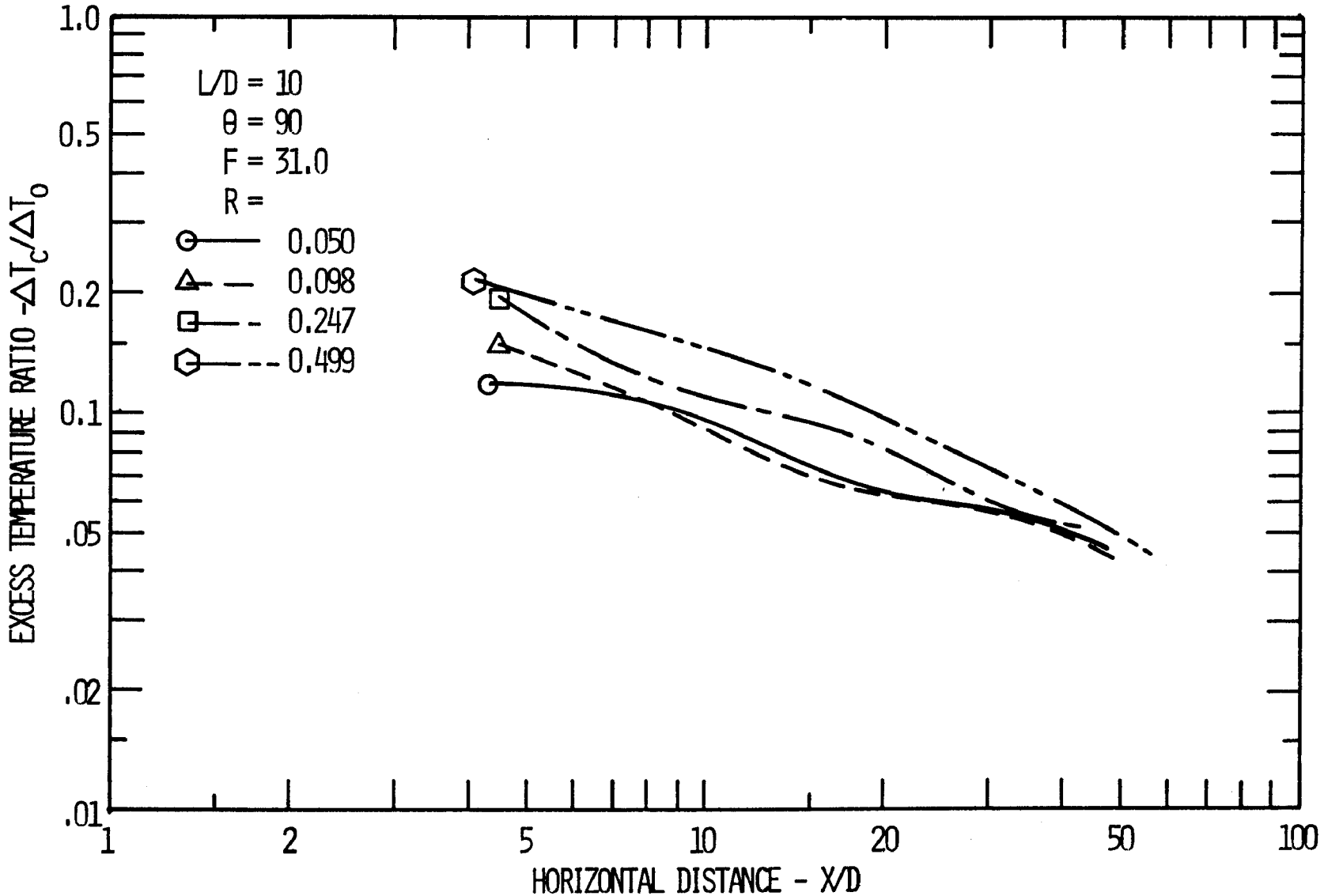

Figure 16. Effect of varying R on excess temperature ratio for L/D=10., θ=90, F=31.0.

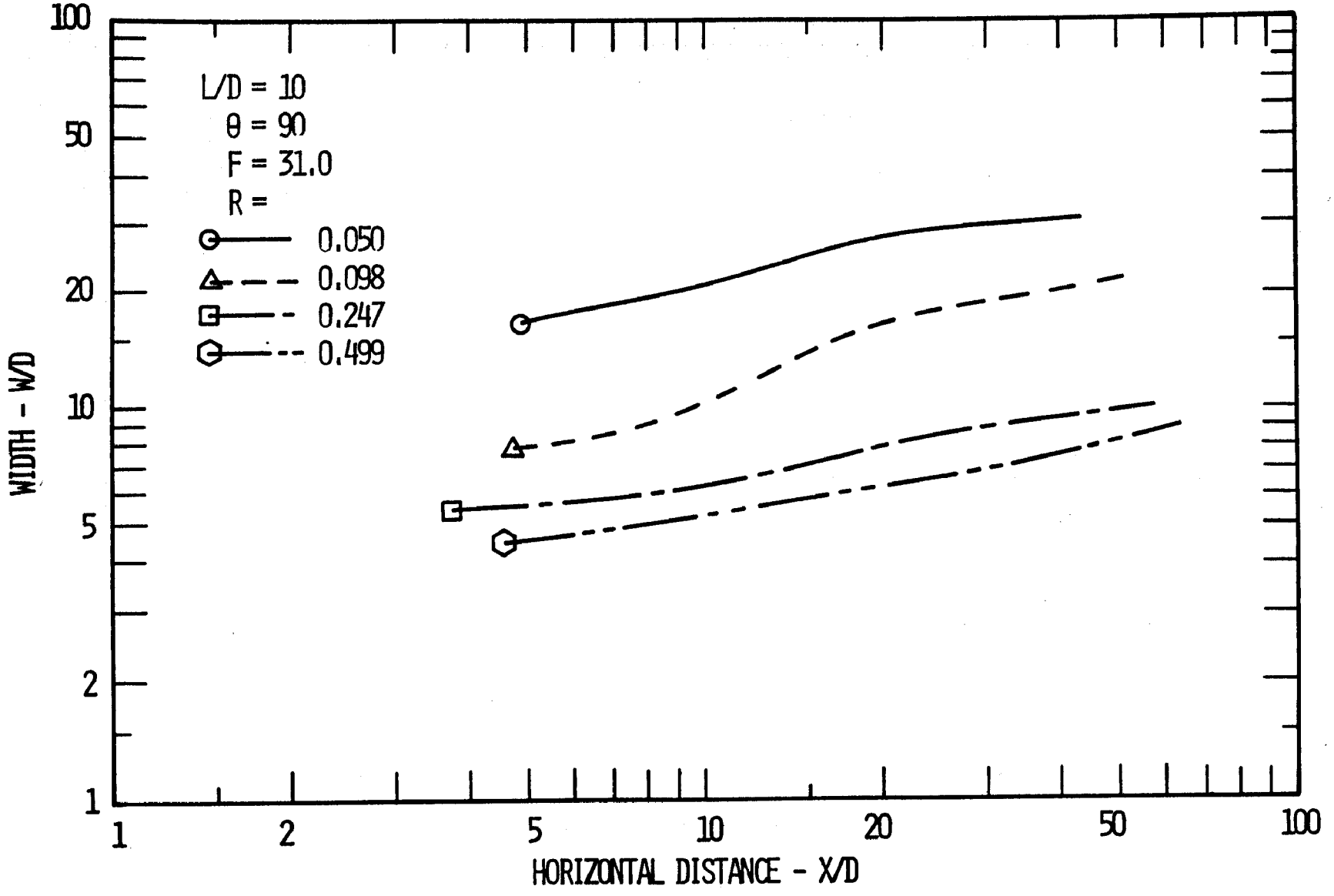

Figure 17. Effect of varying R on width for L/D=10., θ=90, F=31.0.

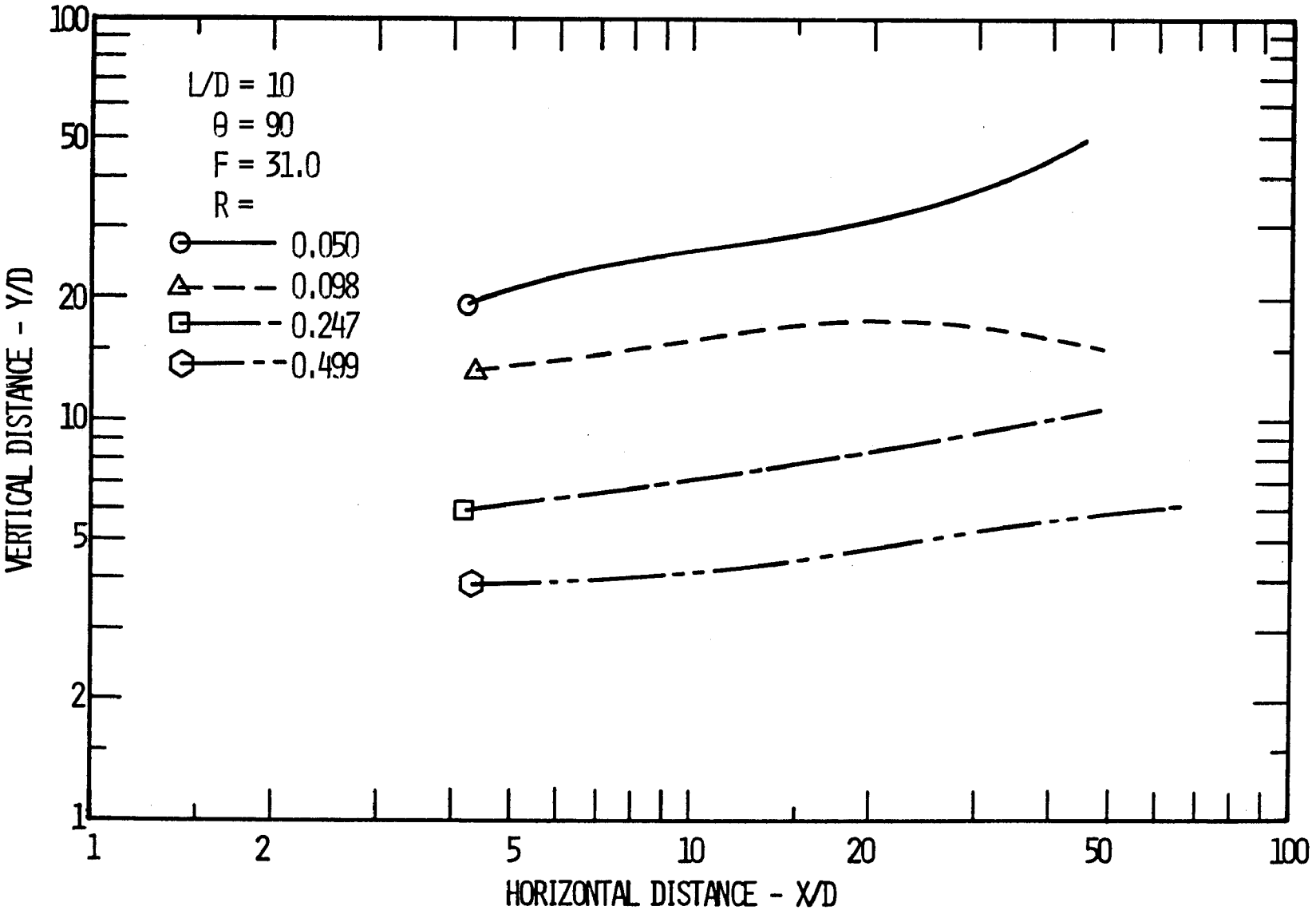

Figure 18. Effect of varying R on trajectory for L/D=10., θ=90, F=31.0.

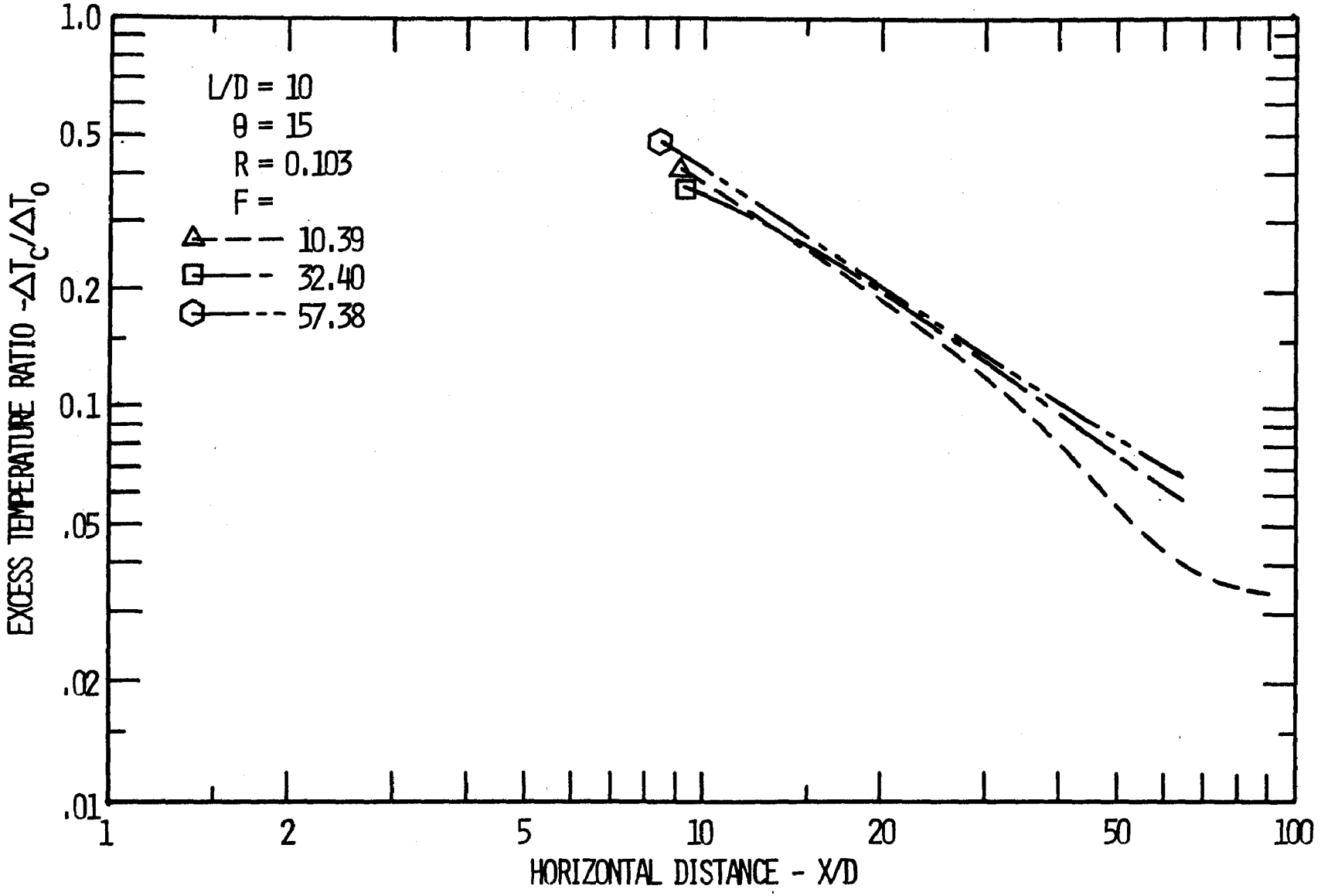

Figure 19. Effect of Froude Number on excess temperature ratio for L/D=10., θ=15, R=0.103.

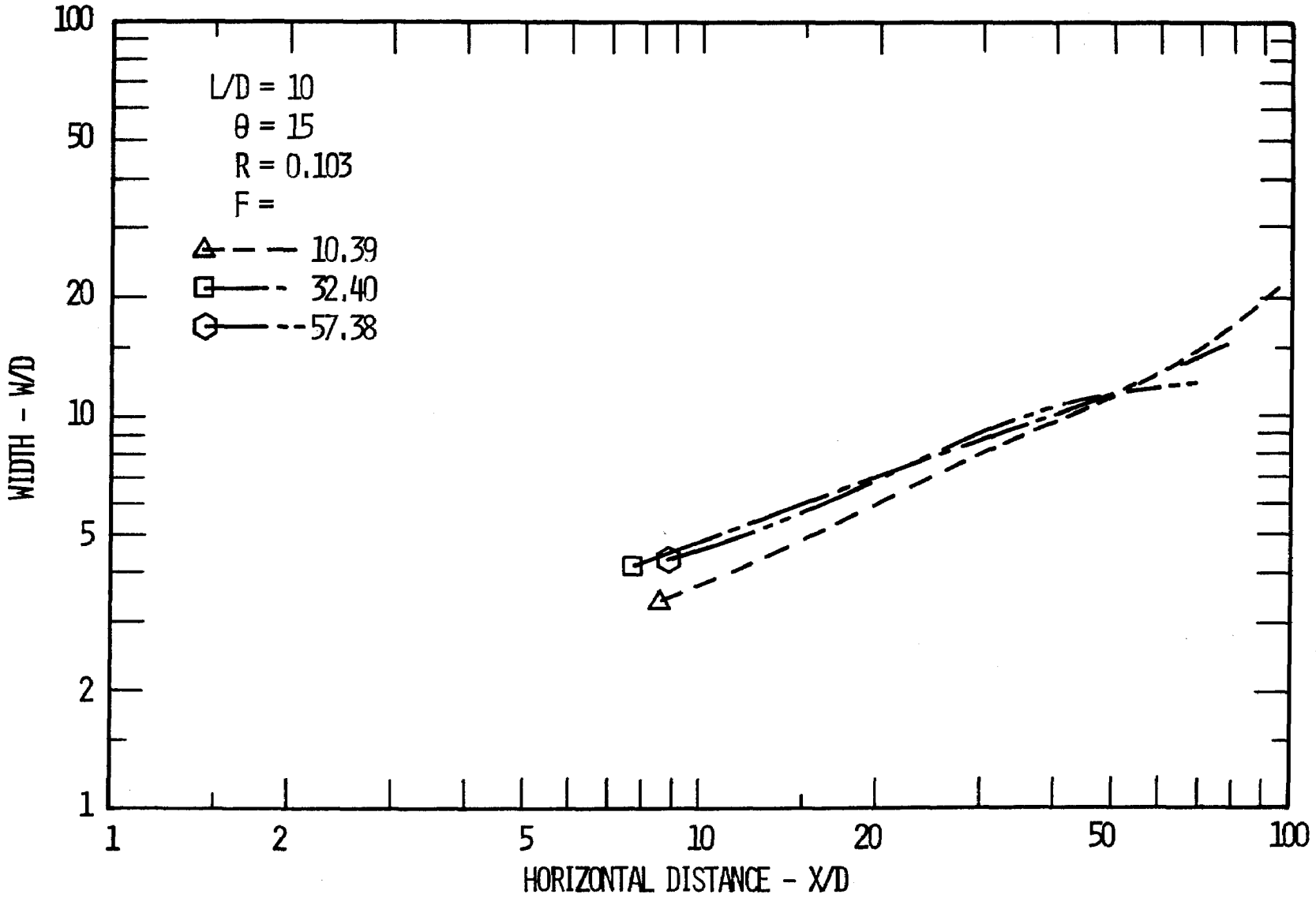

Figure 20. Effect of Froude Number on width for L/D=10., θ=15, R=0.103.

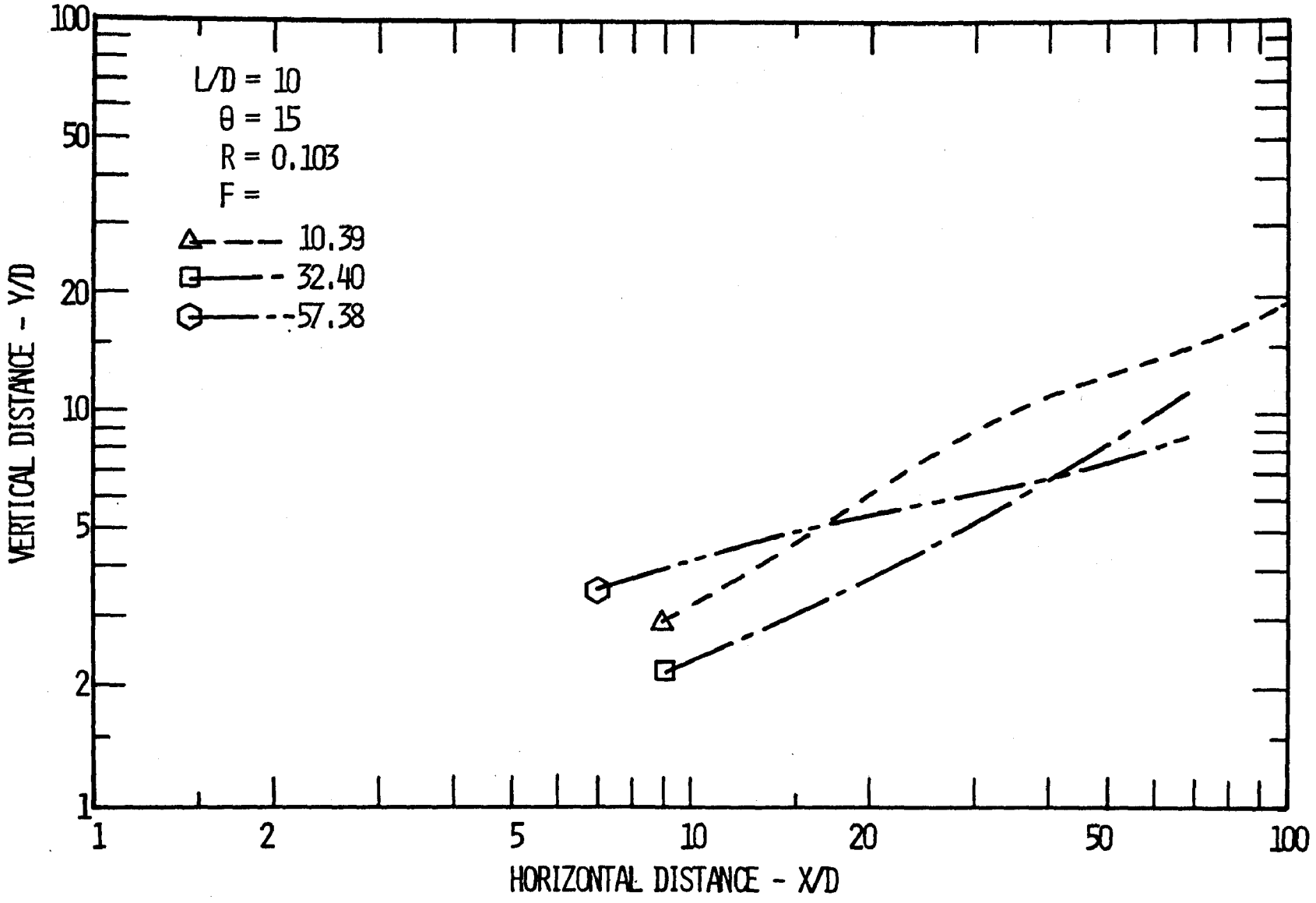

Figure 21. Effect of Froude Number on trajectory for L/D=10., θ=15, R=0.103.

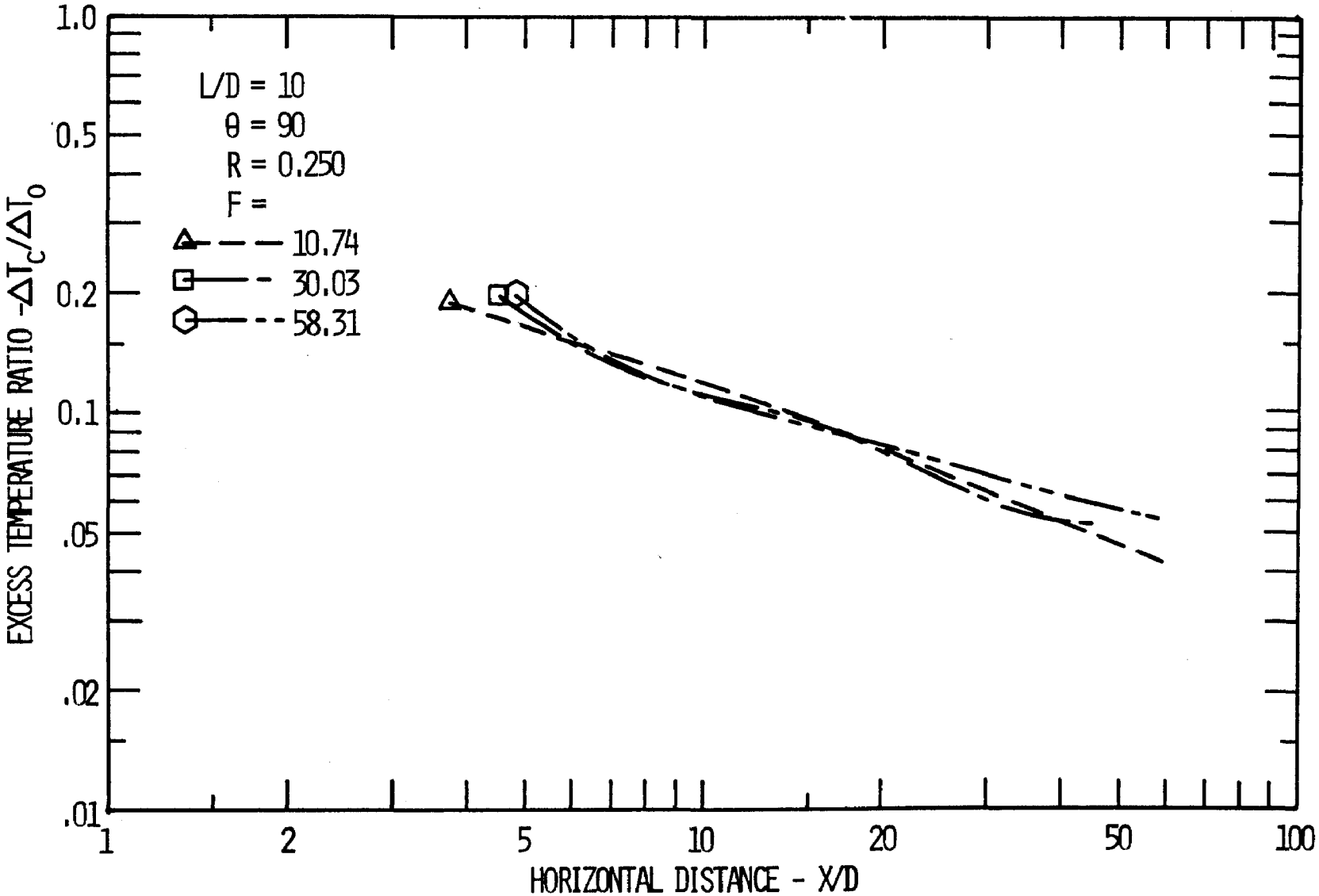

Figure 22. Effect of Froude Number on excess temperature ratio for L/D=10., θ=90, R=0.250.

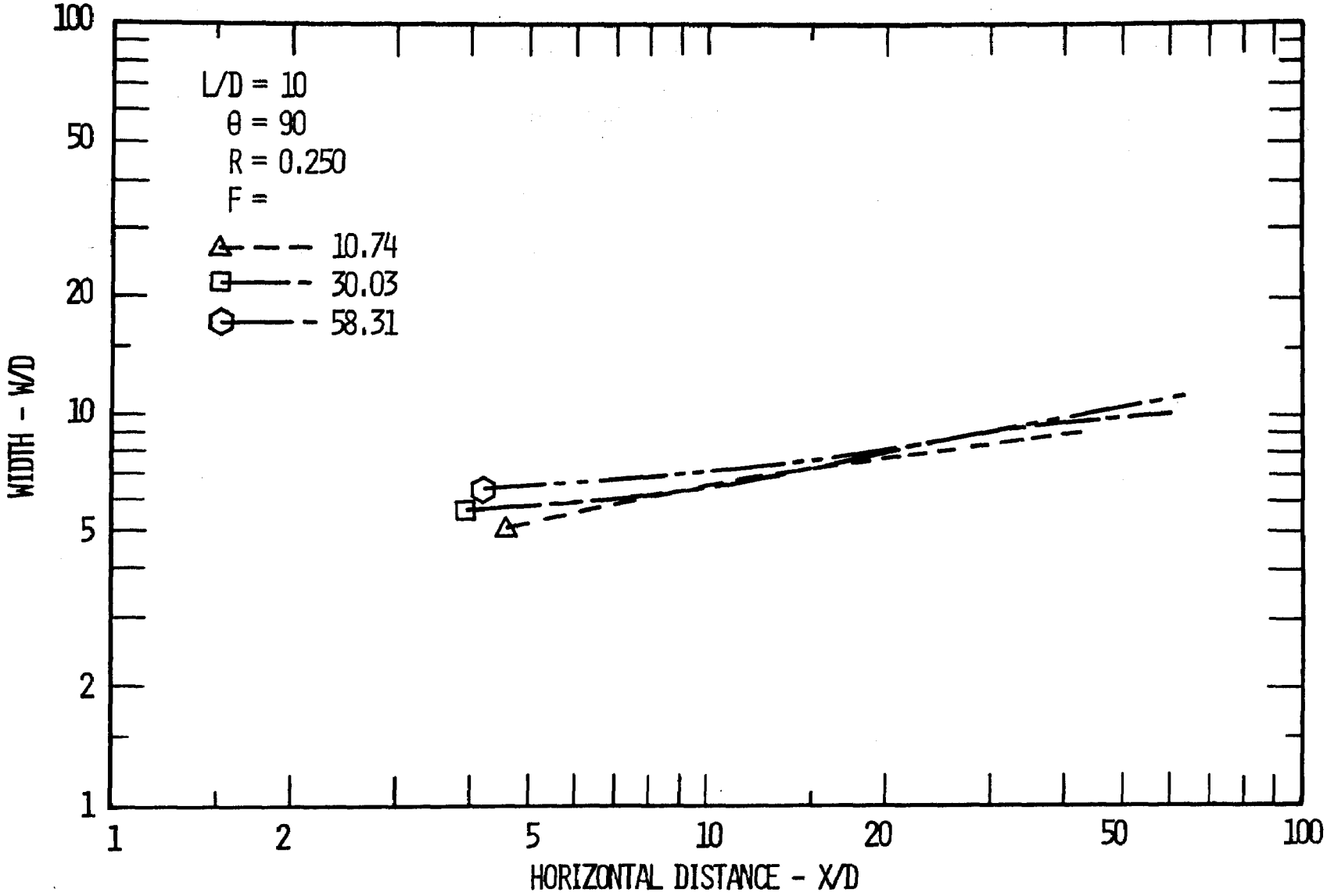

Figure 23. Effect of Froude Number on width for L/D=10., θ=90, R=0.250.

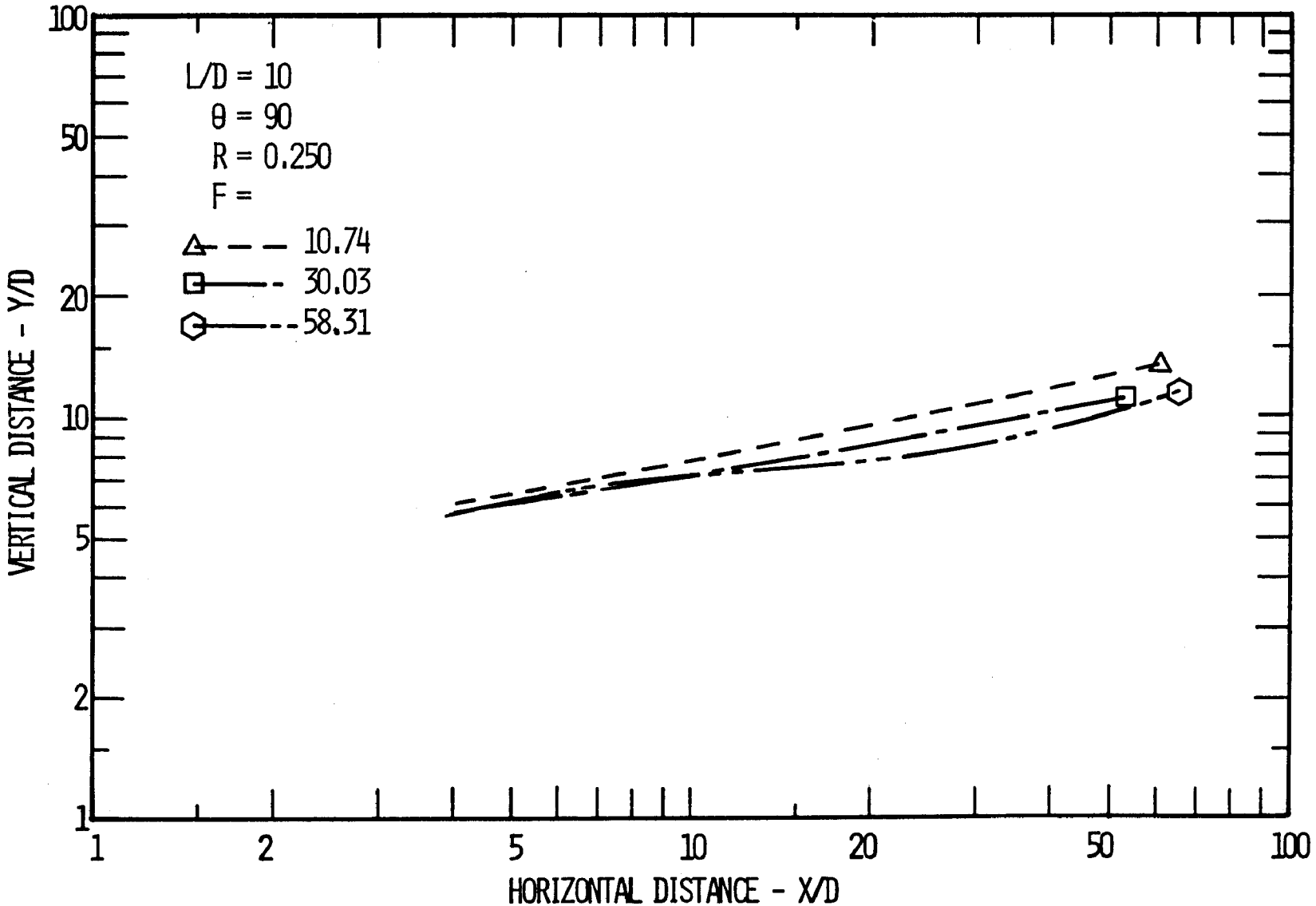

Figure 24. Effect of Froude Number on trajectory for L/D=10., θ=90, R=0.250.

R = .25 are recorded on Figures 25-27. As can be seen, the increase in the angle of discharge increases the dilution. This seems appropriate since greater initial dilution occurs in the 90° discharge as compared to the 15° discharge. A more informative graph is offered in Figure 28 which is a combined trajectory-temperature plot for F = 30, R = 0.25 and L/D = 10. As one notices, the 90° and 60° dilution and trajectory are very similar. It is interesting to note that after X/D = 35 the 15° results show less dilution than the 0° results. Using the results from this graph, attempts were made to predict the results at 45° for cases at extremes of towing ratio and Froude No. using 15° and 90° data previously obtained. While the higher towing rates were predicted quite accurately, the results at lower towing rates were not well predicted. Accordingly, additional runs were taken at 45° for the slower towing rates. Complete data exists for angles of 0°, 15°, and 90° as well as partial data at 45° for L/D = 10. However, only selected runs exist at 90° and 45° for the other L/D's.

Of all the parameters of interest the port spacing seems to be the most critical. It is this variable that will most affect construction costs, and it is probably the most important thermal design parameter related to the siting of a plant. The comparisons offered in this discussion on L/D comprise nearly all the experimental cases. Four cases are offered at 90° and one at 45° for the comparison of L/D effects.

The excess temperature ratio illustrated in Figures 23, 32, 35, 38, and 41 seems to be markedly dependent on L/D. The trend appears to be decreasing dilution with decreasing port spacing.

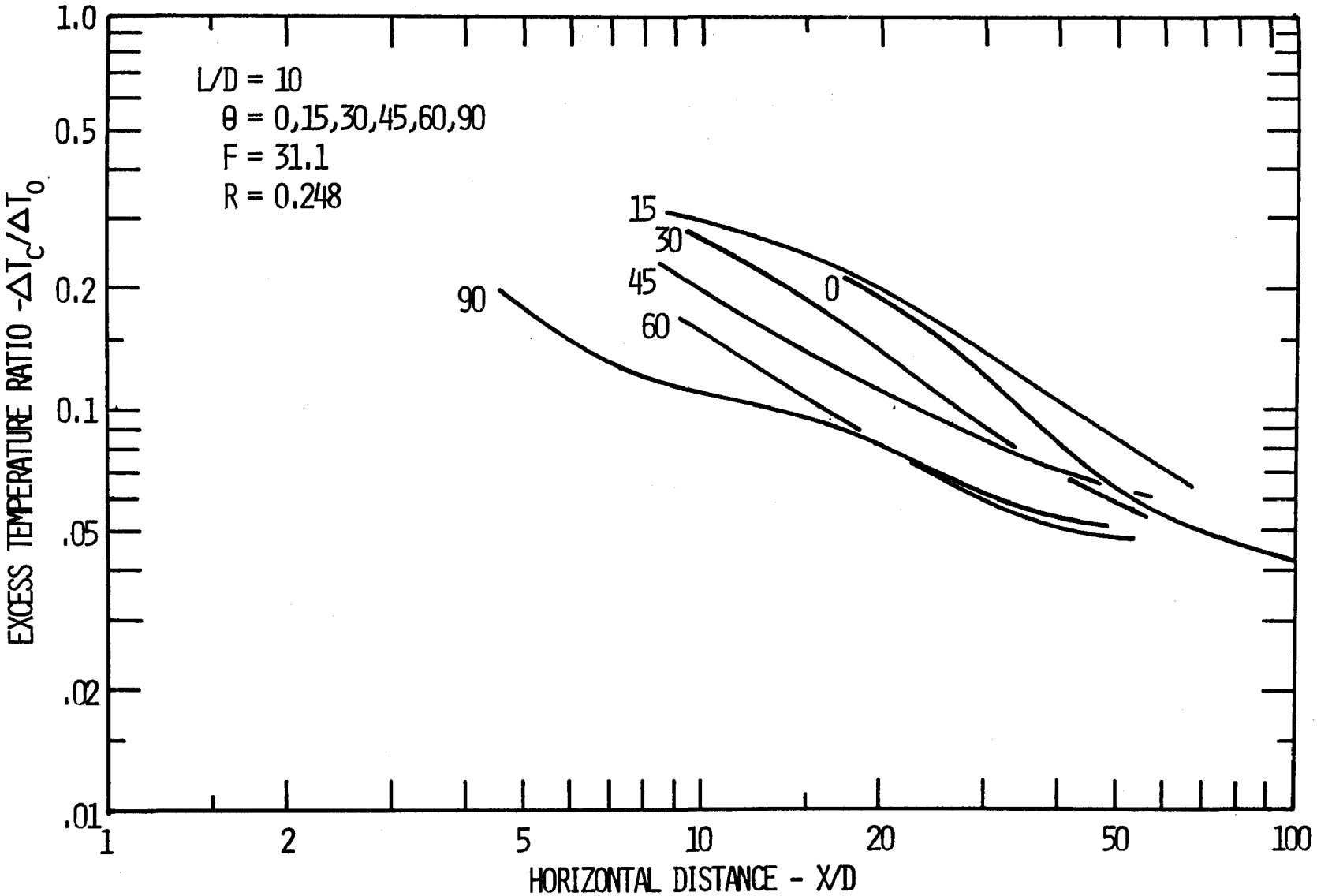

Figure 25. Effect of angle on the excess temperature ratio for L/D=10., F=31.1, R=0.248.

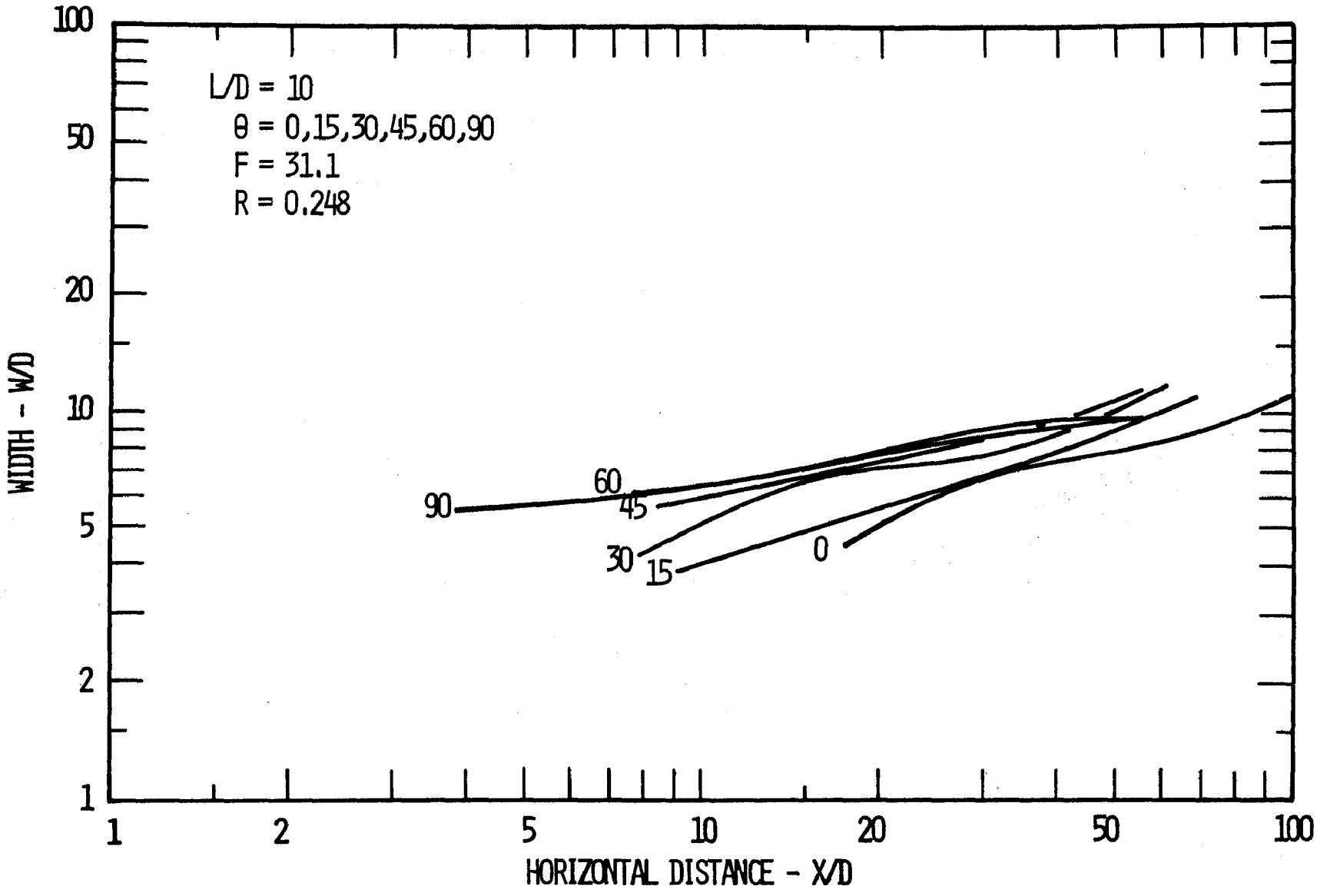

Figure 26. Effect of angle on width for L/D=10., F=31.1, R=0.248.

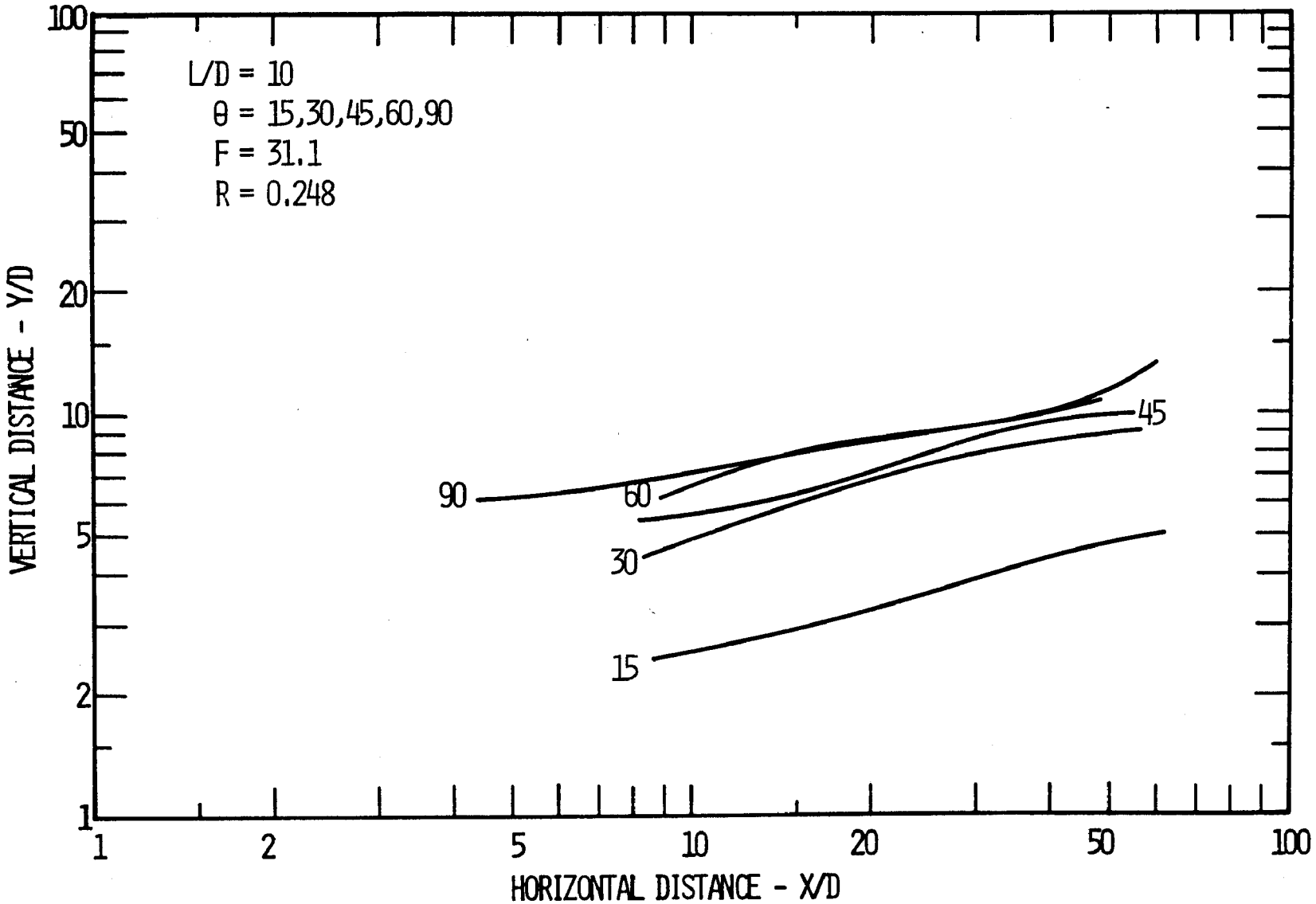

Figure 27. Effect of angle on trajectory for L/D=10., F=31.1, R=0.248.

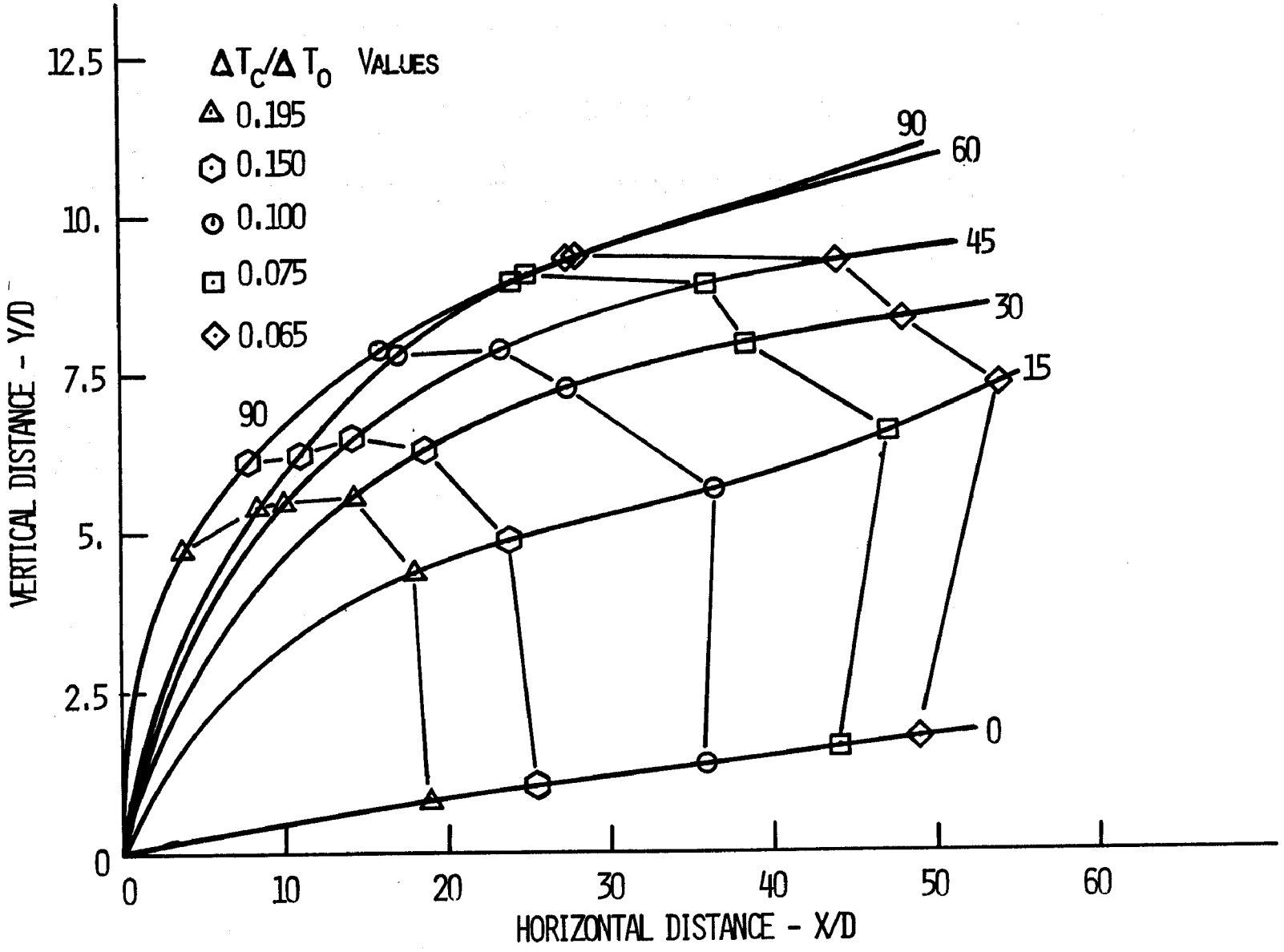

Figure 28. Effect of angle on dilution as plotted with trajectory for L/D=10., F=31.1, R=0.248.

That Figures 29 and 41 show more dramatic trends may be attributable to the fact that the towing ratio is 0.10. As is common with plumes discharged into a current, twin vortices often occur. In the experiments performed, this twin vortex structure seemed to be more defined at R = 0.10. Since the sensor was located in the centerplane of the discharging port, the measurements were actually taken between the two vortices as illustrated in Figure 44, and as cited in Hirst[17], the maximum temperatures often occur near the center of each of these vortices. It is probable that for the distance downstream that the twin vortex structure was maintained our sensor did not pass directly through the region of hottest discharge but rather very close to it. No attempt was made to search for the hottest parts of the discharge except to verify that they were indeed slightly off the center plane.

The vortex effect may increase the lateral entrainment. This effect would be most obvious in comparisons of L/D effect since the jets must compete for lateral entrainment with the competition getting more intense for closer spacings.

Referring to Figures 30, 33, 36, 39, and 42 which present L/D effects on width, the dramatic differences noticed before in excess temperature are not extended to widths. In fact, no clear trend exists in widths. It appears that in all cases though, the width of the jet for L/D = 2.5 is slightly greater than that for the other L/D's. It can be concluded that the width of the jet cannot be used as a measure of dilution for close spaced jets when comparing to larger jet spacings.

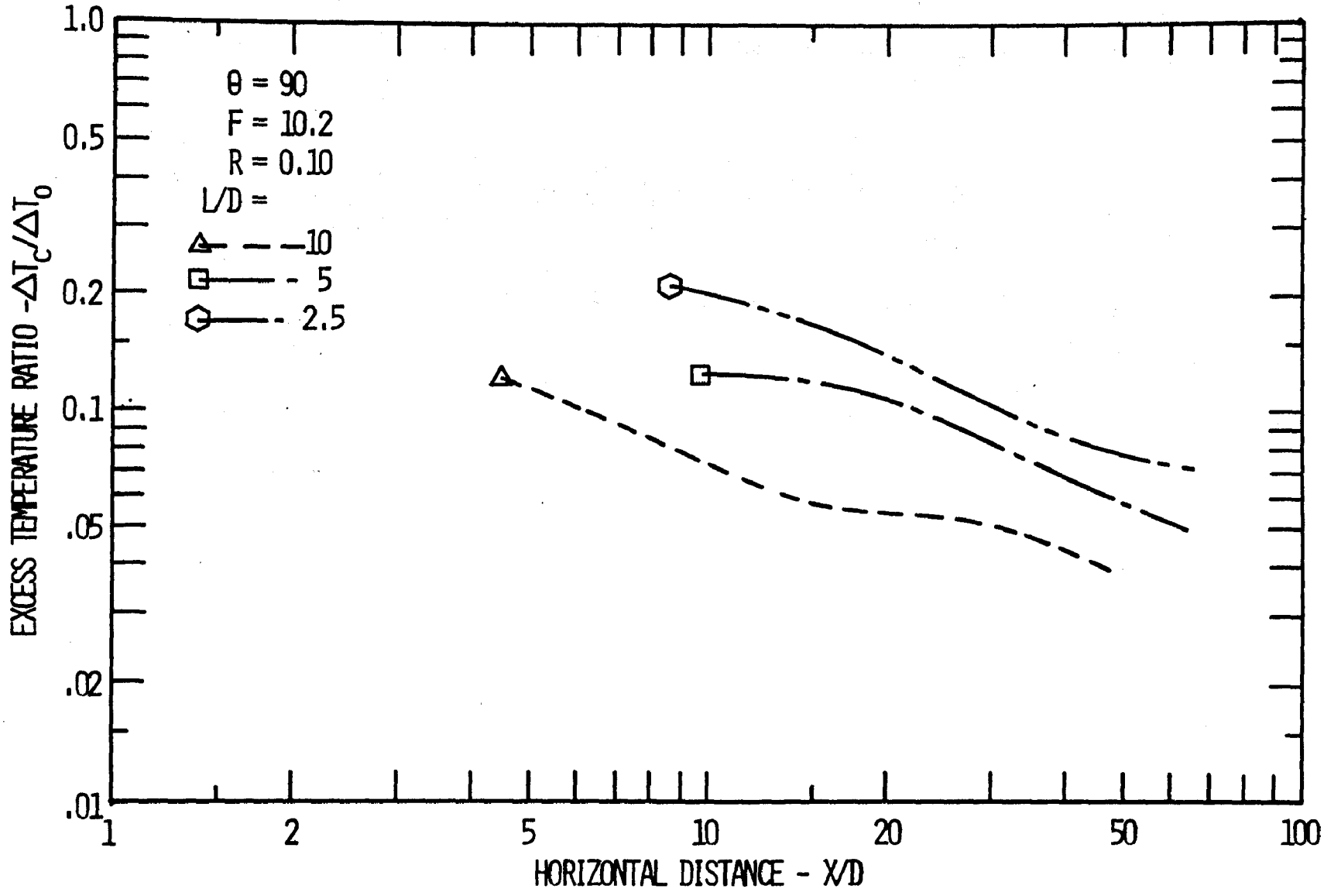

Figure 29. Effect of L/D on excess temperature ratio for θ=90, F=10.2, R=0.10.

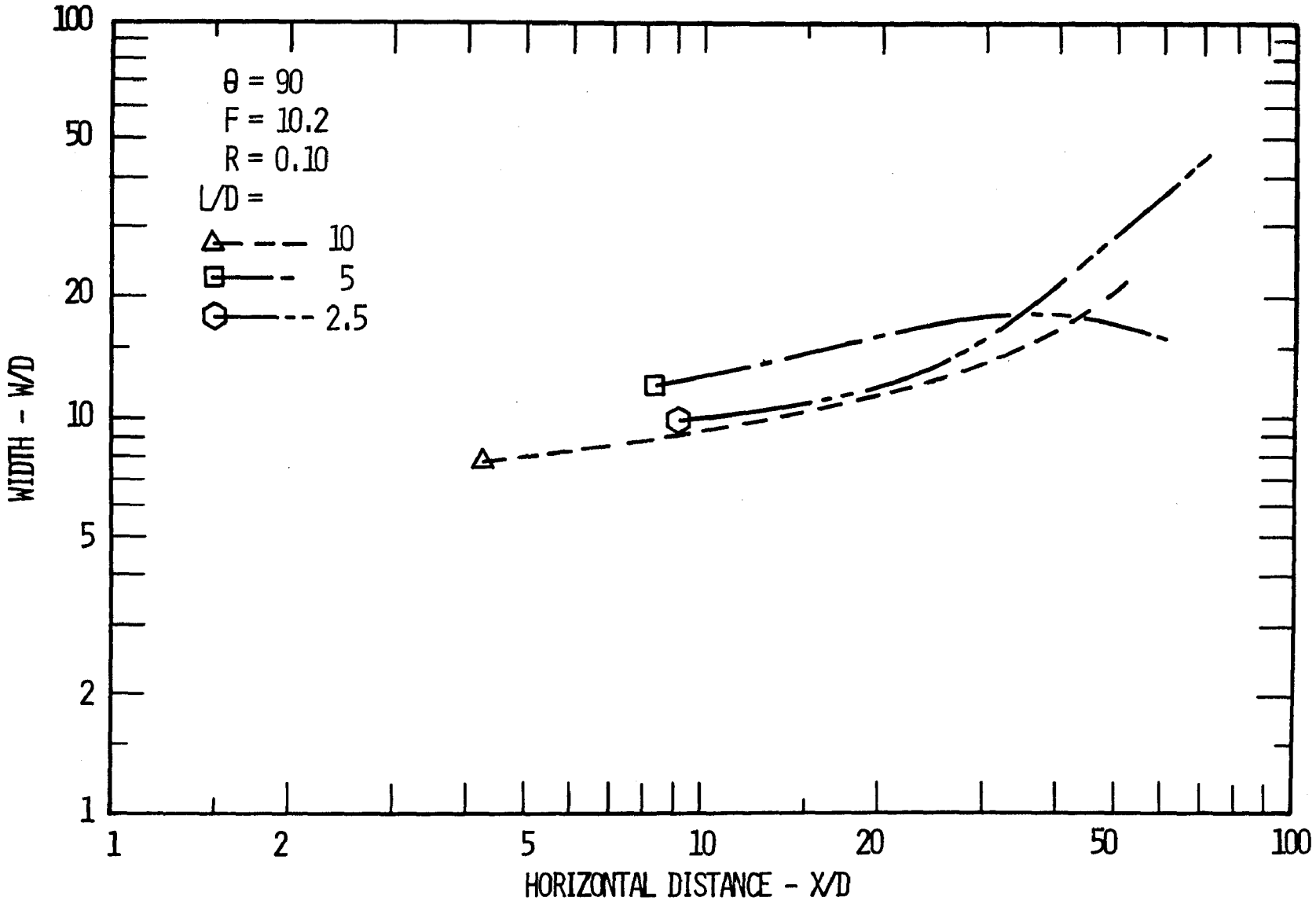

Figure 30. Effect of L/D on width for θ=90, F=10.2, R=0.10.

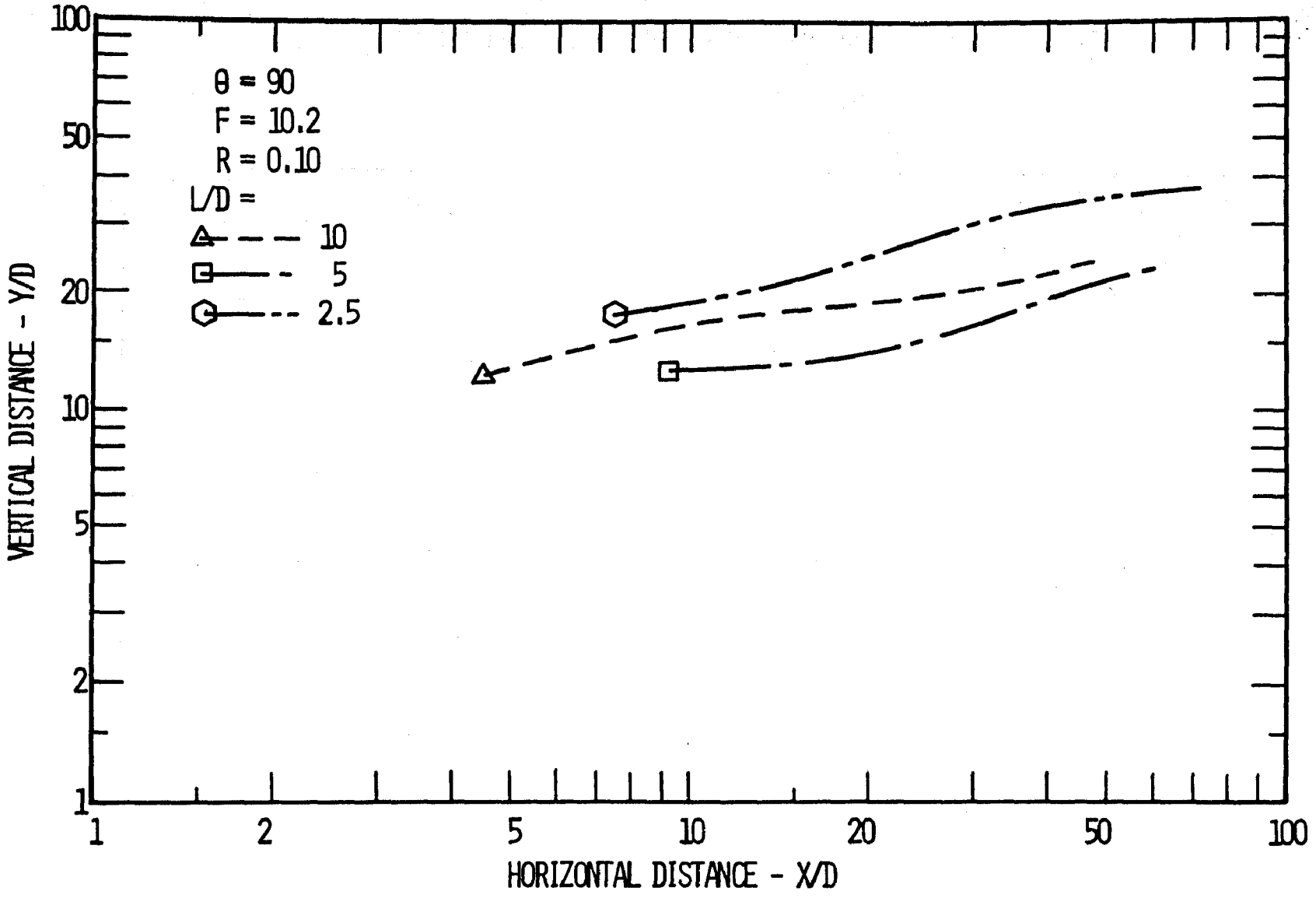

Figure 31. Effect of L/D on trajectory for θ=90, F=10.2, R=0.10.

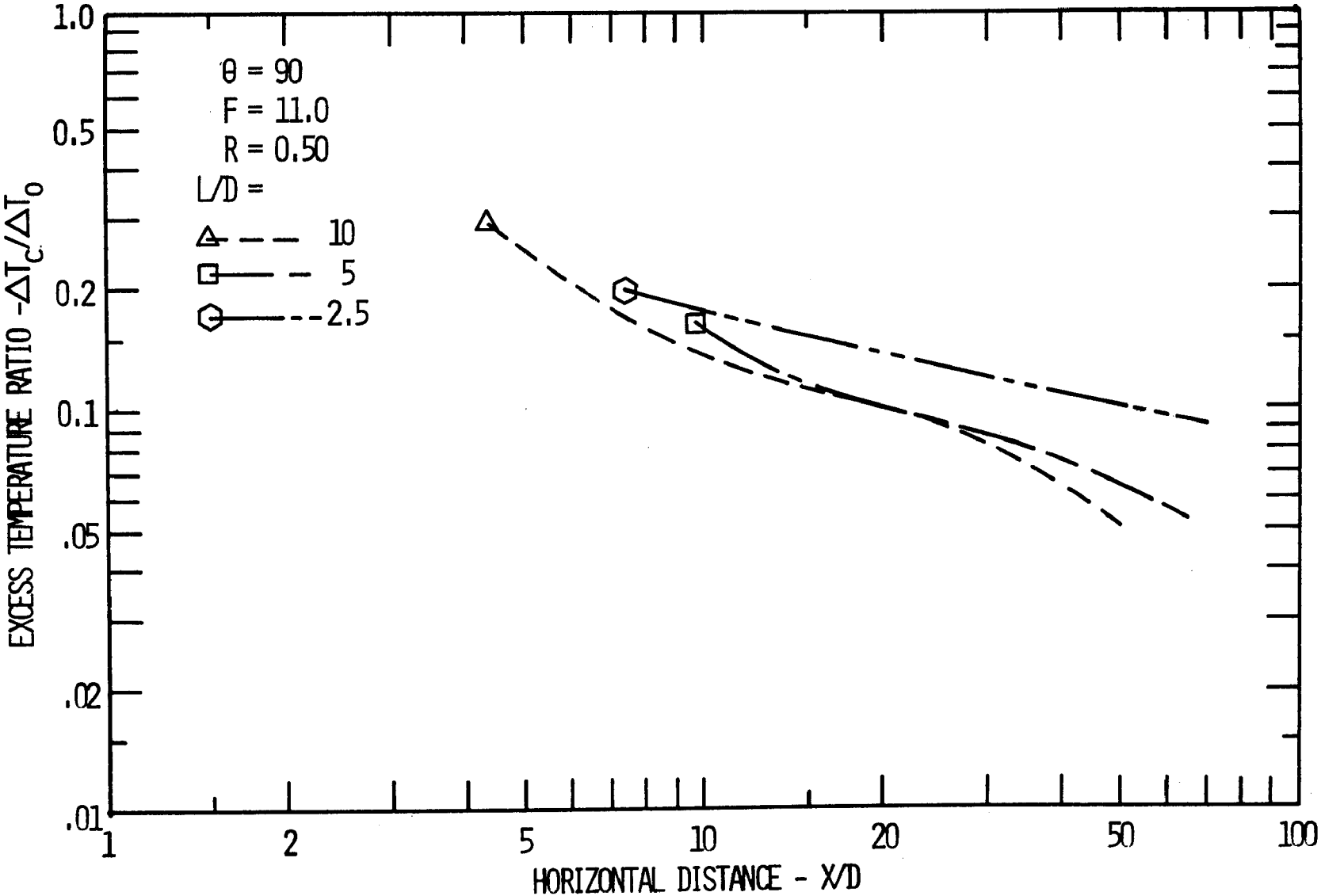

Figure 32. Effect of L/D on excess temperature ratio for θ=90, F=11.0, R=0.50.

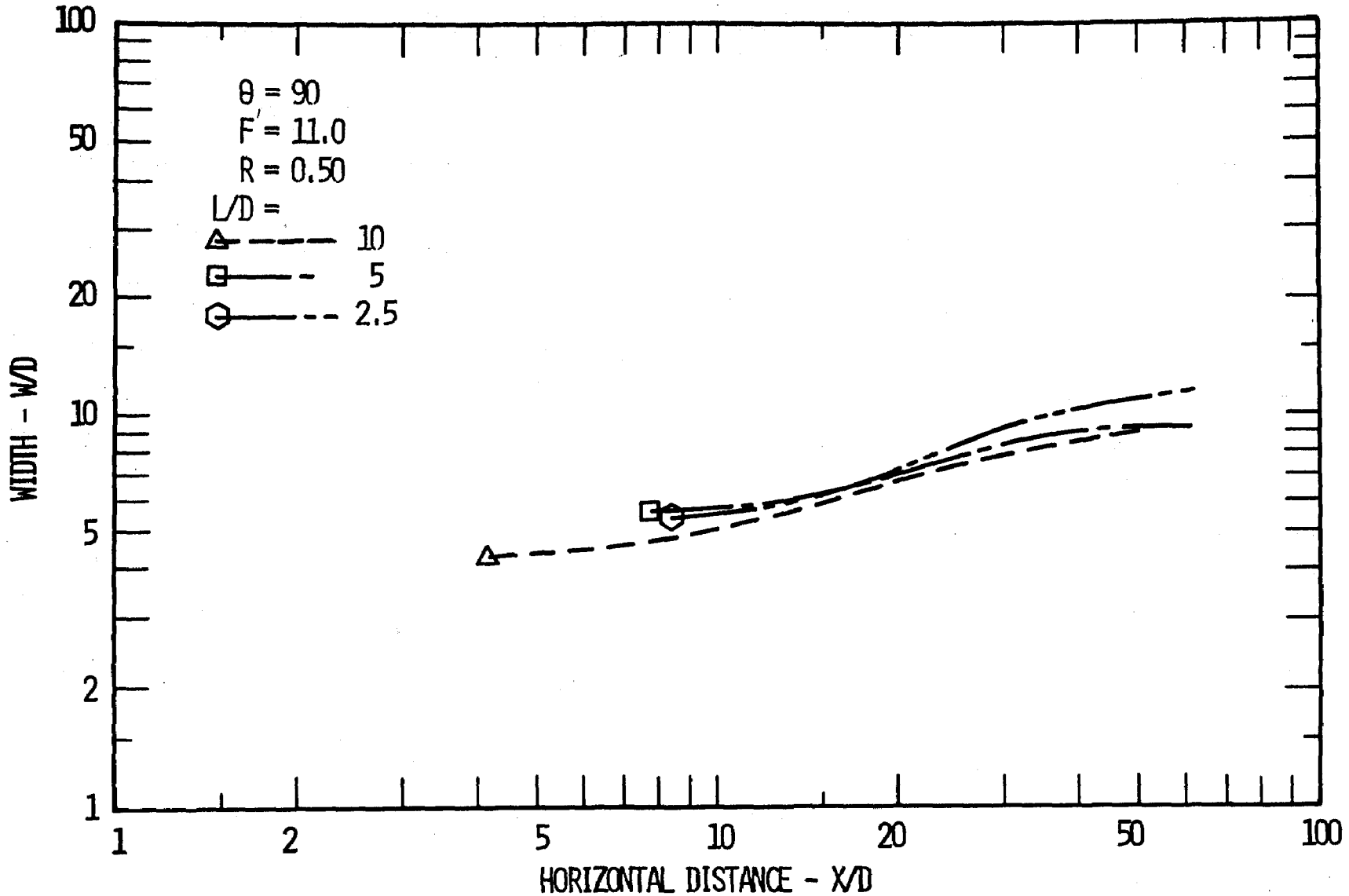

Figure 33. Effect of L/D on width for θ=90, F=11.0, R=0.50.

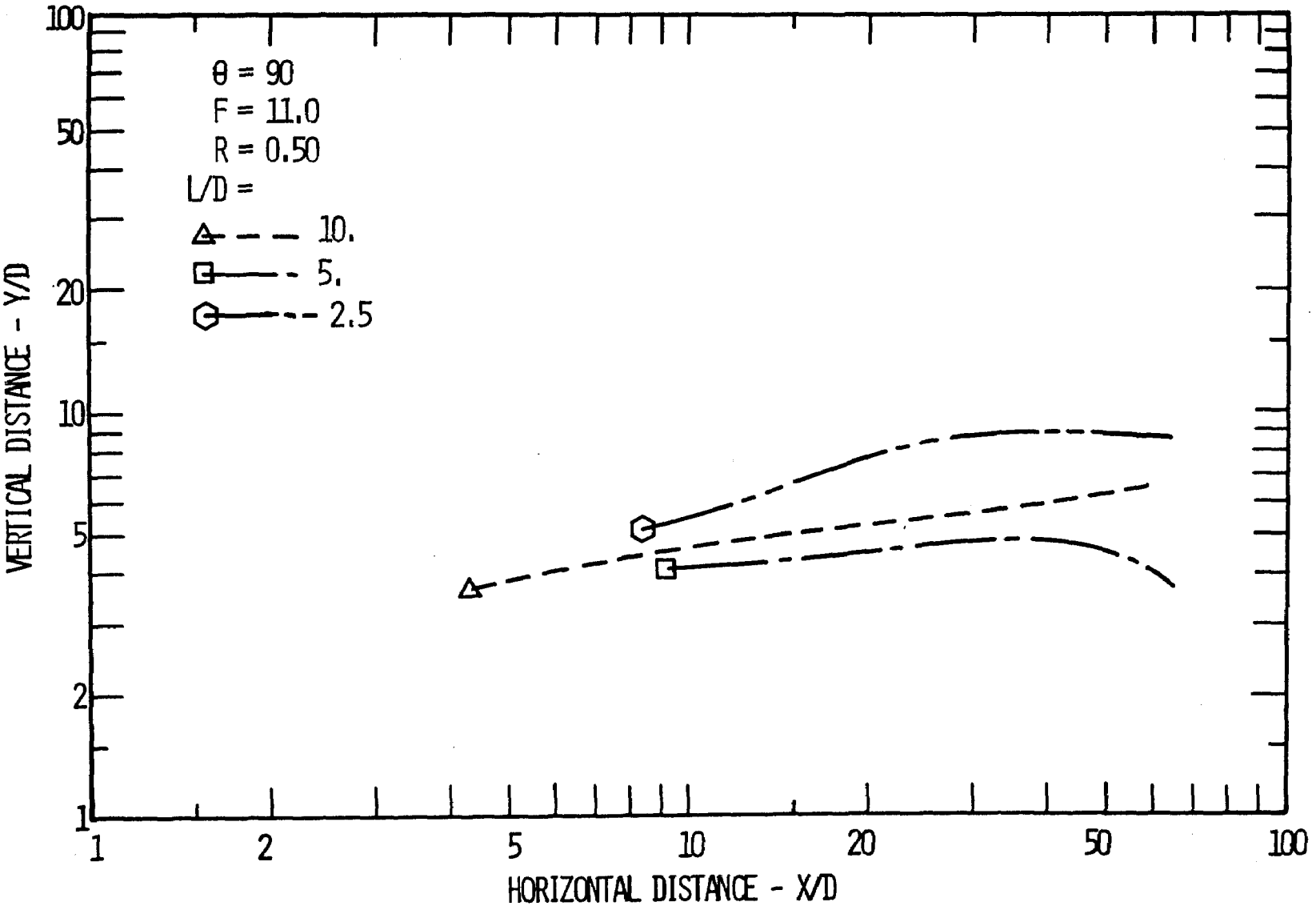

Figure 34. Effect of L/D on trajectory for θ=90, F=11.0, R=0.50

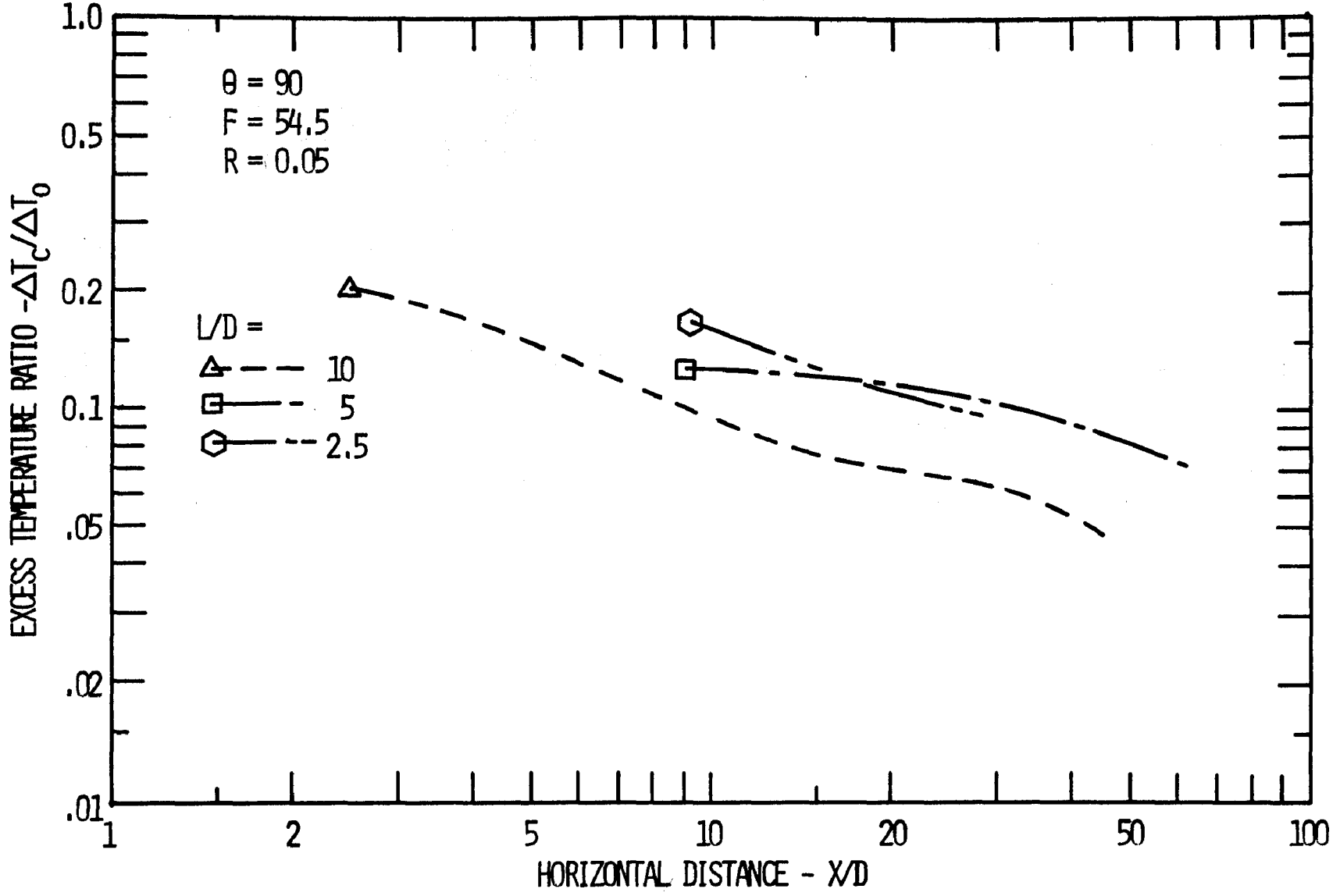

Figure 35. Effect of L/D on excess temperature ratio for θ=90, F=54.5, R=0.05.

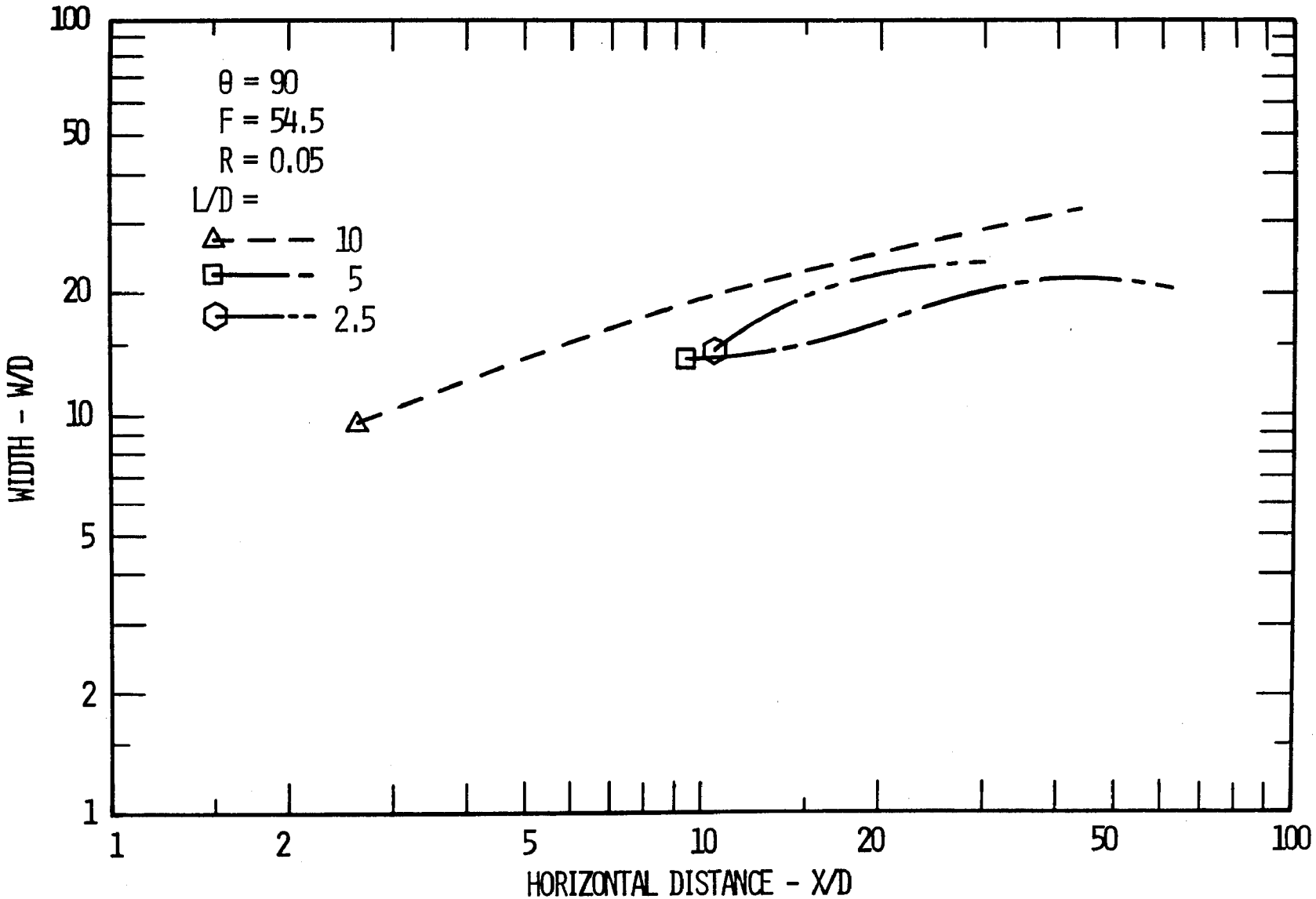

Figure 36. Effect of L/D on widths for θ=90, F=54.5, R=0.05.

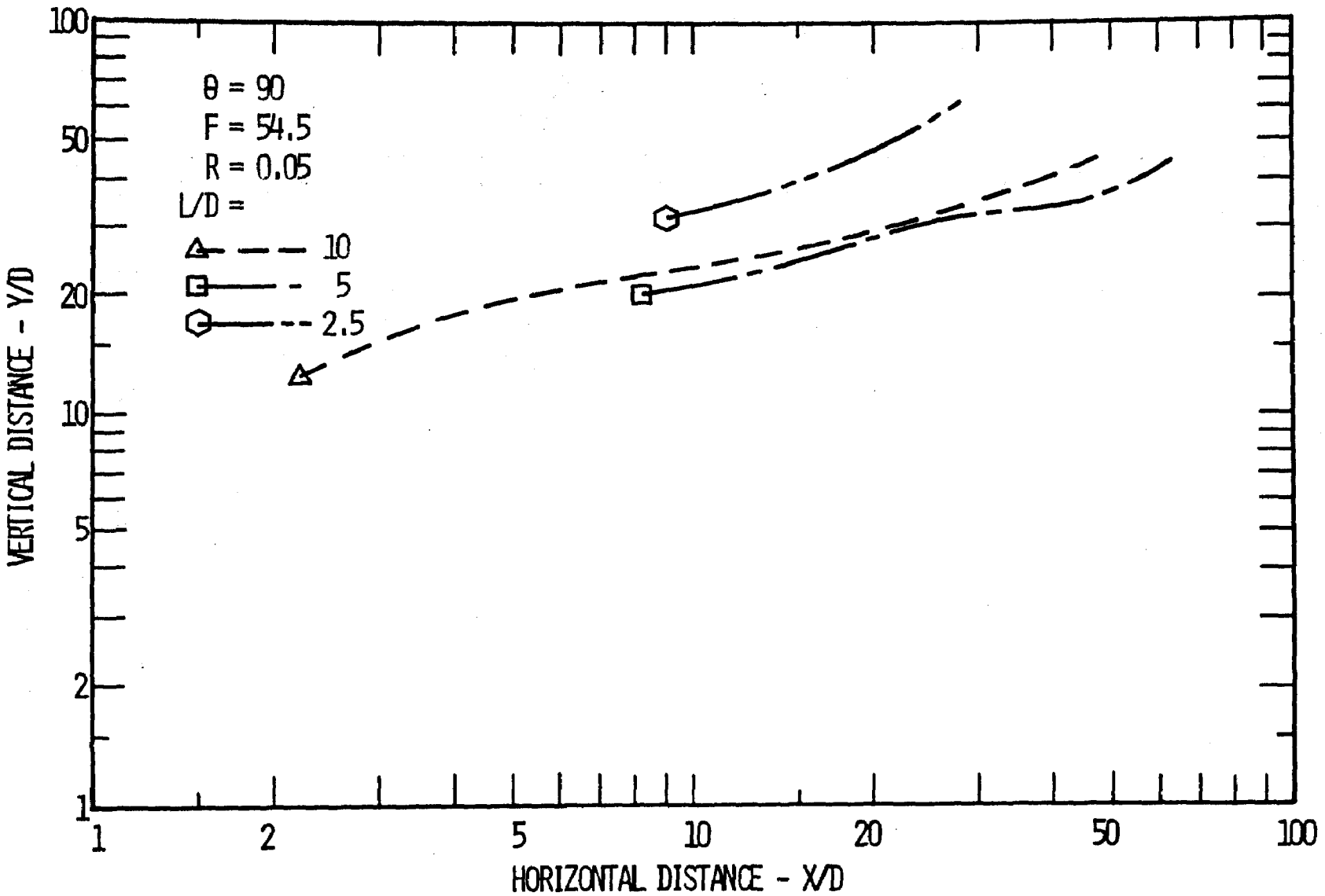

Figure 37. Effect of L/D on trajectory for θ=90, F=54.5, R=0.05.

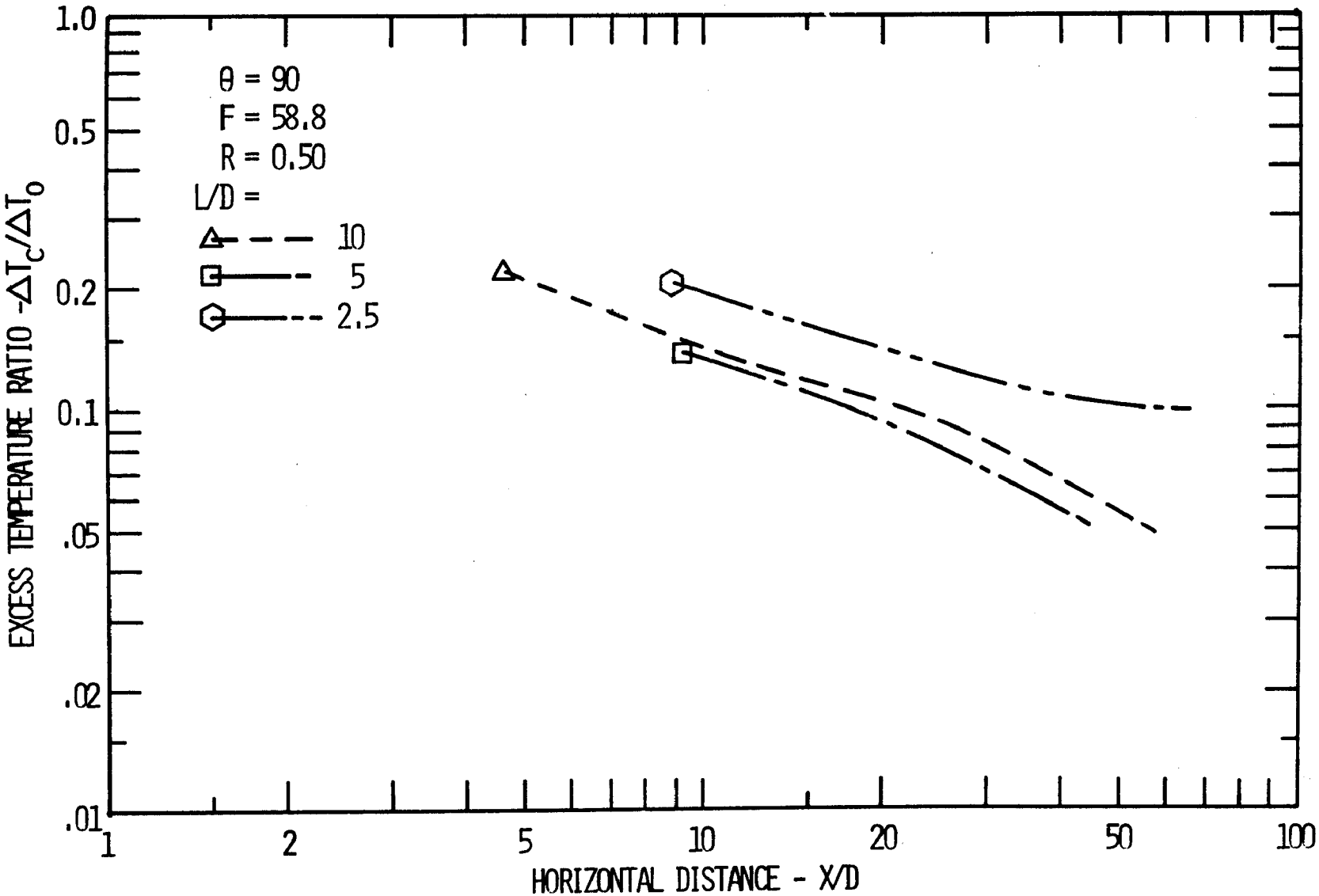

Figure 38. Effect of L/D on excess temperature ratio for θ=90, F=58.8, R=0.50.

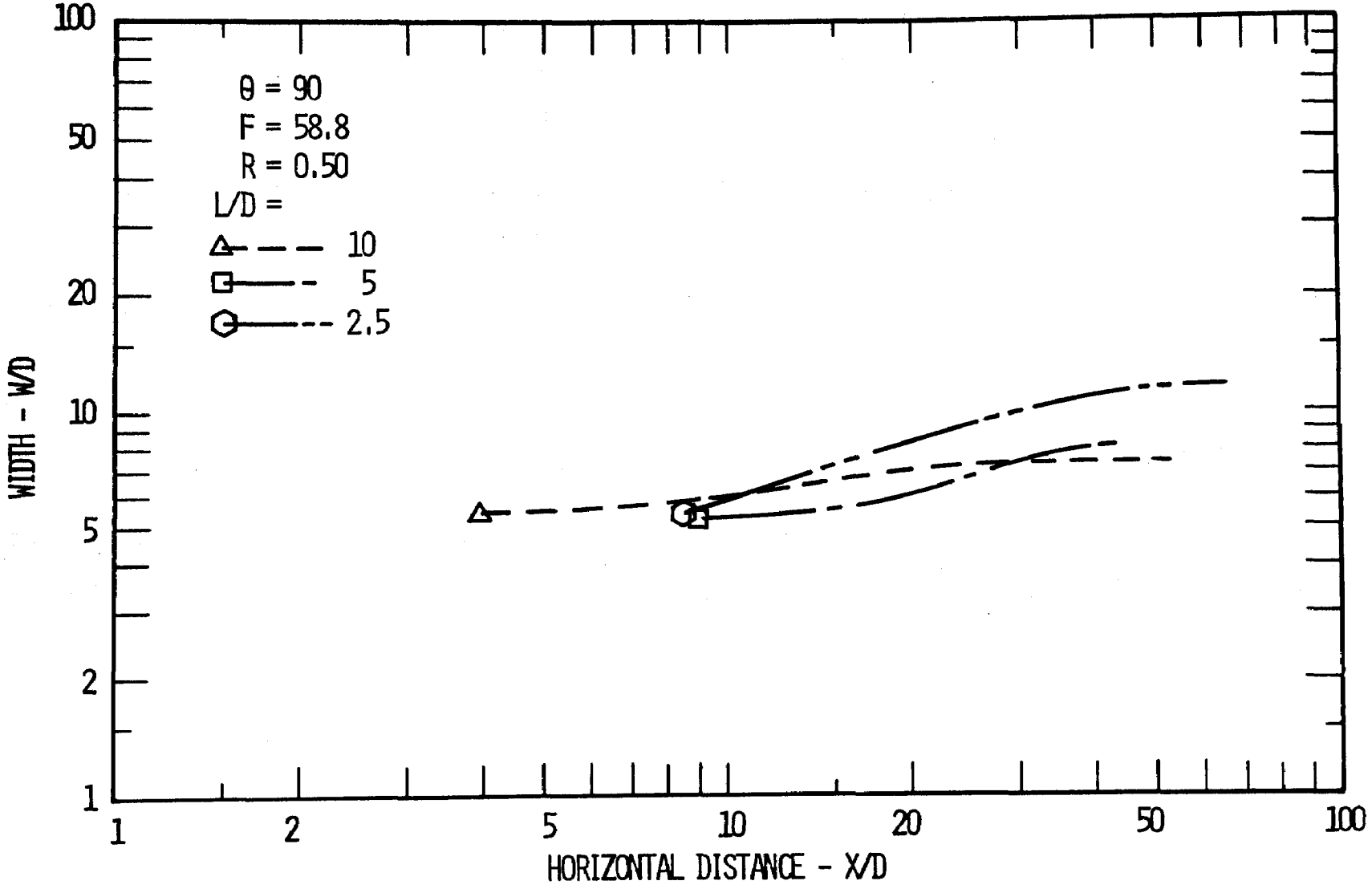

Figure 39. Effect of L/D on width for θ=90, F=58.8, R=0.50.

Figure 39, Effect of L/D on width for θ=90, F=58.8, R=0.50.

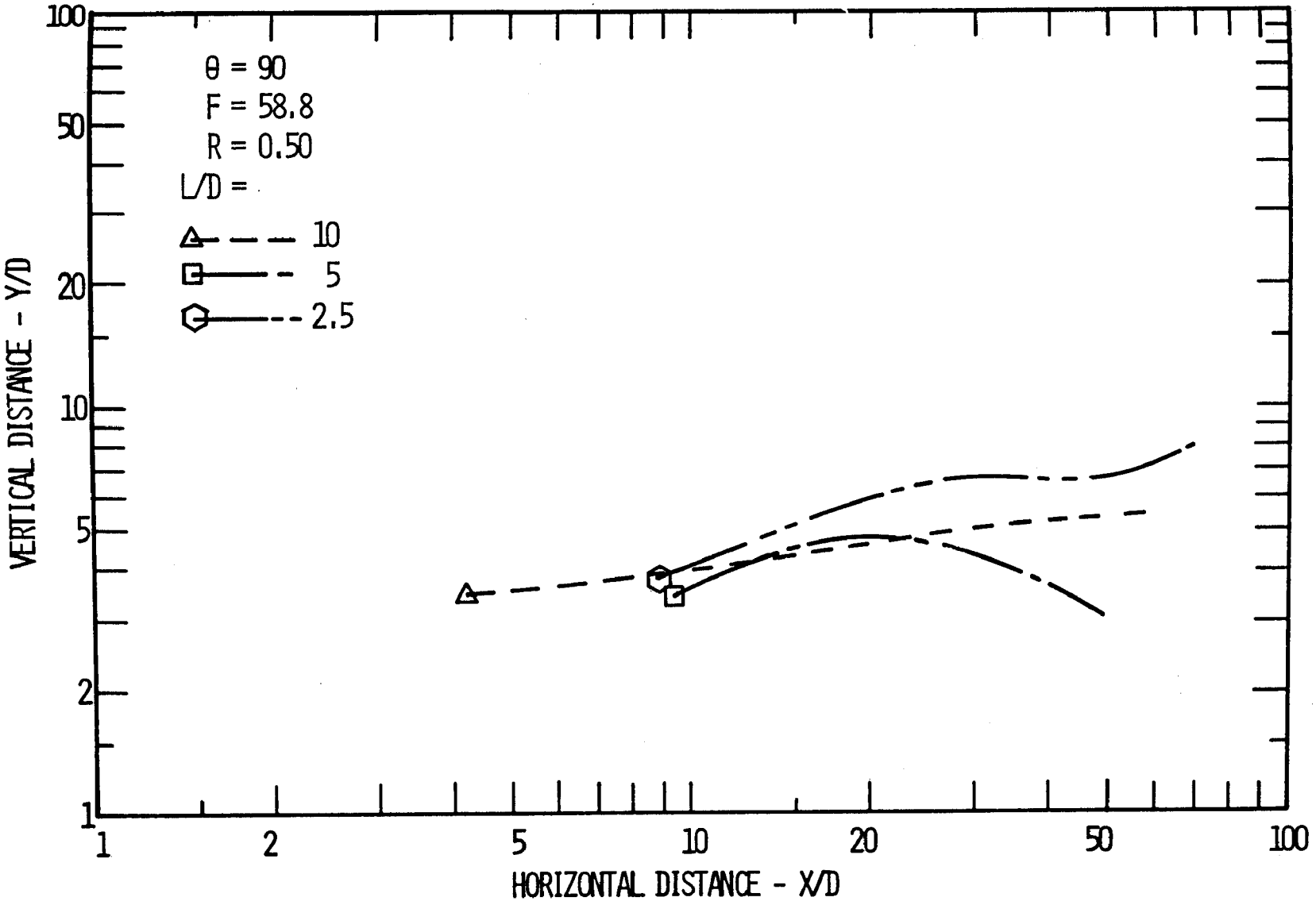

Figure 40. Effect of L/D on trajectory for θ=90, F=58.8, R=0.50.

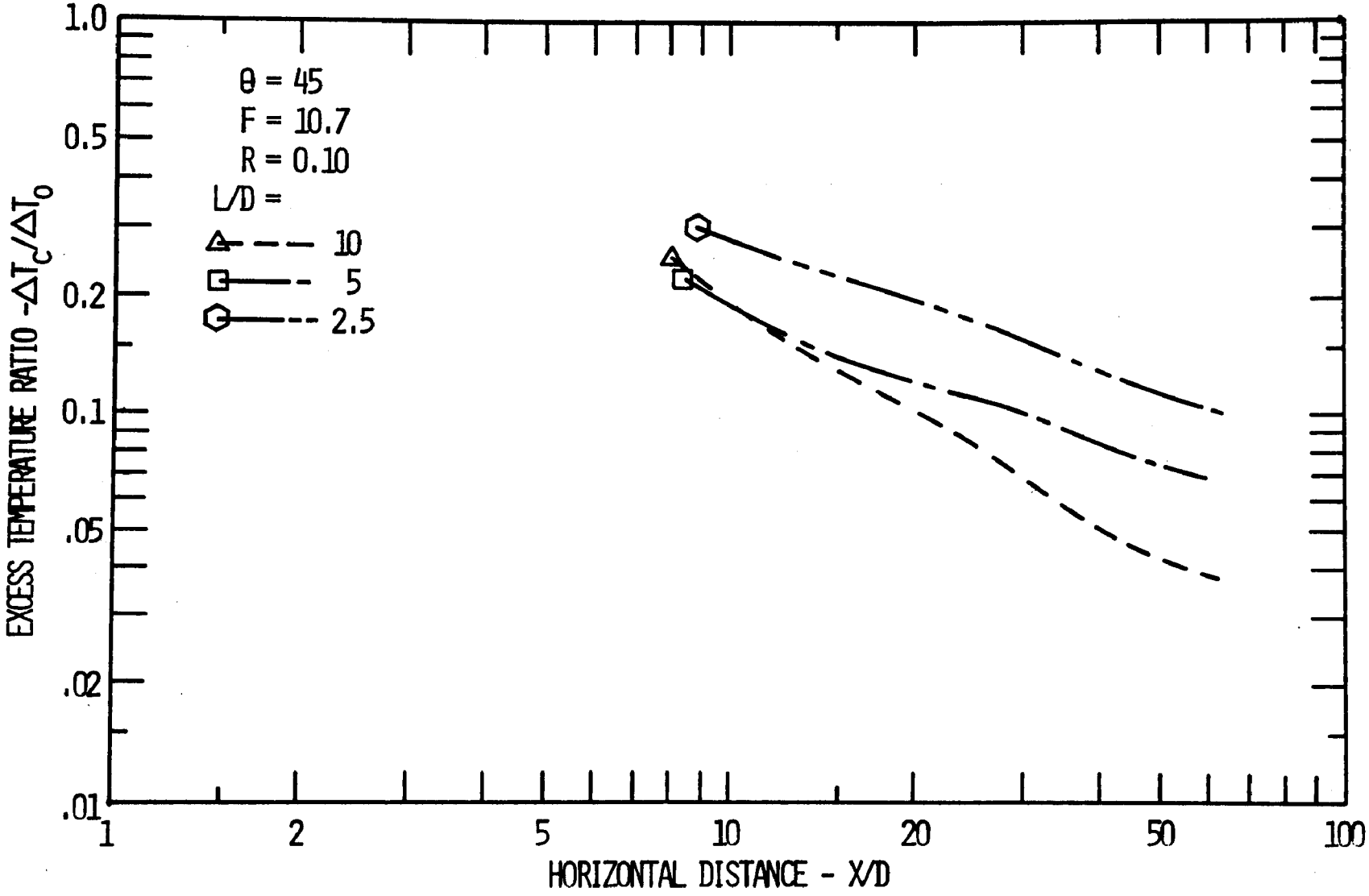

Figure 41. Effect of L/D on excess temperature ratio for θ=45, F=10.7, R=0.10.

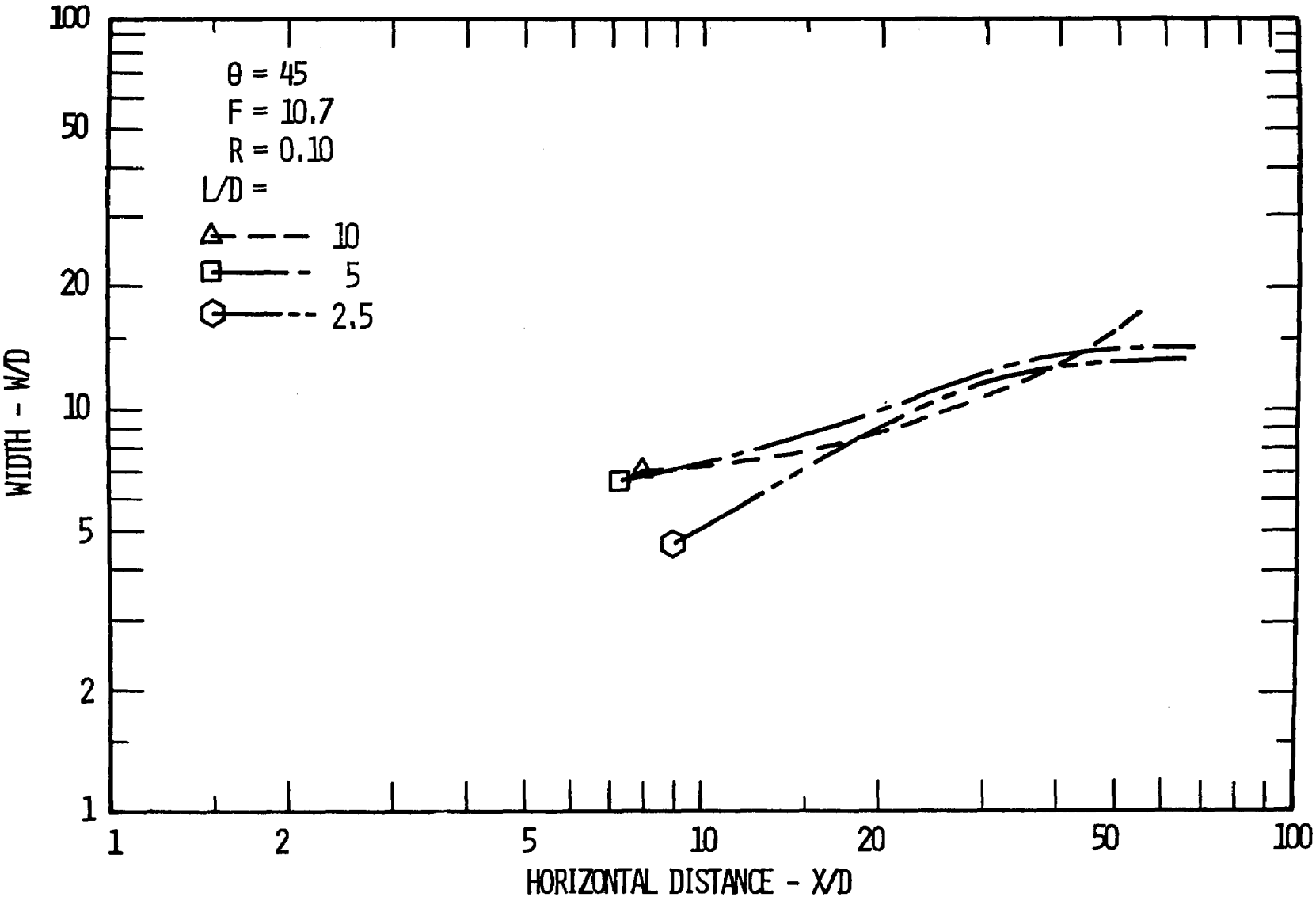

Figure 42. Effect of L/D on width for θ=45, F=10.7, R=0.10.

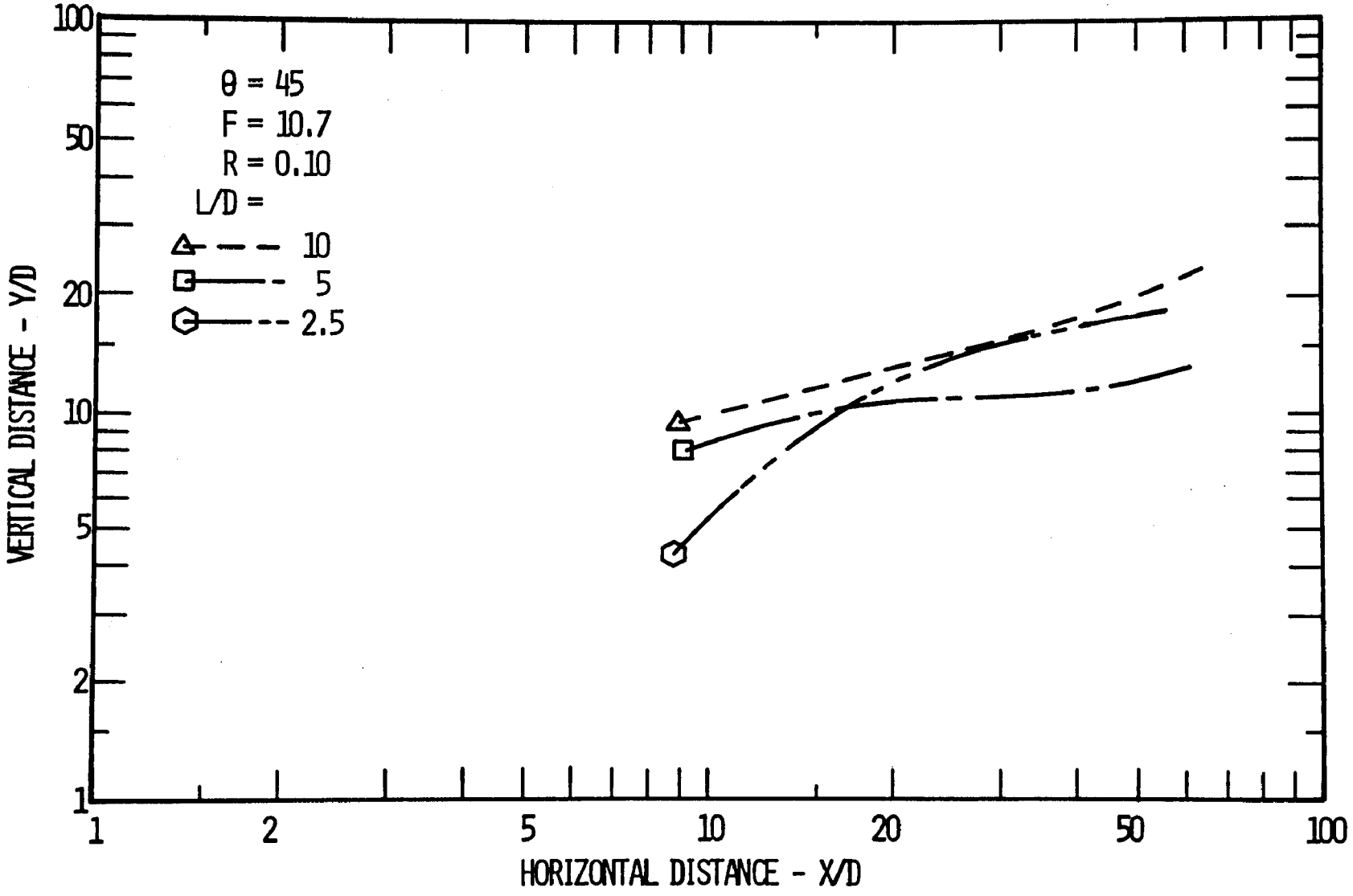

Figure 43. Effect of L/D on trajectory for θ=45, F=10.7, R=0.10.

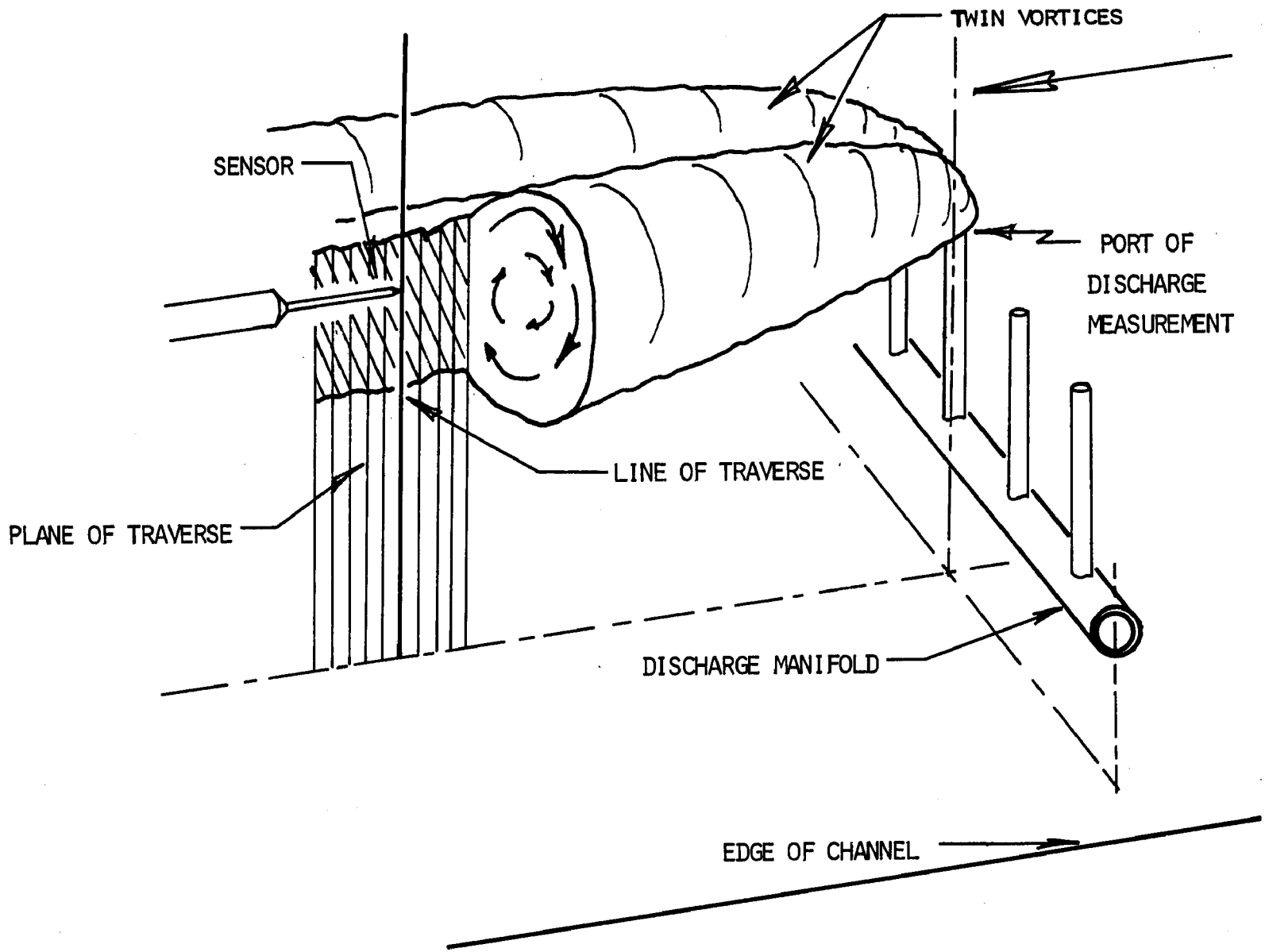

Figure 44. Line of traverse in a current with twin vortex structure.

The trajectory exhibits some rather strange results. In general, one would anticipate that the trajectory would be shifted upward with decreasing L/D. And indeed such seems to be the case when considering only the data for L/D's of 5 and 2.5. But as Figures 31, 34, 37, 40, and 43 show, in all the cases the trajectory for L/D = 10 was between the trajectories for L/D = 5 and L/D = 2.5. The most plausible explanation for this result lies in the fact that the image walls were not used for many runs at L/D = 10. As was mentioned earlier, runs with and without image walls were performed to determine the effect of their presence; the effect measured being the dilution (Excess Temperature Ratio) with no comparisions between trajectories. While the dilution was not significantly affected, the trajectory may have been.

By Regression Curve Fits

In order to offer a homogeneous and unbiased examination of the data collected, a program of regression analysis was performed on the data (except discharge into stagnant ambients). Employment of the Statistical Interactive Programming System (SIPS) available at Oregon State University provided least-squares regression fits where the curve fit provided is in algebraic form. If Y is the dependent variable and X_i (i = 1,2,...m) are the independent variables the regression analysis provides the coefficient, $\bar{a}_i$, in an equation of the type

$$Y = a_o + \sum_{i=1}^{m} a_i X_i;$$

a_i being those coefficients which give the best least-squares fit. By letting Y above be the natural logarithm of a measured dependent variable $\frac{\Delta T_c}{\Delta T_o}$, $\frac{W}{D}$, or $\frac{Y}{D}$, and X_i above be the natural logarithms of the independent variables, $\frac{L}{D}$, θ , F_r , and $\frac{X}{D}$, the algebraic equation may be written as

$$\ln(Y) = a_o + \sum_{i=1}^{m} a_i \ln (X_i) \quad \text{where}$$

$$Y = \frac{\Delta T_c}{\Delta T_o} , \frac{W}{D} , \text{ or } \frac{Y}{D} \text{ and } X_i = \frac{L}{D} , \theta , F_r , R , \text{ and } \frac{X}{D} .$$

This would provide a more suitable final relation of the type

$$Y = e^{a_0} \left(\frac{L}{D}\right)^{a_1} \theta^{a_2} F_r^{a_3} R^{a_4} \left(\frac{X}{D}\right)^{a_5} .$$

The regression analysis was carried out with the natural log's of the dependent and independent variables resulting in a weighted least squares fit. It is likely that the logarithmic weighting provided a better fit than might otherwise be obtained since the magnitudes of the variables are rendered with less absolute variation. Shown in Table 2 are the results of the regression analysis. The coefficients, a_i (i = 0-5) of the curve fits are given for $\frac{\Delta T_c}{\Delta T_o}$, $\frac{W}{D}$, and $\frac{Y}{D}$, at several angles, and for the entire data set (except $\theta = 0°$, and R = 0). The correlation coefficients are also given for each curve as well as the number of observations considered in each curve fit. One is reminded that the correlation coefficient is for the log.-log. curve fit. The regression analysis results for dilution are shown graphically in Figures 45, 46,

TABLE 2 COEFFICIENT MATRIX FOR MULTIPLE REGRESSION ANALYSIS

format $\Phi = e^{a_o}(\frac{L}{D})^{a_1}(\theta)^{a_2}(F_r)^{a_3}(R)^{a_4}(\frac{X}{D})^{a_5}$ - θ -in radians

For Φ =	θ^o	a_o	a_1	a_2	a_3	a_4	a_5	R+**	N
$\Delta T_c/\Delta T_o$	0^o	+.35796	N/A*	N/A	.04842	-.22908	-.90020	.93576	611
	15^o	+.84039	N/A*	N/A	.083518	-.024894	-.94828	.97363	448
	45^o	+.66400	-.36808	N/A	.12021	-.010037	-.78424	.93461	338
	90^o	-.10230	-.41294	N/A	.06786	+.11936	-.50626	.91683	534
	all*** less 0^o	+.54328	-.46867	-.43947	.077242	+.030846	-.67315	.90656	1385
	all less 0^o modified a_4***	+.52258	-.45247	-.26781	+.068075	-.13853 X (1.-.96832 X θ)	-.67836	.91470	1385

N - number of observations

N/A - either Not Applicable or Not Available

* All of the same L/D ($\frac{L}{D}$ = 10).

** R+ is the value of the correlation coefficient

*** θ is in radians

TABLE 2 (cont.)

format $\Phi = e^{a_o}(\frac{L}{D})^{a_1}(\theta)^{a_2}(F_r)^{a_3}(R)^{a_4}(\frac{X}{D})^{a_5}$ - θ is in radians

	$\theta°$	a_0	a_1	a_2	a_3	a_4	a_5	R+**	N
For Φ = W/D	0	-.39863	NA*		+.028992	-.19104	.54616	.91638	611
	15°	-.31603	NA*		+.052352	-.20669	.52352	.86959	448
	45°	+.39420	-.031263		-.011977	-.30276	.42466	.87379	338
	90°	+1.0502	-.8972		+.01337	-.55311	.25288	.90388	534
	all less 0°	.62596	-.088409	.30780	+.036148	-.36893	.34930	.84752	1385
For Φ = Y/D	15°	-.52972	NA*		-.16358	-.47332	.54447	.90734	447
	45°	-.22073	+.067745		-.07233	-.54100	.48679	.94061	338
	90°	+1.1766	-.22950		-.095152	-.79071	.21150	.93038	534
	all less 0°	.43287	-.051189	.53654	-.10060	-.63491	.36350	.91619	1384

N - number of observations

N/A - either Not Applicable or Not Available

* all at same L/D ($\frac{L}{D}$ = 10)

** R+ is the value of the correlation coefficient

and 47. The figures are nomographs showing the isolated effect of several independent variables: towing ratio, angle of discharge, and port spacing.

Shirazi, et. al., [21] have pointed out that experimental evidence indicates that for co-flow the dilution increases with increasing towing ratio while for crossflow the dilution decreases with increasing towing ratio. They also point out that dilution decreases with increasing Froude No. for crossflow discharge while dilution increases with increasing Froude No. for co-flow discharge The curve fits offered for the data collected in this study support the change of dilution trend with towing ratio for the co-flow and cross flow discharge but not the change in effect of Froude No. In fact, the curve fits here suggest very little Froude No. effect. The small and unchanging Froude No. effect is supported by the curve fits of Chasse and Winiarski, [36] as is the change in sign of the towing ratio exponent, a_4 with angle of discharge.[6]

An effort was made to include the variation of the towing rate effect on dilution with discharge angle by placing a factor (1.-.96832θ) (see Table 2) in the exponent. Inclusion of this particular factor was suggested by matching the exponents for co-flow and cross flow cases. With this modified exponent the correlation coefficient increased, but only by about 1%.

The effect of decreasing $\frac{L}{D}$ is to markedly decrease dilution. However, the trajectory and plume width are not nearly so greatly effected by changes in $\frac{L}{D}$.

[6] The co-flow of Chasse and Winiarski, however, employed a false bottom which slightly distorted the trajectory and probably the dilution for that case when compared to the results of this study.

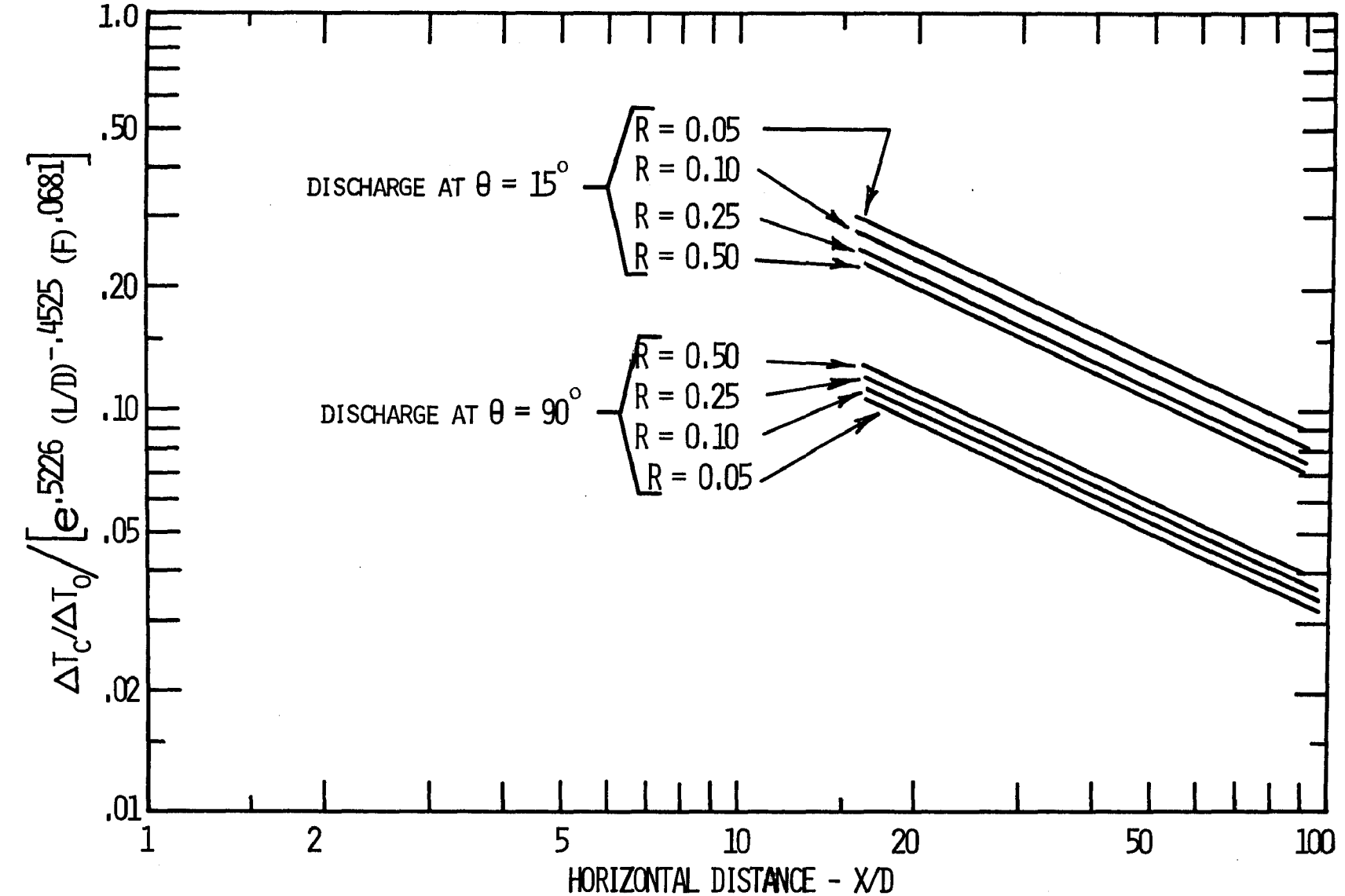

Figure 45. Effect of current to discharge velocity ratio with angle and X/D as predicted by the regression analysis.

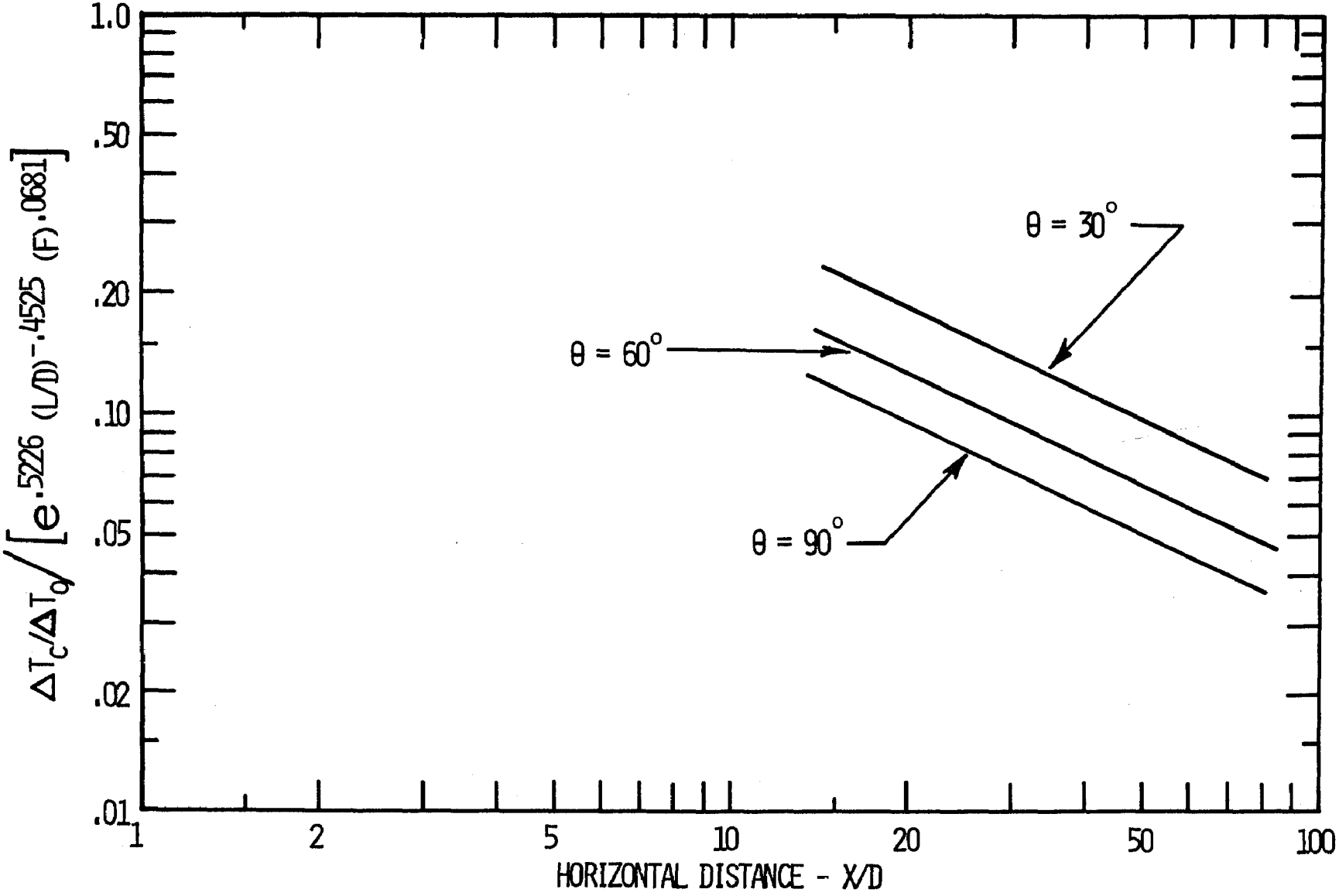

Figure 46. Effect of angle with X/D at R=0.10 as predicted by the regression analysis.

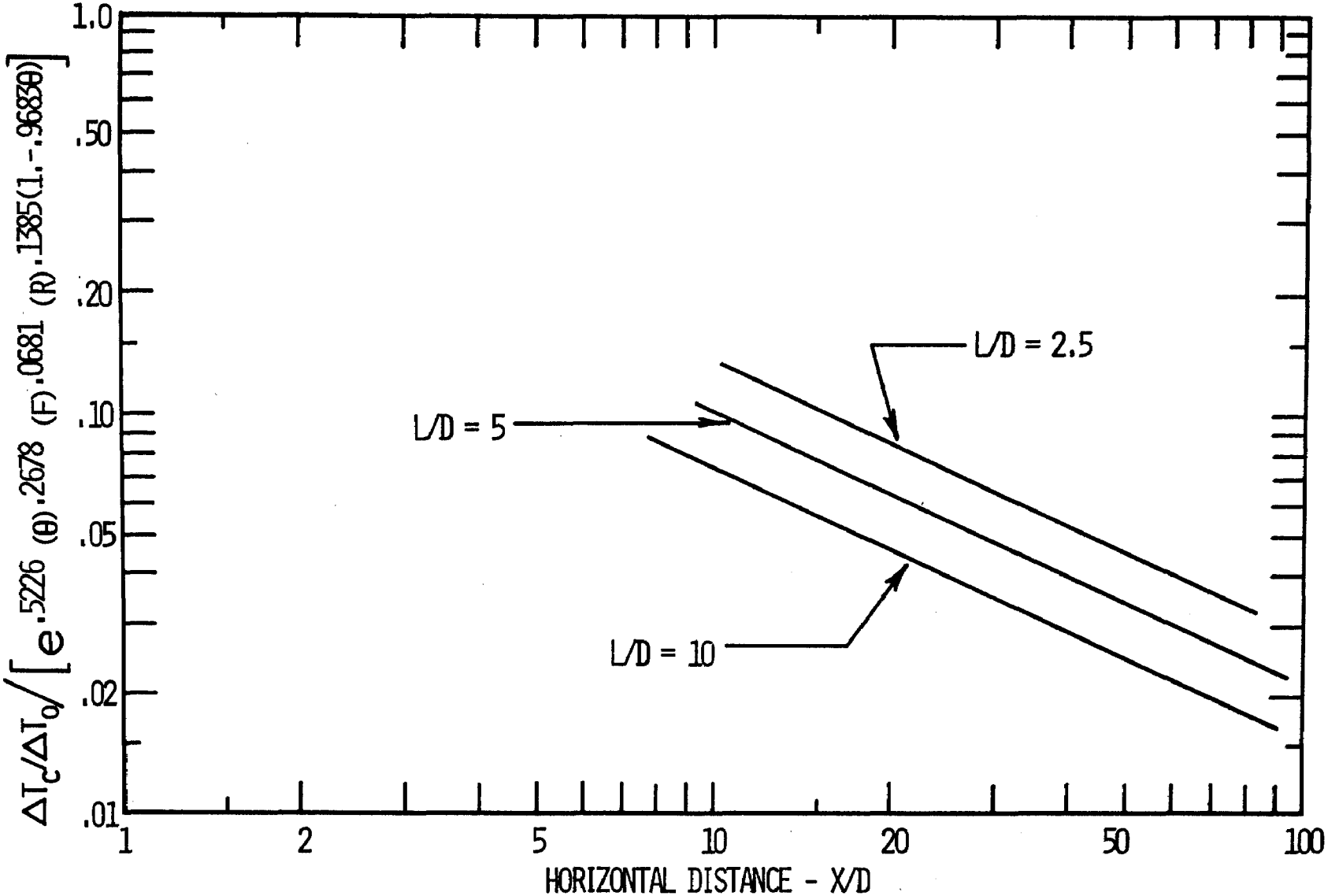

Figure 47. Effect of spacing with X/D as predicted by the regression analysis.

The number of observations is 1931 for cases with current; there were additional stagnant runs which were not considered here.

Care should be used when employing the regression curves. The regression fits for each angle are in general superior to the curve fits which include angle as an independent variable. Care should also be exercised to insure that the case under consideration lies within the experimental data upon which the regression analysis operated. Table 1, given earlier in the text, provides limits for application of the regression curves. It should also be noted that data for port spacings of 5, and 2.5 exist only for crossflow and 45° angle discharge and that there are considerably fewer observations at these smaller spacings than at $\frac{L}{D} = 10$.

The regression analysis offers curves which give a least squares curve fit to the independent variables. These "fits" are by nature one-dimensional (i.e., one regression coefficient per independent variable) and are effectively weighted so that the most deviant cases have the greatest effect. For these reasons, secondary trends such as change of angle effect with changes in $\frac{L}{D}$, or changes in Froude No. effect with $\frac{L}{D}$ are not available from such an analysis. The effects at considerably different values of an independent variable are averaged with weight being thrown to the most deviant cases.

These factors should be kept in mind when dealing with the regression equations.

SECTION VI

ANALYTICAL WORK

INTRODUCTION

The first portion of this thesis has been devoted to the discussion of experimental data describing dilution, trajectory and plume width of multiport thermal discharges. The second portion will be devoted to the description of a mathematical and computer model for predicting these quantities and the method used to determine the necessary coefficients in this model.

Several models have been put forth to describe successively more complex discharge conditions. The first studies were aimed at describing the simple momentum jet. Such studies were carried out primarily in the 1940's and are well documented in References 5, 6, and 38. The buoyant jet in stagnant water was next to be treated followed by the buoyant jet discharged into a flowing stream.

The governing differential equations for these cases involved turbulent terms and were coupled. The treatment undertaken then and which continues now was to use the axisymmetric boundary layer and Boussinesque assumptions and cross sectional jet integrals. Transverse velocity and species profiles were estimated from experimental data and used in the equations. The result was a series of partially coupled, nonlinear, ordinary differential equations in which the streamwise direction was the independent variable. The dependent variables then became the pertinent characteristic measures of the <u>similar</u> profiles, i.e., centerline excess velocity,

centerline excess species, plume half width, and relative growth rate of centerline velocity and temperature. A similar procedure will be described in this work when an attempt is made to include the effects of neighboring plumes.

The model to be presented is a submerged multiport version of the multiple cooling tower plume model proposed by Davis[17]. This model uses the Hirst[6] single port program as a starting point. The multi-port computer program was completed in the present effort and coefficients for entrainment and drag were determined that gave the best agreement with the experimental data presented in this study. The fundamentals of the Hirst and Davis models are presented here for completeness.

THE ANALYTICAL PROBLEM

A model is to be constructed which will determine the plume characteristics of the turbulent discharge of heated water from a single line series of round ports into either a quiescent or a uniform, unconfined ambient. The orientation of the discharge, the spacing between ports and the relative velocity of the ambient fluid are variable. The ambient may be stratified and the discharge diameter, velocity, temperature and species concentration are variable.

The equations which describe conditions throughout the discharge field of the jet are the transport equations of mass, momentum energy, and species. These are,[39] conservation of mass,

$$\frac{\partial \rho}{\partial t} + \bar{\nabla} \cdot (\rho \bar{V}) = 0 \quad , \qquad (1)$$

conservation of energy,

$$\frac{\partial T}{\partial t} + \bar{V}\cdot(\bar{\nabla}T) = \frac{1}{\rho c_v}\bar{\nabla}\cdot(k\bar{\nabla}T) + \frac{\nu}{c_v}\Phi - T\left(\frac{\partial P}{\partial T}\right)_\rho(\bar{\nabla}\cdot\bar{V}) \quad , \quad (2)$$

conservation of momentum,

$$\frac{\partial \bar{V}}{\partial t} + \frac{1}{2}\bar{\nabla}V^2 - \bar{V}\times(\bar{\nabla}\times\bar{V}) = \frac{-\bar{\nabla}P + \rho\bar{F}}{\rho} + \nu\bar{\nabla}^2\bar{V} \quad , \quad (3)$$

and conservation of species,

$$\frac{\partial C}{\partial t} + \bar{V}\cdot(\bar{\nabla}C) = \bar{\nabla}\cdot\left(D_c\bar{\nabla}C\right) \quad . \quad (4)$$

Represented above are six equations with the unknowns being three velocity components, pressure, temperature and species concentration (C). The pressure gradient may be written as

$$\bar{\nabla}P = \rho_\infty\bar{g} + \bar{\nabla}P^+ \quad , \quad (5)$$

where $\rho_\infty\bar{g}$ is the hydrostatic force and $\bar{\nabla}P^+$ is the motion pressure force. The body force term is due to gravitational action on the jet fluid and may be written

$$\rho\bar{F} = \rho\bar{g} \quad . \quad (6)$$

The final equation needed to completely define the equations is an equation of state, i.e.

$$\rho = \rho(T,C,P) \quad (7)$$

which may be considered a seventh equation.

The equations as they appear in (1) - (7) are in their most general form,[7] less considerations for turbulence. However, one must note that these equations are three-dimensional, nonlinear and coupled. Because of these qualities, they are extremely difficult to solve.

By making the following assumptions the equations may be simplified with only a minimal loss in generality and accuracy. The assumptions are (c.f. Hirst[6]):

1) steady flow in the mean,
2) fully turbulent jet flow, molecular diffusion is neglected,
3) incompressible flow; density variations appear only in the buoyancy terms (Boussinesque approximation),
4) all other fluid properties are constant,
5) fluid velocities are low (low Eckert Number) enough to neglect frictional heating,
6) the motion pressure gradient is small so that the only significant pressure variation is purely hydrostatic,
7) changes in density are small enough to assume a linear equation of state (as will be seen, the equation of state may be written as a double Taylor series expansion, here it is assumed to be of linear fashion),

[7] Exception taken for ν, which has been taken as constant.

8) the jet flow is axisymmetric and

9) the flow within the jet is that of the boundary layer type and the boundary layer approximations are valid.

As cited in the experimental discussion, the discharge normal to a current may be decidedly non-axisymmetric for a significant portion of the downstream distance. For this reason, 8) above, must certainly be questionable. However, for the purposes of a general model, axisymmetric flow is assumed (the model will later modify this to account for merging of the plumes).

With the above assumption, the governing equations (1) - (4) and (7) are written as:

continuity,

$$\bar{\nabla}\cdot\bar{V} = 0 \quad , \quad (8)$$

energy,

$$\bar{V}\cdot(\bar{\nabla}T) = 0 \quad , \quad (9)$$

species,

$$\bar{V}\cdot(\bar{\nabla}C) = 0 \quad , \quad (10)$$

momentum,

$$\frac{1}{2}\bar{\nabla}\bar{V}^2 - \bar{V}\times(\bar{\nabla}\times\bar{V}) = \frac{-g\rho_\infty + \rho g}{\rho_o} \quad , \quad (11)$$

and $\rho=\rho(T,C,P)$ can be written as,

state,

$$\rho = \rho_o\left(1 - \beta\left(T - T_o\right) - \gamma\left(C - C_o\right)\right) \quad , \quad (12)$$

where $\beta = -\frac{1}{\rho_o}\left(\frac{\partial\rho}{\partial T}\right)_{P,C}$, $\gamma = -\frac{1}{\rho_o}\left(\frac{\partial\rho}{\partial C}\right)_{P,T}$ and $\left(\frac{\partial\rho}{\partial P}\right)_{T,C}$ has been assumed zero.

Equation (12) may be rewritten as

$$\frac{\rho - \rho_\infty}{\rho_\infty} = \beta\left(T_\infty - T\right) + \gamma\left(C_\infty - C\right) \quad , (13)$$

and then incorporated into (11) as

$$\frac{1}{2}\overline{\nabla}V^2 - \overline{V}x(\overline{\nabla}x\overline{V}) = g\beta\left(T_\infty - T\right) + g\gamma\left(C_\infty - C\right) \quad . (14)$$

Hirst took these equations and employed generalized coordinates to transform them into the so called "natural" coordinate system. Such a system is shown in Figure 48.

Employing the axisymmetric assumption reduces equations (8) - (10) and (14) to:

continuity,

$$\frac{\partial u}{\partial s} + \frac{1}{r}\frac{\partial}{\partial r}(rv) = 0 \quad , (15)$$

energy,

$$u\frac{\partial T}{\partial s} + v\frac{\partial T}{\partial r} = 0 \quad , (16)$$

species,

$$u\frac{\partial C}{\partial s} + v\frac{\partial C}{\partial r} = 0 \quad , (17)$$

s-momentum,

$$u\frac{\partial u}{\partial s} + v\frac{\partial u}{\partial r} = \frac{\rho_\infty - \rho}{\rho_o} g \sin\theta_2 \quad , (18)$$

y-momentum

$$\left(u\frac{\partial u}{\partial s} + v\frac{\partial u}{\partial r}\right)\sin\theta_2 + \left(u^2 - \frac{rv}{2}\frac{\partial v}{\partial r}\right)\kappa_2 \cos\theta_2 = \frac{\rho_\infty - \rho}{\rho_o} g \quad , (19)$$

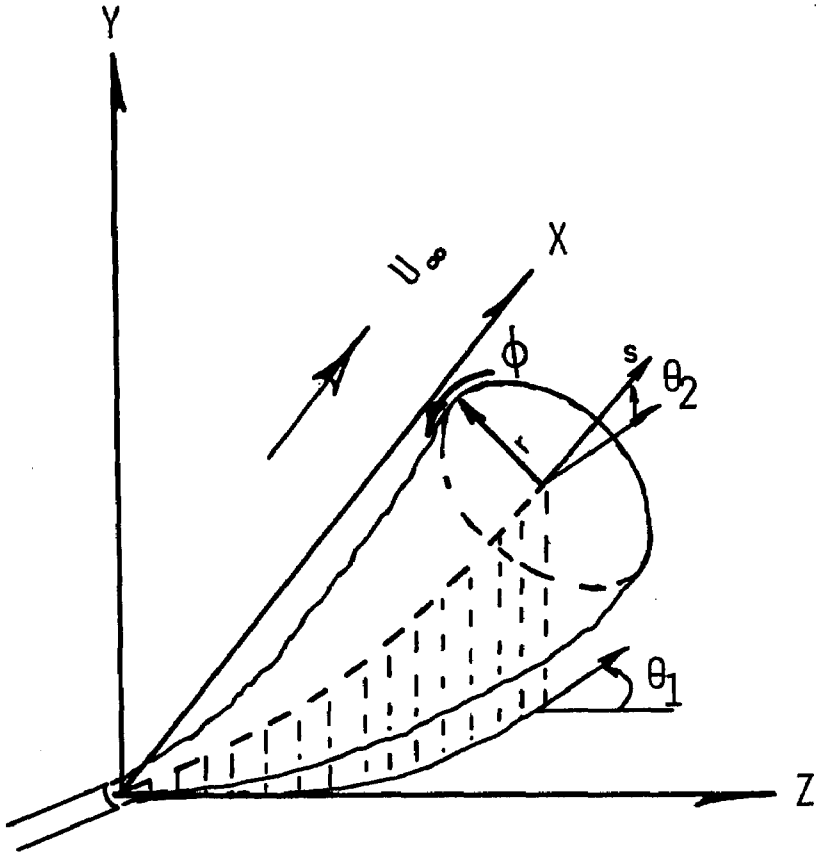

Figure 48. The "natural" coordinate system employed by Hirst[6].

and x-momentum,

$$\left(u\frac{\partial u}{\partial s} + v\frac{\partial u}{\partial r}\right) \sin\theta_1 \cos\theta_2 + \left(u^2 - \frac{rv}{2}\frac{\partial v}{\partial r}\right)$$

$$X \left(\kappa_1 \cos\theta_1 \cos\theta_2 - \kappa_2 \sin\theta_1 \sin\theta_2\right) \quad , \quad (20)$$

where u = component of velocity in the s direction,

v = component of velocity in the r direction,

κ_1 = curvature of s with respect to θ_1,

and κ_2 = curvature of s with respect to θ_2.

By writing the equations above in terms of the fluctuating and steady quantities and taking the time average, i.e.

$$f = \bar{f} + f'$$

where $\bar{f} = \lim_{t_2\to\infty}\left\{\frac{1}{2t_2}\int_{-t_2}^{t_2} f\,d\zeta\right\}$, the time averaged quantity

and f' is the fluctuating component (note that

$$\lim_{t_2\to\infty}\left\{\frac{1}{2t_2}\int_{-t_2}^{t_2} f'\,d\zeta\right\} = 0),$$

the turbulence effects can be included in the model. Hirst did this and employed boundary layer assumptions $\left(\bar{u}>>\bar{v}, \text{ and } \frac{\partial}{\partial r}>>\frac{\partial}{\partial s}\right)$ to arrive at the following relations:

continuity,

$$\frac{\partial \bar{u}}{\partial s} + \frac{1}{r}\frac{\partial (r\bar{v})}{\partial r} \quad , \quad (21)$$

energy,

$$\bar{u}\frac{\partial \bar{T}}{\partial s} + \bar{v}\frac{\partial \bar{T}}{\partial r} = -\frac{1}{r}\frac{\partial (r\overline{v'T'})}{\partial r} \quad , \quad (22)$$

species,

$$\bar{u}\frac{\partial \overline{C}}{\partial s} + \bar{v}\frac{\partial \overline{C}}{\partial r} = -\frac{1}{r}\frac{\partial (r\overline{v'C'})}{\partial r} \qquad , (23)$$

s-momentum,

$$\bar{u}\frac{\partial \overline{U}}{\partial s} + \bar{v}\frac{\partial \overline{U}}{\partial r} = \frac{\rho_\infty - \bar{\rho}}{\rho_o} g \sin\theta_2 - \frac{1}{r}\frac{\partial (r\overline{u'v'})}{\partial r} \qquad , (24)$$

y-momentum,

$$\left(\bar{u}\frac{\partial \bar{u}}{\partial s} + \bar{v}\frac{\partial \bar{u}}{\partial r}\right)\sin\theta_2 = \frac{\rho_\infty - \bar{\rho}}{\rho_o} g - q^+\kappa_2 \cos\theta_2 - \frac{1}{r}\frac{\partial (r\overline{u'v'})}{\partial r}\sin\theta_2 \qquad , (25)$$

and x-momentum,

$$\left(\bar{u}\frac{\partial \bar{u}}{\partial s} + \bar{v}\frac{\partial \bar{u}}{\partial r}\right)\cos\theta_1 \cos\theta_2 = q^+\left\{\kappa_1 \sin\theta_1 \cos\theta_2 + \kappa_2 \cos\theta_1 \sin\theta_2\right\} + \frac{1}{r}\frac{\partial (r\overline{u'v'})}{\partial r}\cos\theta_1 \cos\theta_2 \qquad , (26)$$

where $q^+ = \bar{u}^2 - \frac{r}{4}\left(\frac{\partial \bar{v}^2}{\partial r} + \frac{\partial \overline{v'^2}}{\partial r}\right)$

One notes that the assumption of axisymmetric flow has been extended to the turbulent fluctuations in the ϕ direction so that those terms do not appear. The remaining Reynolds Stress term[8] is present, $\overline{u'v'}$, as are the turbulent convective terms $\overline{v'T'}$ and $\overline{v'C'}$. The inclusion of the turbulent convective terms and the Reynolds Stress term make the equations significantly more complex than would be obtained for laminar flow. The six equations (21) - (26) contain the six terms $\bar{u}$, $\bar{v}$, $\overline{C}$, $\overline{T}$, θ_1 and θ_2,

[8] Other terms have been dropped via the boundary layer assumptions.

but they also contain $\overline{u'v'}$, $\overline{v'^2}$, $\overline{v'T'}$, and $\overline{v'C'}$. In order to obtain closure, we assume the following for treatment of these turbulent terms:

$$\overline{u'v'} = -\varepsilon_m \frac{\partial \bar{u}}{\partial r} \quad ,$$

$$\overline{v'T'} = -\varepsilon_h \frac{\partial T}{\partial r} \quad ,$$

$$v'C' = -\varepsilon_c \frac{\partial \overline{C}}{\partial r} \quad ,$$

and $\overline{v'v'} = 0$.

Often the relations are further simplified by $\varepsilon_m = \varepsilon_h = \varepsilon_c = \varepsilon$, the Reynolds Analogy where ε is a general eddy viscosity. Even with these simplifications the relations remain difficult to solve, for although they are now of only two dimensions, they are still non-linear and coupled.

The initial conditions for $\bar{u}$, $\bar{v}$, $\overline{T}$, and $\overline{C}$ etc., for these parabolic differential equations must be specified at $s = 0$ and will be the discharge conditions of the jet. The boundary conditions are:

$$\bar{u} \to U_\infty \sin \theta_1 = \cos \theta_2 \qquad \text{as } r \to \infty \quad ,$$

$$\bar{v} \to \frac{\partial}{\partial s} \frac{1}{r} \int_0^r \zeta \bar{u} \partial \zeta \qquad \text{as } r \to \infty \quad ,$$

$$\text{or} \quad \bar{v} \to \frac{E}{r} \qquad \text{where} \qquad E = \frac{\partial}{\partial s} \int_0^\infty \bar{u} r \partial r \quad ,$$

$$\overline{T} \to T_\infty \qquad \text{as } r \to \infty \quad ,$$

$$\overline{C} \to C_\infty \qquad \text{as } r \to \infty \quad ,$$

and $\left.\frac{\partial \bar{u}}{\partial r}\right|_{r=0} = \left.\frac{\partial \bar{v}}{\partial r}\right|_{r=0} = \left.\frac{\partial T}{\partial r}\right|_{r=0} = \left.\frac{\partial \bar{C}}{\partial r}\right|_{r=0} = 0$

At this point Hirst reduces the complexity of the equations by another degree with the formal integration of the equations with respect to r. As he states[10], the process of integration represents an averaging process which obscures some of the information contained in the differential equations. The obvious intent of integrating the governing equations is to lump the problem in the r-direction and thereby avoid solving the boundary value type problem obtained above. Not only will integration reduce the dimensions of the problem but it will provide a purely parabolic, albeit coupled, problem in six variables. However, it will be necessary to provide $\bar{u}$, $\overline{T}$ and $\overline{C}$ profiles in r for the integration. The profiles of $\bar{u}$, $\overline{T}$ and $\overline{C}$ cannot be expected to be constant in s. However, by judicious expression of these profiles, one can create profiles which will be similar in shape at all s and whose only differences (in s) will be the changing of certain characteristic measures of the jet. Most often these characteristic measures are the centerline values of velocity, temperature, species and width of the jet.

It shall be assumed that such similar profiles exist although they are yet to be specified. The integration proceeds as: continuity,

$$\frac{d}{ds}\left[\int_o^\infty \bar{u} r dr\right] + \int_o^\infty \frac{1}{r}\frac{\partial (r\bar{v})}{\partial r} r dr = 0 \quad , \quad (27)$$

[10] Reference 6, page 11.

energy,

$$\int_o^\infty \bar{u}\frac{\partial \overline{T}}{\partial s}\, rdr + \int_o^\infty \bar{v}\frac{\partial \overline{T}}{\partial r}\, rdr = -\int_o^\infty \frac{1}{r}\frac{\partial\left(r\overline{v'T'}\right)}{\partial r}\, rdr \quad , \quad (28)$$

species,

$$\int_o^\infty \bar{u}\frac{\partial \overline{C}}{\partial s}\, rdr + \int_o^\infty \bar{v}\frac{\partial \overline{C}}{\partial r}\, rdr = -\int_o^\infty \frac{1}{r}\frac{\partial\left(r\overline{v'C'}\right)}{\partial r}\, rdr \quad , \quad (29)$$

s-momentum,

$$\frac{d}{ds}\int_o^\infty \frac{\bar{u}^2}{2}\, rdr + \int_o^\infty \bar{v}\frac{\partial \bar{u}}{\partial r}\, rdr = \int_o^\infty \frac{\rho_\infty - \bar{\rho}}{\rho_o}\, grdr \sin\theta_2$$

$$- \int_o^\infty \frac{1}{r}\frac{\partial\left(r\overline{u'v'}\right)}{\partial r}\, rdr \quad , \quad (30)$$

y-momentum,

$$\left[\frac{d}{ds}\int_o^\infty \frac{\bar{u}^2}{2}\, rdr + \int_o^\infty \bar{v}\frac{\partial \bar{u}}{\partial r}\, rdr\right] \sin\theta_2 = \int_o^\infty \frac{\rho_\infty - \bar{\rho}}{\rho_o}\, grdr$$

$$- q^*\kappa_2 \cos\theta_2 \sin\theta_2 \int_o^\infty \frac{1}{r}\frac{\partial\left(r\overline{u'v'}\right)}{\partial r}\, rdr \quad , \quad (31)$$

and x-momentum,

$$\left[\frac{d}{ds}\int_o^\infty \frac{\bar{u}^2}{2}\, rdr + \int_o^\infty \bar{v}\frac{\partial u}{\partial r}\, rdr\right] \cos\theta_1 \cos\theta_2$$

$$= q^*\left(\kappa_1 \sin\theta_1 \cos\theta_2 + \kappa_2 \cos\theta_1 \sin\theta_2\right)$$

$$- \int_o^\infty \frac{1}{r}\frac{\partial\left(r\overline{u'v'}\right)}{\partial r}\, rdr \cos\theta_1 \cos\theta_2 \quad , \quad (32)$$

where $$q^* = \int_0^\infty \bar{u}^2 r dr - \frac{1}{4}\int_0^\infty r^2 \left(\frac{\partial \bar{v}^2}{\partial r} + \frac{\partial \overline{v'^2}}{\partial r} \right) dr$$

With the evaluation of certain terms, requiring the use of integration by parts and the continuity relation, and employing the truncated equation of state, it is possible to render the equations (27) - (32) in their most useful forms. These are given below.

Conservation of Mass,

$$\frac{d}{ds}\int_0^\infty \bar{u} r dr = - \lim_{r\to\infty} (r\bar{v}) = E \qquad , (33)$$

Conservation of Energy,

$$\frac{d}{ds}\int_0^\infty \bar{u}\left(\bar{T} - \bar{T}_\infty\right) r dr = - \frac{d\bar{T}_\infty}{ds}\int_0^\infty \bar{u} r dr - \lim_{r\to\infty}\left(r\overline{v'T'}\right) \qquad , (34)$$

Conservation of Species,

$$\frac{d}{ds}\int_0^\infty \bar{u}\left(\bar{C} - \bar{C}_\infty\right) r dr = - \frac{d\bar{C}_\infty}{ds}\int_0^\infty \bar{u} r dr - \lim_{r\to\infty}\left(r\overline{v'C'}\right) \qquad , (35)$$

and Conservation of S-Momentum,

$$\frac{d}{ds}\int_0^\infty \bar{u}^2 r dr = \bar{U}_\infty E \sin\theta_1 \cos\theta_2 + \int_0^\infty g\left[\beta\left(\bar{T} - \bar{T}_\infty\right) + \gamma\left(\bar{C} - \bar{C}_\infty\right)\right] r dr \sin\theta_2 - \lim_{r\to\infty}\left(r\overline{u'v'}\right) \qquad . (36)$$

Now, the other two momentum equations may be put in the form $\kappa_1 = \ldots$ and $\kappa_2 = \ldots$ by simple rearrangement of the equations. If one divides (31) by $\sin\theta_2$ and subtracts (30) from the result, one obtains

$$-\bar{q}\,\kappa_2\,\frac{\cos\theta_2}{\sin\theta_2} - EU_\infty \sin\theta_1 \cos\theta_2 + \int_o^\infty \frac{\bar{\rho}_\infty - \bar{\rho}}{\bar{\rho}_o}\, grdr\, \frac{\cos^2\theta_2}{\sin\theta_2} = 0 \quad ,$$

or

$$\frac{d\theta_2}{ds} = \kappa_2 = \left(g\int_o^\infty \left[\beta\left(\overline{T} - \overline{T}_\infty\right) + \gamma\left(\overline{C} - \overline{C}_\infty\right)\right] rdr \cos\theta_2 - EU_\infty \sin\theta_1 \sin\theta_2\right) / \bar{q} \quad . \quad (37)$$

Likewise, if one divides (32) by $\cos\theta_1 \cos\theta_2$ and subtracts (30) from the result one obtains

$$\bar{q}\left(\kappa_1 \sin\theta_1 \cos\theta_2 + \kappa_1 \cos\theta_1 \sin\theta_2\right) = \left[\int_o^\infty \frac{\rho_\infty - \bar{\rho}}{\bar{\rho}_o}\, grdr \sin\theta_2 + EU_\infty \sin\theta_1 \cos\theta_2\right] \cos\theta_1 \cos\theta_2 \quad ,$$

or, rearranging and substituting for κ_2,

$$\frac{d\theta_1}{ds} = \kappa_1 = \frac{EU_\infty \cos\theta_1}{\bar{q}\cos\theta_2} \quad , \quad (38)$$

where

$$\bar{q} = \int_o^\infty \bar{u}^2 rdr - \frac{E^2}{4} - \lim_{r\to\infty}\left(r^2\overline{v'^2}\right) \quad . \quad (39)$$

These then become the final two differential equations of our six problem equations.

EMPLOYING SIMILAR PROFILES

The processes which characterize the buoyant jet lead to a natural separation of the jet into several regimes. In the past

these have been given as; (I) The zone of flow establishment near the discharge port, (II) The zone of fully developed velocity, temperature and species profiles, (III) The transition region at the free water surface or the maximum height of rise in stratified environments and (IV) The region of drift flow after transition. For multiport discharges there is a fifth region where neighboring plumes merge due to entrainment and plume growth. This fifth zone (V) can start anywhere along the plume depending on the distance between discharge ports, current, Froude Number, etc. These zones are illustrated in Figure 49.

The zone of flow establishment is usually only a few discharge diameters long and is characterized by jet type flow where velocity, temperature and species profiles change from top-hat shapes at the point of discharge to bell-shaped profiles at the end of the zone. Zone II is characterized by a continuation of similar bell-shaped profiles.

The zone of merging plumes is characterized by a gradual change from a series of axisymmetric plumes to a long, two-dimensional slot plume. This region may exist for a considerable distance along the plume before two-dimensional slot flow is realized. In zone III the flow changes from a rising plume to a drifting layer of zone IV.

For deep submerged buoyant jets, the zone of flow establishment, the zone of established flow and the merging zone are where most of the dilution occurs. Only these three zones are of concern in the problem of present interest.

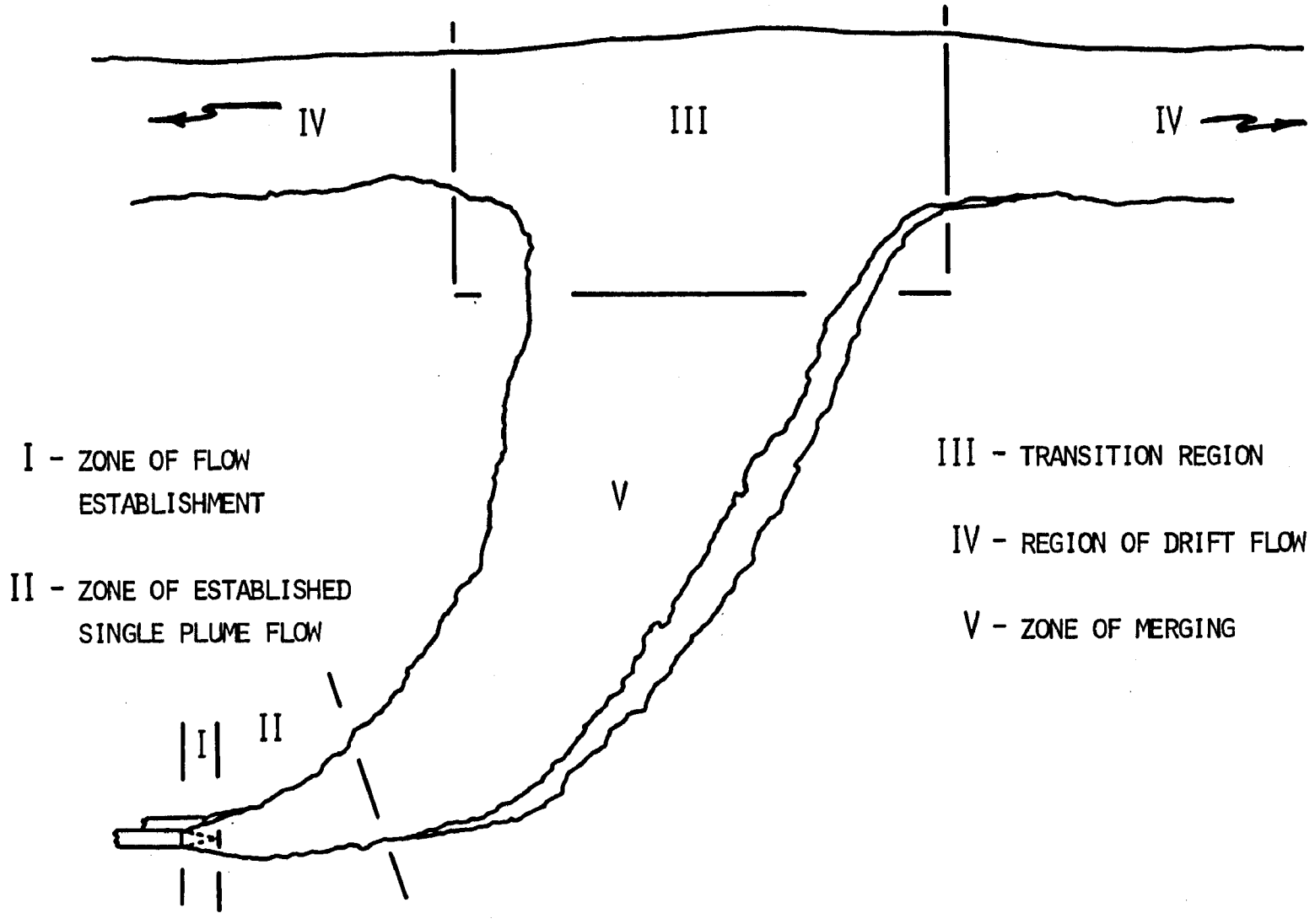

Figure 49. The dominant zones of flow for multiple port discharges.

Equations (33) - (38) may be reduced to simple differential equations by employing similar profiles for $\bar{u}$, $\overline{T}$, and $\overline{C}$ as mentioned above. However, the similar profiles employed differ according to the characteristic zone of the jet; i.e., the zone of flow establishment requires a different set of profiles than required for the zones of established flow or merging. The method of modeling the discharge is to employ the applicable profiles in each successive region. The equations for zone I are solved numerically using the port discharge conditions as initial conditions. The solution advances until zone II is reached. The conditions at the end of zone I are used as initial conditions to zone II. The zone II equations are solved (with modified profiles) successively as the solution continues on in s until merging begins. Here slightly different profiles are employed and the solution to the equations continues until a desired limit is reached. In this manner the differential equations are approximately solved in each of the characteristic regions.

The profiles often employed are the Gaussian profiles in which excess velocity, excess temperature, and excess species are written as $\Delta\bar{u} \propto e^{-\left(\frac{r}{b_1}\right)^2}$, $\Delta\overline{T} \propto e^{-\left(\frac{r}{\lambda b_1}\right)^2}$, and $\Delta\overline{C} \propto e^{-\left(\frac{r}{\lambda b_1}\right)^2}$,

where λ is a measure of the relative spreading of temperature, species and velocity profiles. However, Davis [17] found that employment of these profiles in the integral equations was not possible for merging plumes. This was due to the Gaussian profiles

extending all the way to infinity. It was, therefore, necessary to adopt another basic profile,[40] of the 3/2 power profile used successfully by Stolzenbach and Harleman to facilitate merging, the same profile is assumed for temperature, velocity and species. They are written as:

$$\Delta\overline{U} \propto \left(1 - \left(\frac{r}{b}\right)^{3/2}\right)^2 , \quad \Delta\overline{T} \propto \left(1 - \left(\frac{r}{b}\right)^{3/2}\right)^2 , \text{ and}$$

$$\Delta\overline{C} \propto \left(1 - \left(\frac{r}{b}\right)^{3/2}\right)^2$$

where b differs from b_1 given in the Gaussian profile. A comparison of these two basic profiles is shown in Figure 50. Employing the 3/2 power profile, it is now possible to carry out the integrations in r and arrive at the final nonlinear, coupled, ordinary differential equations for the various zones of interest. The development will be curtailed slightly by not giving the species equation. The species equation is identical to the energy equation with changes of T to C, T_∞ to C_∞, and T_o to C_o.

ZONE OF FLOW ESTABLISHMENT

The similar profile relationships for the zone for flow establishment are[12]:

$$u = U_o \quad , \qquad r \leq r_u \qquad ; (40)$$

$$u = \left(U_o - U_\infty \cos\theta_2 \sin\theta_1\right)\left(1 - \left(\frac{r - r_u}{b}\right)^{3/2}\right)^2$$

$$+ U_\infty \cos\theta_2 \sin\theta_1, \qquad r \geq r_u \qquad ; (41)$$

[12] All terms are time averaged.

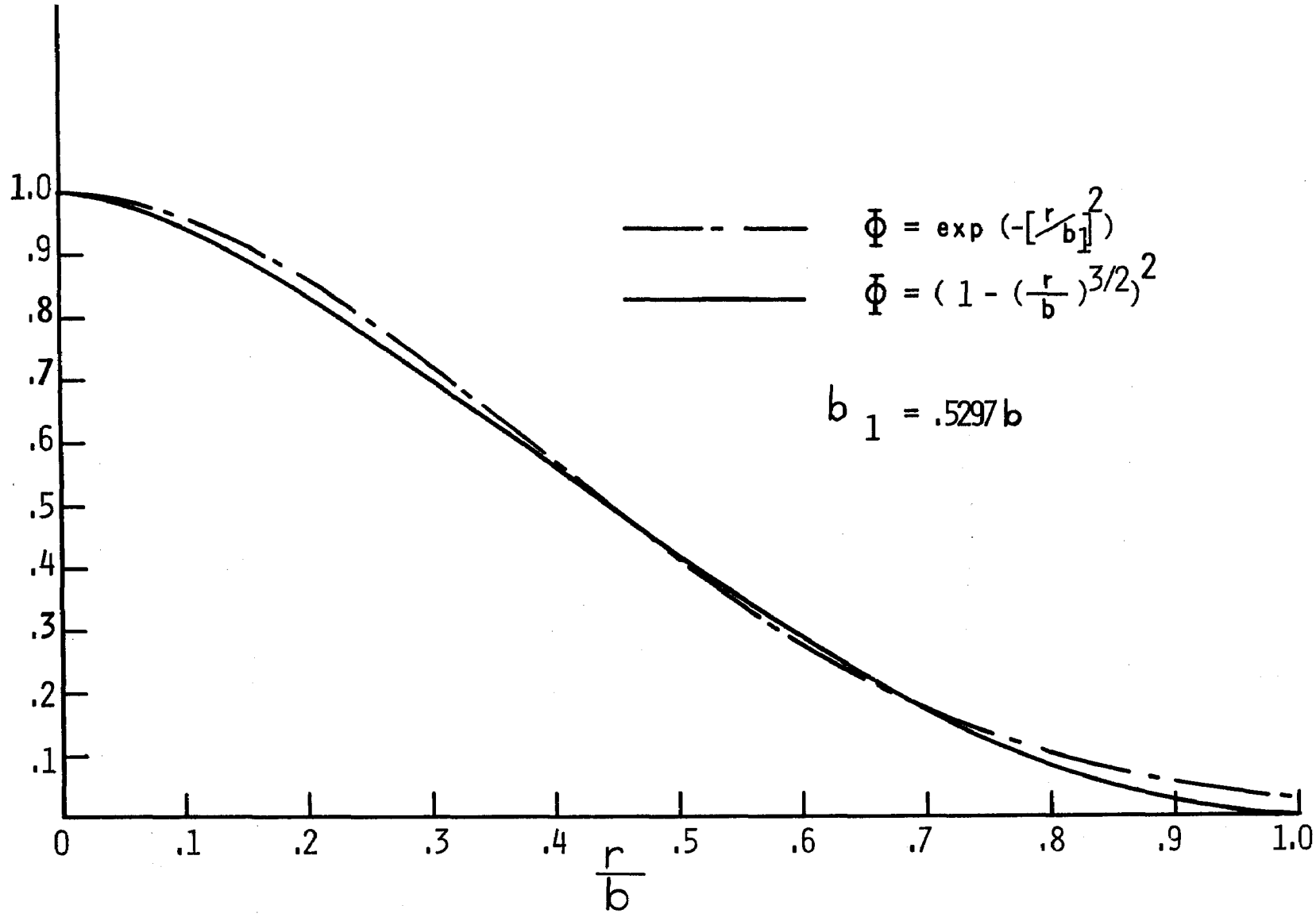

Figure 50. Comparison of the Gaussian and 3/2 power profiles.

$$T - T_\infty = T_o - T_\infty , \quad r \leq r_t \qquad ; (42)$$

$$T - T_\infty = \left(T_o - T_\infty\right)\left(1 - \left(\frac{r - r_t}{b}\right)^{3/2}\right)^2 , \quad r \geq r_t \qquad . (43)$$

If $\frac{\partial T_\infty}{\partial z}$ and $\frac{\partial C_\infty}{\partial z}$ are the same, T and C will grow at the same rate.

Employing these relationships, equations (33) - (38) become:

continuity,

$$\frac{d}{ds}\left[\frac{U_o r_u^2}{2} + r_u b d_1 + \frac{b^2}{2} d_2\right] = E \qquad , (44)$$

energy,

$$\frac{d}{ds}\left[\frac{U_o \Delta T_o r_t^2}{2} + \Delta T_o b r_t d_3 + \Delta T_o \frac{b^2}{2} d_4\right]$$

$$= \frac{dT_\infty}{ds}\left(\frac{U_o r_u^2}{2} + b r_u d_1 + \frac{b^2}{2} d_2\right) - \lim_{r\to\infty}\left(r\overline{v'T'}\right) \qquad , (45)$$

s-momentum,

$$\frac{d}{ds}\left[\frac{U_o^2 r_u^2}{2} + d_5 b r_u + d_6 \frac{b^2}{2}\right] = E U_\infty \cos\theta_2 \sin\theta_1$$

$$+ g \sin\theta_2 \left(\beta \Delta T_o i_{51} + \gamma \Delta C_o i_{52}\right) - \lim_{r\to\infty}\left(r\overline{u'v'}\right) \qquad , (46)$$

and curvatures,

$$\frac{d\theta_2}{ds} = \frac{- E U_\infty \sin\theta_1 \sin\theta_2 + g\left(\beta \Delta T_o i_{51} + \gamma \Delta C_o i_{52}\right)}{\frac{U_o^2 r_u^2}{2} + d_5 b r_u + d_6 \frac{b^2}{2} - \frac{E^2}{4} - \lim_{r\to\infty}\left(r^2\overline{v'^2}\right)} \qquad , (47)$$

$$\frac{d\theta_1}{ds} = \frac{EU_\infty \cos\theta_1}{\left[\frac{U_o^2 r_u^2}{2} + d_5 b r_u + d_6 \frac{b^2}{2} - \frac{E^2}{4} - \lim_{r\to\infty}\left(r^2\overline{v'^2}\right)\right]\cos\theta_2} \quad , \quad (48)$$

where

$$d_1 = .45U_o + .55U \cos\theta_2 \sin\theta_1$$

$$d_2 = .25714U_o + .74286U_\infty \cos\theta_2 \sin\theta_1$$

$$d_3 = .31558U_o + .13442U_\infty \cos\theta_2 \sin\theta_1$$

$$d_4 = .13352U_o + .12362U_\infty \cos\theta_2 \sin\theta_1$$

$$d_5 = .31558U_o^2 + .26885U_oU_\infty \cos\theta_2 \sin\theta_1$$

$$d_6 = .13552U_o^2 + .24724U_oU_\infty \cos\theta_2 \sin\theta_1$$

$$i_{51} = \frac{r_t^2}{2} + .45r_t b + .25714\,\frac{b^2}{2}$$

$$i_{52} = \frac{r_c^2}{2} + .45r_c b + .25714\,\frac{b^2}{2}$$

Taking the implied differentials and holding θ_2 constant for (44) - (46)[13] one obtains:

continuity,

$$U_o r_u r_u' + d_1\left(r_u b' + b r_u'\right) + d_2 bb' = E \quad , \quad (49)$$

energy,

$$U_o \Delta T_o r_t r_t' + \Delta T_o d_3\left(b r_t' + r_t b'\right) + \Delta T_o d_4 bb'$$

$$= \frac{dT_\infty}{ds}\left(\frac{U_o}{z}\left(r_t^2 - r_u^2\right) + b\left(r_t d_3 - r_u d_1\right)\right) - \lim_{r\to\infty}\left(r\overline{v'T'}\right) \quad , \quad (50)$$

and s-momentum,

[13] Hirst argues that this will be of small contribution and will simplify the algebra. While one might question the argument he offers, it seems well worth its exclusion since its inclusion would further couple the equations.

$$U_o^2 r_u r_u' + d_5'\left(b r_u' + r_u b'\right) + d_6 b b' = EU_\infty \cos\theta_2 \sin\theta_1$$

$$+ g \sin\theta_2 \left(\beta \Delta T_o i_{51} + \gamma \Delta C_o i_{52}\right) - \lim_{r\to\infty} \left(\overline{ru'v'}\right) \quad . \quad (51)$$

The variables to be solved for are r_u, r_t, b, θ_1, and θ_2. The solution technique for these equations is: 1) get simultaneous solution where the equations are setup in the form:

$$\left[a_{lm}\right] \begin{bmatrix} r_u' \\ r_t' \\ b' \\ \theta_1' \\ \theta_2' \end{bmatrix} = \begin{bmatrix} f_1 \\ f_2 \\ f_3 \\ f_4 \\ f_5 \end{bmatrix} \quad ; \quad (52)$$

(the species equation may be added as required)

where

$a_{11} = U_o r_u + d_1 b$

$a_{12} = 0$

$a_{13} = d_1 r_u + d_2 b$

$a_{14} = 0$

$a_{15} = 0$

$a_{31} = U_o^2 r_u + d_5 b$

$a_{32} = 0$

$a_{33} = d_5 r_u + d_6 b$

$a_{34} = 0$

$a_{35} = 0$

$a_{51} = 0$

$a_{21} = 0$

$a_{22} = U_o \Delta T_o r_t + \Delta T_o d_3 b$

$a_{23} = \Delta T_o d_3 r_t + \Delta T_o b d_4$

$a_{24} = 0$

$a_{25} = 0$

$a_{41} = 0$

$a_{42} = 0$

$a_{43} = 0$

$a_{44} = 1$

$a_{45} = 0$

$a_{52} = 0$

$$a_{53} = 0 \qquad a_{54} = 0$$

$$a_{55} = 1$$

$$f_1 = E$$

$$f_2 = \frac{\partial T_\infty}{\partial s}\left(\frac{U_o}{2}\left(r_t^2 - r_u^2\right) + b\left(r_t d_3 - r_u d_1\right) + b^2\left(d_4 - d_2\right)\right) - \lim_{r\to\infty}\left(r\overline{v'T'}\right)$$

$$f_3 = EU_\infty \cos\theta_2 \sin\theta_1 + g \sin\theta_2\left(\beta\Delta T_o i_{51} + \gamma\Delta C_o i_{52}\right) - \lim_{r\to\infty}\left(r\overline{v'u'}\right)$$

$$f_4 = EU_\infty \cos\theta_1 \Big/ \left[\left(\frac{U_o^2 r_u^2}{2} + d_5 b r_u + d_6\frac{b^2}{2} - \frac{E^2}{4} - \lim_{r\to\infty}\left(r^2\overline{v'^2}\right)\right)\cos\theta_2\right]$$

and $$f_5 = \left(-EU_\infty \sin\theta_1 \sin\theta_2 + g\left(\beta\Delta T_o i_{51} + \gamma\Delta C_o i_{52}\right)\right)\Big/ \left[\frac{U_o^2 r_u^2}{2} + d_5 b r_u + d_6\frac{b^2}{2} - \frac{E^2}{4} - \lim_{r\to\infty}\left(r^2\overline{v'^2}\right)\right]$$

then 2) use a Hamming Predictor-Corrector scheme[14] to solve equations (51) for r_u, r_t, r_c, b, θ_1 and θ_2.

The calculation continues until either r_u, r_c or r_t reaches zero. At that point the equations must be changed since from then on the centerline values of the quantities whose core radii have already reached zero will begin to diminish.

In most cases r_t will reach zero before r_u since the scalar properties diffuse more rapidly in ambients where great scalar gradients do not exist. In this event the relations that change

[14] The simultaneous solution scheme is called from the IBM Hamming Predictor-Corrector subprogram employed.

are i_{51}, i_{52}, energy and species. If r_t reaches zero before r_u, the new relations are

$$i_{51} = i_{52} = 0.12857b^2 \quad ,$$

and energy,

$$\frac{b^2}{2} d_4 \Delta T_c' + \Delta T_c b d_4 b' = - \frac{dT_\infty}{ds} \left(\frac{U_o r_u^2}{2} + d_1 b r_u + d_2 \frac{b^2}{2} \right) - \lim_{r \to \infty} \left(\overline{rv'T'} \right) \quad . \quad (53)$$

The process remains as before, simultaneous solution and integration but with the variables now being r_u, ΔT_c, ΔC_c, b, θ_1, and θ_2.

If the velocity core expires before the scalar cores, the equations must be changed as well and Δu_c $\left(\Delta u_c = u_c - U_\infty \cos \theta_2 \sin \theta_1\right)$ replaces r_u as a variable. However, all the relations change. The new equations are:

continuity,

$$.12855b^2 \Delta u_c' + \left(.2571 \Delta u_c b + .4858 b U_\infty \cos \theta_2 \sin \theta_1\right) b' = E \quad , \quad (54)$$

energy,

$$\left[\left(\Delta u_c + U_\infty \cos \theta_2 \sin \theta_1\right) r_t + d_7 b\right] r_t' + \left[\frac{r_t^2}{2} + .31588 r_t b + .13552 \frac{b^2}{2}\right] \Delta u_c' + \left[d_7 r_t + d_8 b\right] b' = \frac{1}{\Delta T_o} \frac{dT_\infty}{ds} \left(- \frac{b^2}{2} \left(.2571 \Delta u_c + .4858 U_\infty \cos \theta_2 \sin \theta_1\right) + \left(\Delta u_c + U_\infty \cos \theta_2 \sin \theta_1\right) \frac{r_t^2}{2} + r_t b d_7 + \frac{b^2}{2} d_8 \right) - \frac{1}{\Delta T_o} \lim_{r \to \infty} \left(\overline{rv'T'} \right) \quad , \quad (55)$$

s-momentum,

$$\left[.13352b^2\Delta u_c + .25714b^2U_\infty \cos\theta_2 \sin\theta_1\right]\Delta u_c'$$
$$+ b'\left[.13352b\Delta u_c{}^2 + .51824b\Delta u_c U_\infty \cos\theta_2 \sin\theta_1\right.$$
$$\left. + bU_\infty{}^2 \cos{}^2\theta_2 \sin{}^2\theta_1\right] = EU_\infty \cos\theta_2 \sin\theta_1$$
$$+ g \sin\theta_2 \left(\beta\Delta T_o i_{51} + \gamma\Delta C_o i_{52}\right) - \lim_{r\to\infty}\left(r\overline{u'v'}\right) \quad , (56)$$

and curvatures,

$$\frac{d\theta_1}{ds} = \left(EU_\infty \cos\theta_1\right)\Big/\left[\frac{b^2}{2}\left(.13352\Delta u_c{}^2 + .51428\Delta u_c U_\infty \cos\theta_2 \sin\theta_1\right.\right.$$
$$\left.\left. + U_\infty{}^2 \cos{}^2\theta_2 \sin{}^2\theta_1\right) - \frac{E^2}{4} - \lim_{r\to\infty}\left(r^2\overline{v'^2}\right)\right]\cos\theta_2 \quad , (57)$$

and

$$\frac{d\theta_2}{ds} = \left(-EU_\infty \sin\theta_2 \sin\theta_1 + g\left(\beta\Delta T_o i_{51} + \gamma\Delta C_o i_{52}\right)\right)\Big/$$
$$\left[\frac{b^2}{2}\left(.13352\Delta u_c{}^2 + .51428\Delta u_c U_\infty \cos\theta_2 \sin\theta_1\right.\right.$$
$$\left.\left. + U_\infty{}^2 \cos{}^2\theta_2 \sin{}^2\theta_1\right) - \frac{E^2}{4} - \lim_{r\to\infty}\left(r^2\overline{v'^2}\right)\right] \quad , (58)$$

where

$$d_7 = .31558\Delta u_c + .45U_\infty \cos\theta_2 \sin\theta_1$$
$$d_8 = .13352\Delta u_c + .25714U_\infty \cos\theta_2 \sin\theta_1$$

and i_{51} and i_{52} are the same as those first given in the general development zone analysis.

The initial conditions for the zone of flow establishment are simply the conditions of jet discharge:

$$r_u = .5D \ , \ r_t = .5D \ , \ b = 0.0 \ , \ \theta_1 = \theta_{1_0} \ , \text{ and } \theta_2 = \theta_{2_0}$$

The equations and solution techniques are now completed for the zone of flow establishment with the exception of the entrainment, E, which will be discussed later.

ZONE OF ESTABLISHED SINGLE PLUME FLOW

The calculation of plume properties has proceeded through the zone of flow establishment, according to the differential equations given in the previous section, until r_u and r_t are all zero. Generally, $\Delta T_c/\Delta T_o$ is less than 1.0 and often $\Delta u_c/\Delta U_o$ is less than 1.0 because of the definition of Δu_c and ΔU_o. At this time the plume width will be about 2.6 port diameters and merging will not begin if the port spacing is greater than this. In such a case the plume will continue growing with the geometry and character of a single, fully developed, buoyant jet until merging begins. In this region the profiles remain axisymmetric and similar. The characteristic variables of the jet are Δu_c, ΔC_c, ΔT_c, b, θ_1, and θ_2. The similar profiles adopted for this region are:

$$u = \Delta u + U_\infty \cos \theta_2 \sin \theta_1$$

where

$$\Delta u = \Delta u_c \left(1 - \left(\frac{r}{b}\right)^{3/2}\right)^2$$

and $$\Delta T = \Delta T_c \left(1 - \left(\frac{r}{b}\right)^{3/2}\right)$$

(the species will have the same profile as temperature).

With these profiles the integrals in equations (33) - (38) can be evaluated to yield:

continuity,

$$\frac{d}{ds}\left(.12857\Delta u_c b^2 + U_\infty \cos \theta_2 \sin \theta_1 \frac{b^2}{2}\right) = E \quad , (59)$$

energy,

$$\frac{d}{ds}\left(.066758\Delta u_c \Delta T_c b^2 - .12857\Delta T_c U_\infty \cos\theta_2 \sin\theta_1 b^2\right)$$
$$= -\frac{dT_\infty}{ds}\left(.12857\Delta u_c b^2 + \frac{b^2}{2} U_\infty \cos\theta_2 \sin\theta_1\right) - \lim_{r\to\infty}\left(r\overline{v'T'}\right), \quad (60)$$

s-momentum,

$$\frac{d}{ds}\left[b^2\left(.066758\Delta u_c^2 + .25714\Delta u_c U_\infty \cos\theta_2 \sin\theta_1\right.\right.$$
$$\left.\left. + \frac{1}{2}U_\infty^2 \cos^2\theta_2 \sin^2\theta_1\right)\right] = EU_\infty \cos\theta_2 \sin\theta_1$$
$$+ .12857b^2 g \sin\theta_2\left(\beta\Delta T_c + \gamma\Delta C_c\right) - \lim_{r\to\infty}\left(r\overline{v'u'}\right), \quad (61)$$

and curvatures,

$$\frac{d\theta_1}{ds} = EU_\infty \cos\theta_1 \Big/ \left(\left[b^2\left(.066758\Delta u_c^2 + .25714\Delta u_c U_\infty \cos\theta_2 \sin\theta_1\right.\right.\right.$$
$$\left.\left.\left. + \frac{1}{2}U_\infty^2 \cos^2\theta_2 \sin^2\theta_1\right) - \frac{E^2}{4} - \lim_{r\to\infty}\left(r^2\overline{v'^2}\right)\right]\cos\theta_2\right) \quad (62)$$

and

$$\frac{d\theta_2}{ds} = \left(-EU_\infty \sin\theta_2 \sin\theta_1 + .12857b^2 g\left(\beta\Delta T_c + \gamma\Delta C_c\right)\cos\theta_2\right)\Big/$$
$$\left[b^2\left[.066758\Delta u_c^2 + .25714\Delta u_c U_\infty \cos\theta_2 \sin\theta_1\right.\right.$$
$$\left.\left. + \frac{1}{2}U_\infty^2 \cos^2\theta_2 \sin^2\theta_1\right] - \frac{E^2}{4} - \lim_{r\to\infty}\left(r^2\overline{v'^2}\right)\right] . \quad (63)$$

These may be written as:

$$\frac{d}{ds} G_1 = E \quad , (64)$$

$$\frac{d}{ds} G_2 = - \frac{dT_\infty}{ds} G_1 - \lim_{r\to\infty} \left(r\overline{v'T'}\right) \quad , (65)$$

$$\frac{d}{ds} G_3 = EU_\infty \sin\theta_1 \cos\theta_2 + G_4 g \sin\theta_2 - \lim_{r\to\infty} \left(r\overline{v'u'}\right) \quad , (66)$$

$$\frac{d\theta_1}{ds} = EU_\infty \cos\theta_1 \Big/ \left[\left(G_3 - \frac{E^2}{4} - \lim_{r\to\infty} \left(r^2\overline{v'^2}\right)\right) \cos\theta_2\right] \quad , (67)$$

and

$$\frac{d\theta_2}{ds} = \left(- EU_\infty \sin\theta_2 \sin\theta_1 + g \cos\theta_2 G_4\right) \Big/ \left(G_3 - \frac{E^2}{4} - \lim_{r\to\infty} \left(r^2\overline{v'^2}\right)\right) \quad . (68)$$

These equations may be integrated for G_i ($i = 1,2,3,4$) using the Hamming Predictor-Corrector method. Then the variables Δu_c, ΔC_c, ΔT_c, and b (θ_1 and θ_2 will already have been obtained) may be obtained once G_i ($i = 1,2,3,4$) are known, from the relations below:

$$G_1 = .12857\Delta u_c b^2 + \frac{b^2}{2} U_\infty \cos\theta_2 \sin\theta_1 \quad , (69)$$

$$G_2 = .066758\Delta u_c \Delta T_c b^2 - .12857 b^2 \Delta T_c U_\infty \cos\theta_2 \sin\theta_1 \quad , (70)$$

$$G_3 = .066758\Delta u_c{}^2 b^2 + .25714 b^2 \Delta u_c U_\infty \cos\theta_2 \sin\theta_1 + \frac{b^2}{2} U_\infty{}^2 \cos{}^2\theta_2 \sin{}^2\theta_1 \quad , (71)$$

and

$$G_4 = .12857b^2\left(\beta\Delta T_c + \gamma\Delta C_c\right) \quad . \quad (72)$$

Put in a more direct form, from (69) and (71),

$$b = \left(-\frac{BB}{2AA} - \sqrt{\frac{BB^2}{4AA^2} - \frac{CC}{AA}}\right)^{1/2} \quad , \quad (73)$$

where

$$AA = -.37019U_\infty^2 \cos^2\theta_2 \sin^2\theta_1 \quad , \quad (74)$$

$$BB = 2G_1U_\infty \cos\theta_2 \sin\theta_1 - G_3 - 4.0386G_1U_\infty \cos\theta_2 \sin\theta_1 \quad , \quad (75)$$

and

$$CC = 4.0386G_1^2 \quad . \quad (76)$$

With b determined, Δu_c is found to be

$$\Delta u_c = \frac{G_1 - \frac{b^2}{2} U_\infty \cos\theta_2 \sin\theta_1}{.12857b^2} \quad , \quad (77)$$

and likewise

$$\Delta T_c = \frac{G_2}{b^2\left(.066758\Delta u_c - .12857U_\infty \cos\theta_2 \sin\theta_1\right)} \quad . \quad (78)$$

G_4 may be determined with (78) (and its species equivalent when necessary) above.

The quantities G_i (i = 1,2,3,4) are the local mass flux, energy flux, species flux (when used), momentum flux and density

difficiency respectively. The integration of these "secondary" variables (G_i) as opposed to the "primary" variables, Δu_c, ΔC_c, ΔT_c, and b, is advantageous in two ways. First, the fluxes are of the natural properties of the jet. Second, and more importantly, the integration of the secondary variables does not involve the matrix solution of simultaneous equations, as does integration of the equations employing the primary variables.

Employing the values of Δu_c, ΔC_c, ΔT_c and b calculated at the end of the zone of flow establishment as the initial values for the governing equations in the zone of established single plume flow, one may proceed using the equations developed above.

ZONE OF MERGING PLUMES

At some point, the edges of the adjacent plumes will begin to merge. When this occurs, the discharge loses its axisymmetry and the profiles become dependent on the angle with respect to the neighboring plume. This does not invalidate the lumping integral process nor is the concept of similarity threatened. However, certain adjustments must be made.

The original equations (33) - (38) could have included an asymmetric quality if the integrals had been considered as area integrals rather than line integrals, with the surface integration being

$$\int_o^{2\pi}\int_o^{\infty} \Gamma(r,\phi,s)\,r\,dr\,d\phi$$

Now when axisymmetry is assumed, as was done earlier, the integral in ϕ can be brought outside the integral in r, evaluated to be 2π, and divided out from both sides to obtain the relations (33) -

(38). However, now that axisymmetric profiles no longer exist it is necessary to include this integral into the equations, i.e., where one has $\int_0^\infty \Gamma(r,s)rdr$ in (33) - (38) one now has

$$\int_0^{2\pi}\int_0^\infty \Gamma(r,\phi,s)\ rdrd\phi \tag{79}$$

In this form the equations are quite general and assuming one knows the complete profiles of velocity, temperature, and species, the integrals could be carried out numerically if not in closed form.

Rather than deal with profile integrals of the (79) type, it is more convenient to employ a different coordinate system when merging begins. This new coordinate system is shown in Figure 51. In the new coordinate system ζ lies through the axis of a line of adjacent jets and η is perpendicular to the ζ-s plane and hence is perpendicular to the line of jets. If the profiles are symmetric with respect to both these axes (to ∞ in η and to L/2 in ζ), then the integration is simplified greatly. However, this case is only attainable when the adjacent plumes have the same velocity, temperature, and species profiles; are of equal spacing from the origin ($\eta = \zeta = 0$) jet and all have centerlines lying on the ζ-axis. This is tantamount to saying that the jets are line discharged normal to a uniform free stream (if one exists) in a common hydrostatic plane and experience the same dilution and ambient history. The most likely deviation from these conditions would be a line discharge into a non-normal uniform free stream. It is not likely that small deviations from the normal would

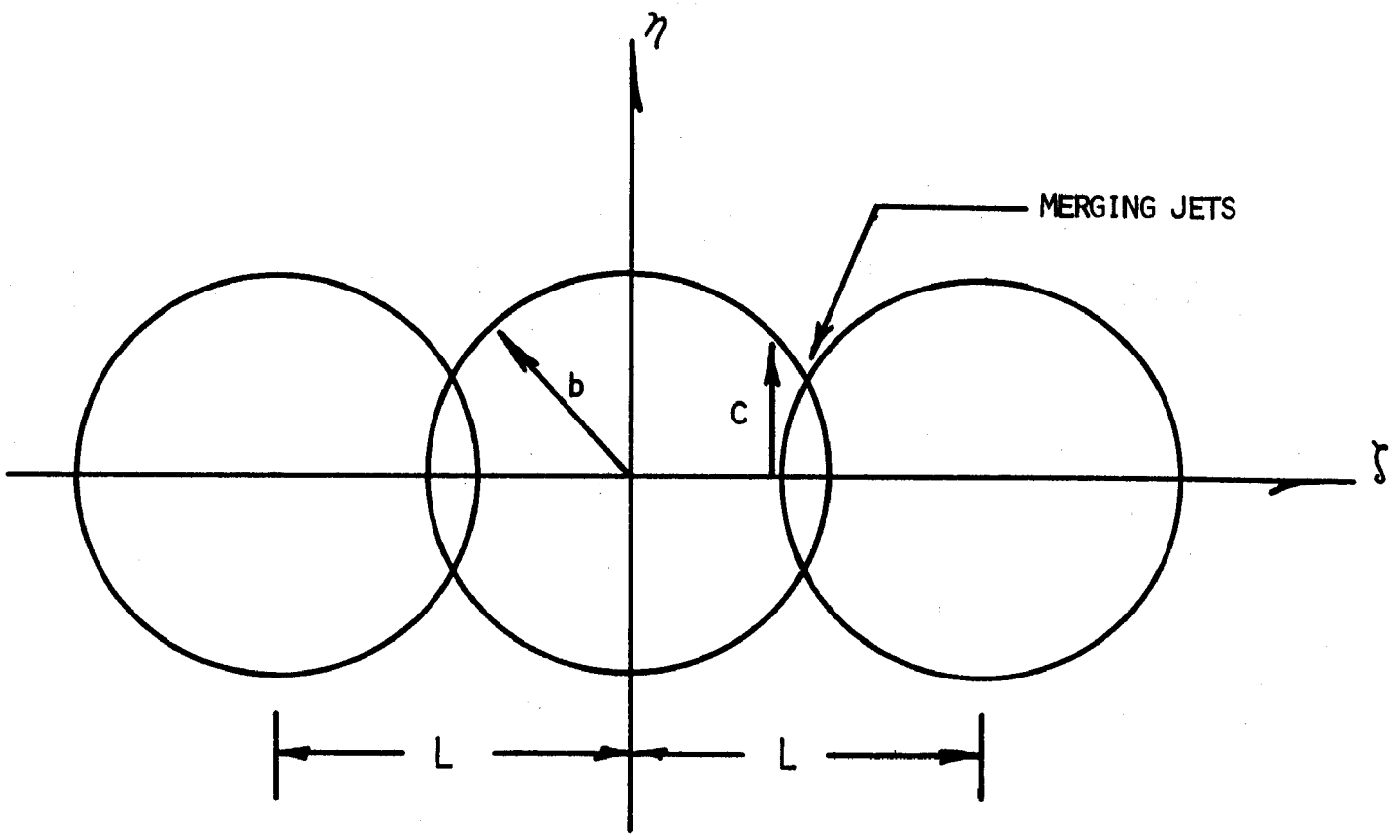

Figure 51. The coordinate system for the merging plume analysis.

severely affect the calculations, but no experimental evidence exists with which to determine the allowable extent of the deviation.

If symmetry exists only with respect to ζ, then the development becomes more difficult since the integration of the profiles are more complex. However, this is probably the only way to include other multiple discharge geometries once merging is initiated. In the final analysis it may be necessary to forgo any symmetry conditions and treat the most complex of multiple discharge configurations three dimensionally. The analysis presented here (as in Reference 17) will restrict itself to the case where symmetry exists with respect to both η and ζ.

Experiments made in this study indicate that the temperature at $\zeta = L/2$, $\eta = 0$ is approximately twice that of the temperature at $\zeta = 0$, $\eta = L/2$ during merging. This suggests that the profiles may be assumed to simply be the superposition of adjacent single plume profiles. Considering this, the merging profiles should satisfy the following:

a) the profiles should be smooth in all directions,

b) the slopes should be zero at $\zeta = 0$, $\eta = 0$, and $\zeta = L/2$, $\eta = 0$,

c) when the plumes just begin to merge they should retain their single plume profiles,

d) the profiles should be the superposition of the single plume profiles (where applicable) with no point allowed to exceed centerline properties.

In keeping with the similar profiles developed prior to this, and the discussion above, the following are the assumed profiles in the zone of merging:

$$u = \Delta u + U_\infty \cos \theta_2 \sin \theta_1 \quad , \quad (80a)$$

$$\Delta u = \Delta u_\eta = \Delta u_\zeta \left[1 - \left(\frac{\eta}{c}\right)^{3/2}\right]^2 \quad , \quad (80b)$$

$$\Delta u_\zeta = \Delta u_c \left[1 - \left(\frac{\zeta}{b}\right)^{3/2}\right]^2 \quad \text{for } 0 \leq \zeta \leq L-b \quad , \quad (80c)$$

$$\Delta u_\zeta = \Delta u_c \left[\left(1 - \left(\frac{\zeta}{b}\right)^{3/2}\right)^2 + \left(1 - \left(\frac{L-\zeta}{b}\right)^{3/2}\right)^2\right] \quad \text{for } L-b \leq \zeta \leq L/2 \quad , \quad (80d)$$

where

$$c = \sqrt{b^2 - \zeta^2} \quad ;$$

also

$$\Delta T = \Delta T_\eta = \Delta T_\zeta \left[1 - \left(\frac{\eta}{c}\right)^{3/2}\right]^2 \quad , \quad (81a)$$

$$\Delta T_\zeta = \Delta T_c \left[1 - \left(\frac{\zeta}{b}\right)^{3/2}\right]^2 \quad \text{for } 0 \leq \zeta \leq L-b \quad , \quad (81b)$$

and,

$$\Delta T_\zeta = \Delta T_c \left[\left(1 - \left(\frac{\zeta}{b}\right)^{3/2}\right)^2 + \left(1 - \left(\frac{L-\zeta}{b}\right)^{3/2}\right)^2\right] \quad \text{for } L-b = L/2 \quad . \quad (81c)$$

After $\Delta u_\zeta = \Delta u_c$ at $\zeta = L/2$, then $\Delta u_\zeta = \Delta u_c$, and after $\Delta T_\zeta = \Delta T_c$ at $\zeta = L/2$, then $\Delta T_\zeta = \Delta T_c$.

In order to make the treatment homogeneous, the governing equations will be divided by 2π, as appropriate to the area integrals. This was also done in the first two zones. With the profiles described above, the governing relations (33) - (38) may be written as follows.

The continuity equation becomes,

$$\frac{d}{ds}\left[\frac{1}{2\pi}\int_A\int u dA\right] = \frac{d}{ds}\left[\frac{2}{\pi}\int_o^{L/2}\int_o^{c}\left(\Delta u_\eta + U_\infty \cos\theta_2 \sin\theta_1\right) d\eta d\zeta\right] \quad , \quad (82)$$

$$= \frac{d}{ds} H_1 = E$$

where

$$H_1 = \frac{.90}{\pi} b^2 \Delta u_c h_1(\alpha) + \frac{b^2}{\pi} U_\infty \cos\theta_2 \sin\theta_1 h_2(\alpha) \quad , \quad (83)$$

$$\alpha = \frac{L}{b} \quad ,$$

$$h_1(\alpha) = \int_o^{\frac{\alpha}{2}} \sqrt{1 - \chi^2}\left(1 - \chi^{3/2}\right) d\chi$$

$$+ \int_{\alpha-1}^{\alpha/2} \sqrt{1 - \chi^2}\left(1 - \left(\alpha - \chi\right)^{3/2}\right)^2 d\chi \quad , \quad (84)$$

and

$$h_2(\alpha) = 2\int_o^{\alpha/2} \sqrt{1 - \chi^2}\, d\chi = \frac{\alpha}{2}\sqrt{1 - \left(\frac{\alpha}{2}\right)^2} + \sin^{-1}\left(\frac{\alpha}{2}\right) \quad . \quad (85)$$

Now after $\Delta u_\zeta = \Delta u_c$ at $\zeta = L/2$, then $\Delta u_\zeta = \Delta u_c$ and one obtains,

$$H_1 = \frac{b^2}{\pi}\left[.45\Delta u_c + U_\infty \cos\theta_2 \sin\theta_1\right] h_2(\alpha) \quad . \quad (86)$$

In the equations $\alpha = L/b$ represents the degree of merging since for $\alpha = 2.$, $b = L/2$ and the plumes are just beginning to merge and for $\alpha = 1.$, $b = L$ and the plumes are nearly merged.

For the energy equation,

$$\frac{d}{ds}\left[\frac{1}{2\pi}\int_A\int u\Delta T dA\right] = \frac{d}{ds}\left[\frac{2}{\pi}\int_o^{L/2}\int_o^c \left(\Delta u_\eta + U_\infty \cos\theta_2 \sin\theta_1\right)\Delta T_\eta d\eta d\zeta\right]$$

$$= \frac{d}{ds} H_2 = -\frac{dT_\infty}{ds} H_1 - \lim_{r\to\infty}\left(\overline{rv'T'}\right) \quad , \quad (87)$$

where

$$H_2 = \frac{.63116}{\pi} b^2 \Delta T_c \Delta u_c h_3(\alpha) + \frac{.90}{\pi} b^2 \Delta T_c U_\infty \cos\theta_2 \sin\theta_1 h_1(\alpha) \quad , \quad (88)$$

and where

$$h_3(\alpha) = \int_o^{\alpha/2} \sqrt{1-\chi^2}\left(1-\chi^{3/2}\right)^4 d\chi + \int_{\alpha-1}^{\alpha/2} \sqrt{1-\chi^2}$$

$$\left[\left(1-\chi^{3/2}\right)^2\left(1.-(\alpha-\chi)^{3/2}\right)^2 + \left(1-(\alpha-\chi)^{3/2}\right)^4\right] d\chi \quad . \quad (89)$$

When $\Delta T_\zeta = \Delta T_c$ at $\zeta = L/2$, $\Delta T_\zeta = \Delta T_c$. With the profile description used, Δu_ζ approaches Δu_c at $\zeta = L/2$ to the same degree that ΔT_ζ approaches ΔT_c. Hence, when $\Delta T_\zeta = \Delta T_c$, $\Delta u_\zeta = \Delta u_c$. So with $\Delta T_\zeta = \Delta T_c$ and $\Delta u_\zeta = \Delta u_c$ one obtains,

$$H_2 = \frac{b^2}{\pi}\Delta T_c \left(.31558\Delta u_c + .45U_\infty \cos\theta_2 \sin\theta_1\right) h_2(\alpha) \quad . \quad (90)$$

The species equation would take on the same form as the energy equation under the same assumptions that in this region T, C, and u profiles are the same.

The s-momentum equation takes the following form for the zone of merging:

$$\frac{d}{ds}\left[\frac{1}{2\pi}\int_A\int u^2 dA\right] = \frac{d}{ds}\left[\frac{2}{\pi}\int_o^{L/2}\int_o^{c}\left(\Delta u_\eta + U_\infty \cos\theta_2 \sin\theta_1\right)^2 d\eta d\zeta\right]$$

$$= \frac{d}{ds} H_3 = EU_\infty \cos\theta_2 \sin\theta_1 + H_4 g \sin\theta_2 - \lim_{r\to\infty}\left(r\overline{u'v'}\right) \quad , \quad (91)$$

where

$$H_3 = \frac{.63116}{\pi} b^2 \Delta u_c{}^2 h_3(\alpha) + \frac{1.8}{\pi} b^2 \Delta u_c U_\infty \cos\theta_2 \sin\theta_1 \, h_1(\alpha)$$

$$+ \frac{1}{\pi} b^2 U_\infty{}^2 \cos{}^2\theta_2 \sin{}^2\theta_1 \, h_2(\alpha) \quad , \quad (92)$$

and

$$H_4 = \frac{.9}{\pi} b^2 \left(\beta\Delta T_c + \gamma\Delta C_c\right) h_1(\alpha) \quad . \quad (93)$$

After $\Delta u_\zeta = \Delta u_c$, equations (92) and (93) become

$$H_3 = \frac{b^2 h_2(\alpha)}{\pi}\left(.31558\Delta u_c{}^2 + .9\Delta u_c U_\infty \cos\theta_2 \sin\theta_1\right.$$

$$\left. + U_\infty{}^2 \cos{}^2\theta_2 \sin{}^2\theta_1\right) \quad , \quad (94)$$

and

$$H_4 = \frac{.45 b^2}{\pi}\left(\beta\Delta T_c + \gamma\Delta C_c\right) h_2(\alpha) \quad . \quad (95)$$

For the zone of merging the curvature equations take the forms,

$$\frac{d\theta_1}{ds} = \frac{EU_\infty \cos\theta_1}{\left(H_3 - \frac{E^2}{4} - \lim_{r\to\infty}\left(r\overline{v'^2}\right)\right)\cos\theta_2} \quad , \quad (96)$$

and

$$\frac{d\theta_2}{ds} = \frac{-EU_\infty \sin\theta_2 \sin\theta_1 + H_4 g \cos\theta_2}{H_3 - \frac{E^2}{4} - \lim_{r\to\infty}\left(r^2\overline{v'^2}\right)} \quad . \quad (97)$$

The functions $h_1(\alpha)$, $h_2(\alpha)$ and $h_3(\alpha)$ are incomplete integrals in α. These integrals are not solved in closed form at present but may be readily solved numerically. In fact, the results of this numerical integration show that the integrals may be adequately represented by a simple interpolating scheme between various values of the evaluated integrals. The computer program evaluates the integrals in this form.

The quantities H_i (i = 1,2,3,4) are the same as G_i (i = 1,2,3,4) in the previous subsection. They represent the local mass flux, energy flux, momentum flux, and density deficiency. The advantages of using these secondary variables was pointed out earlier.

In the process of solving the differential equations it is necessary (as in the previous subsection) to solve for the primary variables. Once H_i (i = 1,2,3,4) are known, the relations for $H_i = H_i(\Delta u_c, \Delta C_c, \Delta T_c, b, \theta_1, \theta_2, h_{1,2,3}(\alpha))$ may be used to obtain Δu_c, ΔC_c, ΔT_c, and b. The following equations are the result of the simultaneous solution of those equations. Taken in sequence for the region after merging is initiated,

$$b = \left(-\frac{BB}{2AA} - \sqrt{\frac{BB^2}{4AA^2} - \frac{CC}{AA}}\right)^{1/2} \quad , \quad (98)$$

where

$$AA = .31831h_2(\alpha)U_\infty^2 \cos^2\theta_2 \sin^2\theta_1 \left(.77921\frac{h_2(\alpha)h_3(\alpha)}{h_1^2(\alpha)} - 1\right) , \quad (99)$$

$$BB = 2H_1U_\infty \cos\theta_2 \sin\theta_1 - 1.5584H_1U_\infty \cos\theta_2 \sin\theta_1 \frac{h_2(\alpha)h_3(\alpha)}{h_1^2(\alpha)} - H_3 , \quad (100)$$

and

$$CC = 2.4480H_1^2 \frac{h_3(\alpha)}{h_1(\alpha)} ; \quad (101)$$

$$\Delta u_c = \frac{H_1 - \frac{b^2}{\pi}U_\infty \cos\theta_2 \sin\theta_1 h_2(\alpha)}{.28648b^2h_1(\alpha)} , \quad (102)$$

and

$$\Delta T_c = \frac{H_2}{\frac{b^2}{\pi}\left(.63116\Delta u_c h_3(\alpha) + .9U_\infty \cos\theta_2 \sin\theta_1 h_1(\alpha)\right)} . \quad (103)$$

When the primary variables at $\zeta = L/2$ sum to the centerline values, due to merging, the relations above change to the following:

$$b = \left(-\frac{BB}{2AA} - \sqrt{\frac{BB^2}{4AA^2} - \frac{CC}{AA}}\right)^{1/2} ; \quad (104)$$

where

$$AA = .1777h_2(\alpha)U_\infty^2 \cos^2\theta_2 \sin^2\theta_1 , \quad (105)$$

$$BB = -1.1168H_1U_\infty \cos\theta_2 \sin\theta_1 - H_3 , \quad (106)$$

and

$$CC = 4.8959 \frac{H_1^2}{h_2(\alpha)} \quad ; \quad (107)$$

$$\Delta u_c = 6.9813 H_1 \frac{1}{b^2 h_2(\alpha)} - 2.2222 U_\infty \cos \theta_2 \sin \theta_1 \quad ; \quad (108)$$

and finally

$$\Delta T_c = \frac{\pi H_2}{b^2 h_2(\alpha) \left(.31558 \Delta u_c + .45 U_\infty \cos \theta_2 \sin \theta_1\right)} \quad . \quad (109)$$

The initial conditions for the merging zone equations are the values of G_i $(i = 1,2,3,4)$ when $\alpha = 2$.

The appropriate governing differential equations have now been established. During the discussions suitable initial conditions have been specified. No boundary conditions remain to be specified with the possible exception of those boundary turbulence terms, of the type $\lim_{r\to\infty} (r\overline{v'T'})$, and the entrainment, $E = \lim_{r\to\infty}(r\bar{v})$. Discussion follows on these subjects.

BOUNDARY TURBULENCE TERMS

Most analytical discussions deal with discharges where the boundary turbulence terms are neglected, since describing these terms is somewhat difficult. The only experimental work found that has included such a description in relation to submerged discharges has been that of McQuivey, Keefer, and Shirazi[19], supplemented by their summarization in Reference 20. The information provided by those reports was used by Shirazi, Davis, and Byram[21] in the Hirst single port plume model in order to model co-flow

discharge. While their results were less than conclusive, it appears necessary to include these terms (at least for co-flow) but at higher magnitudes than suggested by experiment[20]. The model presented here employs the same boundary turbulence model that Shirazi, Davis, and Byram used.

If it is assumed that

$$\overline{v'c'} = -\varepsilon_c \frac{d\bar{C}}{dr}\ ,\ \overline{v'u'} = -\varepsilon_m \frac{d\bar{u}}{dr}\ ,\ \overline{v'T'}\ ,\ \text{and}\ \varepsilon_h = \varepsilon_c = \frac{\varepsilon m}{\lambda}\ ,$$

where

ε_m = momentum eddy diffusivity,

ε_h = thermal eddy diffusivity,

ε_c = species eddy diffusivity,

and λ = turbulent Schmidt Number (approximately 1.13); and if Gaussian profiles are assumed, the turbulence terms may be written as

$$\lim_{r \to \sqrt{2}b_1} \left(\frac{r\overline{v'u'}}{r_o U_o U_o}\right) = \left(\frac{\varepsilon_m}{r_o U_o}\right)\left(4e^{-2}\right)\left(\frac{\Delta u_c}{U_o}\right) = \left(\frac{\varepsilon_h}{r_o U_o}\right)\left(4\lambda e^{-2}\right)\left(\frac{\Delta u_c}{U_o}\right), \quad (110)$$

$$\lim_{r \to \sqrt{2}b_1} \left(\frac{r\overline{v'T'}}{r_o U_o T_o}\right) = \left(\frac{\varepsilon_h}{r_o U_o}\right)\left(\frac{4}{\lambda^2}\, e^{\frac{-2}{\lambda^2}}\right)\left(\frac{\Delta T_c}{T_o}\right) \quad , \quad (111)$$

and

$$\lim_{r \to \sqrt{2}b_1} \left(\frac{r\overline{v'C'}}{r_o U_o C_o}\right) = \left(\frac{\varepsilon_h}{r_o U_o}\right)\left(\frac{4}{\lambda^2}\, e^{\frac{-2}{\lambda^2}}\right)\left(\frac{\Delta C_c}{C_o}\right) \quad . \quad (112)$$

The $\overline{v'v'}$ term is assumed to be,

$$\lim_{r \to \sqrt{2}b_1} \left(\frac{r^2\overline{v'v'}}{r_o U_o U_o}\right) = \lim_{r \to \sqrt{2}b_1} \left(\frac{r^2\overline{u'u'}}{r_o U_o U_o}\right), \text{ i.e. } \overline{v'v'} = \overline{u'u'} \quad . \quad (113)$$

By suitable approximation to the downstream interval and making use of the empirical relations developed in Reference 20, an approximate relationship may be developed for ε_h in terms of Froude Number, ambient discharge velocity ratio, and $\sqrt{\overline{u'u'}}/U_\infty$ [15]. The boundary turbulence terms can then be written as

$$\lim_{r \to \sqrt{2}b_1} \left(\frac{r\overline{v'u'}}{r_o U_o U_o} \right) = \left[.192 \left(\frac{\sqrt{\overline{u'u'}}}{U_\infty} \right)^{1.182} R^{2.182} F^{1.131} \right] 4\lambda e^{-2} \frac{\Delta u_c}{U_o} \quad , \quad (114)$$

$$\lim_{r \to \sqrt{2}b_1} \left(\frac{r\overline{v'T'}}{r_o U_o T_o} \right) = \left[.192 \left(\frac{\sqrt{\overline{u'u'}}}{U_\infty} \right)^{1.182} R^{2.182} F^{1.131} \right] \frac{4}{\lambda^2} e^{\frac{-2}{\lambda^2}} \frac{\Delta T_c}{T_o} \quad , \quad (115)$$

$$\lim_{r \to \sqrt{2}b_1} \left(\frac{r\overline{v'C'}}{r U_o C_o} \right) = \left[.192 \left(\frac{\sqrt{\overline{u'u'}}}{U_\infty} \right)^{1.182} R^{2.182} F^{1.131} \right] \frac{4}{\lambda^2} e^{\frac{-2}{\lambda^2}} \frac{\Delta T_c}{T_o} \quad , \quad (116)$$

$$\lim_{r \to \sqrt{2}b_1} \left(\frac{r^2\overline{v'v'}}{r_o^2 U_o U_o} \right) = \left(\frac{\sqrt{2}b_1}{r_o} \right)^2 \frac{\overline{u'u'}}{U_o^2} R^2 = .5618 \left(\frac{b}{r_o} \right)^2 \frac{\overline{u'u'}}{U_o^2} R^2 \quad . \quad (117)$$

Shirazi, et.al.[21], reported that employing the above relationships in the equations had little if any effect on the dilution in crossflow but had a significant effect on co-flow. However, the values employed for $\left(\overline{u'^2}/U_\infty^2\right)^{1/2}$ were significantly larger than those measured by McQuivey, et.al.[19]. As is noted by Shirazi, et. al.[21], the entrainment term is considerably larger than the boundary turbulence terms. Therefore, the inclusion of turbulent effects in entrainment would probably give more satisfying results.

[15] Personal communication with M. A. Shirazi, Research Engineer, U. S. Environmental Protection Agency, Corvallis Environmental Research Laboratories, Corvallis, OR.

Shirazi, et.al.[21] found it necessary to change $\left(\overline{u'^2}/U_\infty^2\right)^{1/2}$ depending on towing ratio, R, and Froude Number in order to get satisfactory agreement with data.

ENTRAINMENT

The mathematical definition of entrainment has been given as $\lim_{r\to\infty} (r\bar{v}) = E$. Physically, entrainment is the rate of ambient fluid brought into the jet by virtue of the shear or turbulent transport action at the jet boundary. By continuity, it is also the local rate of change of total mass flux through the cross-section of the jet. The entrainment is important in the development of a suitable model since it controls the growth of the jet, and via the governing equations determines the dilution and trajectory. Unfortunately, this term has eluded explicit definition and thus appears in the form of a postulated function. How this function is postulated determines the value of the model as a predictive tool.

Lack of an explicit definition for entrainment is a mixed blessing. On the one hand, some of the information lost through integration may be returned to the model in the entrainment function. On the other hand, the roles of the various physical elements must be estimated and weighted into the entrainment function. Determining which physical actions should be included and to what degree is enlightened guesswork at best, especially when the discharges are physically complex. If the model is physically sound, any conceptual errors in the entrainment function will plague efforts to match model predictions to experiment.

The entrainment for the simple plume was first discussed by Taylor[22] who was seeking to simplify the entrainment concept by using the bulk properties of the plume to describe entrainment rather than the mixing length concepts used previously. Morton, et.al.[4] employed the assumption that entrainment was proportional to the relative plume centerline velocity and the local characteristic width measure of the plume, i.e.

$$E = ab_1\Delta u_c \tag{118}$$

This type of entrainment term remains today as the most basic entrainment function form. Most models employing it yield reasonable prediction of dilution and trajectory for discharge into deep quiescent stratified or unstratified ambients. In the above equation "a" is the entrainment coefficient. For Gaussian distributions (i.e. b_1 is the characteristic width measure) the best values for "a" have been found to be 0.057[16] for the simple momentum jet and 0.085[17] for the low Froude Number discharges. Observing that different values were necessary for different Froude Numbers, Fox [23] developed an entrainment function of the form,

$$E = \left[a_1 + \frac{a_2}{F_L}\right] b_1\Delta u_c \tag{119}$$

by arguing that consistency among the differential equations and similar profiles (extended to $\overline{u'v'}$as well) requires the above relationship. This entrainment function implies that the local buoyancy influences entrainment processes. The concept is rather weak when one considers that the dominant processes are primarily

[16] Albertson, et.al.[3]
[17] Abraham, G.[24]

turbulent and are in fluids of only average Prandtl Number (0.7 to about 7). Perhaps the most compelling reason for inclusion of the local Froude Number term is that Hirst[6] found this function to give better prediction than the Morton, et.al.[4] relation in his model. With equation (119) and the proper entrainment coefficient (about 0.80) the dilution could be predicted for discharge of a buoyant jet at all angles with acceptable agreement.

Discharges to flowing ambients have not been modeled yet with complete satisfaction. Agreement has been obtained between models and experiment, but in reaching such agreement the models require entrainment functions whose coefficients vary with the discharge conditions. Fan[25] conducted experimental research into buoyant jet discharge into a crossflow which he used to determine the entrainment coefficients of his computer model. He employed the same entrainment function as Morton, et.al.[4] but with the vector ambient-to-jet velocity difference. Fan included the drag force due to the pressure variation around the jet in his horizontal and vertical momentum equations. His vertical and horizontal momentum equations were

$$\frac{d}{ds}\left(\int_0^\infty u^2 r dr \cos\theta_2\right) = EU_\infty + F_D \sin\theta_2 \quad , \quad (120)$$

and

$$\frac{d}{ds}\left(\int_0^\infty u^2 r dr \sin\theta_2\right) = -\int_0^\infty \frac{\Delta\rho}{\rho_o} r g dr - F_D \cos\theta_2 \quad . \quad (121)$$

With this and the drag force equation,

$$F_D = C_D U_\infty^2 \sin^2\theta_2 \sqrt{2} b_1 \quad , \quad (122)$$

the coefficients left to be determined by matching model to experiment were the entrainment coefficient, "a", and the drag coefficient, C_D. Unfortunately, Fan could not obtain good agreement except by varying "a" and C_D with the discharge conditions. The variation was considerable for C_D, ranging from 0.1 to 1.7, while "a" ranged from 0.4 to 0.5.

Platten and Keffer[26] as well as Hoult, et.al.[27], chose to alter the entrainment function rather than employ the drag force. Platten and Keffer dealt only with non-buoyant jets in a crossflow. The entrainment function they employed had two terms,

$$E = a_1 b \left(u_c - U_\infty \sin \theta_1\right) + a_2 b U_\infty \left(\sin \theta_1 - \sin \theta_{1_o}\right) \quad . \quad (123)$$

The first term is the familiar entrainment term due to jet turbulence. The second term is a function included to "account for the vortex shear inflow." As has already been mentioned, the crossflow discharge induces twin vortices to form in the jet, which persist downstream for some distance. The influence of these vortices on entrainment is supposedly modeled by the second term of Platten and Keffer's entrainment function. Despite the inclusion of this second term and second entrainment coefficient, they were unable to get agreement without varying both coefficients.

Hoult, et.al.[27] also employed an entrainment function with two terms;

$$E = a_1 b \left|u_c - U_\infty \cos \theta_2\right| + a_2 b U_\infty \sin \theta_2 \quad , \quad (124)$$

the first term being jet turbulence entrainment, the second one associated with forced entrainment due to a normal external

velocity. The agreement with experiment obtained by Hoult, et.al. was better than that of Platten and Keffer, since the entrainment "constants" did not vary as much. Platten and Keffer's entrainment coefficients ranged over a factor of 3, while the values given by Hoult, et.al., $a_1 = 0.12$ and a_2 ranging from 0.6 to 0.9 (in a leter report, $a_1 = 0.11$ and $a_2 = 0.6$), varied to a smaller degree.

Hirst[6] employed an entrainment function of the form

$$E = \left(a_1 + \frac{a_2}{F_L}\right)\left[b\left|u_c - U_\infty \sin\theta_1 \cos\theta_2\right| + a_3 U_\infty b \sqrt{1 - \left(\sin\theta_1 \cos\theta_2\right)^2}\right] \quad . \quad (125)$$

This is seen to be a combination of Fox's entrainment function and a generalized Hoult, et.al. entrainment function. Hirst compared computer runs for a Gaussian profile model with data from fourteen other authors for conditions of crossflow and co-flow (as well as $\theta_2 = 135°$ and $45°$) discharge into stratified and unstratified, flowing and stagnant ambients. The values he obtained for entrainment coefficients were $a_1 = 0.057$, $a_2 = 0.97$, and $a_3 = 9.0$ for Gaussian profiles; when altered for the 3/2 power profile these values become 0.029, 0.51, and 4.8 respectively.

Since the computer routine used to solve the 3/2 power profile merging equations presented here is essentially that of Hirst (with appropriate profile and merging changes) an examination of the results of his modeling effort might prove valuable.

Hirst obtains excellent agreement for the simple momentum jet, ($a_1 = 0.057$, Gaussian). However, when buoyancy is also con-

sidered, the agreement is not as good. He notes that the predicted trajectories lie considerably below the experimental results of Fan[25], especially for higher Froude Numbers. By placing a_1 = 0.082 better agreement was obtained, but this value gave less acceptable predictions for many other flows. For co-flow cases Hirst's predictions are less dilute than corresponding experiments, especially for higher R's. This he attributes to the longer starting lengths proposed by Abramovich[29] (c.f. Hirst[6][18]) than supposedly really exist. For the discharges into a crossflow Hirst obtains good agreement (trajectory) for R = 0.125. However, the predicted trajectories are slightly lower than experiment for R<0.10 and are higher than experiment for R>0.10. In general, the dilutions Hirst obtained for crossflow were greater than that predicted from experiment. His results for stratified ambient discharges gave good agreement with experiment.

In summary, Hirst's work involved the use of constant entrainment coefficients but did not give exceptional agreement with experimental data for all discharge conditions. Inability to match the data for all discharge conditions may imply that the true entrainment is not accurately modeled by the proposed entrainment function; it may also imply that assumptions made during the development of the model render the model less universal than hoped. The predictions of Hirst give adequate agreement for a moderate range of all the parameters with constant entrainment coefficients.

[18] Hirst modifies the original starting length function of Abramovich to obtain agreement with Albertson, et.al.[3], for R = 0.0.

Hirst discusses what elements an entrainment function should include. These are:

1) local mean flow conditions within the jet, u_c and b;

2) local buoyancy within the jet, F_L;

3) velocity ratio, R;

4) initial jet orientation, θ_{1_o} and θ_{2_o};

and 5) ambient turbulence.

The entrainment function of Fan[25] and Morton, et.al.[4] include only 1). Fox's[23] entrainment function includes 1) and 2). Platten and Keffer's entrainment function employs only terms due to 1), 3), and 4). Hoult, et.al.[27], used an entrainment function having only 1), and 3), with 4) included somewhat implicitly. The Hirst entrainment function contained 1), 2), and 3) with 4) involved implicityly. None of the entrainment functions contain effects of ambient turbulence (although the terms in the governing equations accounting for ambient turbulence are in the Hirst program but set to zero).

Koh and Fan[13] were one of the first to deal with the case of merging adjacent plumes. They used a computer routine which would begin with a single round port solution and at some point switch to a slot solution. Two criteria were given for determining the transition point (when $b = L/2$, and $E_{round} = E_{slot}$), however, the two criteria gave essentially the same solution. While this was a way of handling the multiport case, it did not model the merging region.

Harleman and Jirka[7] approached the problem slightly differently. They stated that the multiport case could be adequately modeled by an "equivalent slot" solution. By making the multiport discharge

momentum and mass fluxes per unit length equal to those of a slot discharge, an equivalent slot discharge width may be defined. Combining this with a newly defined slot Froude Number provides sufficient information so that the standard slot solutions may be used to predict the trajectory and dilution of the multiport discharge. However, a recent report on deep submerged multiple port discharges into stagnant and coflowing ambients (Kannberg and Davis[14]) seems to dispute the acceptability of an equivalent slot solution. According to that report, both the transition model and the equivalent slot model over-predicted dilution. In each of these cases no attempt has been made to include merging effects in the entrainment function, except to switch from a round jet entrainment function to a slot jet entrainment function.

Kannberg and Davis[14] speculate that the entrainment model should be sensitive to the area of entrainment which diminishes as the plumes merge. And indeed, effects of adjacent plumes may be evident long before the jet boundaries touch, since the jets are always competing for common entrainment fluid. In this light Davis[17] proposed that the entrainment function contain an additional term to allow for effects of competition and reduction of the entrainment surface. Before boundary contact, the form of the entrainment function is given as

$$E = \left(a_1 + \frac{a_2}{F_L}\right)\left[b\left|u_c - U_\infty \cos\theta_2\right|\left(1 - \frac{a_4 b}{L}\right) + a_3 U_\infty b \sin\theta_2\right] \quad ; \quad (126)$$

while after boundary contact (when $b \geq L/2$) it takes the form,

$$E = \left(a_1 + \frac{a_2}{F_L}\right)\left[b\left|u_c - U_\infty \cos\theta_2\right|\left(1 - \frac{a_4'}{2}\right)\left(1 - \frac{2}{\pi}\cos^{-1}\frac{L}{2b}\right) + a_3 U_\infty \frac{L}{2}\sin\theta_2\right] \quad . \quad (127)$$

The change in entrainment functions is due to the change in entrainment area. Before merging, the entrainment area was π on a side, but after merging begins, the entrainment area becomes approximately $A_{entr.} = b\,(\pi - 2\cos^{-1}[L/(2b)])$ on each side. Ideally there should be no difference between a_4 and a_4' since at $b = L/2$ the two entrainment functions are the same. The entrainment equations of Davis are the same as Hirst's except for the modification due to merging, and like Hirst's include elements 1), 2), 3) and 4) (implicityly). As Davis mentions, the entrainment coefficients other than a_4 (a_4') in his entrainment function should be approximately those of Hirst. Since the Davis entrainment function is similar to the Hirst function, it should suffer the same deficiencies for single port discharges if the same coefficients are used as Hirst recommended.

The entrainment function(s) adopted initially in the present modeling effort were those of Davis. Since the model here includes the zone of flow establishment, the Davis entrainment function,

$$\frac{E}{r_o U_o} = C_1\left[.0204 + .0144\frac{b}{r_o}\right]\left[\left|1 - R\cos\theta_2\right|\left(1 - \frac{c_4 r_o}{L}\right) + C_3 R\sin\theta_2\right]\left[1 + \frac{c_2}{F}\right] \quad , \quad (128)$$

is used in that zone.

The values suggested by Davis for use in the entrainment function employed in this study are essentially those of Hirst, altered to the different plume width definition;

$$c_1 = 1.05, \qquad c_2 = 34., \qquad c_3 = 4.3,$$

$$a_1 = 0.029, \qquad a_2 = 0.51, \qquad \text{and } a_3 = 4.8.$$

One notes that the terms in the entrainment function appear in linear combination. This speaks for the simplicity of the entrainment models presently available.

TUNING THE MODEL - RESULTS

The governing differential equations have been determined, the entrainment specified, and expressions provided for boundary turbulence. All that remains is to determine the best entrainment coefficients. The calculations were carried out on an IBM 370/158 computer operated by Optimum Systems, Inc., of Bethesda, Maryland. The computer code employed was originally for the Hirst model. Extensive revision of the code was performed in order to accomodate the different profiles and the merging process. The code was then used in the present study by tuning the entrainment coefficients. Alterations were made as necessary to examine the influence of various entrainment and turbulence terms. The terms of the entrainment function allow for a successive evaluation of the entrainment coefficients. For the case of the momentum jet in a quiescent ambient, only c_1 and a_1 are involved. Therefore, to tune the model for these coefficients, various values of c_1 and a_1 were used in the model. The results were compared with the data

of Morton, et.al.[4], with the conclusion that c_1 = 1.06, and a_1 = 0.029 gave the best fit. The model prediction and results of Morton, et.al.[4], are shown in Figure 52. As can be seen, excellent agreement results. The coefficients are very nearly those suggested by Hirst when converted to the definition of plume width used here.

For the case of the buoyant jet, the coefficients c_2 and a_2 are the additional terms to be determined. No attempt was made to tune c_2; the value, 34., given by Hirst was considered adequate. However, problems arose when attempts were made to tune a_2. Use of values near those suggested by Hirst resulted in trajectories considerably below those of experiment, primarily for moderate Froude Numbers (30-100). In order to reach acceptable agreement with experiment, a_2 had to be set to zero and a_1 raised to 0.05, rather than 0.029 as given for the momentum jet. Model predicted trajectories (a_2 = 0.0, a_1 = 0.05) are compared with experimental trajectories and predicted trajectories from other models in Figures 53 and 54. The comparison of dilution for experiments and models are given in the Cederwall[19] type graph of Figure 55. As is evident from these graphs, the coefficients suggested give good agreement at low and moderate Froude Numbers but less satisfactory results at high Froude Numbers. It would seem that there is some Froude Number effect that is not included in the entrainment function. However, since no rational explanation exists for how and why such a term should be included, its inclusion is not justified.

[19] Originally attributed to Cederwall[30] (c.f. Fan[25]).

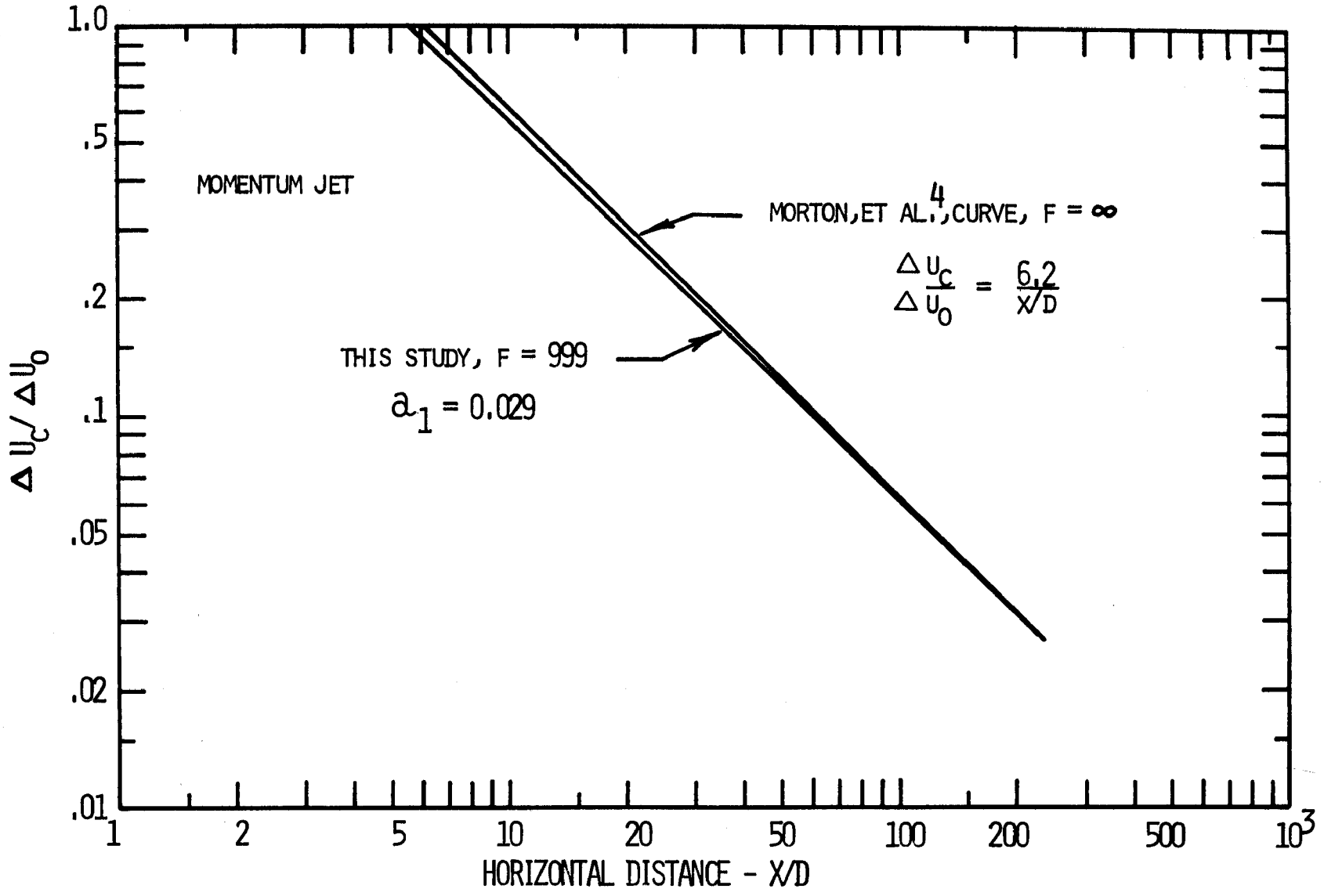

Figure 52. Model prediction and the Morton, et al.[4] empirical curve for the momentum jet.

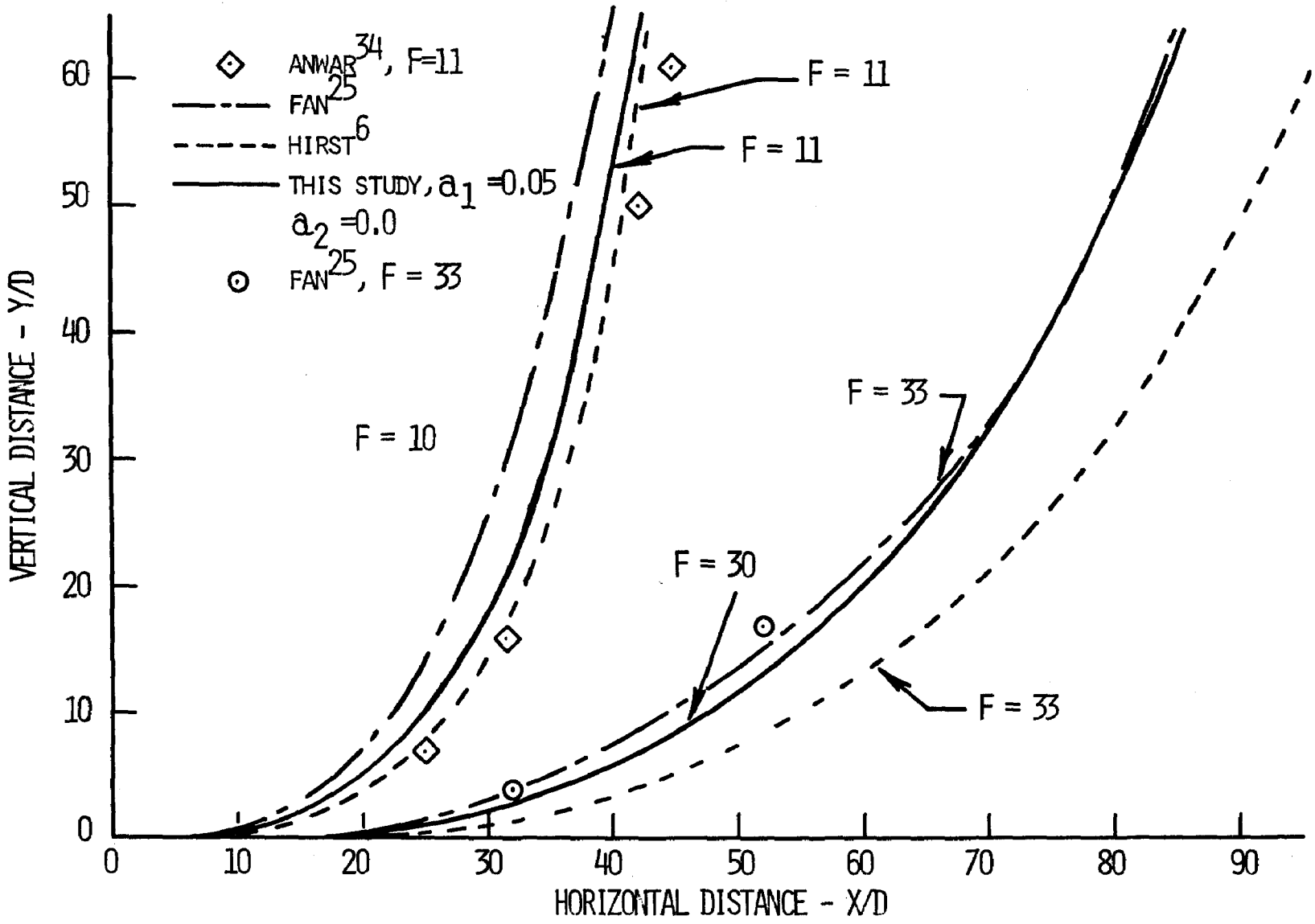

Figure 53. Model prediction and experimental data for trajectory of single port discharges.

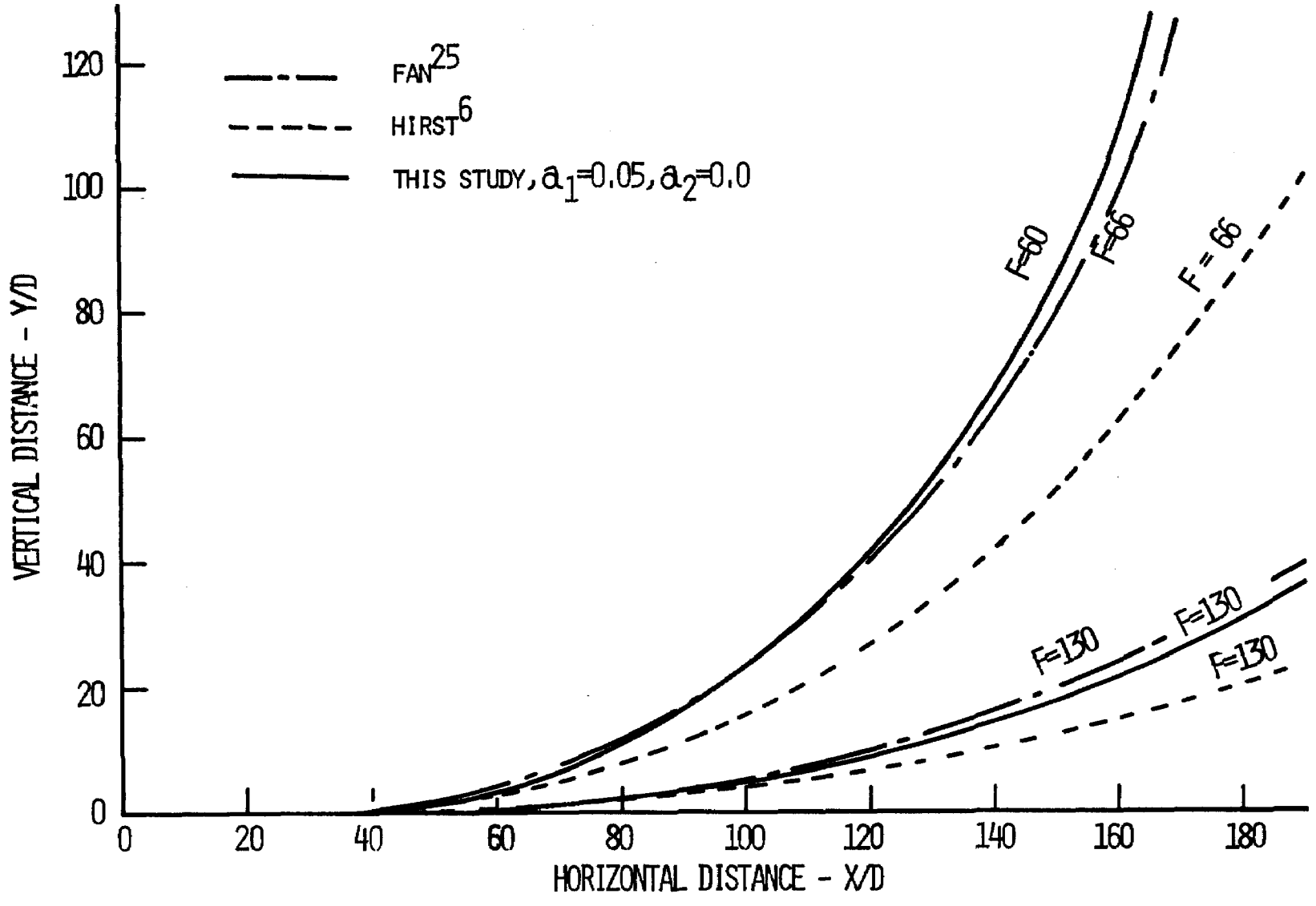

Figure 54. Model prediction of trajectory of single port discharges.

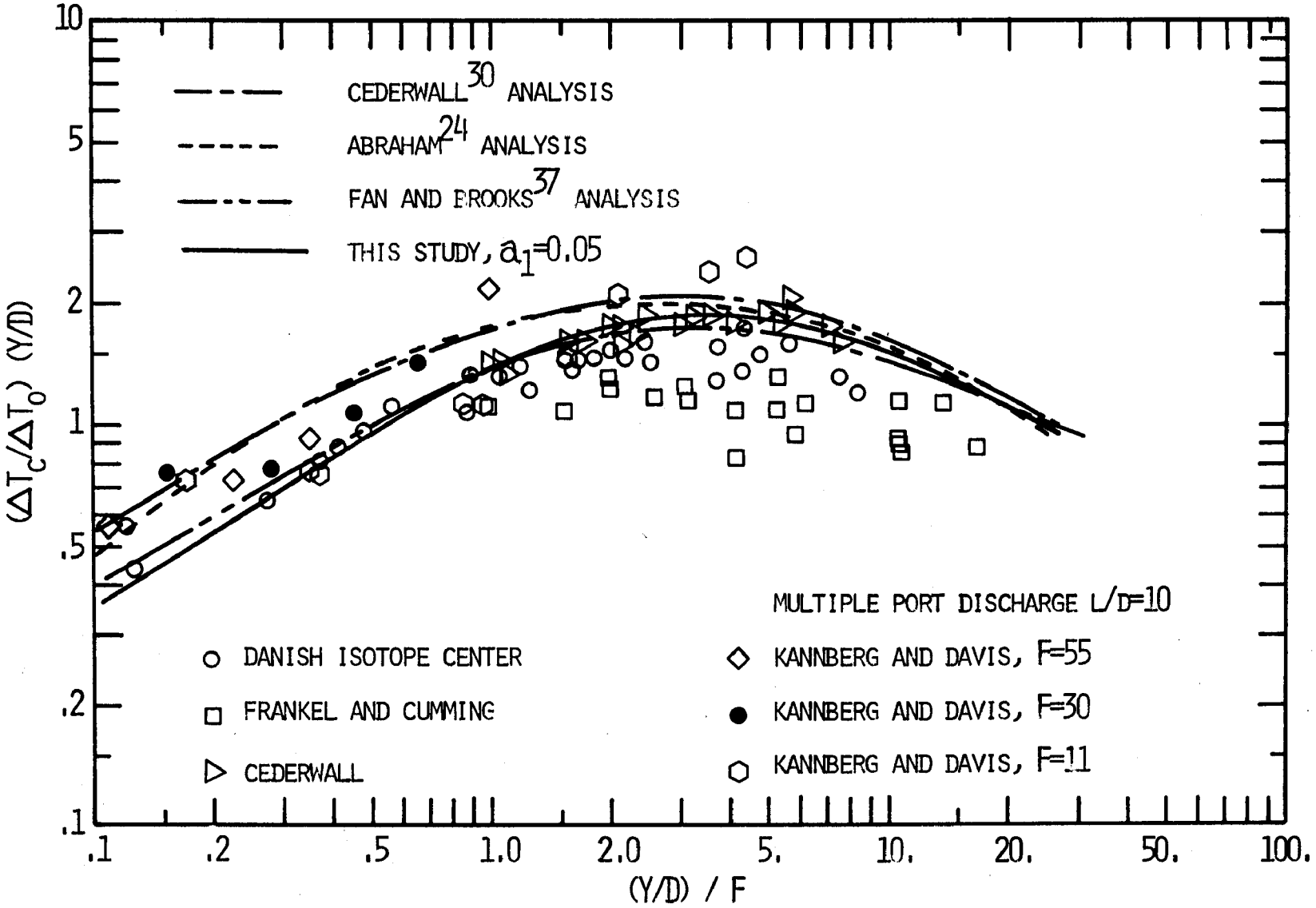

Figure 55. Model predictions and experimental data of dilution for single port discharges (original graph by Cederwall[30]).

Crossflow discharge provides the means of tuning the best value for c_3 and a_3. The primary source of experimental data concerning this discharge is Fan[25]. c_3 was obtained by tuning to match predicted starting lengths with the starting length curve offered by Hirst[18], $S_e = 6.2\ De^{-3.4R}$. This curve is the same one obtained by Fan[25] and given graphically for the data by Gördier[31] (c.f. Fan). The best value found for c_3 was 6.0. With this c_3 value, the starting lengths are as shown in Figure 56.

Considerable difficulty was encountered when trying to tune for a_3. The final value determined for a_3 was 11.5 and, as is pointed out in Figure 57, agreement with Fan's trajectory data for high and low current ratios is not exceptionally good.

The comparisons of dilution are somewhat hindered by the fact that experimental values were taken in the cleavage between the twin vortices observed. Hence the measured dilutions are depressed below the true profile maximums located at the centers of each vortex. The measured maximum concentration may be depressed as much as 65% from the vortex center concentration according to Fan's measurement. Liberty was taken to reproduce two figures presented by Fan in Figures 58 and 59. The profiles amply testify to the twin vortex structure and the depressed centerline values. No attempt was made to tune to these depressed measurements. However, as is seen in Figures 60-63, the centerline concentrations predicted by the model range from 45% to 100% higher than measured values depending on R. It can then be assumed that the program predicts the approximate local <u>maximum</u> concentrations likely to occur downstream from the crossflow discharge.

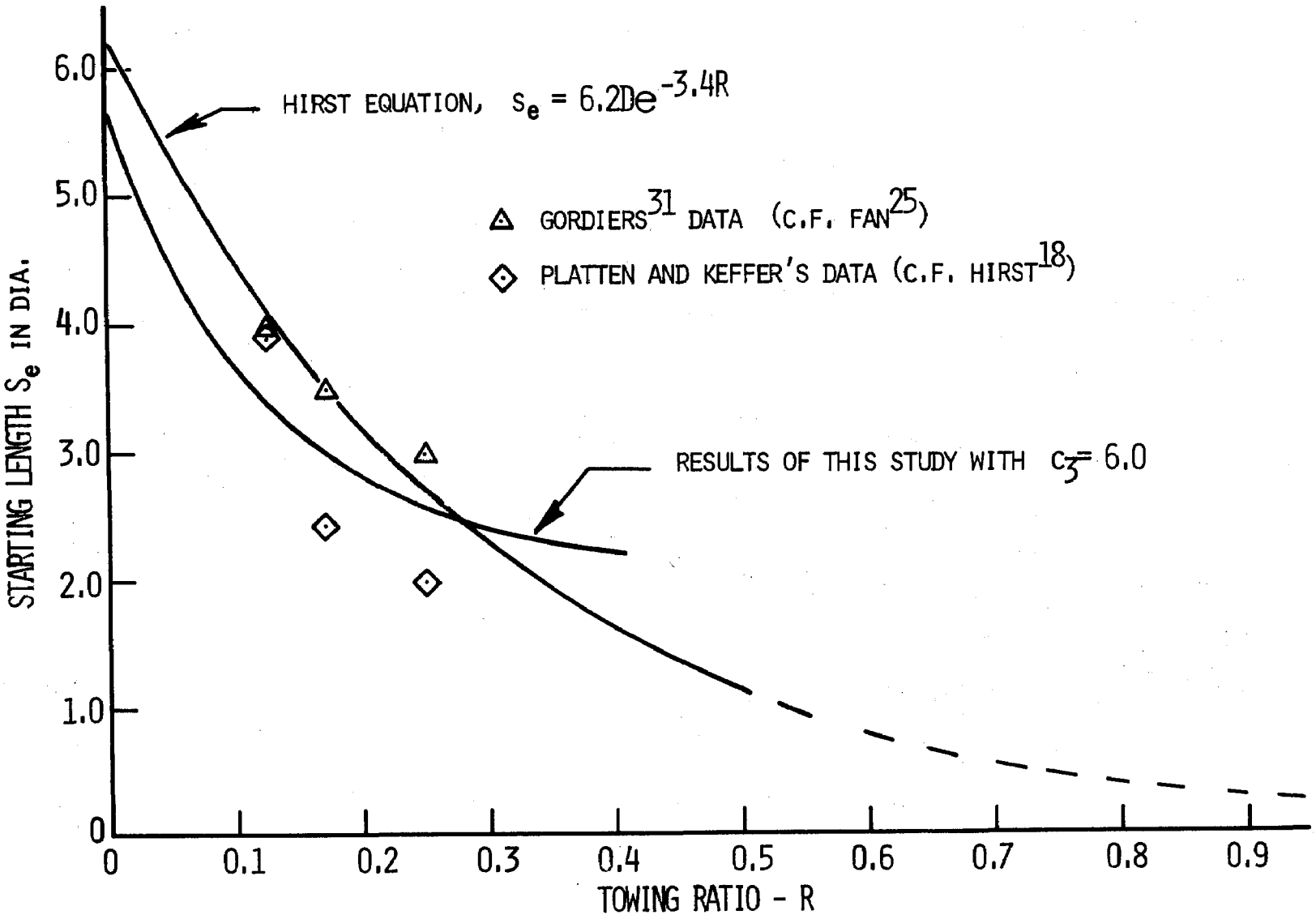

Figure 56. Model and experimental crossflow starting lengths.

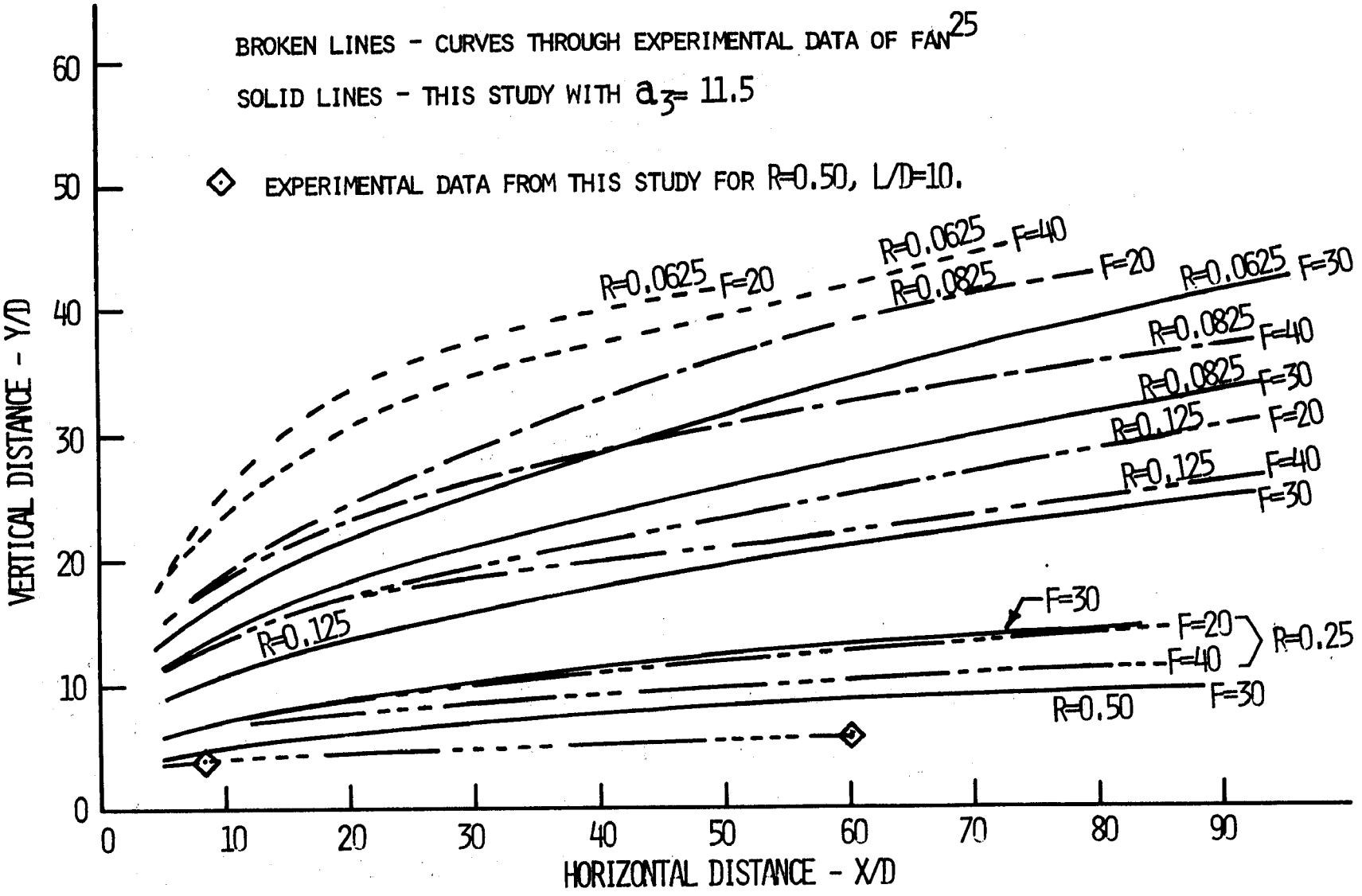

Figure 57. Crossflow model prediction and experimental data trajectory comparison.

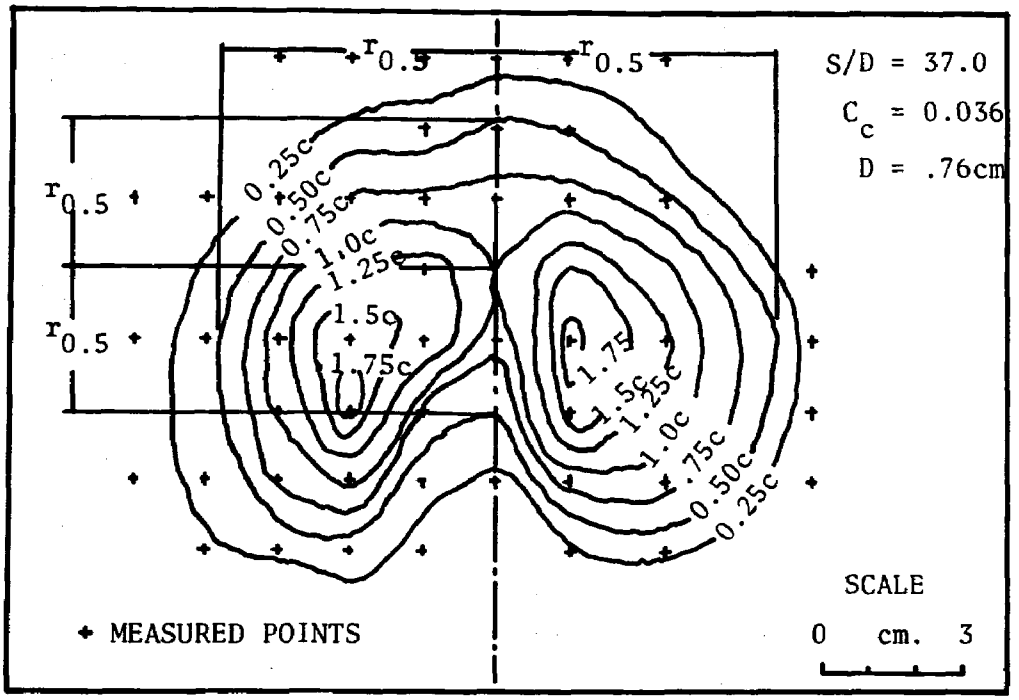

Figure 58. Concentration profile for F=20. and R=0.125. Ambient flow strikes plume from top of figure, (taken from Fan[25], pg. 127)

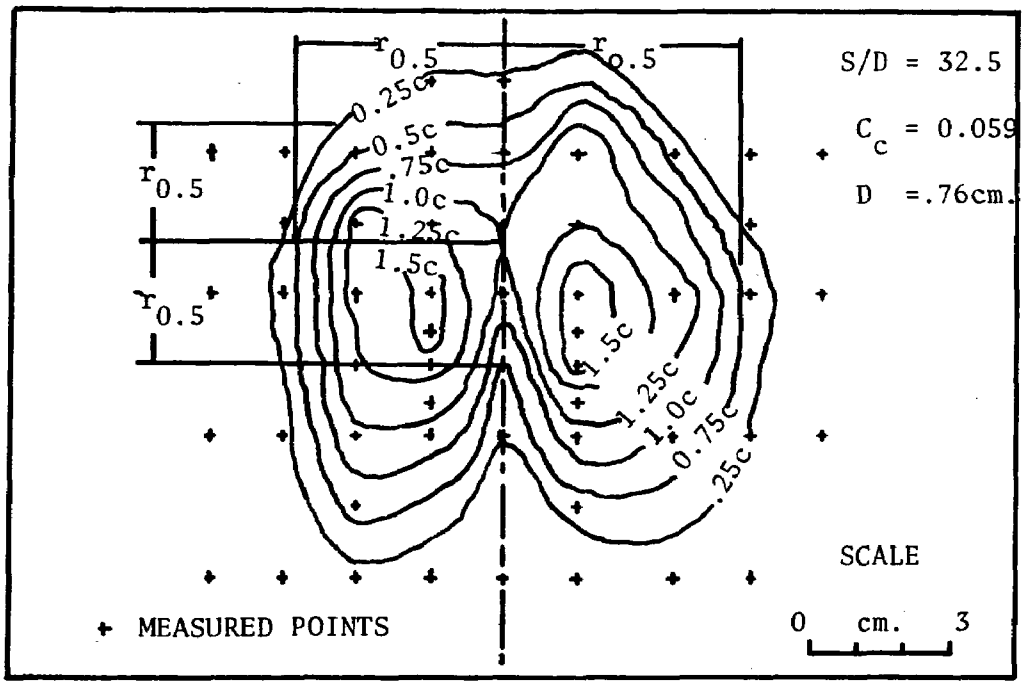

Figure 59. Concentration profile for F=40. and R=0.125. Ambient flow strikes plume from top of figure. (taken from Fan[25])

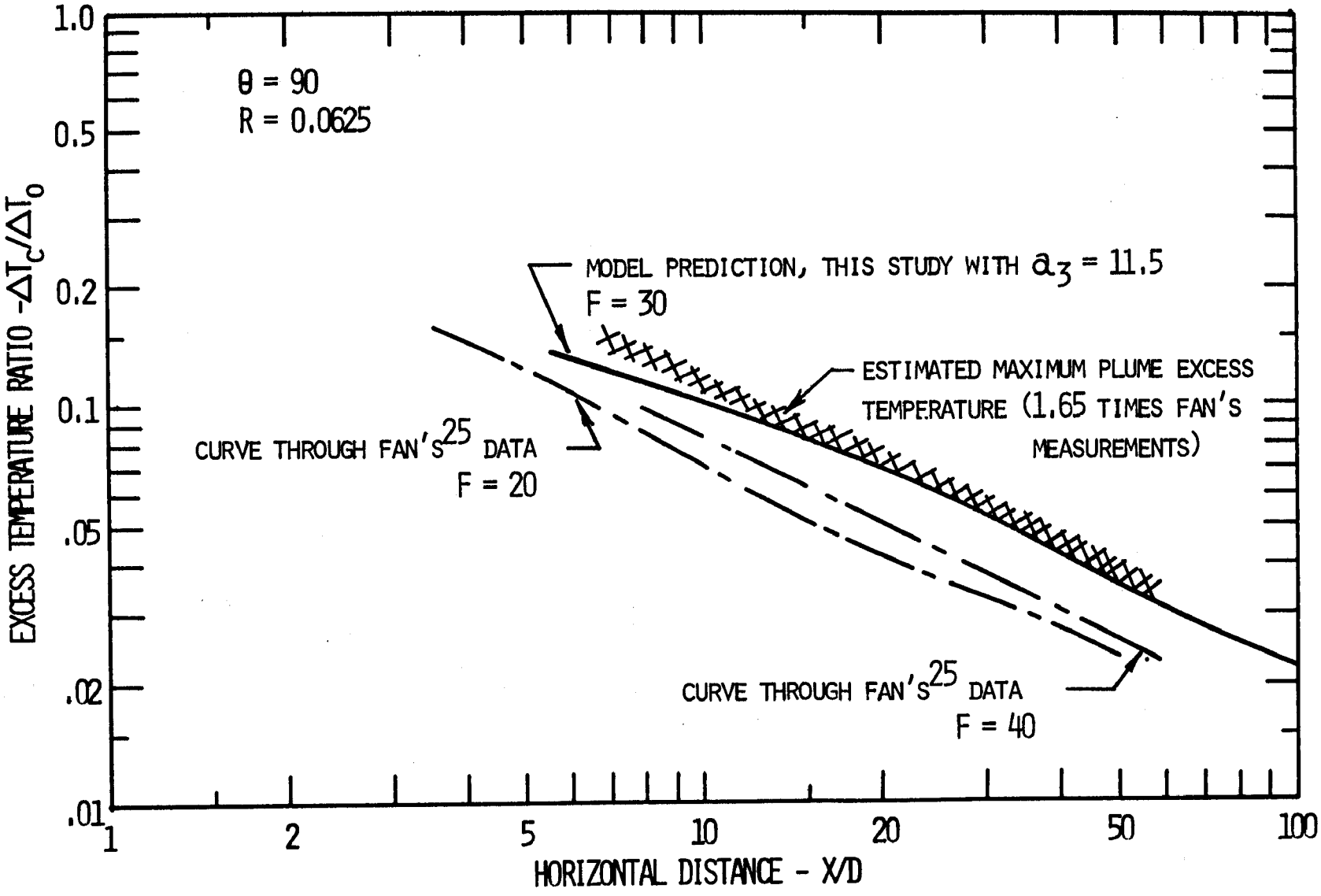

Figure 60. Dilution for crossflow discharge from a single port, R=0.0625, compared to Fan^{25}.

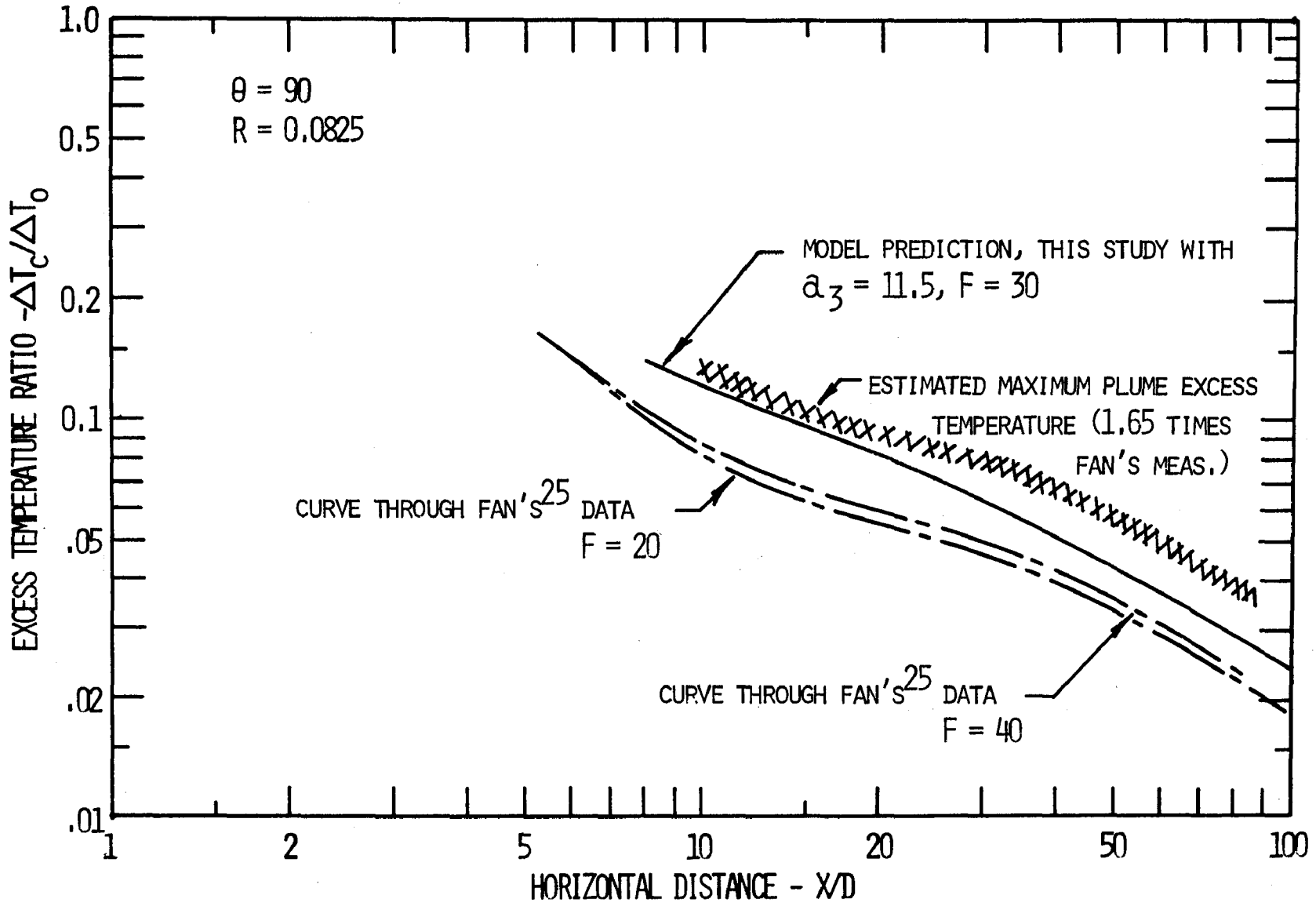

Figure 61. Dilution for crossflow discharge from a single port, R=0.0825.

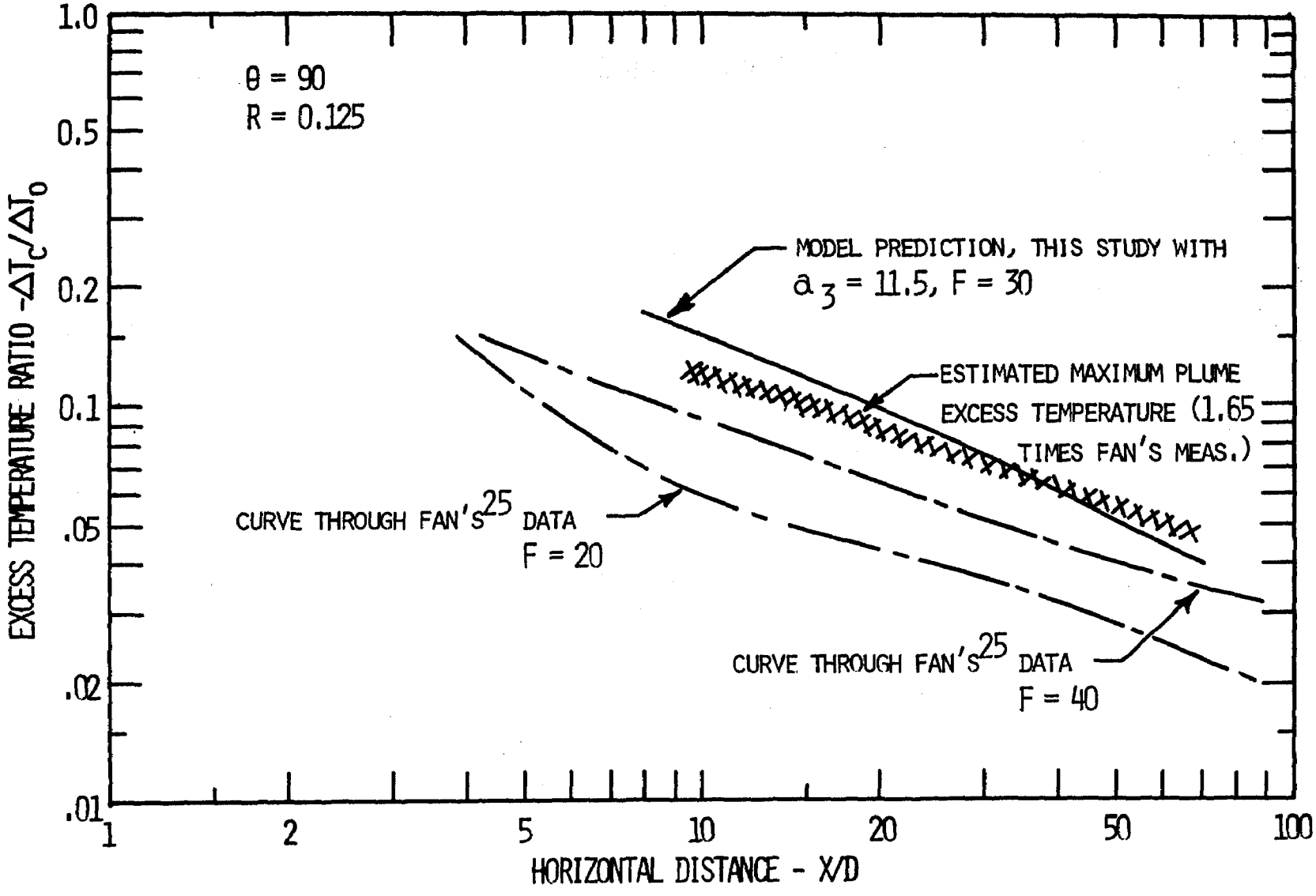

Figure 62. Dilution for crossflow discharge from a single port, R=0.125.

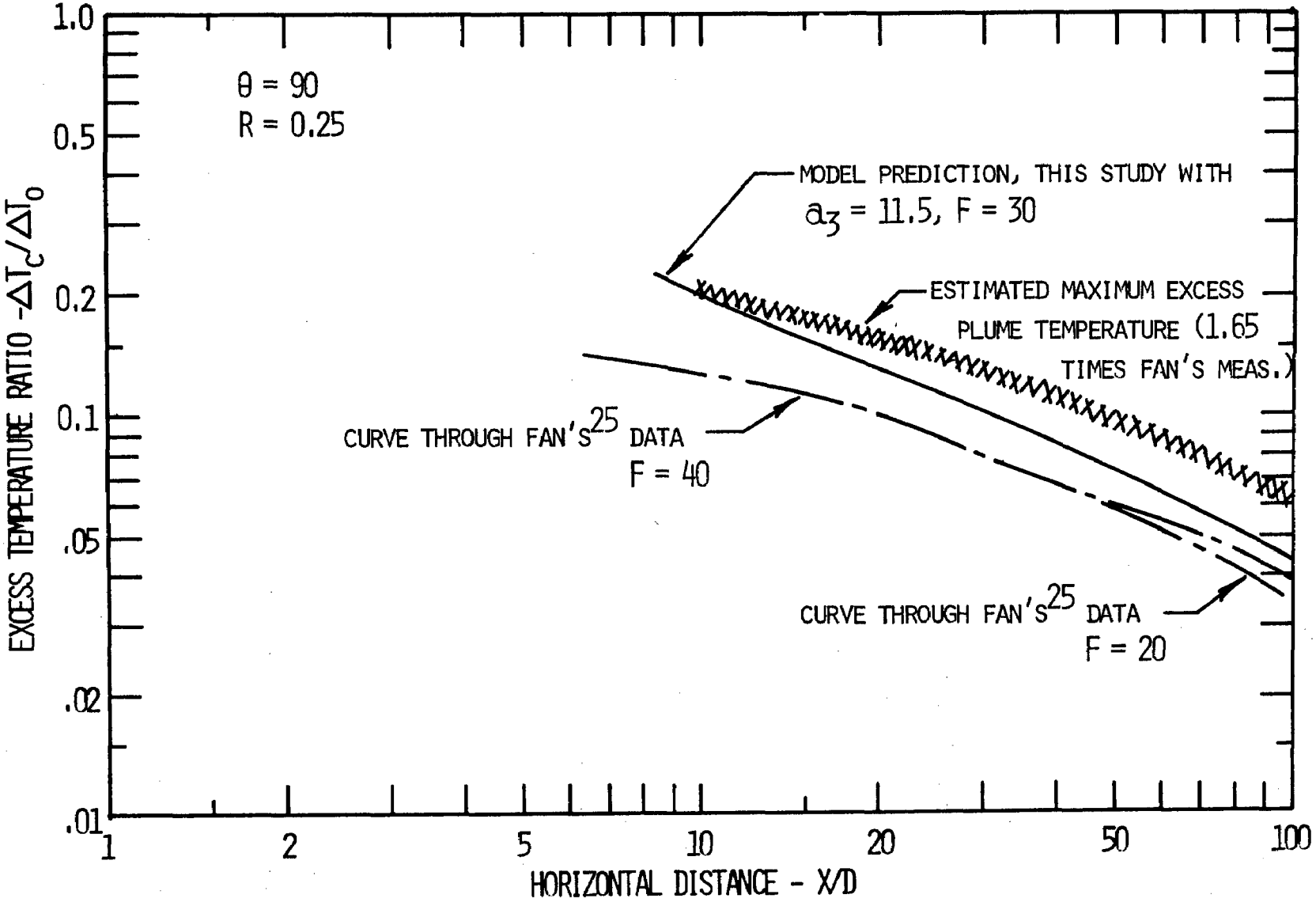

Figure 63. Dilution for crossflow discharge from a single port, R=0.25.

The inability to match the trajectory for several current ratios initiated a search for methods that would give better agreement. The drag force on the crossflow discharge was included (as was done by Fan), but the results were not an improvement. Likewise, several alterations were considered in the R sin θ_2 term of the entrainment function, notably, raising R to exponents other than one. While exponents of 3/2 and 2 gave good trajectory and dilution fits, there was no physical explanation as to why powers other than one should be employed. However, an argument based on the curvature and vortex action of the jet might provide better agreement and involve physical insight into the entrainment processes.

The twin vortices are probably generated by a combination of bending and edge shearing on the jet. The fluid at the edge of the jet is of lower axial momentum and hence is easily sheared downstream by the flowing ambient. As is well known, when fluid in a circular conduit is forced through a bend, the high velocity center fluid resists bending and pushes to the top of the bending conduit thereby forcing the slower fluid around the edge of the conduit to the bottom. Continued action of this sort results in twin vortices in the conduit and an increase in momentum loss due to viscous shear at the walls. In conduits the twin vortices have been observed to persist as far as 50 to 75 pipe diameters downstream (see Reference 32). The strength of the vortex may be measured by the curvature of the pipe.

The same action occurs in the jets discharged to a crossflow. Here the jet is bent over by the oncoming free stream rather than

the confines of the pipe, with the result being the formation of the twin vortices, increased entrainment and increased dilution. It is important to note that the increased entrainment and increased dilution are a result of the curvature induced vortex initiation and hence is not represented by the R sin θ_2 entrainment term.

Although inclusion of the effects of curvature and shear induced vortices in the entrainment function certainly seems desirable in light of the above discussion, care must be exercised. Certainly when curvature is high and a significant amount of warm, high velocity, centerline fluid is being pumped into immediate contact with the ambient, entrainment is going to be enhanced. But what about downstream? It has been stated that the vortex structure persists far downstream for pipe flow, and indeed for free twin vortices, as are formed in the wake of aircraft, the vortices decay as $x^{-1/3}$. However, Brown[33] notes that vortex wakes are found to grow at <u>much slower</u> rates than those of non-rotating wakes. It is now known that the rotation produces a certain stabilizing effect on the system and appears to cause a reduction in turbulent eddy diffusivity at least in the radial direction. Apparently, an entrainment term modeling curvature and shear induced vortices should be short lived axially.

An attempt was made to add a term to the entrainment function of the form $a_5 R \frac{d\theta_2}{ds}$, the thought being that additional entrainment due to initial vortex action would be proportional to the curvature as is indicated from pipe flow (see Reference 33).

The entrainment function would then be,

$$E = \left(a_1 + \frac{a_2}{F_L}\right)\left(b\left|u_c - U_\infty \cos\theta_2\right|\right)\left(1 - \frac{a_{4b}}{L}\right) + a_3 b U_\infty \sin\theta_2 + a_5 U_\infty b R \frac{d\theta_2}{ds} \quad . \quad (129)$$

The attempt failed due to instabilities in the predictor-corrector integration probably attributable to coupling between entrainment and the curvature equation. It is possible that another integrating scheme (Runge-Kutta for example) might not be plagued by these difficulties. A function, $\frac{.75}{R}\frac{\theta_{2o}-\theta_2}{s^2}$ which approximates $\frac{d\theta_2}{ds}$ to within 60% at all ambient to current ratios (0.05 to 0.50) $\left(\frac{d\theta_2}{ds}\right.$ ranges over three orders of magnitude for high towing rates$\left.\right)$ was tried. The trajectories and dilutions obtained, for cases where a_5 was 45 and a_3 was 5.0 are shown in Figures 64, 65, and 66. While agreement is quite good (remembering the depressed experimental concentration values) the term given above is an imprecise alternative for the $\frac{d\theta_2}{ds}$ term and without more refinement renders the results mere speculation. But the results using this term are promising. Until further investigation of initial entrainment in crossflow discharges, the curvature entrainment term remains unproven and therefore was not included in subsequent tuning work.

Co-flow discharge has presented prediction and tuning problems to nearly all modelers. Hirst[18] was able to get acceptable starting lengths (greater than experiment but very close to the curve given by Abramovich[28]). However, as pointed out by Shirazi, et.al.[21], the dilution trends are opposite those of experiment for R and Froude Number. Shirazi, et.al.[21] proceed to include the boundary turbu-

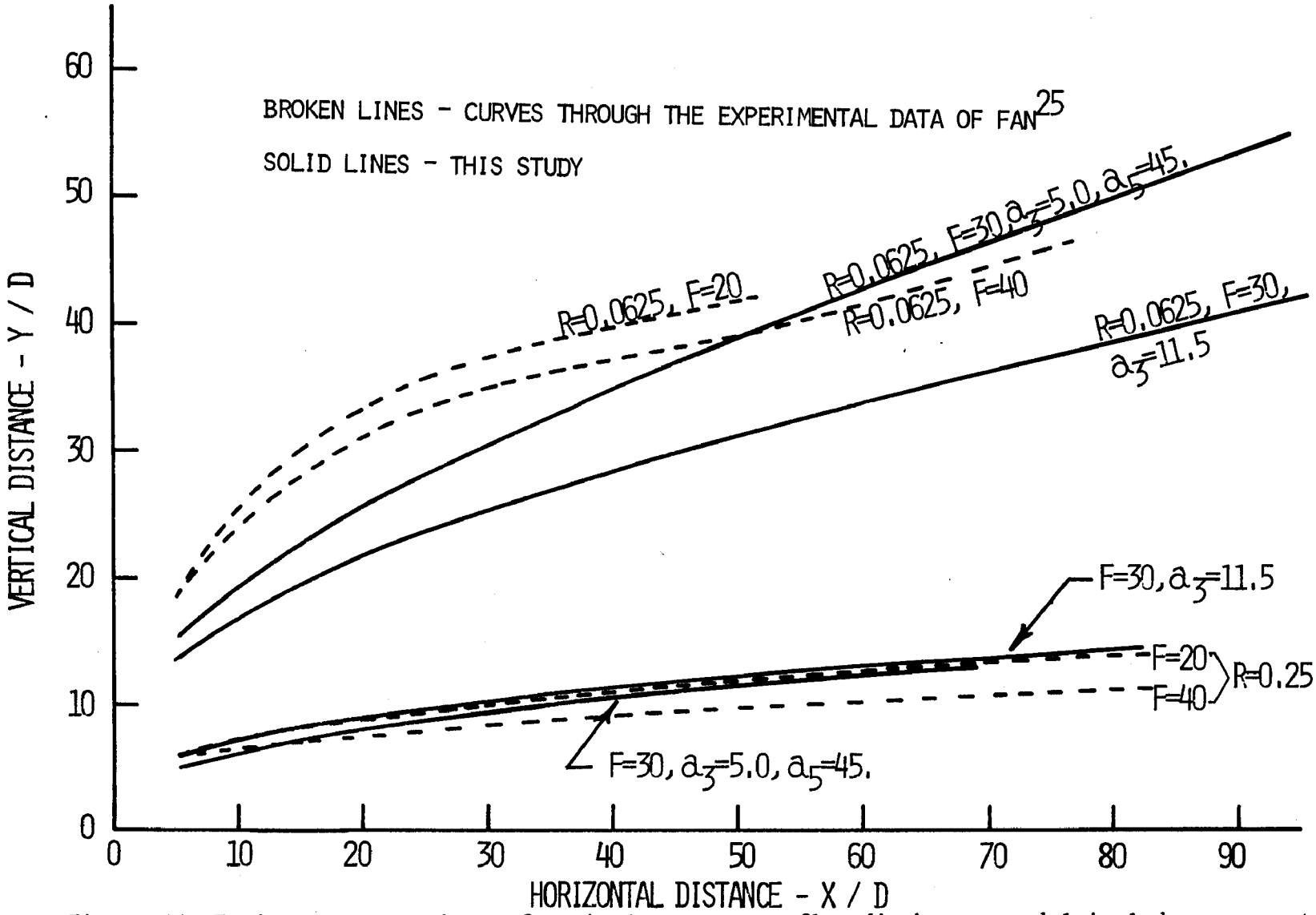

Figure 64. Trajectory comparisons for single port crossflow discharge, model includes a curvature term in the entrainment function.

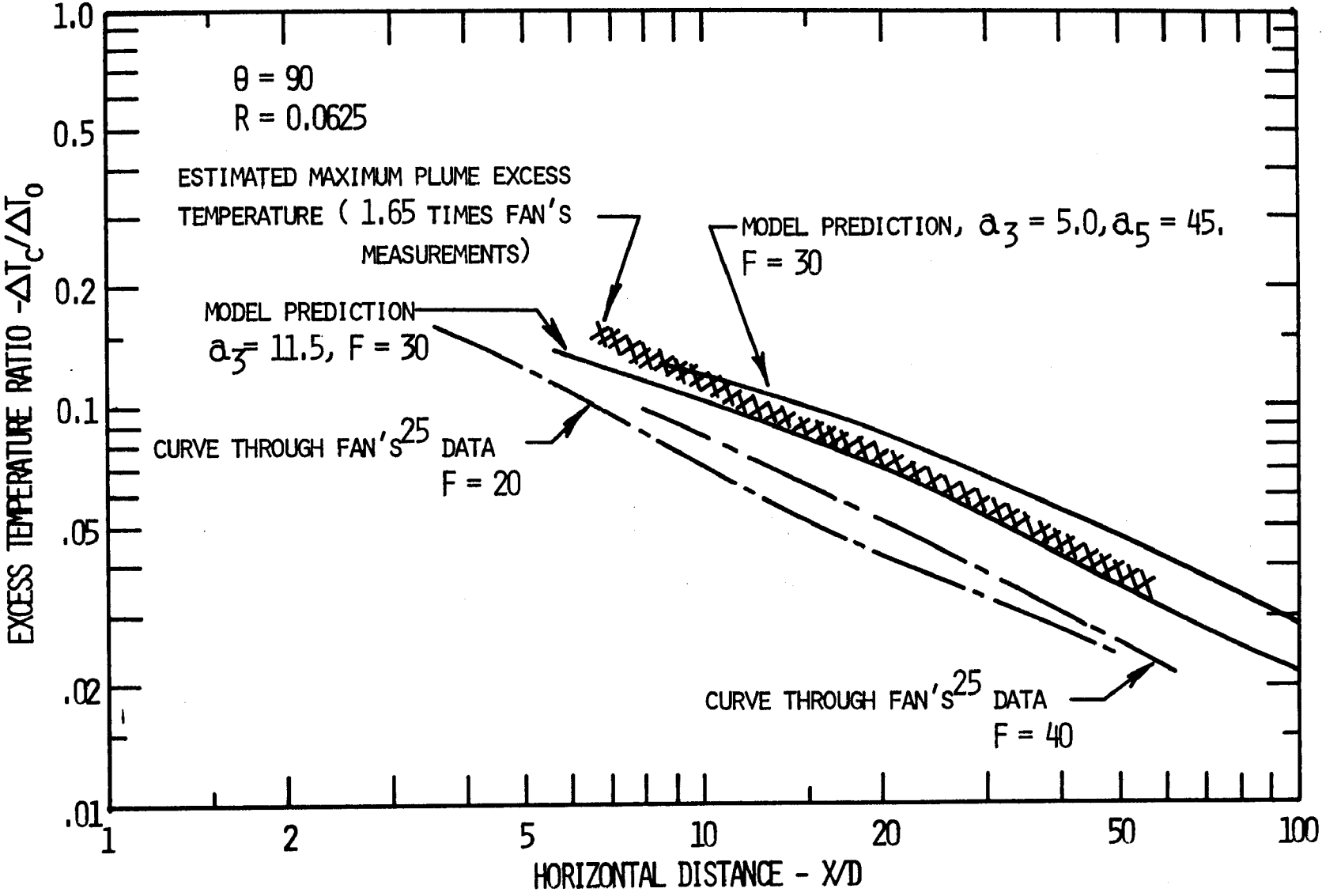

Figure 65. Dilution comparisons for single port crossflow discharge. Curves include predictions by the model with a curvature term in the entrainment function, R=0.0625.

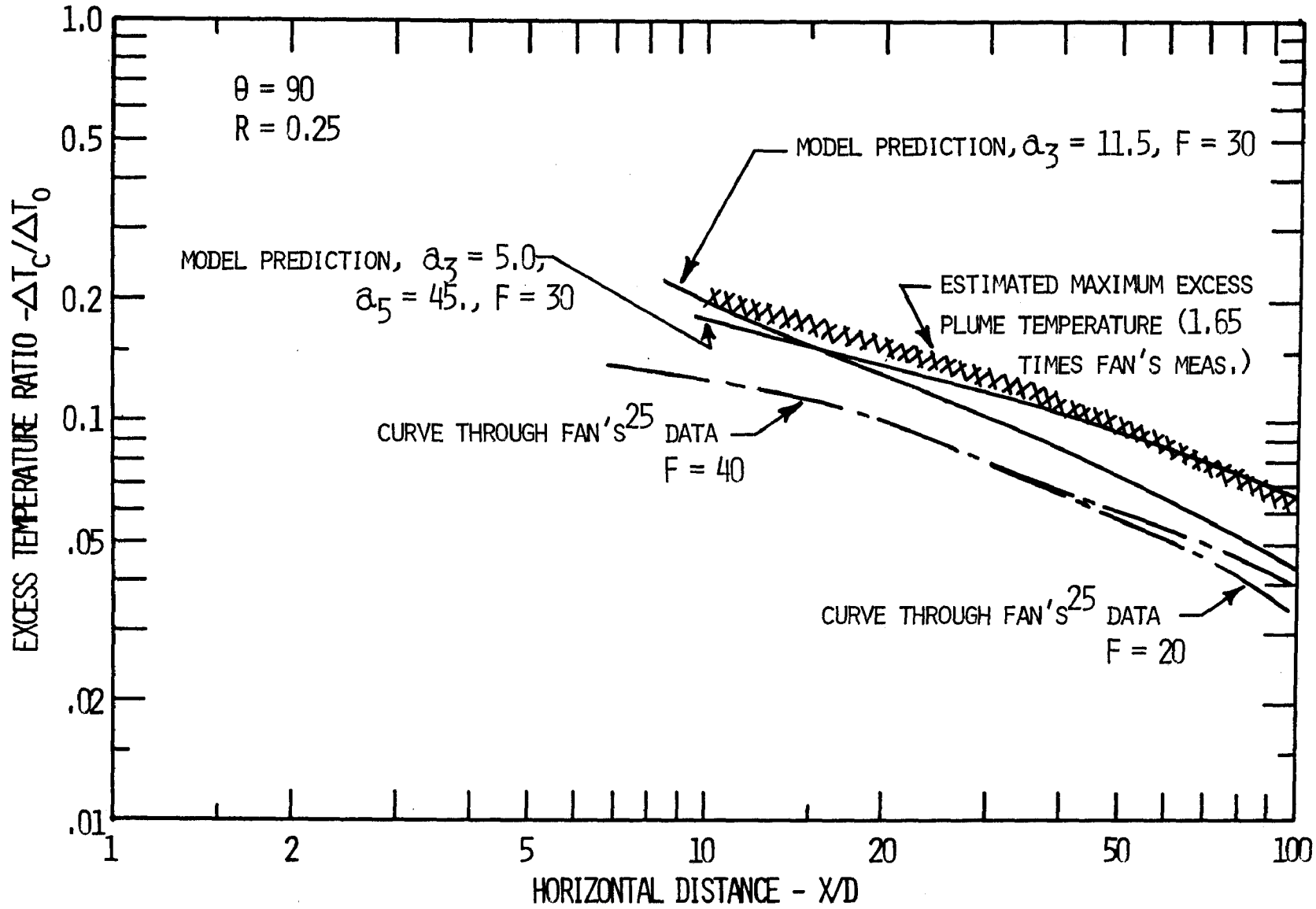

Figure 66. Dilution comparisons for single port cross flow discharge. Curves include predictions by the model with a curvature term in the entrainment function, R=0.25.

lence terms discussed earlier and obtain acceptable agreement although artificially high turbulence values were needed. Without turbulence terms the merging model predicts starting lengths which greatly exceed both Hirst's predictions and experiment. It was necessary to include the boundary turbulence terms discussed earlier in order to diminish starting lengths and get the proper dilution trends with R. The effects of including boundary turbulence terms on the starting length for the merging model are shown in Figure 67. The higher the values of $\sqrt{\overline{u'^2}}/U_\infty$, the greater the boundary turbulence. Included in Figure 67 are correlations and experimental data of other authors. While there appears to be some disagreement in the exact values of the starting length, there is little doubt of its trend with R. This trend makes it quite difficult to match experimental data beyond the starting length since the starting length increases with R while the downstream concentration decreases with R. The best results (shown in Figure 68) are not very satisfactory, however, they are an improvement over results without turbulence terms and it appears that the values of $\sqrt{\overline{u'^2}}/U_\infty$ which give the improved fit are near those obtained experimentally by McQuivey, et.al.[19] (McQuivey, et.al., found $\sqrt{\overline{u'^2}}/U_\infty$ to be about 0.033 for discharge to a smooth walled flume, the value giving "ball park" dilutions for the model is 0.025 (although comparison is rather difficult without accurate starting lengths).

The results of Forstall and Shapiro[38], also shown in Figure 68, are somewhat misleading since the dilution is reduced with increasing velocity ratio, R. The studies offered by Shirazi, et.al.[20]

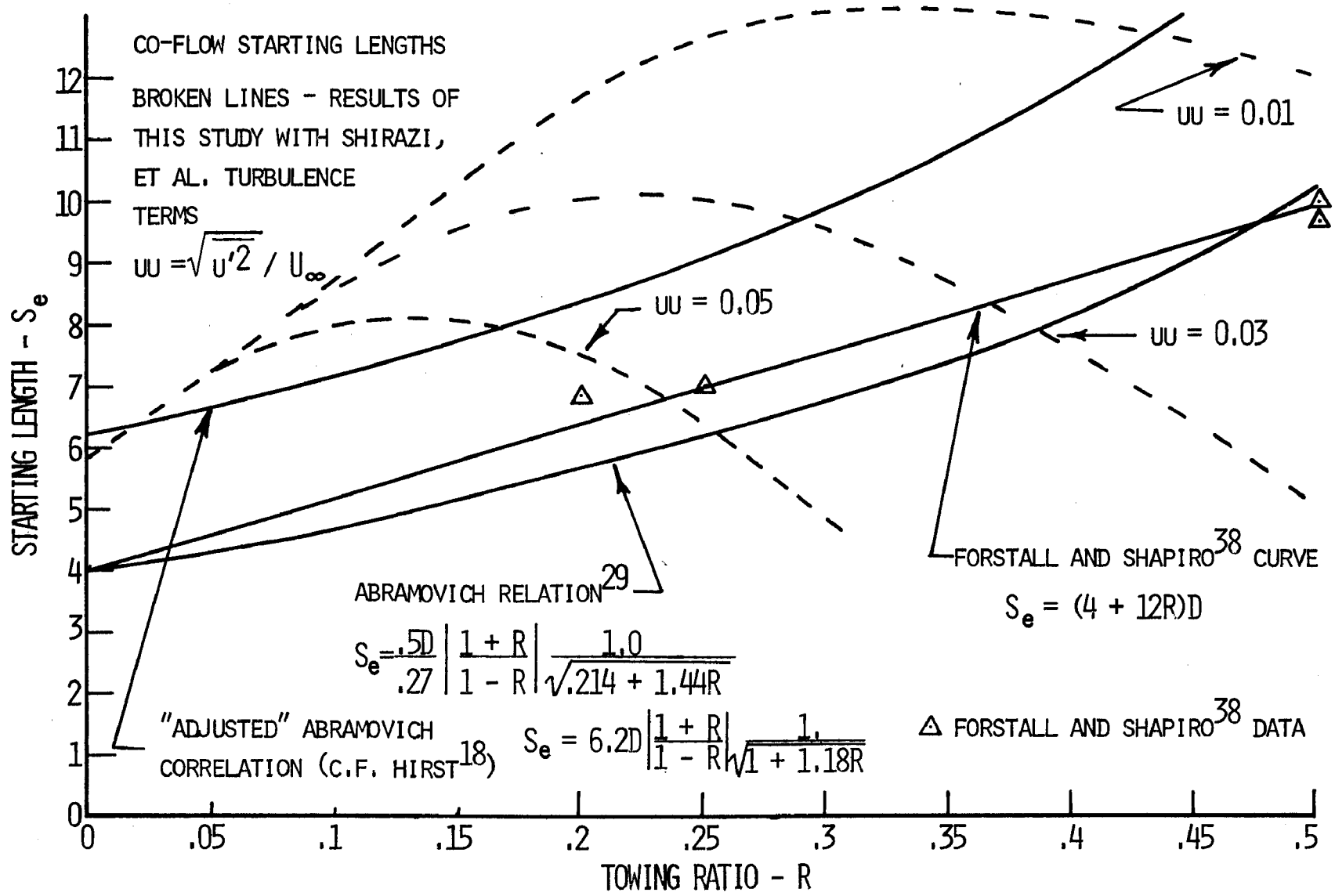

Figure 67. Co-flow starting length comparison, single port discharge, model contains the turbulence terms.

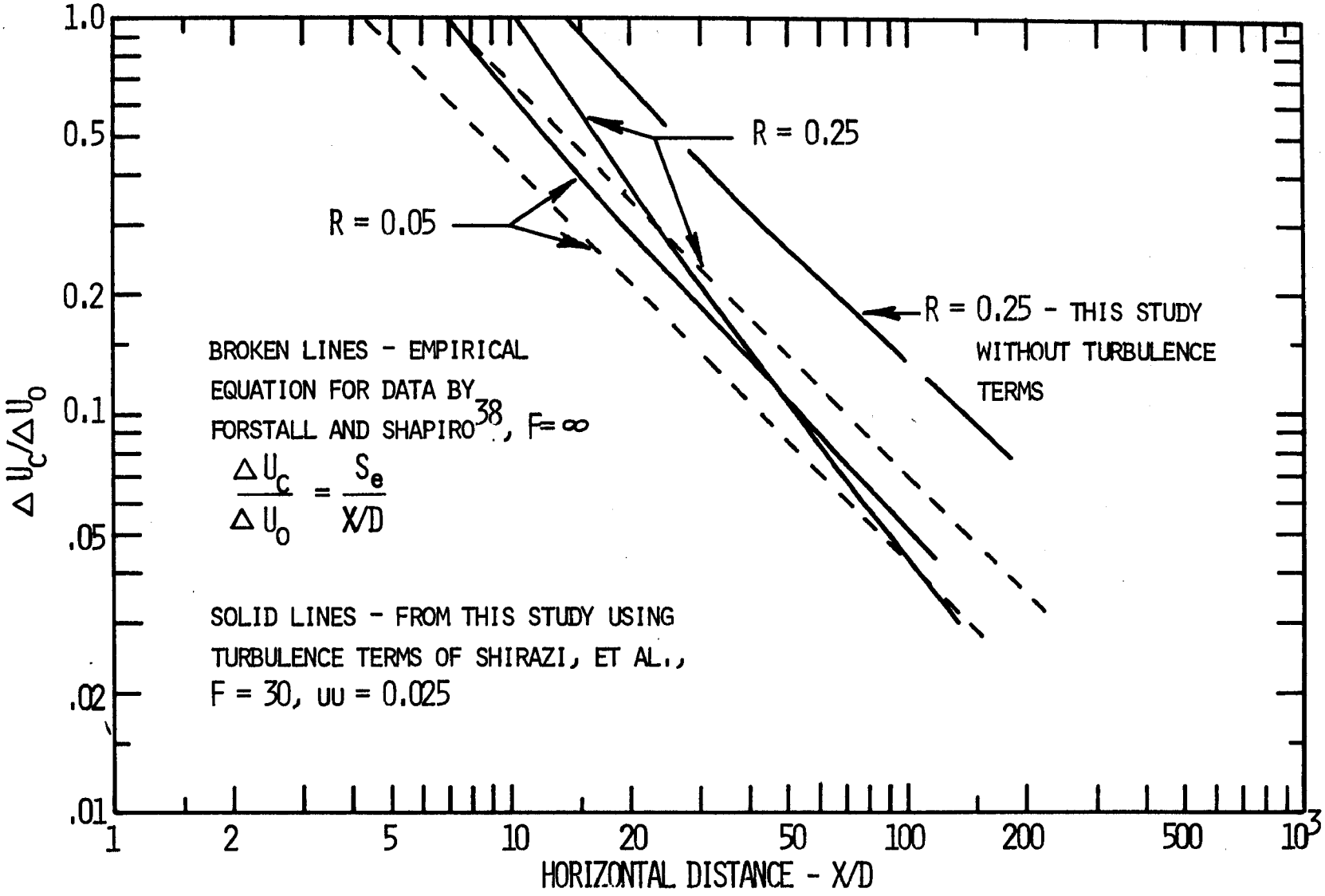

Figure 68. Velocity dilution for co-flow single port discharge, the model employs turbulence terms.

as well as Chassi and Winiarski[36] give the opposite trend for co-flow discharge. Some results of the experimental work presented earlier in this text are given in Figure 69. These results definitely show the dilution increasing with increasing velocity ratio, R.

Shirazi, et.al.[21] speculate that more satisfactory model prediction would be obtained if the turbulence were included in the entrainment function. The results given in the present study seem to support this speculation. However, too many unsupported assumptions are necessary in the formulation of the boundary turbulence terms used here to provide any confidence in the method. In the present study, for R>0.10, the velocity decayed faster than the concentration in the zone of flow establishment. This may be due to the scaling of the turbulent terms, however, there may be many other causes.

In any event, co-flow discharges cannot as of yet be accurately predicted, although ball park numbers and trends may be duplicated.

The only coefficients remaining to be tuned are a_4 (a_4') and c_4 associated with the effect of merging plumes. It is reasonable to expect that the entrainment should be near that for a single round port before merging begins and near that of a slot jet after a long period of merging. If one takes the single round port entrainment to be $E_r = 2\pi a \Delta u_c b$ (a is the entrainment coefficient) as suggested by Morton, et.al.[4], one sees that $\frac{E_r}{\Delta u_c} \propto b$. If the slot jet entrainment is taken as $E_s = 2Le_s\Delta u_c$ as suggested by Fan and Brooks[37], and Koh and Fan[13] as well as others, with $e_s = 0.16$, then

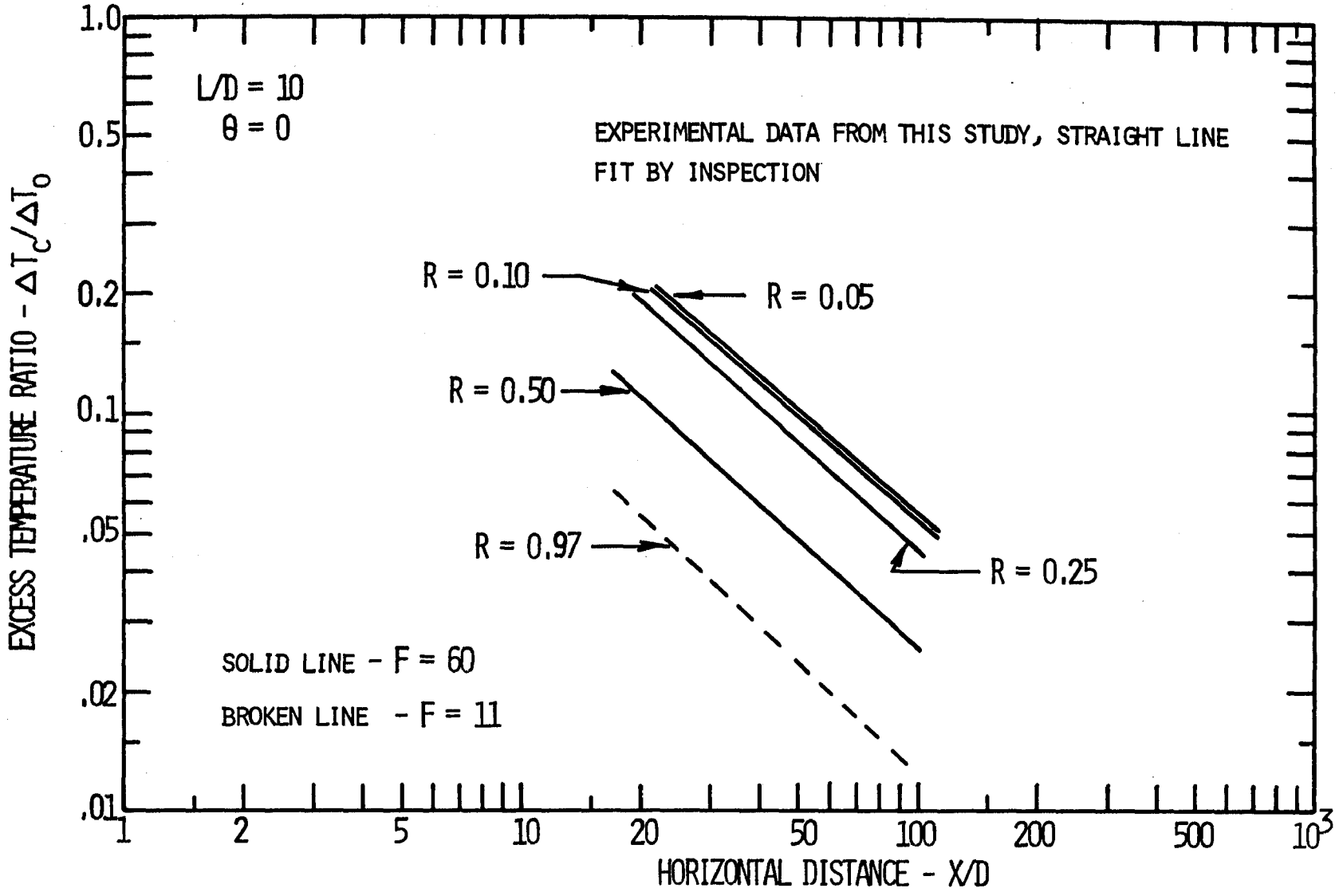

Figure 69. Experimentally obtained co-flow thermal dilutions of this study for L/D=10 and various R's.

$\frac{E_s}{\Delta u_c} \propto L$ and is constant for any L. It would seem plausible that the entrainment should move smoothly from the round port case to the slot case as merging progresses. The value of these functions may be graphed along with that of the Davis[17] "entrainment surface" entrainment function. Such a graph is shown in Figure 70. Here a = 0.043, e_s = 0.16 and L is taken to be 5. As can be seen, the round port entrainment continues to grow as the entraining area $2\pi b$ grows. The slot jet entrainment remains constant since its entrainment area is constant and the Davis[17] "entrainment area" function (which starts at b = L/2) diminishes to a constant since the available entrainment area of the merging jets diminishes to a constant. It is noticed that the Davis entrainment function is only about 27% of the slot entrainment function in the limit as b approaches infinity.

The Davis entrainment function was employed with a_4 and c_4 tuned to give the most satisfactory agreement with experimental data. When tuning the model for the merging jets, the model predictions were matched against the crossflow experimental data. The values found most suitable were a_4 = 0.2 although the results did not allow for good comparison of c_4 values and a_4 = 0.0 would probably yield nearly identical results over the range of comparison. When tuning to crossflow discharges, it was found necessary to include the drag force analysis previously used by Fan[25]. Since no such drag force was necessary for the single port case, the drag force was written in the following manner:

Zone of Flow Establishment, $F_D = \frac{C_D}{L/D} U_\infty{}^2 N/2$, (130)

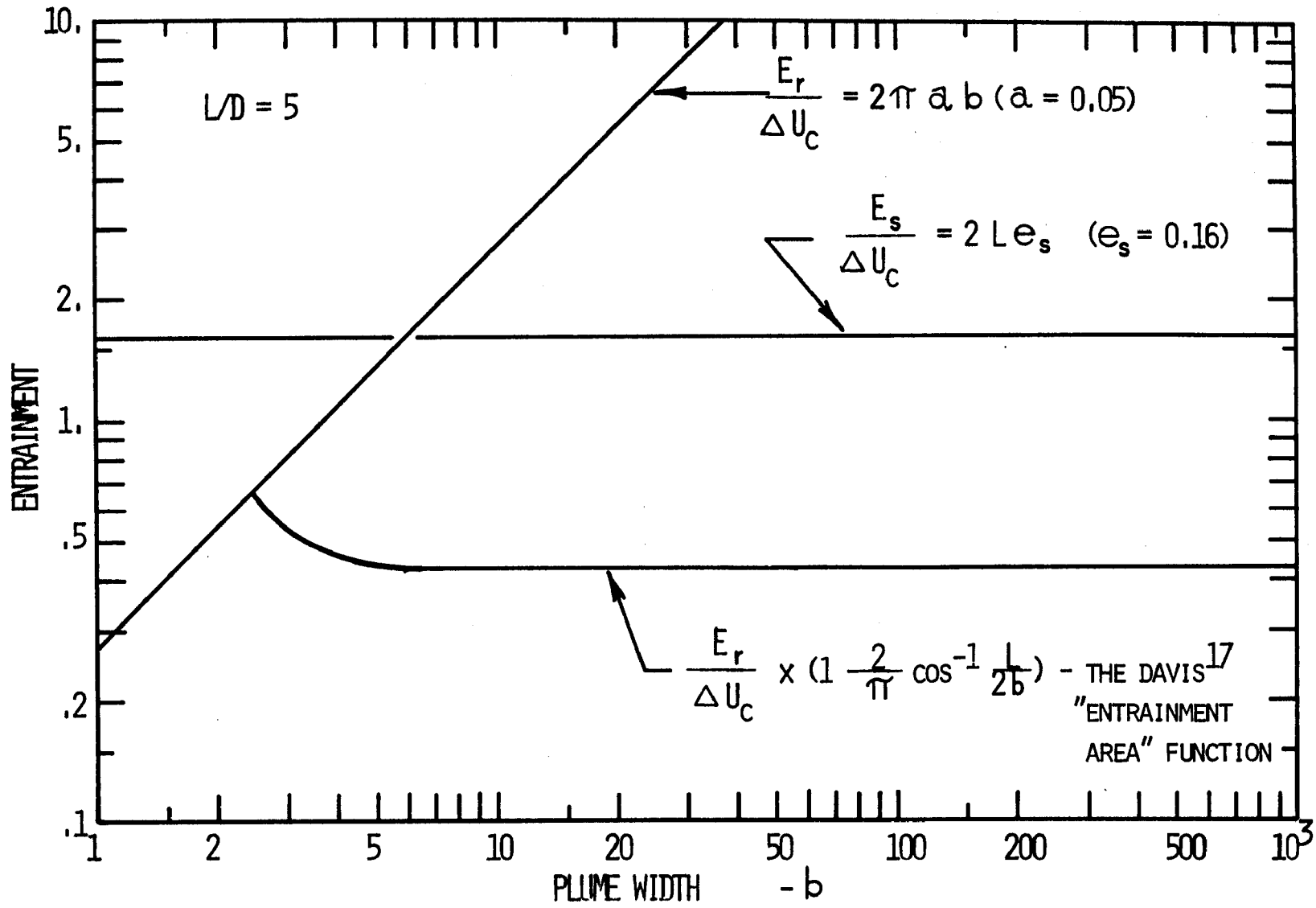

Figure 70. The value of various entrainment models as plotted against plume width b.

where

$$N = N_1^2 + N_2^2 + N_3^2 \quad ,$$

and

$$N_1 = -\cos^2\theta_2 \sin\theta_1 \cos\theta_1 \quad ,$$

$$N_2 = \sin^2\theta_2 + \cos^2\theta_2 \cos^2\theta_1 \quad ,$$

$$N_3 = -\sin\theta_2 \cos\theta_2 \sin\theta_1 \quad ;$$

Zone of Single Plume Established Flow,

$$F_D = \frac{C_D b^2}{L} U_\infty \frac{N}{2\pi} \quad , \quad (131)$$

where N, N_1, N_2, and N_3 are the same as above;

and the Zone of Merging Plumes,

$$F_D = C_D L U_\infty^2 \frac{N}{2\pi} \quad , \quad (132)$$

where N, N_1, N_2, and N_3 are the same as above.

The only equations which change are the curvature equations.

These now become

$$\frac{d\theta_1}{ds} = \left(EU_\infty \cos\theta_1 + F_D \frac{\left(\sin^2\theta_2 + \cos^2\theta_2 \cos^2\theta_1 - \sin^2\theta_1 \sin^2\theta_2\right)}{\cos\theta_1} \right) \Big/ \bar{q} \cos\theta_2 \quad , \quad (133)$$

and

$$\frac{d\theta_2}{ds} = \left(g \int \left[\beta\left(\bar{T} - \bar{T}_\infty\right) + \gamma\left(\bar{C} - \bar{C}_\infty\right) \right] r\,dr \cos\theta_2 - \left(EU_\infty + F_D\right) \sin\theta_1 \sin\theta_2 \right) \Big/ \bar{q} \quad . \quad (134)$$

In the expression for F_D, the drag coefficient, C_D, must be determined. The values of C_D which gave reasonable agreement were $C_D = 3.0$ for $R = 0.10$, and $C_D = 0.70$ for $R = 0.50$. The trajectories obtained with these values are given in Figures 71, 72, and 73, for L/D values of 2.5, 5., and 10. respectively. As can be seen, the model matches the data for the most part, especially for what would be moderate Froude Numbers. However, there appears to be a significant change in trajectory with Froude Number for the model predictions. The effect of Froude Number is not nearly as noticeable in the experimental data. One also notes that the plume seems to follow a straight line trajectory after the jet is initially bent over. The straight line represents a balance between the drag force, buoyancy force, and added vertical momentum due to entrainment. Additional experimental data further downstream would have been useful in assessing this effect.

The dilution comparisons are given in Figures 74-79 for various L/D's. In general, the predicted excess temperature concentrations match the data quite well. At L/D = 10 the dilution is greater in experiment than prediction. But this is probably due to the depressed temperature measurements made between the twin axial vortices. It is expected that as merging proceeds this vortex structure would be broken down. The improved thermal dilution agreement at closer spacings tends to support this idea.

The results of tuning the merging coefficients would be much more satisfactory if the drag coefficient were a single value for all flows. The model employed by Fan[25] also utilized a drag coefficient, and the value he found necessary to match experiment also

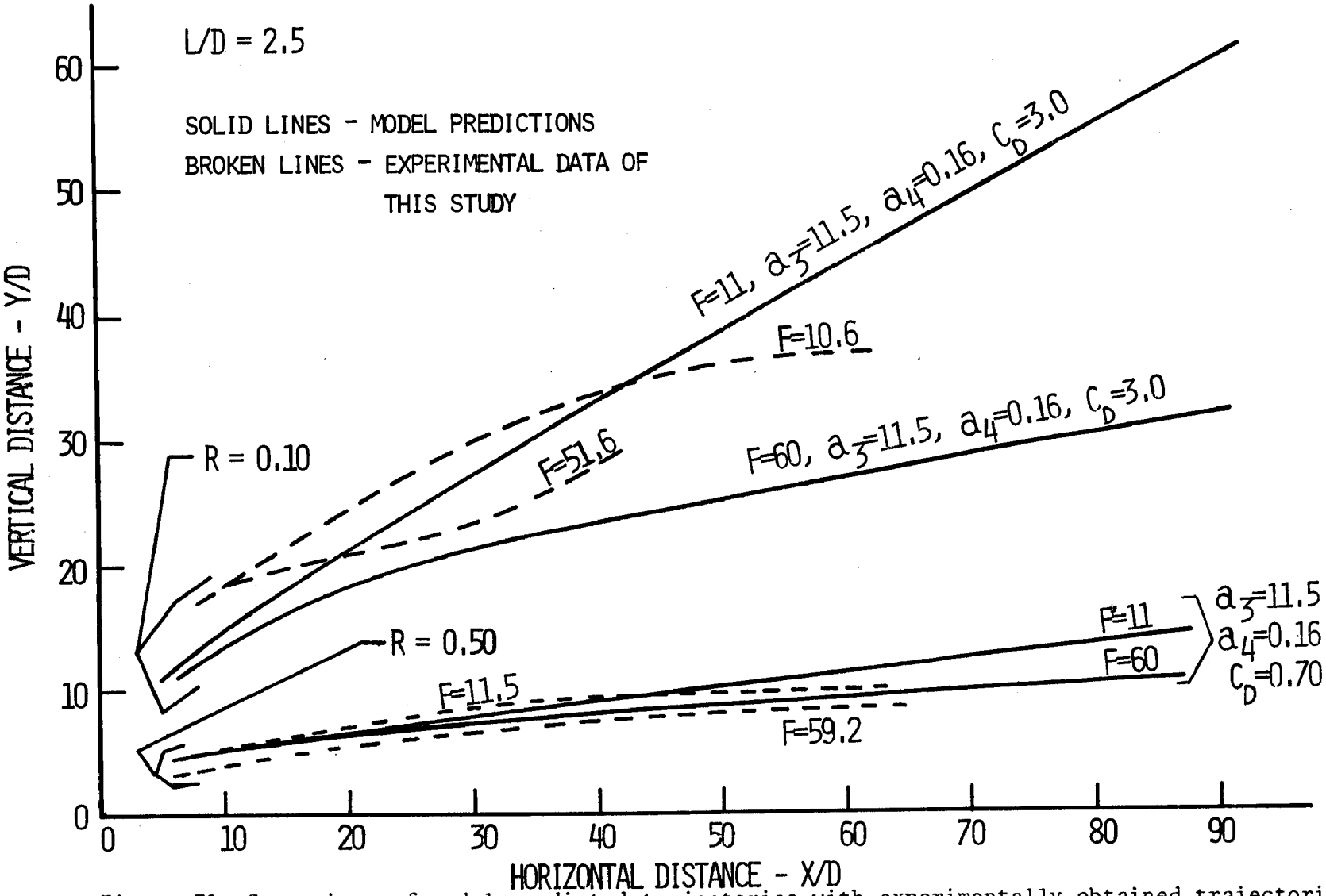

Figure 71. Comparison of model predicted trajectories with experimentally obtained trajectories for L/D=2.5, crossflow discharge.

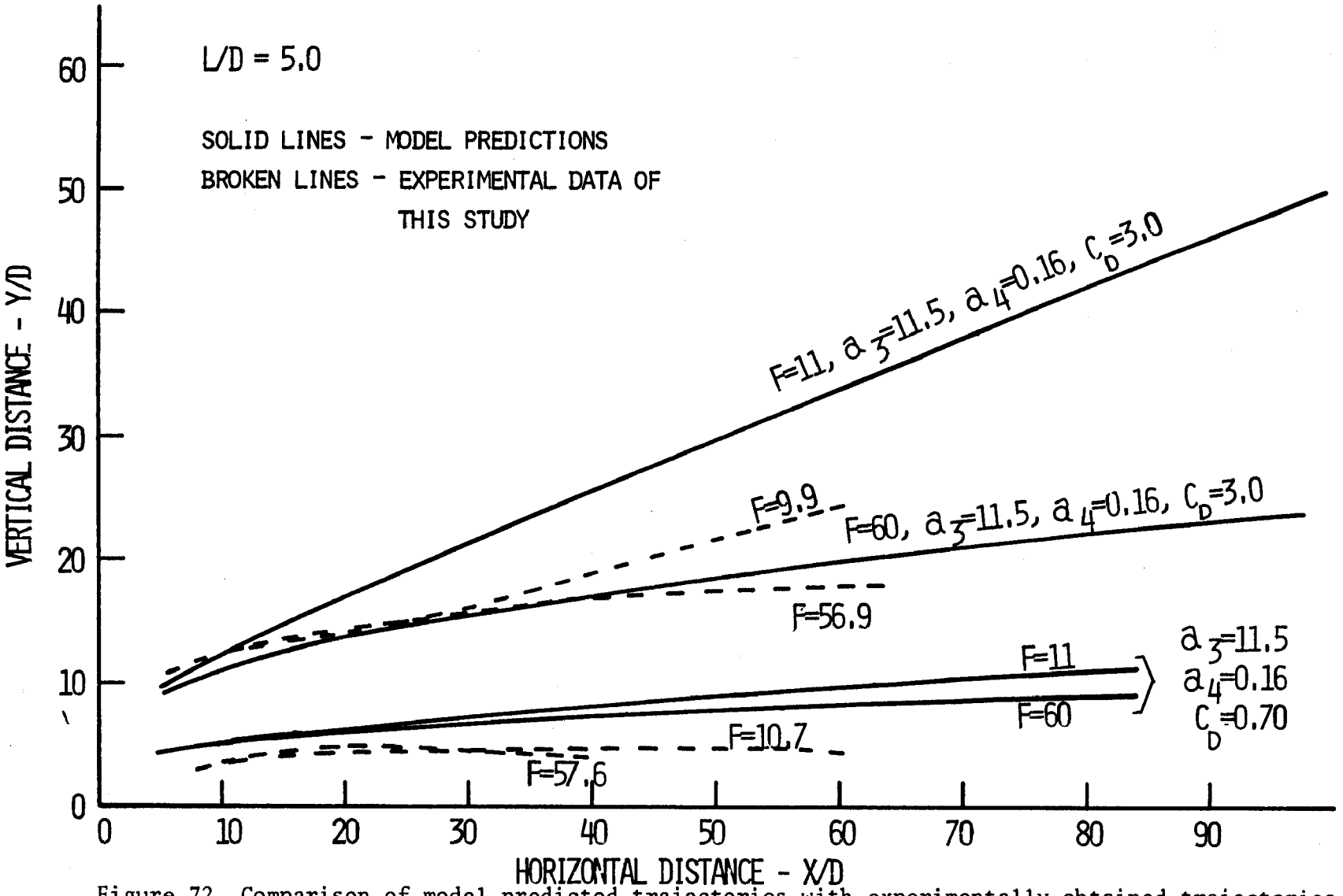

Figure 72. Comparison of model predicted trajectories with experimentally obtained trajectories for L/D=5.0, crossflow discharge.

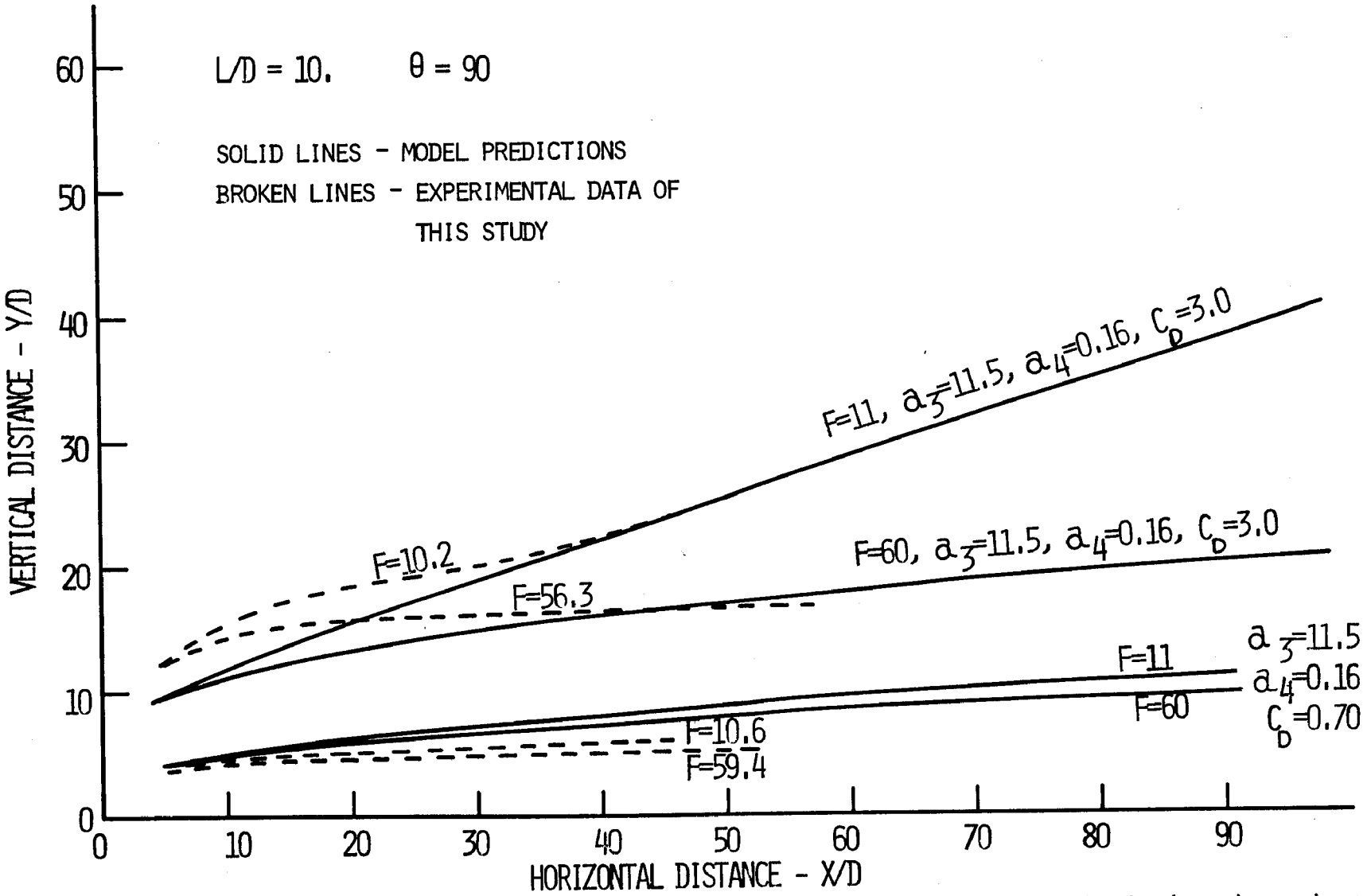

Figure 73. Comparison of model predicted trajectories with experimentally obtained trajectories for L/D=10, crossflow discharge.

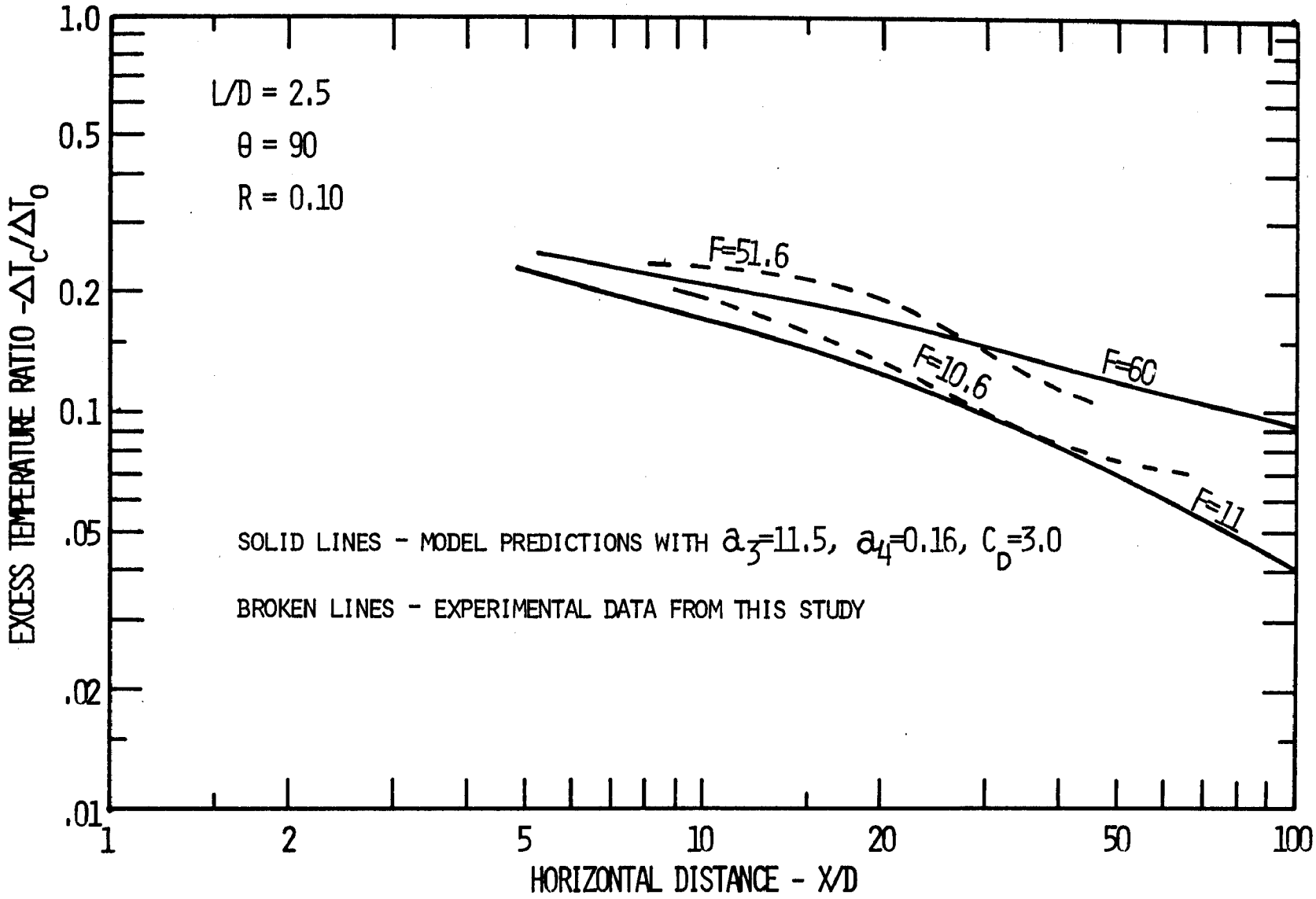

Figure 74. Comparison of experimental and model predicted excess temperature for L/D=2.5, R=0.10, crossflow discharge.

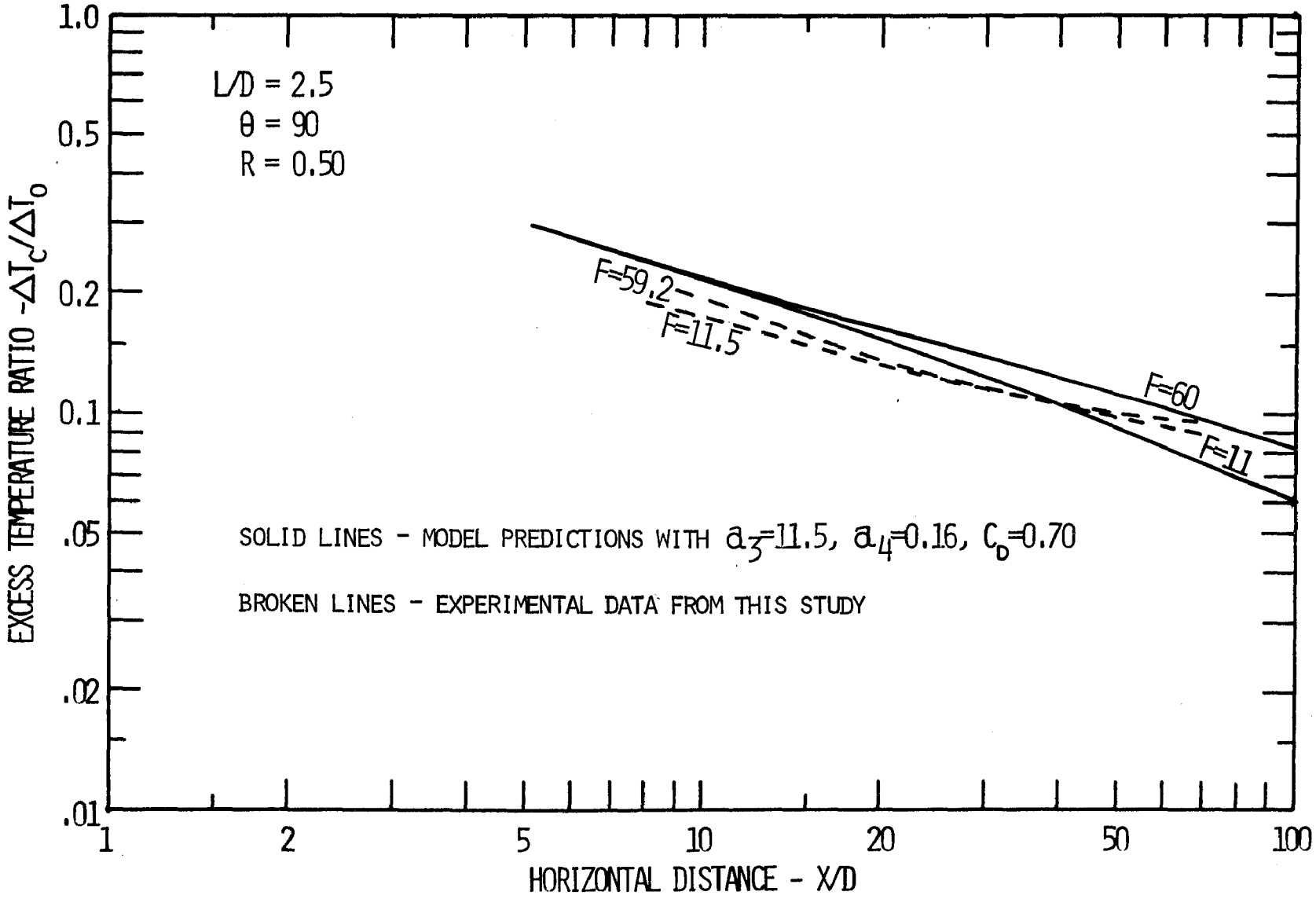

Figure 75. Comparison of experimental and model predicted excess temperature for L/D=2.5, R=0.50, crossflow discharge.

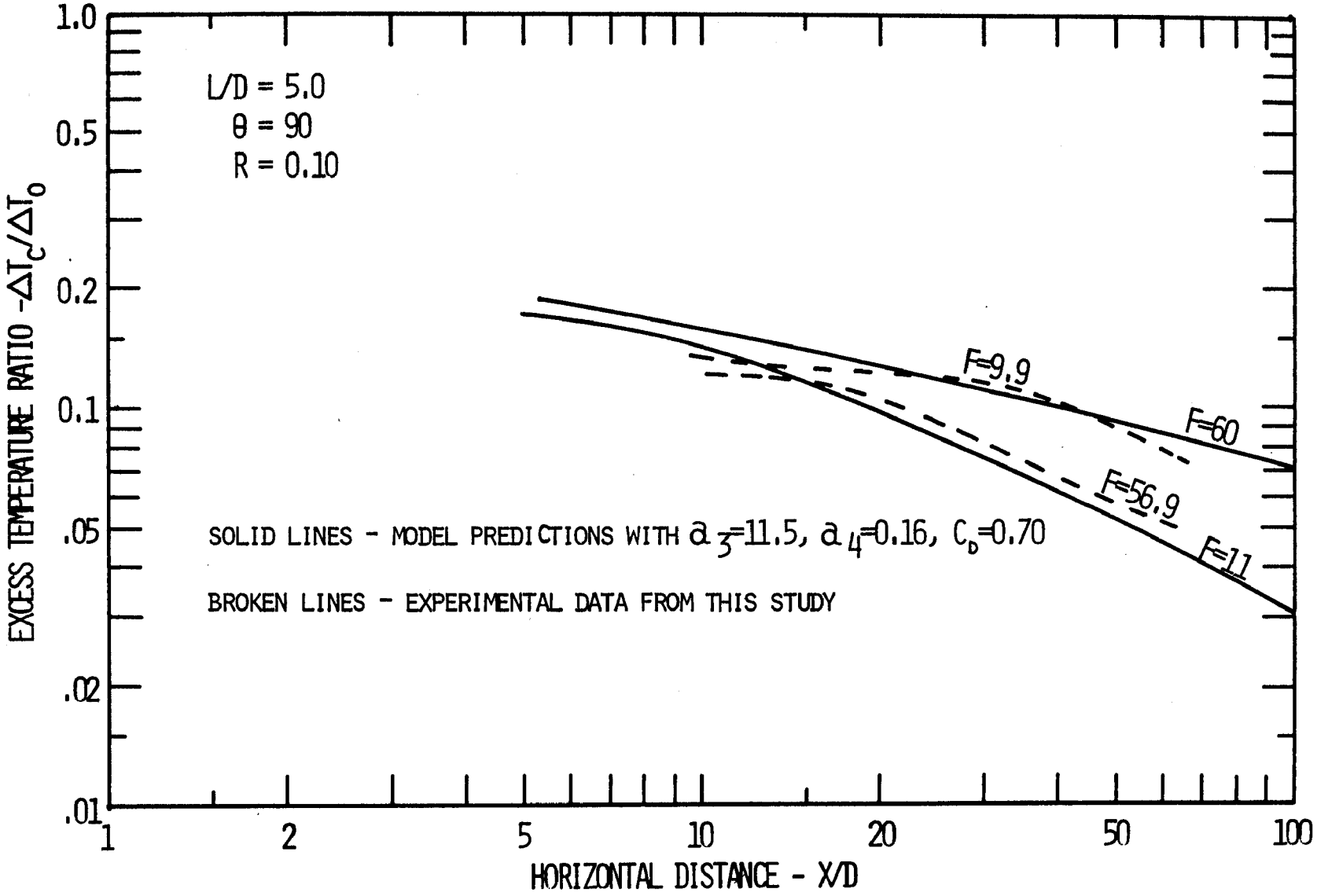

Figure 76. Comparison of experimental and model predicted excess temperature for L/D=5.0, R=0.10, crossflow discharge.

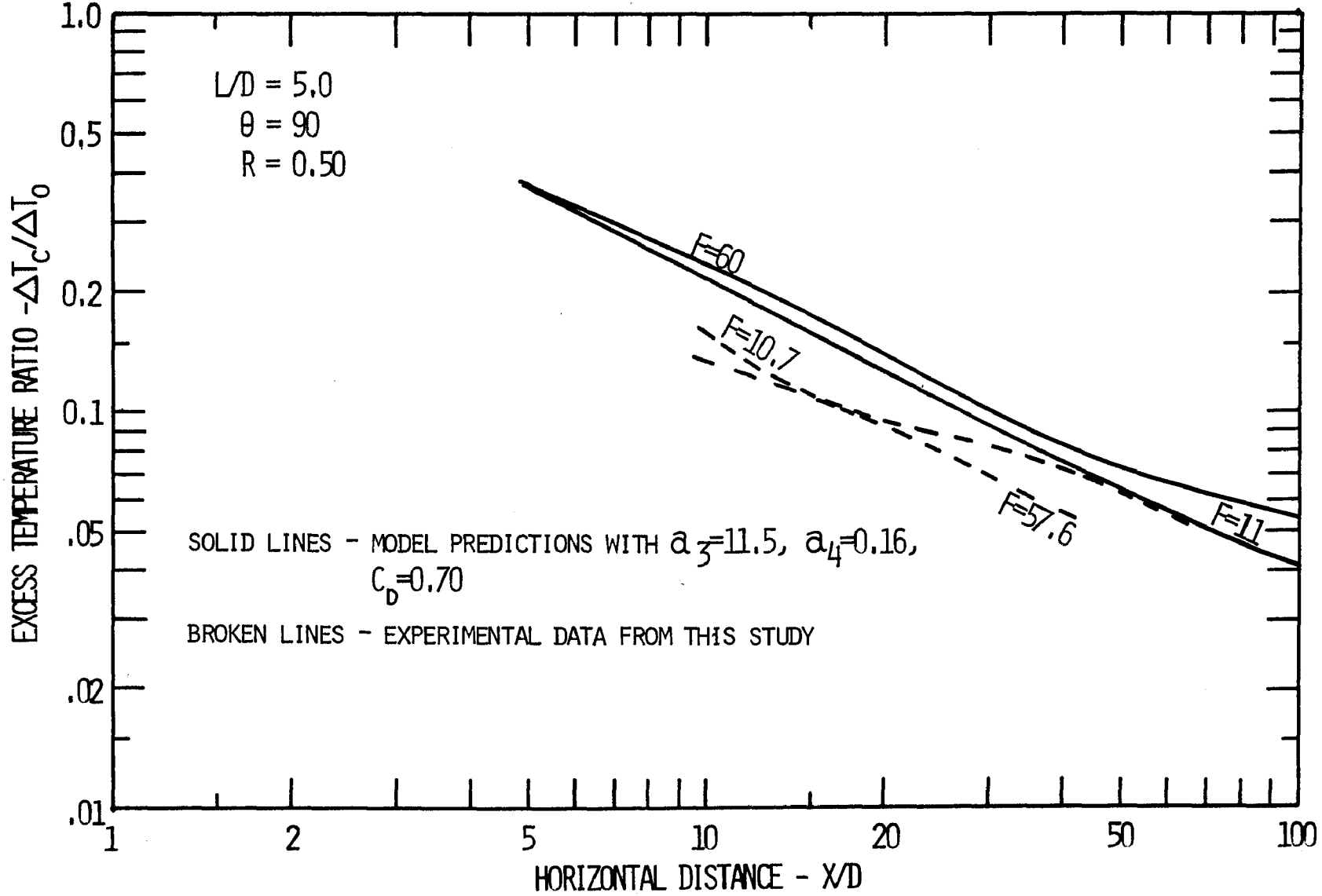

Figure 77. Comparison of experimental and model predicted excess temperature for L/D=5.0, R=0.50, crossflow discharge.

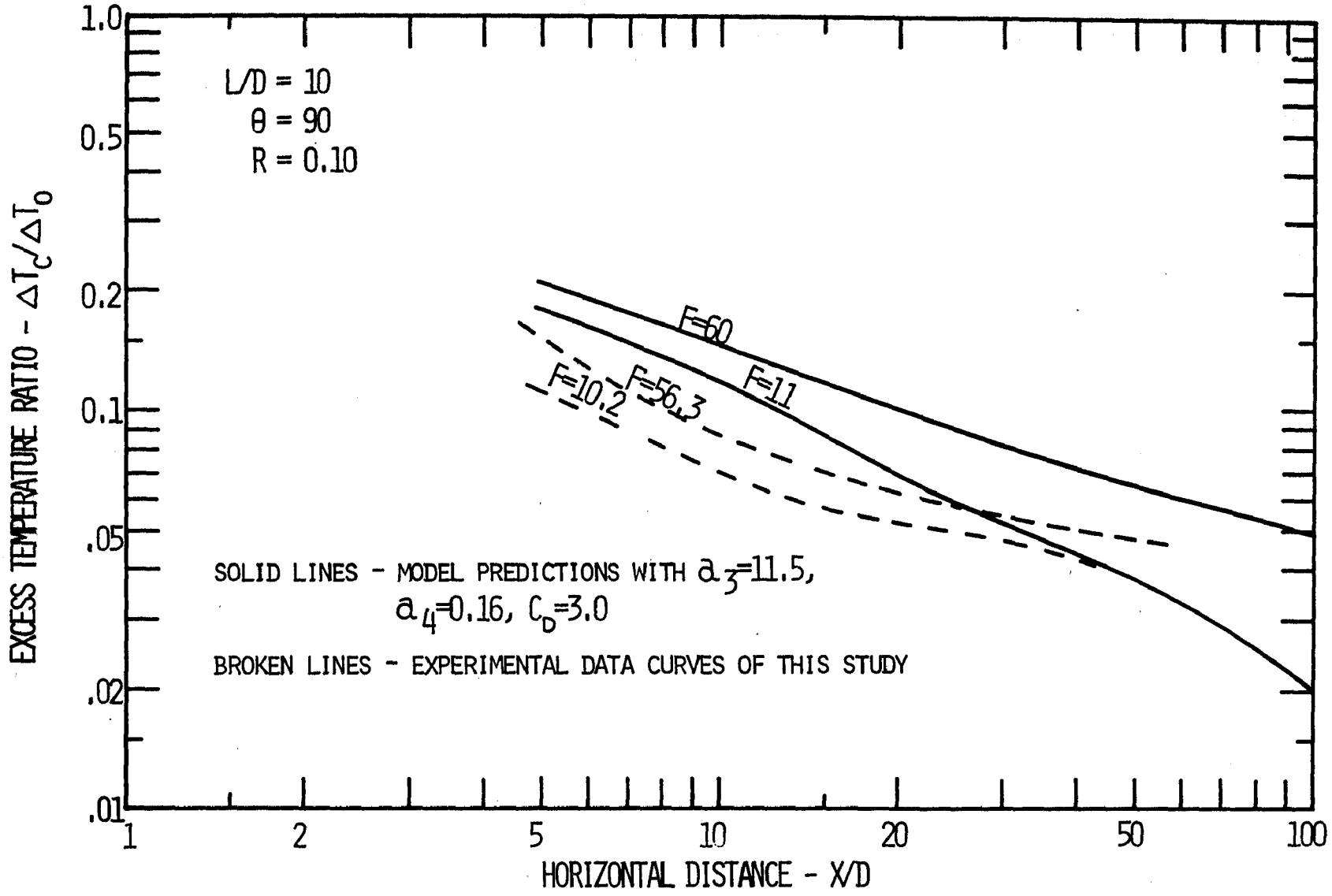

Figure 78. Comparison of experimental and model predicted excess temperature for L/D=10., R=0.10, crossflow discharge.

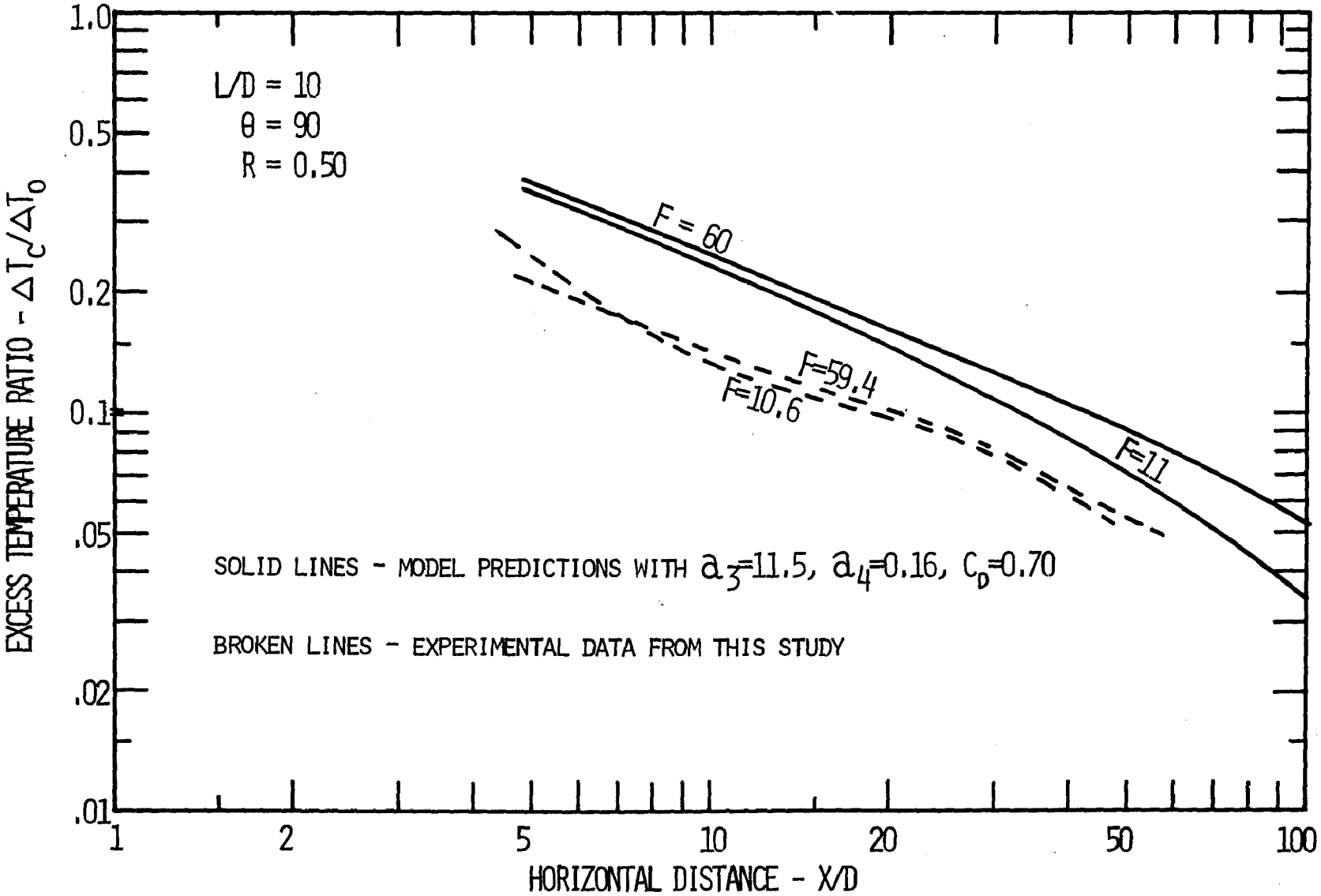

Figure 79. Comparison of experimental and model predicted excess temperature for L/D=10., R=0.50, crossflow discharge.

varied (from 0.1 at R = 0.0625 to 1.7 at R = 0.25). However, while his coefficient increased with increasing R, the results for this study required that C_D decrease with increasing R. This trend is more in line with the results for flows around cylinders and spheres.

It should be noted that the drag is also dependent on spacing. Inherent in the expressions offered here for drag force is the variation of the effective C_D with spacing. For wide spacings the drag force is very small. The drag force grows during plume growth and merging of the jets. Once the width of the jet is the same as the port spacing, the drag force is independent of width of the jet.

Setting aside the questions and problems raised in these attempts to tune the model to experimental data; the model is now complete. All of the necessary entrainment coefficients are specified and the model predicts trajectory and dilution with acceptable accuracy for a wide variety of discharge conditions. The co-flow discharge, even with the turbulence parameters discussed earlier, will not, however, give exceptional prediction.

The final recommended entrainment coefficient values are:

$c_1 = 1.06$, $c_2 = 34.$, $c_3 = 6.0$, $c_4 = 0.20$,

$a_1 = 0.05$, $a_2 = 0.0$, $a_3 = 11.5$, $a_4 = 0.16$,

$C_D = 3.0$ at $R = 0.10$, and $C_D = 0.70$ at $R = 0.50$.

SOME COMPARISONS AND PREDICTIONS

The purpose of the analytical development of the model presented in this study was to obtain a predictive tool to handle multiple port discharges. It was important that this model did

not suffer from the same difficulties as the Koh and Fan[13] "transition" model or the Jirka and Harleman[7] "equivalent slot" model. The major problem of these models was that they over-predicted dilution. The transition model had some additional difficulties. When the transition point was reached, several of the plume characteristics underwent step changes in value in order to accomodate the shift from the round port solution to the slot solution and still maintain a conservation of momentum, energy and mass flow.

By referring to Reference 14 we may reproduce the predictions of these two models, experimental data and the "merging" model discussed here for horizontal discharge into a quiescent ambient of a multiport diffuser with an L/D of 10. The comparison of the predictions is offered in Figures 80, 81, and 82 (the predictions of Jirka and Harleman were taken from Figure 2.4 of Reference 7 with the aid of experimental trajectories from this study). The Davis[17] model of this study with the entrainment coefficients already arrived at, accurately predicts the dilution of the multiple port discharge for the cases presented. The plume characteristics of the Davis solution remain smooth and continuous functions during merging. As shown in Figure 83, the trajectories of the experimental data are matched quite well by the predictions of the Davis merging model, although the Koh and Fan transition model also matched the data.

With the model developed exhibiting the desired merging properties (smooth, continuous, and accurate), certain aspects of the merging process may be explored. The notable interest is in the effect of port spacing on trajectory and dilution.

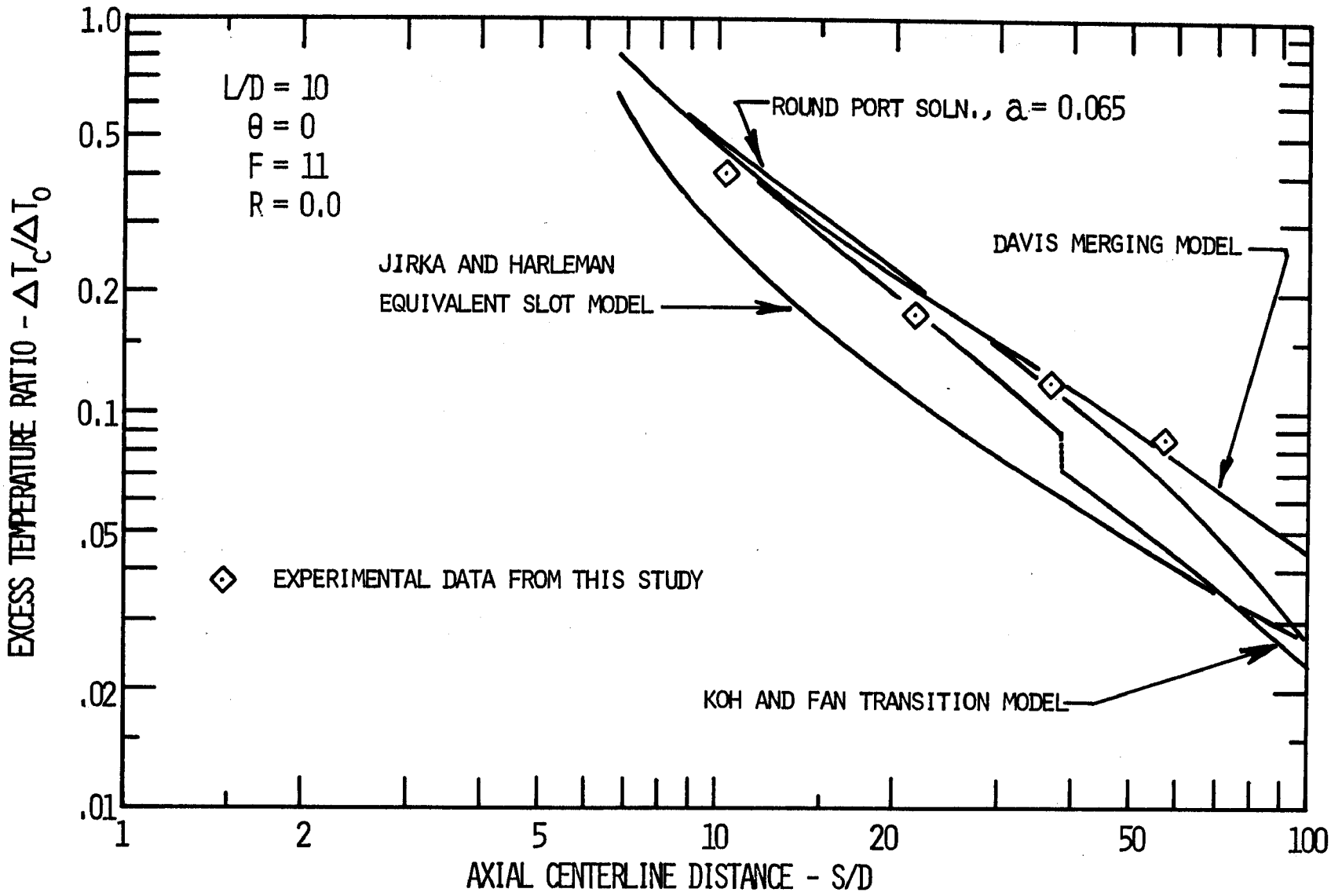

Figure 80. Comparison of excess temperature predicted by several models and experimental data for L/D=10, R=0.0, F=11, horizontal discharge.

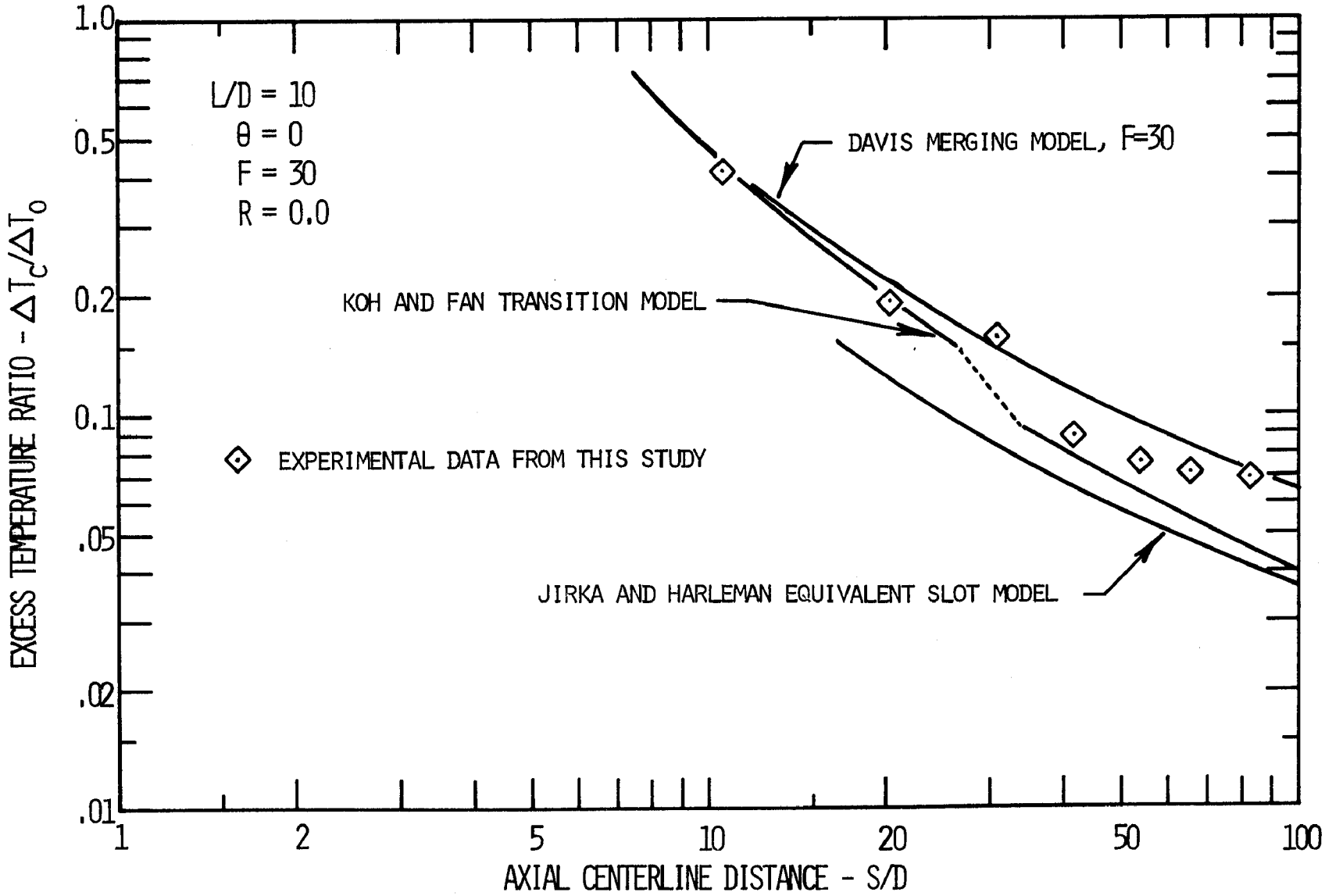

Figure 81. Comparison of excess temperature predicted by several models and experimental data for L/D=10., R=0.0, F=30, horizontal discharge.

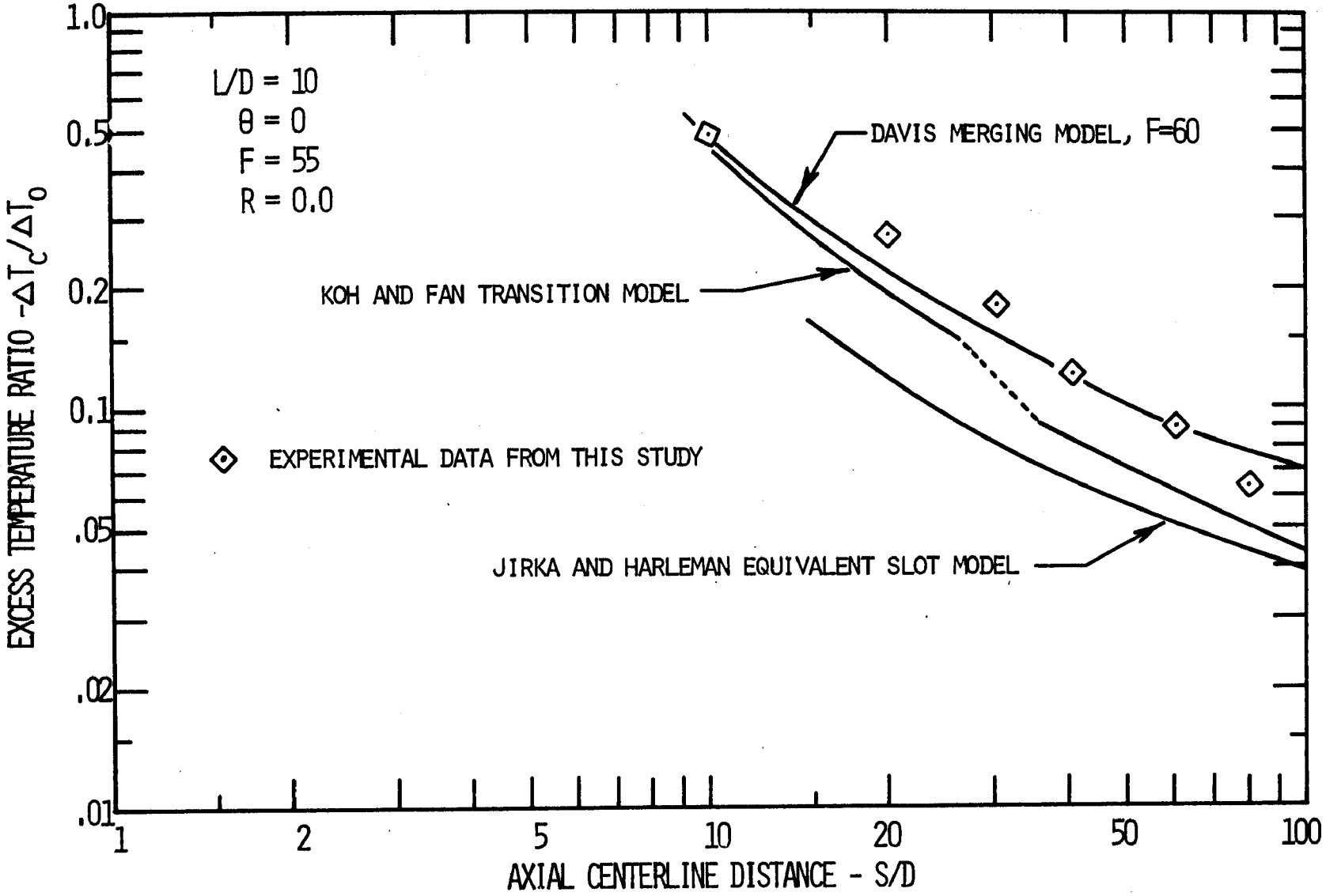

Figure 82. Comparison of excess temperature predicted by several models and experimental data for L/D=10., F=55, R=0.0, horizontal discharge.

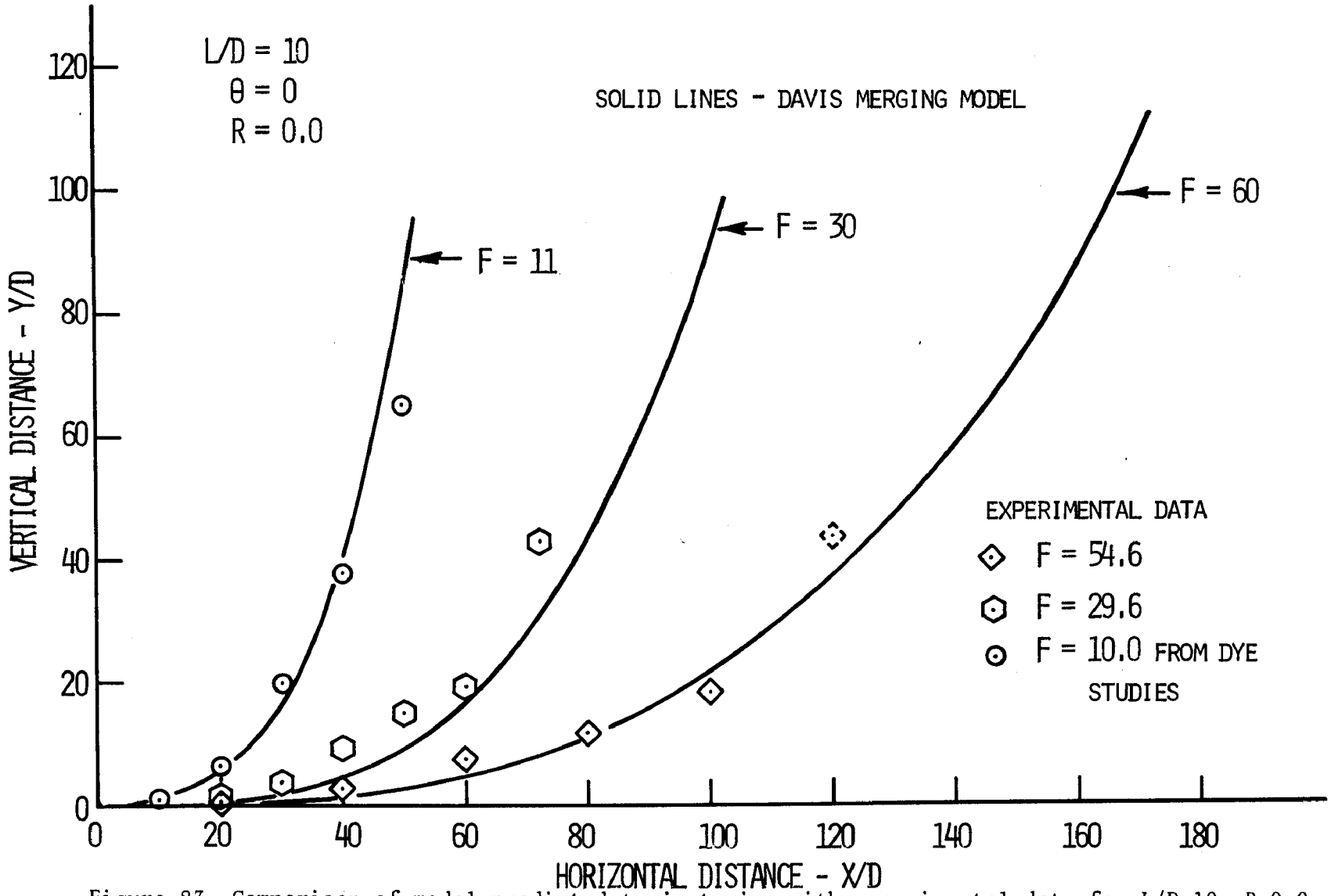

Figure 83. Comparison of model predicted trajectories with experimental data for L/D=10, R=0.0, horizontal discharge.

In Figure 84 the trajectory and dilution points for horizontal discharge into a quiescent ambient is given for port spacings of 10, 5, and 2.5. The results demonstrate that with the merging model having the Davis "entraining area" entrainment function, the port spacing has a large affect on both the trajectory and the excess temperature concentration. No attempt was made to compare this with experimental data that might be available for comparison for discharge from close spaced jets (L/D = 2.5) into a quiescent ambient.

It is tempting to wonder about the effect of raising the entrainment value for the fully merged plume from the Davis "entraining area" value,

$$E = 0.05\ L\Delta U_c/\pi$$

to that of the slot jet,

$$E_s = 0.16 L\Delta u_c/\pi \text{[20]}$$

The entrainment increase would be greater than three-fold. With such an increase, it is expected that the effect of reducing port spacing would be less than that illustrated in Figure 84.

In an attempt to satisfy such speculation, an entrainment function similar to that used in the Koh and Fan transition model was used in the merging model developed here. The entrainment was allowed to grow with b, as does the round jet entrainment, until some limit was reached, after which it remained constant. The entrainment function before reaching the limit was

[20] The entrainment functions are divided by 2π.

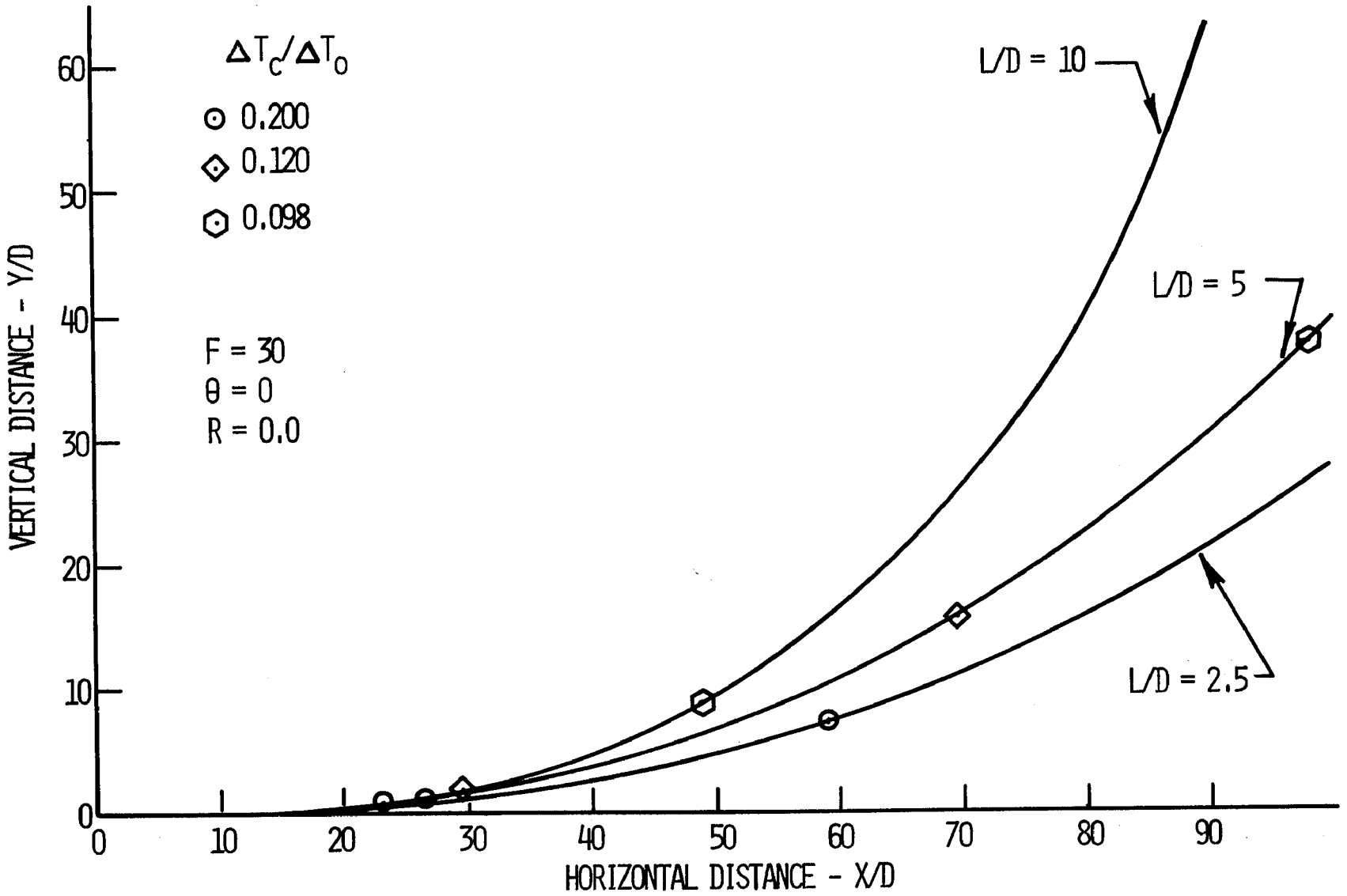

Figure 84. Trajectory and dilution prediction for various port spacings, F=30, R=0.0, horizontal discharge.

$$E = 0.05b\ \Delta u_c(1. - 2a'_{41}/L) \quad ;$$

when the value for E reached

$$E_s = 0.16L\ \Delta u_c(1. - a'_{41})/\pi$$

the entrainment remained constant at that value of E_s. The above entrainment functions would be the same as those employed by the Koh and Fan transition model if a'_{41} were 0.0, and the value 0.05 were 0.043. The model, employing $a'_{41} = 0.5$, seemed to give good agreement with experimental data for crossflow (L/D = 2.5, 5, 10) and stagnant horizontal discharge (L/D = 10). It is interesting that with $a'_{41} = 0.0$ the dilution was greatly over-predicted resulting in excess temperatures much lower than experimentally measured. Figure 85 shows the dilutions as predicted by the merging model employing the entrainment functions considered above with $a'_{41} = 0.50$, for stagnant horizontal discharge and L/D = 10. It is seen that for the case offered, agreement is good for dilution.

From the consideration of this alternate entrainment function it is apparent that the merging model of Davis provides a physically accurate treatment of the merging process and that in the limit (as b approaches infinity) the entrainment does not seem to approach the value obtained for the slot jet but rather approaches a value between 0.0159L and 0.025L[21].

PLUME WIDTH

One consideration may have become conspicuous due to its absence. All of the comparisons and careful tuning of the model

[21] Multiply these values by 2π for the entrainment associated with models where the governing equations are not divided by 2π.

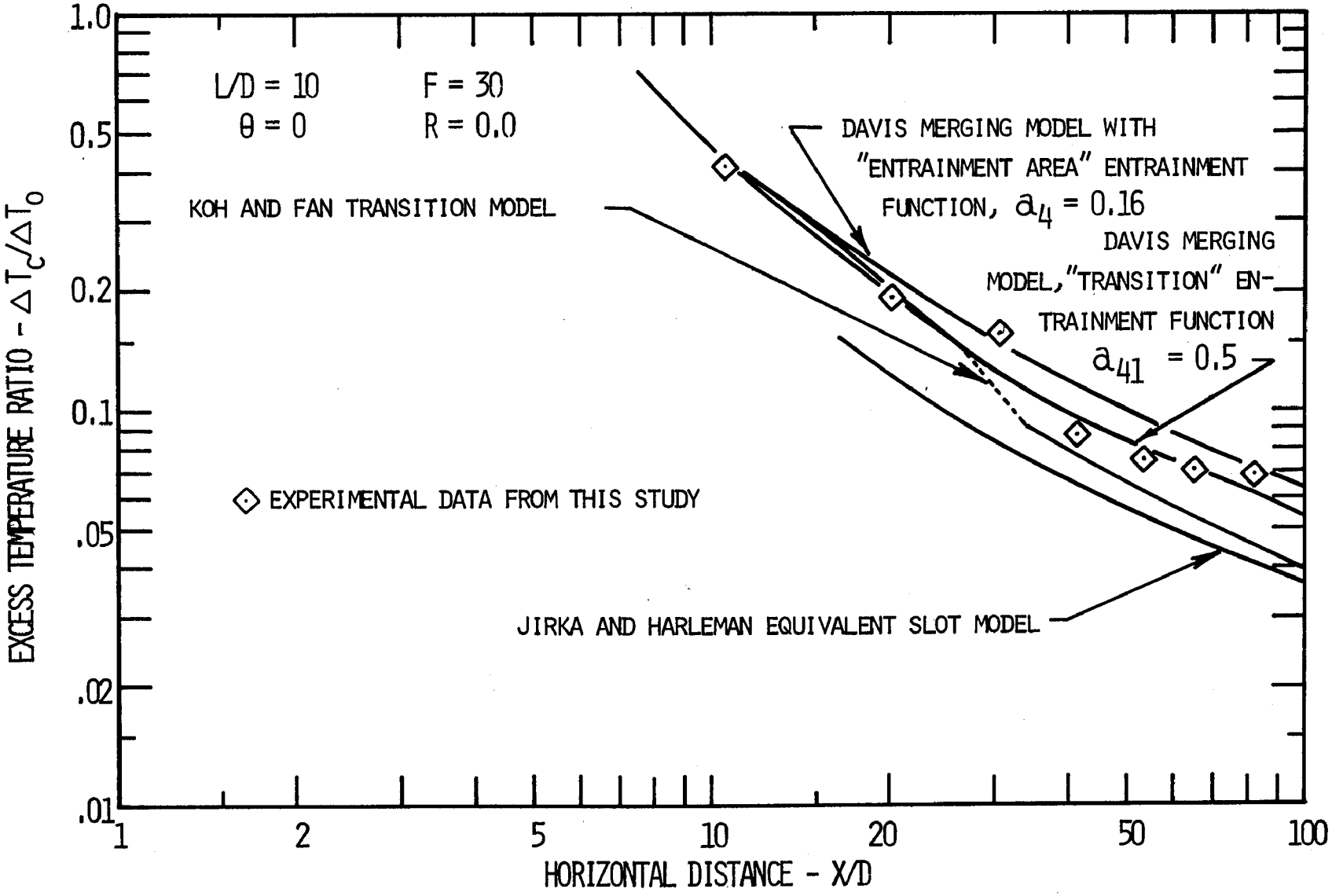

Figure 85. Comparison of various models and experiment for merging jets excess temperature, emphasis on comparison of the "entrainment area" and transition" entrainment results.

dealt with the thermal dilution and trajectory; no comparisons have been made between model predictions and experimental values of plume width or centerline velocity. Part of the reason is that these quantities are more difficult to measure than plume temperature and trajectory. Very little velocity data exists for complex flow conditions or widely varying discharge parameters. Plume width has been difficult to define experimentally although the profile half-radii (radius to the point where axial velocity is one half of the centerline value) may be determined if accurate velocity or temperature profiles are known. The bulk of the experimental data then is for concentration and trajectory downstream from the discharge.

The centerline velocity and plume half-radii for several models, the experimental work of Morton, et.al.[4], and some experimental work from this study are given in Figures 86 and 87. Figure 86 reveals that the centerline velocities predicted by the Fan model (using $a_1 = 0.043$, where a_1 has been adjusted to the plume definition used here) and the model discussed in this study (using $a_1 = 0.05$) are less than the Morton, et.al., values or the predictions of the model offered in this study when $a_1 = 0.029$. With $a_1 = 0.029$ the results are very similar to those of the Hirst[6] model for the momentum jet.

When one examines Figure 87 it is seen that the plume width agreement between prediction and experiment for the Fan model ($a_1 = 0.043$) and the tuned model given here with $a_1 = 0.029$ is good (again this is similar to the Hirst model). However, with $a_1 = 0.05$ the model developed in this text over-predicts plume width for high Froude Number single port discharges.

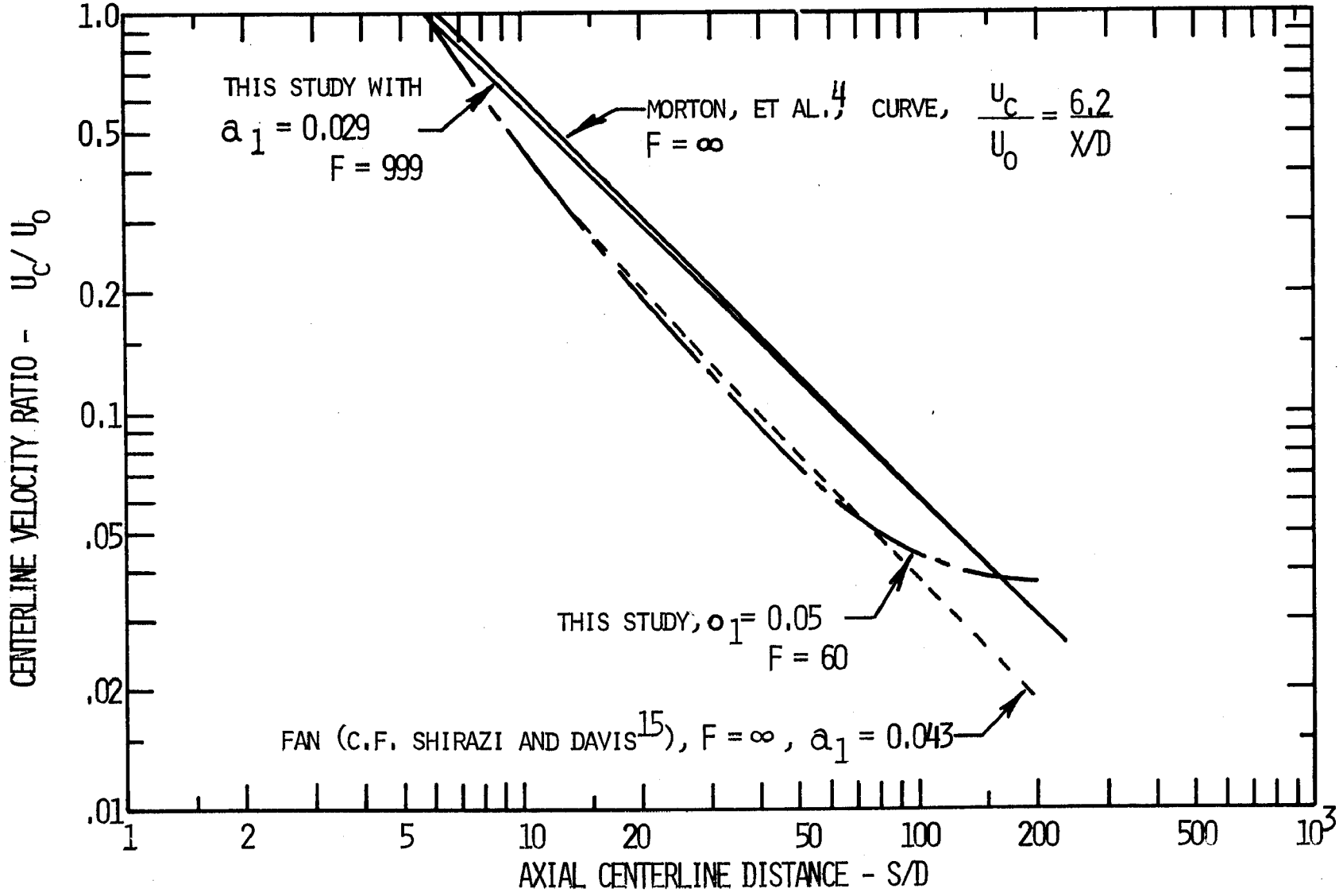

Figure 86. Comparison of momentum jet centerline velocity predictions of several models and the empirical curve of Morton, et al.[4].

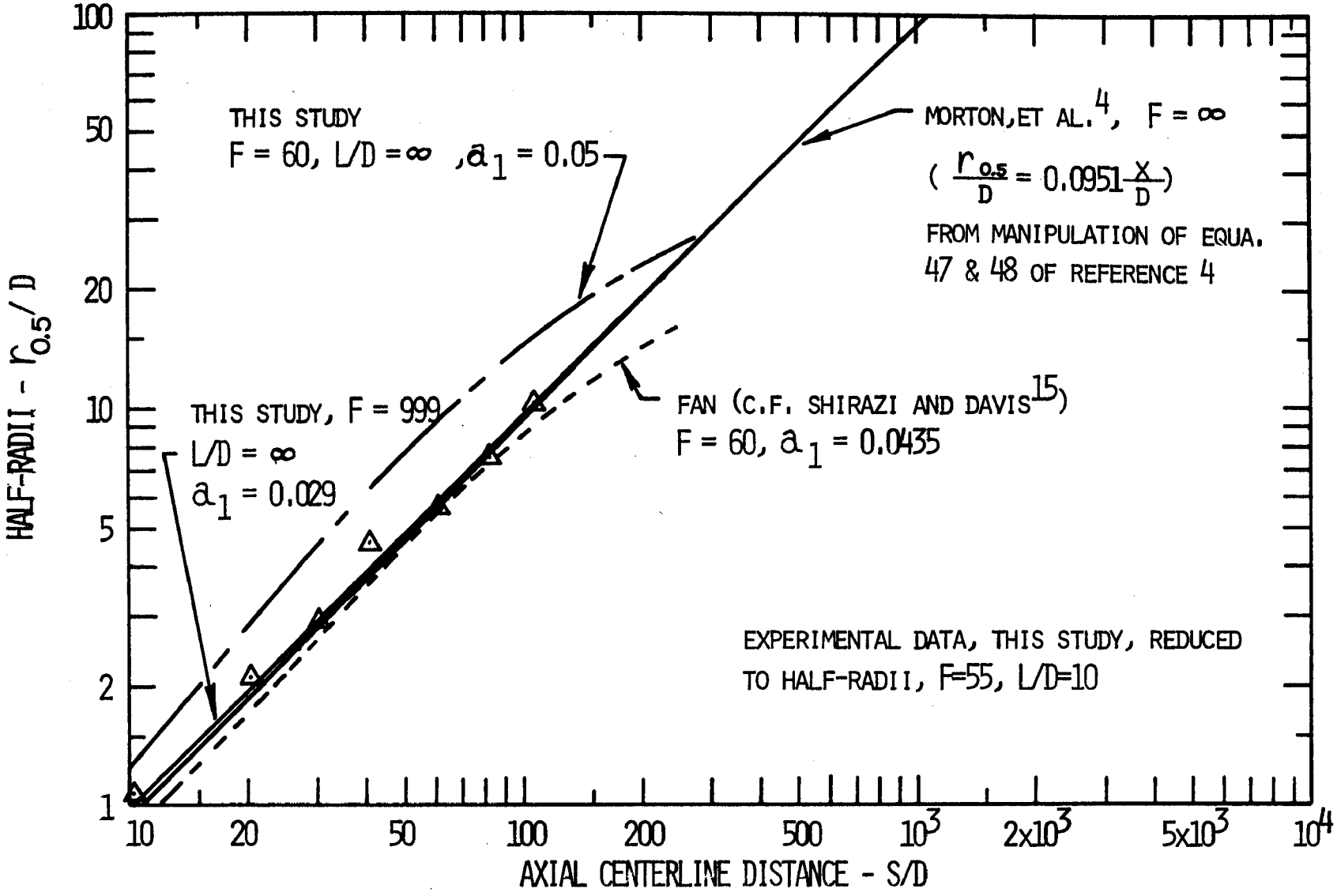

Figure 87. Comparison of momentum jet half-radii predictions of several models with experimental data and the empirical curve of Morton, et al.[4].

The tuning process recommendation was that $a_1 = 0.05$. It was felt that accuracy in thermal concentrations and trajectories was more ecologically useful than accurate plume widths. Therefore, the modeling here of single port discharges is deficient in that the model predicts exaggerated widths for high Froude Number single port discharges. However, for multiple port discharges the predicted plume widths compare quite nicely with experimental values. Shown in Figure 88 are the width predictions of the Davis merging model and the Koh and Fan transition model for horizontal multiple port discharge (L/D = 10) into a quiescent ambient. Also offered in Figure 88 are reduced data from this study (measured widths divided by 0.8). As can be seen, the Davis merging model provides excellent agreement for the widths of these buoyant discharges. The Koh and Fan model, however, overpredicts the widths. This is probably due to the use of the slot entrainment function which is significantly larger than the value employed in the Davis entrainment model when merging approaches completion. The lack of a smooth, continuous transition to the slot jet flow may also contribute to this. One may conclude that the width predictions are accurate for the merging model when multiple port discharges are considered but are not as accurate for single port high Froude Number discharges.

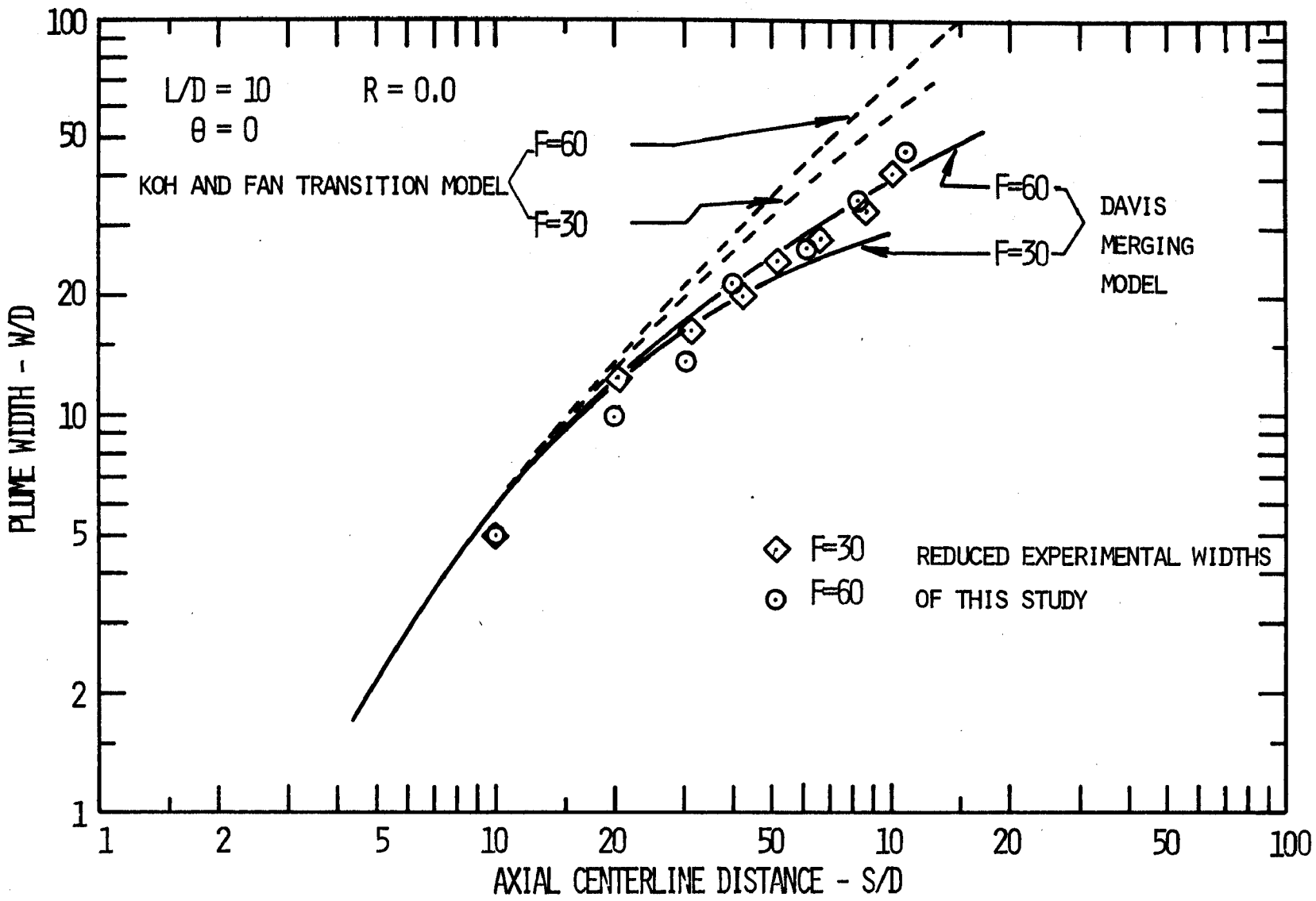

Figure 88. Comparison of the width predictions of the Koh and Fan[13] transition model and the Davis merging model with experimental data.

SECTION VII

REFERENCES

1. Reichardt, H., Impuls- Und Warmeaustausch in freier Turbulenz, Z. agnew. Math. Mech., Volume 24, num. 5, pp. 268-72, 1944.

2. Schmidt, W., Z. Agnew. Math. Mech., Vol. 21, pp. 265, 351, 1941.

3. Albertson, M. L., Y. B. Dai, R. A. Jensen, and Hunter Rouse, D iffusion of Submerged Jets, A.S.C.E., Dec. 1948, pp. 1571-96.

4. Morton, B. R., Sir Geoffrey Taylor, J. S. Turner, Turbulent Gravitational Convection from Maintained and Instantaneous Sources. Proceedings of the Royal Society of London, Ser. A, 234; 1-23.

5. Trent, Donald S., and J. R. Welty, Numerical Thermal Plume Model for Vertical Outfalls in Shallow Water, Environmental Protection Technology Series, EPA-R2-73-162, March 1973.

6. Hirst, E. A., Analysis of Round Turbulent, Buoyant Jets Discharged to Flowing Stratified Ambients. Oak Ridge, Oak Ridge National Laboratory, Dept. No. ORNL-4685, 36 p., 1971.

7. Jirka, G., and D. R. F. Harleman, The Mechanics of Submerged Multiport Diffusers for Buoyant Discharges in Shallow Water, MIT Ralph M Parsons Laboratory for Water Resources and Hydrodynamics, Report No. 169, March 1973.

8. Argue, J., The Mixing Characteristics of Submerged Multiple Port Diffusers for Heated Effluents in Open Channel Flow, University of Iowa, Masters Thesis, May 1973.

9. Larsen, J. and G. E. Hecker, Design of Submerged Diffusers and Jet Interactions, ASCE National Water Resources Engineering Meeting, Jan. 24-28, 1972, Atlanta, GA, Reprint No. 1614.

10. Koh, R. C., N. H. Brooks, E. H. Wolanski, and E. J. List, Basin Model Studies of Diffusers, SCE Report No. 4, W. M. Keck Hydraulics Laboratory, CIT, May 1973.

11. Liseth, P., Mixing of Merging Buoyant Jets from a Manifold in Stagnant Receiving Water of Uniform Density, Hydraulic Engineering Laboratory Report HEL 23-1, University of California, Berkeley, November, 1970.

12. Iwasa, Yoshiaki, and Mashio Yatsuzuka, Spread of Heated Waters from Multiport Diffuser, Proceedings of the U. S. - Japan Joint Seminar on Engineering and Environmental Aspects of Waste Heat Disposal, Paper #9, Tokyo, Japan, April 15, 1974.

13. Koh, R. C. and L. N. Fan, Mathematical Models for the Prediction of Temperature Distributions Resulting from the Discharge of Heated Water in Large Bodies of Water, E.P.A. Water Pollution Control Research Series Report No. 1613DW)1)/70, October 1970.

14. Kannberg, L. D. and L. R. Davis, Experimental Investigation of Deep Submerged Multiple Buoyant Jets into Stagnant and Co-moving Ambients, Paper presented at Thermal Pollution Analysis Conference held at VPL & SU, Blacksburg, Virginia, May 1974.

15. Shirazi, M. A., and L. R. Davis, Workbook of Thermal Plume Prediction Vol. I: Submerged Discharge, E.P.A. Environmental Protection Technology Series, EPA-R2-72-005a, August, 1972.

16. Benedict, R. P., Engineering Analysis of Experimental Data, Transaction of ASME, Journal of Engineering for Power, January 1969, pp. 21-30.

17. Davis, L. R., Analysis of Multiple Cell Mechanical Draft Cooling Towers, E.P.A. Natl. Envir. Res. Cntr., Corvallis, OR Ecological Res. Series, EPA-660/3-75-039, June 1975.

18. Hirst, E. A. Analysis of Buoyant Jets Within the Zone of Flow Establishment, Oak Ridge National Lab., Report No. ORNL-TM-3470, August 1971.

19. McQuivey, R. S., T. N. Keefer, and M. A. Shirazi, Basic Data Report on the Turbulent Spread of Heat and Matter, U. S. Department of the Interior, Geological Survey, and the U. S. Environmental Protection Agency, Open-file Report, Fort Collins Colo., August 1971.

20. Shirazi, M. A., R. S. McQuivey, and T. N. Keefer, Heated Water Jet in Coflowing Turbulent Stream, Journal of the Hydraulics Division, A.S.C.E., Vol. 100, No. HY7, Proc. Paper 10661, July 1974, pp. 919-934.

21. Shirazi, M. A., L. R. Davis, K. V. Byram, An Evaluation of Ambient Turbulence Effects on a Buoyant Plume Model, Proceedings of the 1973 Summer Computer Simulation Conference, July 17, 18, 19, Montreal, P.Q., Canada.

22. Taylor, Sir Geoffrey, Dynamics of a Mass of Hot Gas Rising in Air, U. S. Atomic Energy Commission, MDDC 919, LADC 276, 1945.

23. Fox, D. G., Forced Plume in a Stratified Fluid, J. Geophys. Res., Vol. 75, No. 33, pp. 6818-35, 1970.

24. Abraham, G., Horizontal Jets in Stagnant Fluid of Other Density, J. Hyd. Div., A.S.C.E., Vol. 91, No. HY4, 1969, pp. 139-153.

25. Fan, L-N., Turbulent Buoyant Jets into Stratified or Flowing Ambient Fluids, Keck Lab of Hyd. and Water Resources, California Inst. of Tech., Rept No. KH-R-15, June 1967.

26. Platten, J. L., and J. F. Keffer, Entrainment in Deflected Axisymetric Jets at Various Angles to the Free Stream, Univ. of Toronto, Mech. Engr. Dept., UTME-TP-6808, 1968.

27. Hoult, D. P., J. A. Fay, and L. J. Forney, A Theory of Plume Rise Compared with Field Observations, J. Air Pollut. Cntrl. Asso., Vol. 19, No. 9, pp. 585-90, 1969.

28. Hoult, D. P., and J. C. Weil, Turbulent Plume in a Laminar Cross Flow, MIT Fluid Mechanics Lab., Pub. No. 70-8, 1970.

29. Abramovich, G. N., The Theory of Turbulent Jets, Translation by Scripta Technica, M.I.T. Press, 1963.

30. Cederwall, K., Jet Diffusion: Review of Model Testing and Comparison with Theory, Hyd. Div., Chalmers Inst. of Tech. Goteborg, Sweden, Feb. 1967.

31. Gordier, R. L., Studies on Fluid Jets Discharging Normally into Moving Fluids, St. Anthony Falls Hyd. Lab., Tech. Rpt. 28, Ser. B., Univ. of Minn., 1959.

32. Rouse, Hunter, Fluid Mechanics for Hydraulic Engineers, Dover, 1961; McGraw Hill, 1938; Copyright-United Engineering Trustees, Inc.

33. Brown, C. E., Aerodynamics of Wake Vortices, AIAA Journal, Vol. II, No. 4, pp. 531-536, Apr. 1973.

34. Anwar, H. O., Behavior of Buoyant Jet in Calm Fluid, ASCE J. Hydraulics Div., Vol. 95, No. HY4, pp. 1289-1303, 1969.

35. Schlichting, H., Boundary-Layer Theory, translated by J. Kestin, McGraw-Hill Co., 6th Edition, 1968.

36. Chasse, J. P., and L. Winiarski, Laboratory Experiments of Submerged Discharges with Current, Environ. Prot. Agency, Pacific NW. Environ. Research Lab., Working Paper #12, June 1974.

37. Fan, L-N, and N. H. Brooks, Numerical Solution of Turbulent Buoyant Jet Problems, W. M. Keck Laboratory, Calif. Inst. of Tech., Report No. KH-R-18, January 1969.

38. Forstall, W., and A. H. Shapiro, The Turbulent Mixing of Co-axial Gas Jets, J. Appl. Mech., Vol. 17, pp. 399-408, 1950.

39. Bird, R. B., W. E. Stewart, and E. N. Lightfoot, Transport Phenomena, John Wiley & Sons, Inc., New York, 1960.

40. Stalzenbach, K. D., Harleman, D. R. F., An Analytical and Experimental Investigation of Surface Discharge of Heated Water, EPA Water Pollution Control Series 16130 DJV 02/71, February 1971.

SECTION VIII

APPENDIX A

Appendix A contains a complete list of the normalized experimental data. Data is listed successively according to L/D, θ, F, R, and $\frac{X}{D}$ with the discharge velocity and temperature and ambient temperature also given. In this listing

L/D = port spacing, L, in port diameters, D,

θ = vertical angle of discharge from the horizontal downstream direction in degrees

$F = \dfrac{V_o}{\sqrt{\dfrac{\rho - \rho_a}{\rho_o} g D}}$ = Discharge densimetric Froude Number,

R = Discharge to ambient velocity ratio,

X/D = Distance downstream, X, in port diameters, D,

$\dfrac{\Delta T_c}{\Delta T_o} = \dfrac{T_c - T_a}{T_o - T_a}$ = Dimensionless normalized thermal concentration,

$\dfrac{W}{D}$ = Vertical jet width, W, in port diameters, D,

$\dfrac{Y}{D}$ = Vertical distance, Y, to jet thermal centerline in port diameters, D,

V_o = port discharge velocity in cm/sec.,

T_o = port discharge temperature in degrees Celsius,

and

T_a = ambient water temperature in degrees Celsius.

APPENDIX A. TABULATED DATA

L/D	θ	F	R	X/D	$\Delta T_c/\Delta T_o$	W/D	Y/D	V_o	T_o	T_a
10.	0	11.15	0	10	0.41	6.7	1.0*	25.00	45.05	20.00
		11.89	0	20	0.18	8.3	6.4*	26.50	45.12	20.40
		11.50	0	30	0.12	12.	20.0*	26.4	46.06	21.01
		11.8	0	40	0.086	15.	38.0*	26.7	46.16	21.08
		11.0	0	50	0.045	18.	65.0*	26.4	48.42	20.84
10.	0	11.09	0.093	20	0.188	4.5		26.50	44.31	5.96
					0.195	5.0				
					0.197	4.9				
					0.203	7.0				
10.	0	10.70	0.107	30	0.134	6.3		25.44	44.04	5.75
					0.123	7.1				
					0.130	8.3				
10.	0	10.68	0.093	40	0.112	9.1		26.5	45.73	5.4
					0.114	8.1				
					0.102	9.0				
10.	0	10.84	0.102	50	0.082	10.2		26.2	44.78	5.64
					0.086	7.5				
					0.072	8.6				
10.	0	10.30	0.100	60	0.057	11.0		23.18	41.67	5.23
					0.065	12.8				
					0.066	13.1				
10.	0	11.66	0.102	80	0.046	12.7		26.38	41.90	5.10
					0.040	13.5				
					0.043	12.8				
					0.053	13.7				
					0.055	13.8				
10.	0	11.32	0.098	100	0.033	12.3		26.80	43.78	4.97
					0.041	12.1				
					0.032	9.8				
					0.040	12.1				
10.	0	11.38	0.088	140	0.037	23.3		27.50	44.67	4.76
					0.039	12.3				
					0.042	13.5				
					0.045	13.8				
10.	0	10.83	0.254	20	0.191	5.3		25.77	44.42	7.88
					0.199	5.7				
					0.196	5.2				
					0.199	5.7				

*As determined from dye studies.

APPENDIX A (continued). TABULATED DATA

L/D	θ	F	R	X/D	$\Delta T_c/\Delta T_o$	W/D	Y/D	V_o	T_o	T_a
10.	0	11.26	0.251	30	0.128	5.9		25.7	42.65	7.79
					0.131	4.8				
					0.121	5.0				
10.	0	10.96	0.248	40	0.125	5.8		25.3	43.16	8.03
					0.106	6.2				
					0.117	5.7				
10.	0	10.81	0.244	50	0.083	8.9		25.79	44.55	8.02
					0.072	6.2				
					0.069	6.3				
10.	0	10.77	0.255	60	0.063	9.7		25.58	44.39	8.13
					0.054	5.9				
					0.054	7.3				
10.	0	10.62	0.257	80	0.044	7.3		25.16	44.32	8.24
					0.043	8.3				
					0.049	7.4				
10.	0	11.07	0.251	100	0.040	10.9		25.71	43.47	8.30
					0.041	7.4				
					0.043	12.9				
10.	0	10.59	0.459	20	0.148	4.7		26.82	47.50	9.57
					0.154	4.5				
					0.124	3.8				
					0.147	5.4				
					0.143	4.4				
					0.121	4.2				
10.	0	11.07	0.501	30	0.091	5.4		25.44	43.29	9.49
					0.093	5.0				
					0.119	5.4				
					0.101	5.2				
					0.090	5.8				
10.	0	10.82	0.486	40	0.091	7.0		25.5	44.27	9.3
					0.079	7.4				
					0.077	5.5				
					0.066	4.5				
					0.064	7.7				
					0.067	6.0				
10.	0	10.38	0.511	50	0.065	8.5		24.44	44.27	9.36
					0.064	8.6				
					0.072	8.3				
					0.059	8.0				
					0.059	6.4				
					0.062	10.2				

APPENDIX A (continued). TABULATED DATA

L/D	θ	F	R	X/D	$\Delta T_c/\Delta T_o$	W/D	Y/D	V_o	T_o	T_a
10.	0	11.03	0.485	60	0.040	9.4		25.59	43.60	9.11
					0.049	9.3				
					0.043	7.7				
					0.043	10.5				
					0.051	8.3				
10.	0	10.57	0.486	80	0.042	9.2		25.13	44.58	8.99
					0.040	6.5				
					0.042	8.1				
					0.046	9.0				
					0.048	9.6				
					0.042	10.1				
10.	0	11.25	0.500	100	0.019	12.3		25.69	42.87	8.84
					0.018	12.1				
					0.017	11.2				
10.	0	10.25	0.962	20	0.057	4.0		25.73	47.35	13.34
10.	0	10.59	0.962	40	0.030	5.4		25.72	45.80	13.24
10.	0	10.67	0.944	60	0.018	7.5		25.70	45.43	13.19
10.	0	10.49	0.946	80	0.014	8.9		25.68	46.11	13.04
10.	0	10.14	0.946	100	0.013	10.5		25.66	48.00	12.96
10.	0	10.70	0.955	140	0.011	12.9		25.66	45.53	12.94
10.	0	29.0	0	10	0.420	4.0	0.0*	49.4	36.00	21.11
		29.0	0	20	0.196	10.	1.5*	49.4	36.60	21.28
		28.8	0	30	0.160	13.	4.0*	49.4	37.75	21.41
		29.8	0	40	0.088	16.	9.3*	49.4	37.00	21.34
		29.6	0	50	0.076	19.5	15.3*	49.6	37.30	21.51
		29.2	0	60	0.071	23	19.5*	49.5	37.20	21.74
		30.6	0	72	0.069	26.4	43. *	49.5	36.13	21.74
		30.7	0	80	**	33.	**	49.5	36.09	21.75
10.	0	25.73	0.057	20	0.177	7.3		48.72	34.19	11.52
					0.158	5.4				
					0.166	6.3				
					0.178	7.3				
					0.163	6.5				

APPENDIX A (continued). TABULATED DATA

L/D	θ	F	R	X/D	$\Delta T_c/\Delta T_o$	W/D	Y/D	V_o	T_o	T_a
10.	0	30.36	0.050	20	0.219	5.6		50.48	32.10	9.85
					0.210	7.2				
					0.240	6.0				
					0.217	6.0				
					0.228	6.2				
					0.203	5.6				
					0.212	7.5				
10.	0	29.29	0.045	30	0.150	8.0		50.33	33.15	11.73
					0.128	8.9				
					0.132	9.9				
10.	0	29.20	0.054	30	0.145	7.7		48.66	32.23	10.06
					0.135	7.7				
					0.141	8.1				
					0.139	8.4				
					0.130	7.3				
					0.134	7.0				
10.	0	30.01	0.050	40	0.108	10.2		49.64	31.80	12.09
					0.122	10.6				
					0.112	10.8				
					0.118	10.3				
					0.116	10.7				
10.	0	30.50	0.054	40	0.112	10.5		49.87	31.67	10.30
					0.113	11.1				
					0.115	11.0				
					0.118	9.2				
10.	0	28.93	0.050	50	0.089	12.0		50.31	33.16	11.90
					0.080	11.7				
					0.093	12.5				
					0.081	12.2				
					0.085	12.3				
10.	0	30.29	0.053	50	0.086	12.3		49.55	31.74	10.20
					0.087	11.0				
					0.074	11.1				
					0.092	13.4				
					0.079	11.2				
					0.079	12.3				
10.	0	29.66	0.050	60	0.060	11.4		49.37	32.04	12.25
					0.057	14.2				
					0.057	12.6				
					0.059	11.1				
					0.057	11.5				

APPENDIX A (continued). TABULATED DATA

L/D	θ	F	R	X/D	$\Delta T_c/\Delta T_o$	W/D	Y/D	V_o	T_o	T_a
10.	0	31.30	0.049	60	0.068	13.2		50.10	31.20	10.43
					0.074	14.9				
					0.077	14.7				
					0.068	12.2				
					0.072	15.2				
10.	0	31.82	0.050	70	0.051	11.4		52.06	31.67	12.59
					0.052	16.4				
					0.051	15.9				
					0.054	13.9				
					0.059	16.1				
10.	0	30.81	0.054	80	0.068	18.7		48.47	31.39	14.35
					0.061	13.6				
					0.065	12.1				
					0.059	14.9				
					0.070	13.2				
10.	0	29.89	0.047	80	0.066	13.4		49.61	32.28	10.57
					0.066	15.8				
					0.057	14.9				
					0.058	15.3				
					0.069	14.1				
10.	0	29.79	0.045	100	0.048	15.8		49.70	32.45	10.66
					0.048	18.0				
					0.053	17.3				
					0.051	15.6				
					0.057	14.9				
10.	0	29.96	0.050	140	0.046	24.4		49.70	32.34	10.82
					0.050	23.5				
					0.054	19.1				
					0.047	25.3				
					0.048	18.9				
10.	0	31.10	0.095	20	0.209	5.2		52.53	31.87	10.53
					0.213	6.6				
					0.207	5.1				
10.	0	31.59	0.104	20	0.200	7.2		49.39	32.13	14.40
					0.230	5.4				
					0.228	5.8				
					0.193	6.1				
					0.230	5.3				
					0.221	7.8				
					0.228	4.5				

APPENDIX A (continued). TABULATED DATA

L/D	θ	F	R	X/D	$\Delta T_c/\Delta T_o$	W/D	Y/D	V_o	T_o	T_a
10.	0	31.04	0.096	30	0.221	5.8		49.11	30.98	10.30
					0.206	5.9				
10.	0	31.53	0.107	30	0.152	7.3		47.94	31.44	14.43
					0.128	5.8				
					0.141	6.4				
					0.141	5.7				
					0.154	6.9				
10.	0	29.45	0.105	40	0.114	9.2		47.77	32.50	15.03
					0.101	6.9				
					0.105	8.3				
					0.082	6.9				
					0.093	7.9				
10.	0	30.94	0.104	40	0.112	9.2		49.78	32.80	14.27
					0.108	6.9				
					0.110	8.9				
					0.110	9.3				
					0.118	7.7				
10.	0	31.15	0.111	50	0.066	8.7		48.80	31.53	14.70
					0.059	11.3				
					0.071	7.6				
					0.073	8.9				
					0.062	8.1				
10.	0	30.96	0.110	50	0.089	7.5		50.92	32.60	13.91
					0.103	9.1				
					0.090	7.5				
					0.094	8.0				
10.	0	30.17	0.119	60	0.051	10.5		47.60	32.35	14.80
					0.052	12.6				
					0.054	12.4				
					0.060	9.1				
10.	0	31.73	0.095	60	0.085	10.4		50.92	32.60	13.91
					0.088	12.8				
					0.088	12.8				
					0.082	13.3				
					0.080	11.9				
10.	0	31.60	0.094	80	0.046	11.7		50.96	32.17	14.62
					0.053	11.5				
					0.057	14.3				

APPENDIX A (continued). TABULATED DATA

L/D	θ	F	R	X/D	$\Delta T_c/\Delta T_o$	W/D	Y/D	V_o	T_o	T_a
10.	0	30.32	0.100	80	0.055	15.9		48.73	32.59	13.79
					0.054	15.0				
					0.062	12.5				
					0.058	13.9				
					0.054	11.5				
10.	0	31.87	0.095	100	0.051	17.1		50.30	31.46	14.32
					0.044	15.7				
					0.046	15.8				
					0.051	14.8				
10.	0	29.37	0.113	100	0.059	10.5		48.15	33.05	13.62
					0.050	12.8				
					0.052	14.8				
					0.048	14.3				
10.	0	31.87	0.100	140	0.046	20.1		49.60	32.25	14.23
					0.057	15.8				
					0.038	18.7				
10.	0	28.92	0.104	140	0.043	24.5		48.15	33.45	13.55
					0.043	22.9				
					0.036	16.4				
					0.041	17.5				
					0.042	14.8				
10.	0	30.67	0.250	20	0.147	5.2		50.42	32.15	10.72
					0.160	4.7				
					0.195	5.0				
					0.200	5.4				
10.	0	30.58	0.254	20	0.172	4.0		48.58	33.00	15.41
					0.198	4.8				
					0.203	4.11				
					0.174	4.6				
					0.201	5.5				
					0.190	5.6				
10.	0	20.67	0.247	30	0.120	7.8		50.50	32.34	11.02
					0.128	8.6				
10.	0	32.21	0.243	30	0.146	6.6		50.75	32.75	15.33
					0.130	6.3				
					0.144	6.3				

APPENDIX A (continued). TABULATED DATA

L/D	θ	F	R	X/D	$\Delta T_c/\Delta T_o$	W/D	Y/D	V_o	T_o	T_a
10.	0	30.64	0.249	40	0.093	9.4		52.08	32.30	11.20
					0.083	9.5				
					0.078	8.6				
					0.102	8.6				
10.	0	31.26	0.247	40	0.063	7.4		49.60	33.02	15.52
					0.074	7.1				
					0.067	5.9				
					0.067	6.9				
					0.082	6.6				
					0.078	6.7				
10.	0	31.85	0.239	50	0.066	10.7		52.60	31.97	11.79
					0.061	7.7				
					0.054	7.5				
					0.056	9.5				
10.	0	33.03	0.239	50	0.053	8.5		51.98	32.83	15.57
					0.068	7.5				
					0.061	8.3				
					0.063	7.9				
10.	0	31.82	0.241	60	0.048	8.7		53.20	31.52	11.50
					0.042	9.7				
					0.043	7.6				
10.	0	31.83	0.254	60	0.055	7.7		48.84	33.26	15.70
					0.060	7.9				
					0.052	9.3				
					0.056	7.7				
					0.056	8.3				
					0.049	9.0				
10.	0	31.36	0.239	80	0.050	8.2		52.60	32.13	11.92
					0.052	10.8				
					0.047	10.4				
10.	0	29.98	0.260	80	0.046	10.7		48.21	33.42	15.64
					0.046	10.7				
					0.045	9.2				
					0.042	12.9				
					0.044	11.0				
					0.041	8.6				
10.	0	30.25	0.248	100	0.045	13.5		50.09	31.81	12.05
					0.033	12.0				

APPENDIX A (continued). TABULATED DATA

L/D	θ	F	R	X/D	$\Delta T_c/\Delta T_o$	W/D	Y/D	V_o	T_o	T_a
10.	0	32.44	0.243	100	0.046	12.0		51.52	33.16	15.77
					0.042	11.0				
					0.041	10.9				
					0.040	10.0				
					0.039	10.8				
10.	0	28195	0.262	140	0.040	14.0		47.53	31.63	12.17
					0.025	15.4				
					0.036	11.4				
10.	0	31.09	0.261	140	0.027	10.4		49.01	33.02	15.88
					0.026	12.0				
					0.022	9.6				
					0.022	12.1				
10.	0	34.2	0.450	20	0.131	5.6		55.55	31.63	12.97
					0.145	4.1				
					0.140	5.5				
10.	0	30.89	0.494	20	0.127	3.7		51.05	33.95	15.21
					0.135	6.1				
					0.121	6.0				
					0.131	4.9				
10.	0	28.64	0.518	30	0.083	7.2		48.58	32.80	12.90
					0.088	7.4				
					0.076	5.0				
10.	0	29.65	0.506	30	0.097	4.4		49.58	34.25	15.16
					0.088	6.7				
					0.099	6.2				
					0.074	6.8				
					0.075	3.3				
10.	0	28.32	0.510	40	0.092	6.0		48.97	33.18	12.75
					0.091	5.6				
					0.097	7.8				
10.	0	30.66	0.495	40	0.074	5.9		50.34	33.65	14.93
					0.086	6.1				
					0.065	5.1				
					0.081	6.0				
10.	0	28.72	0.517	50	0.058	8.3		48.58	32.70	12.82
					0.046	9.6				
					0.067	8.5				
					0.046	6.7				

APPENDIX A (continued). TABULATED DATA

L/D	θ	F	R	X/D	$\Delta T_c/\Delta T_o$	W/D	Y/D	V_o	T_o	T_a
10.	0	28.68	0.520	50	0.053	6.4		48.09	34.28	15.04
					0.048	7.3				
					0.059	6.7				
					0.062	4.9				
					0.064	6.6				
10.	0	29.32	0.500	60	0.048	6.7		48.97	32.28	12.67
					0.064	8.8				
					0.055	8.5				
					0.046	7.8				
10.	0	29.05	0.509	60	0.051	9.5		49.13	34.44	14.87
					0.049	5.6				
					0.048	6.5				
10.	0	30.99	0.470	80	0.046	8.9		51.86	32.36	12.75
					0.038	8.3				
					0.048	9.4				
10.	0	26.13	0.512	80	0.036	9.2		44.21	34.41	14.77
					0.036	9.1				
					0.032	11.2				
10.	0	29.53	0.506	100	0.048	11.9		49.00	32.09	12.64
					0.033	10.9				
					0.029	10.0				
10.	0	28.78	0.511	100	0.034	8.5		49.37	34.77	14.69
					0.028	12.9				
					0.029	10.2				
					0.029	9.1				
10.	0	30.65	0.499	140	0.033	12.6		49.60	31.37	12.54
					0.024	13.5				
					0.033	7.9				
10.	0	29.66	0.516	140	0.018	13.7		48.66	33.50	14.64
					0.021	10.3				
					0.017	11.8				
10.	0	54.4	0	10	0.497	4.0*	0.0*	76.4	29.26	18.03
		56.7		20	0.277	8.0	0.8*	73.6	29.16	17.97
		54.4		30	0.181	11.	1.2	76.3	30.53	17.72
		51.4		40	0.121	17.	2.8	75.03	32.51	19.58
		56.4		60	0.090	21.	7.3	70.96	30.10	19.75
		54.9		80	0.063	28.	12.0	70.2	30.16	19.80
		54.9		100	0.048	38.	18.7	70.3	30.28	20.05
		53.8		140	0.042	**	44.	74.6	30.29	17.69

APPENDIX A (continued). TABULATED DATA

L/D	θ	F	R	X/D	$\Delta T_c/\Delta T_o$	W/D	Y/D	V_o	T_o	T_a
10.	0	54.87	0.051	20	0.196	7.7		70.48	26.25	13.07
					0.210	6.5				
					0.210	6.3				
					0.224	7.5				
					0.217	7.7				
10.	0	58.05	0.052	20	0.242	6.5		76.06	28.10	14.50
					0.236	5.9				
					0.231	7.1				
					0.230	6.0				
					0.221	6.6				
					0.224	5.5				
10.	0	53.06	0.052	30	0.156	8.1		70.05	26.85	13.17
					0.160	7.2				
					0.154	8.3				
					0.151	8.7				
					0.155	8.9				
10.	0	53.90	0.055	20	0.192	6.5		74.27	26.52	10.04
					0.237	6.5				
					0.247	7.0				
					0.251	6.5				
10.	0	53.41	0.052	30	0.153	7.2		74.32	26.69	9.81
					0.132	5.7				
					0.160	5.9				
					0.158	8.7				
					0.153	8.6				
10.	0	49.75	0.055	50	0.091	11.0		69.15	26.65	9.80
					0.098	11.4				
					0.097	12.5				
					0.092	9.1				
					0.091	14.2				
10.	0	52.16	0.055	30	0.145	8.3		68.97	28.35	14.62
					0.148	9.0				
					0.148	6.7				
					0.150	7.4				
					0.149	7.8				
10.	0	52.68	0.0512	40	0.113	8.4		74.05	26.85	9.61
					0.103	11.0				
					0.110	10.4				
					0.107	10.2				
					0.115	10.5				

APPENDIX A (continued). TABULATED DATA

L/D	θ	F	R	X/D	$\Delta T_c/\Delta T_o$	W/D	Y/D	V_o	T_o	T_a
10.	0	52.59	0.050	40	0.104	9.6		71.07	28.87	14.74
					0.112	10.9				
					0.108	8.9				
					0.113	12.7				
					0.104	8.6				
10.	0	55.29	0.054	50	0.098	14.0		73.14	26.95	13.29
					0.094	11.7				
					0.098	11.8				
					0.098	10.4				
10.	0	54.00	0.051	50	0.086	11.3		71.96	28.57	14.73
					0.091	11.2				
					0.087	12.4				
					0.091	12.8				
10.	0	54.03	0.052	60	0.070	13.4		75.42	26.64	9.46
					0.075	12.0				
					0.089	11.6				
					0.081	11.6				
					0.075	12.2				
10.	0	53.67	0.048	60	0.076	14.1		72.39	28.86	14.80
					0.080	11.8				
					0.071	13.0				
					0.079	13.5				
					0.066	12.6				
10.	0	53.44	0.052	80	0.060	18.6		75.76	26.94	9.25
					0.065	17.2				
					0.057	18.9				
					0.064	18.8				
10.	0	52.94	0.055	80	0.58	15.2		70.23	28.54	14.86
					0.056	18.2				
					0.048	15.1				
					0.057	16.9				
					0.050	15.9				
10.	0	53.76	0.052	100	0.053	13.1		73.96	26.20	9.10
					0.061	23.1				
					0.065	19.8				
					0.066	18.3				
					0.056	20.1				
10.	0	52.38	0.050	100	0.054	12.7		70.88	29.00	14.94
					0.051	18.7				
					0.047	19.9				
					0.050	19.2				
					0.048	17.9				

APPENDIX A (continued). TABULATED DATA

L/D	θ	F	R	X/D	$\Delta T_a/\Delta T_o$	W/D	Y/D	V_o	T_o	T_a
10.	0	54.39	0.056	140	0.055	18.3		75.05	26.20	8.85
					0.047	24.6				
					0.050	24.0				
					0.038	23.8				
					0.050	20.9				
10.	0	56.80	0.049	140	0.042	24.6		75.14	28.40	14.70
					0.040	23.6				
					0.039	24.0				
					0.038	20.7				
10.	0	54.21	0.101	20	0.186	4.6		74.53	26.53	10.22
					0.185	5.4				
					0.216	6.7				
10.	0	52.54	0.104	20	0.262	5.2		71.96	27.05	9.92
					0.253	6.7				
					0.251	6.6				
10.	0	54.28	0.105	30	0.148	8.6		74.29	26.46	10.31
					0.154	7.1				
					0.154	7.3				
10.	0	52.63	0.104	30	0.152	6.9		70.31	26.43	9.80
					0.167	7.8				
					0.154	8.0				
					0.146	8.9				
					0.155	5.3				
10.	0	55.04	0.100	40	0.113	8.6		75.97	26.73	10.53
					0.091	8.5				
					0.107	9.1				
					0.100	7.1				
10.	0	52.68	0.110	40	0.121	6.7		69.52	28.65	15.27
					0.124	8.7				
					0.127	8.9				
10.	0	54.14	0.110	50	0.086	10.2		73.43	26.29	10.40
					0.083	12.5				
					0.081	10.5				
10.	0	54.16	0.108	50	0.090	11.1		71.10	28.57	15.32
					0.092	9.1				
					0.098	11.2				
					0.094	11.4				

APPENDIX A (continued). TABULATED DATA

L/D	θ	F	R	X/D	$\Delta T_c/\Delta T_o$	W/D	Y/D	V_o	T_o	T_a
10.	0	54.16	0.099	60	0.081	8.9		77.42	26.71	10.61
					0.084	9.9				
					0.080	9.5				
10.	0	54.06	0.109	60	0.088	8.4		70.07	28.55	16.15
					0.088	11.0				
					0.087	8.7				
					0.078	11.2				
10.	0	54.37	0.102	80	0.062	13.8		74.53	26.64	10.73
					0.052	10.9				
					0.057	13.6				
10.	0	54.52	0.105	80	0.060	15.4		70.9	28.27	15.12
					0.055	11.5				
					0.062	13.5				
					0.058	13.3				
					0.060	15.5				
10.	0	53.31	0.107	100	0.047	15.8		73.46	26.79	10.82
					0.013	15.5				
					0.057	14.4				
10.	0	58.50	0.098	100	0.051	17.2		76.4	28.31	15.03
					0.049	12.7				
					0.050	14.1				
					0.053	15.6				
10.	0	52.68	0.105	140	0.047	19.6		72.42	26.76	10.90
					0.046	19.5				
10.	0	55.72	0.100	140	0.039	13.0		76.90	26.82	10.79
					0.044	15.1				
					0.043	18.2				
10.	0	58.51	0.098	140	0.046	18.5		77.16	28.47	14.96
					0.045	19.1				
					0.039	19.2				
					0.039	21.0				
10.	0	56.83	0.254	20	0.200	5.2		73.96	26.39	11.17
					0.207	5.3				
					0.194	5.3				
10.	0	51.38	0.264	20	0.204	5.9		71.18	27.37	10.06
					0.200	4.3				
					0.190	6.5				
					0.193	5.4				

APPENDIX A (continued). TABULATED DATA

L/D	θ	F	R	X/D	$\Delta T_c/\Delta T_o$	W/D	Y/D	V_o	T_o	T_a
10.	0	55.75	0.260	30	0.119	6.1		72.1	26.22	11.10
					0.129	5.6				
					0.120	6.0				
					0.119	6.6				
10.	0	54.40	0.250	30	0.140	6.9		72.07	26.43	10.22
					0.140	6.1				
					0.145	6.9				
					0.142	7.0				
10.	0	55.03	0.260	40	0.087	7.8		71.74	26.38	11.05
					0.098	7.6				
					0.099	7.3				
					0.088	6.1				
10.	0	51.55	0.257	40	0.103	7.1		71.85	27.65	10.42
					0.113	7.7				
					0.112	9.2				
					0.102	8.2				
10.	0	56.77	0.228	50	0.065	9.4		71.9	25.76	11.05
					0.073	8.5				
					0.079	7.8				
					0.081	6.4				
10.	0	51.12	0.260	50	0.072	9.5		70.72	27.43	10.31
					0.086	7.4				
					0.072	8.7				
10.	0	57.96	0.240	60	0.076	8.3		76.01	26.48	10.98
					0.071	6.8				
					0.063	9.4				
					0.070	6.2				
10.	0	50.17	0.266	60	0.060	9.4		69.52	27.53	10.53
					0.071	7.2				
					0.066	7.1				
					0.071	7.5				
10.	0	58.74	0.241	80	0.058	12.4		76.26	26.22	10.89
					0.051	9.7				
					0.054	10.8				
10.	0	52.43	0.261	80	0.049	10.1		70.31	26.85	10.67
					0.057	10.2				
					0.047	11.4				
					0.047	8.0				

APPENDIX A (continued). TABULATED DATA

L/D	θ	F	R	X/D	$\Delta T_c/\Delta T_o$	W/D	Y/D	V_o	T_o	T_a
10.	0	59.83	0.242	100	0.045	9.2		76.26	25.78	10.78
					0.055	11.1				
					0.043	12.7				
					0.043	12.5				
10.	0	57.92	0.250	100	0.043	10.8		75.57	27.34	13.20
					0.045	10.7				
					0.040	10.2				
					0.043	10.1				
10.	0	56.58	0.0250	140	0.047	12.9		74.70	25.91	10.96
					0.037	12.4				
					0.040	16.5				
10.	0	56.56	0.249	140	0.035	18.7		76.1	28.03	13.24
					0.028	14.6				
					0.033	17.1				
					0.032	17.4				
10.	0	55.07	0.451	20	0.133	4.6		69.50	25.71	11.22
					0.130	3.7				
10.	0	54.96	0.525	20	0.105	5.1		71.88	26.04	10.02
					0.115	4.9				
					0.093	5.2				
10.	0	57.39	0.499	30	0.091	6.5		75.43	26.69	11.37
					0.083	6.0				
					0.092	5.5				
					0.082	5.7				
10.	0	57.62	0.496	30	0.091	5.9		75.58	27.71	13.74
					0.087	5.3				
					0.091	5.8				
10.	0	55.84	0.520	40	0.058	7.2		72.76	26.58	11.55
					0.056	6.1				
					0.053	6.4				
					0.070	7.2				
					0.057	6.8				
10.	0	56.59	0.517	40	0.082	5.1		75.56	27.22	13.64
					0.071	5.3				
					0.066	5.8				
10.	0	52.37	0.545	50	0.043	7.8		69.00	26.78	11.45
					0.045	6.3				
					0.040	6.6				

APPENDIX A (continued). TABULATED DATA

L/D	θ	F	R	X/D	$\Delta T_c/\Delta T_o$	W/D	Y/D	V_o	T_o	T_a
10.	0	55.94	0.516	50	0.041	9.3		73.08	27.03	13.69
					0.052	7.5				
					0.050	7.7				
10.	0	50.90	0.566	60	0.047	10.9		66.73	26.75	11.64
					0.037	5.5				
					0.040	8.6				
10.	0	56.29	0.510	60	0.046	8.2		73.70	27.60	13.54
					0.042	7.7				
					0.044	9.4				
10.	0	53.59	0.553	80	0.035	12.7		68.52	26.23	11.67
					0.030	9.1				
10.	0	55.63	0.516	80	0.035	9.3		72.73	27.54	13.48
					0.028	8.5				
					0.023	13.6				
10.	0	55.58	0.536	100	0.019	13.2		70.27	26.05	11.79
					0.025	6.8				
					0.023	8.0				
					0.027	6.1				
10.	0	56.15	0.516	100	0.031	10.3		73.17	27.44	13.41
					0.029	11.8				
					0.023	11.8				
10.	15	10.50	0.110	10	0.364	3.4	3.2	24.08	45.26	16.60
					0.372	3.9	3.3			
					0.393	3.8	3.2			
					0.417	3.7	2.8			
10.	15	10.55	0.106	20	0.193	6.5	6.9	22.60	42.60	16.35
					0.187	4.9	6.4			
					0.185	5.8	4.9			
					0.185	6.6	6.1			
					0.186	5.5	5.9			
					0.188	6.9	6.2			
10.	15	9.77	0.110	20	0.173	4.9	5.7	23.73	48.59	19.27
					0.187	6.7	6.9			
					0.192	7.1	6.3			
					0.172	5.8	5.8			
					0.204	7.7	6.3			
					0.187	6.1	5.5			
					0.190	4.9	6.2			

APPENDIX A (continued). TABULATED DATA

L/D	θ	F	R	X/D	$\Delta T_c/\Delta T_o$	W/D	Y/D	V_o	T_o	T_a
10.	15	9.50	0.106	30	0.109	8.2	9.2	23.28	48.90	19.19
					0.116	6.3	9.5			
					0.127	7.1	8.7			
					0.115	6.1	8.7			
					0.125	9.6	9.4			
					0.128	10.6	9.3			
10.	15	10.63	0.099	30	0.122	8.0	8.9	25.49	47.97	19.09
					0.112	8.2	8.8			
					0.114	8.3	9.4			
					0.120	6.5	9.0			
					0.120	8.7	9.5			
					0.121	6.7	10.2			
10.	15	10.30	0.105	40	0.080	10.5	10.6	24.77	48.08	18.99
					0.079	8.8	10.6			
					0.080	11.5	10.1			
					0.079	13.1	10.1			
10.	15	10.56	0.102	40	0.078	9.6	10.3	25.11	47.54	18.84
					0.087	7.4	10.7			
					0.084	10.5	10.3			
					0.089	7.4	11.5			
					0.080	8.2	12.2			
10.	15	9.32	0.108	50	0.056	13.7	11.8	23.40	49.79	18.80
					0.054	9.9	13.1			
					0.055	8.7	14.2			
					0.054	11.4	13.9			
10.	15	10.05	0.105	50	0.064	12.4	15.3	23.96	47.60	18.68
					0.059	13.5	12.3			
					0.056	15.4	15.4			
					0.058	11.5	12.4			
10.	15	10.10	0.106	60	0.041	15.0	14.9	23.67	46.92	18.69
					0.041	16.5	12.9			
					0.041	16.7	13.5			
					0.040	13.0	17.4			
10.	15	11.07	0.109	60	0.040	10.6	9.0	23.48	43.14	18.56
					0.043	9.4	11.5			
					0.036	12.5	11.5			
					0.043	13.1	12.2			
10.	15	12.20	0.108	60	0.051	10.4	14.6	23.66	40.13	18.52
					0.049	8.8	11.9			
					0.048	10.8	12.5			

APPENDIX A (continued). TABULATED DATA

L/D	θ	F	R	X/D	$\Delta T_o/\Delta T_o$	W/D	Y/D	V_o	T_o	T_a
10.	15	10.56	0.106	100	0.041	21.9	20.4	24.23	45.29	16.71
					0.034	24.3	20.4			
10.	15	10.34	0.260	10	0.346	4.3	2.3	24.40	45.99	15.43
					0.354	2.9	2.9			
10.	15	10.72	0.251	10	0.342	3.4	2.5	25.35	46.13	15.52
					0.360	4.0	2.7			
					0.359	3.2	2.5			
					0.343	3.7	2.6			
10.	15	10.80	0.247	20	0.183	6.3	4.1	25.39	45.88	15.53
					0.177	5.0	4.2			
					0.179	4.4	4.3			
10.	15	11.80	0.237	20	0.163	5.0	5.1	26.14	43.55	15.53
					0.174	5.2	4.9			
					0.168	5.9	5.1			
10.	15	11.47	0.240	20	0.171	5.1	4.3	25.85	44.25	15.65
					0.184	5.7	4.0			
					0.168	5.5	4.6			
					0.188	6.1	4.7			
10.	15	11.85	0.248	30	0.125	5.5	5.9	25.20	42.40	14.01
					0.117	6.0	5.7			
					0.112	5.6	5.6			
10.	15	11.40	0.251	30	0.128	6.9	5.8	25.20	42.99	14.16
					0.141	6.4	5.3			
10.	15	10.94	0.259	40	0.100	8.7	5.4	24.40	43.39	14.26
					0.110	8.0	6.2			
					0.097	9.6	6.8			
10.	15	10.99	0.252	40	0.092	6.9	6.2	24.95	44.10	14.29
					0.084	7.6	5.8			
					0.093	7.9	6.4			
10.	15	11.07	0.254	50	0.065	7.4	7.6	24.91	43.76	14.37
					0.066	8.5	7.5			
					0.068	7.9	7.6			
					0.071	9.0	6.9			
10.	15	11.31	0.248	50	0.076	7.5	6.3	25.09	43.21	14.41
					0.077	8.5	6.5			
					0.087	9.8	7.6			

APPENDIX A (continued). TABULATED DATA

L/D	θ	F	R	X/D	$\Delta T_o/\Delta T_o$	W/D	Y/D	V_o	T_o	T_a
10.	15	11.48	0.242	60	0.055	9.1	7.3	25.53	43.35	14.47
					0.058	7.6	7.5			
10.	15	11.10	0.258	60	0.068	13.4	7.9	23.70	41.82	14.53
					0.066	9.7	7.2			
					0.062	10.9	7.7			
10.	15	10.65	0.497	10	0.314	2.8	1.4	25.38	46.53	15.80
					0.325	2.6	1.4			
10.	15	10.60	0.500	10	0.329	2.8	1.8	25.26	46.37	15.82
					0.328	3.5	1.7			
10.	15	11.13	0.475	10	0.293	2.5	2.0	16.06	45.81	15.76
					0.294	3.2	1.7			
10.	15	10.08	0.495	20	0.151	3.8	2.1	25.49	49.45	17.1
					0.151	4.0	2.5			
10.	15	9.99	0.501	20	0.183	4.8	2.1	25.20	49.33	17.01
					0.166	3.9	2.6			
10.	15	10.14	0.495	20	0.180	4.8	2.9	25.30	48.86	16.90
					0.174	5.0	2.5			
10.	15	10.66	0.489	30	0.147	5.1	3.1	25.39	46.91	16.88
					0.141	6.6	3.4			
10.	15	10.92	0.478	30	0.114	4.8	3.4	26.13	47.06	16.80
					0.119	5.2	2.8			
10.	15	10.44	0.500	30	0.124	4.6	3.3	25.00	47.07	16.72
					0.119	5.1	3.3			
10.	15	10.41	0.499	40	0.117	4.3	4.3	25.35	47.72	16.67
10.	15	10.59	0.483	40	0.098	7.2	3.6	25.97	48.02	16.63
10.	15	10.04	0.505	40	0.096	6.4	3.8	24.83	48.33	16.52
					0.097	6.3	3.5			
10.	15	9.94	0.504	50	0.084	8.1	4.1	24.94	48.97	16.54
					0.080	8.2	4.6			
10.	15	10.03	0.514	50	0.069	7.7	3.8	24.84	48.38	16.47
10.	15	11.12	0.464	50	0.083	5.8	4.2	27.00	47.51	16.37
					0.079	6.1	3.1			
					0.086	6.9	4.2			

APPENDIX A (continued). TABULATED DATA

L/D	θ	F	R	X/D	$\Delta T_c/\Delta T_o$	W/D	Y/D	V_o	T_o	T_a
10.	15	11.44	0.488	60	0.068	8.1	4.4	25.62	44.08	15.86
					0.066	6.2	3.8			
10.	15	11.10	0.513	60	0.079	11.0	3.4	24.83	44.00	15.78
10.	15	11.38	0.496	60	0.075	7.8	3.4	25.62	44.21	15.67
					0.075	6.7	4.0			
10.	15	11.12	0.498	60	0.066	6.6	3.9	25.42	44.77	15.60
					0.068	7.1	4.1			
10.	15	11.63	0.476	80	0.063	8.4	4.2	26.57	44.75	15.50
					0.060	7.6	6.1			
10.	15	10.98	0.501	80	0.059	5.9	5.4	25.19	44.88	15.44
10.	15	30.44	0	10	0.382	6.6	4.2	49.54	36.82	21.52
					0.410	5.1	4.1			
					0.396	5.0	3.3			
					0.402	6.1	4.2			
					0.392	5.5	4.7			
					0.390	4.2	4.2			
					0.384	4.9	4.2			
10.	15	30.42	0	20	0.174	6.1	9.6	50.75	37.30	21.29
					0.192	7.8	8.1			
					0.180	11.8	9.6			
					0.183	10.9	7.8			
					0.194	10.8	7.7			
					0.192	8.4	7.2			
					0.172	7.7	8.1			
10.	15	30.86	0	30	0.140	13.6	12.2	50.53	36.60	20.88
					0.140	14.1	12.0			
					0.153	13.1	12.3			
					0.143	18.6	12.0			
					0.154	13.2	9.8			
					0.150	12.8	10.5			
					0.143	12.5	10.4			
					0.154	13.6	9.6			
					0.157	12.9	11.2			
10.	15	30.48	0	40	0.089	27.9	22.3	50.28	36.63	20.61
					0.084	26.2	19.4			
					0.099	31.9	18.6			
					0.094	28.7	17.0			
					0.086	25.4	19.0			
					0.099	25.8	15.6			
					0.095	21.3	16.4			

APPENDIX A (continued). TABULATED DATA

L/D	θ	F	R	X/D	$\Delta T_c/\Delta T_o$	W/D	Y/D	V_o	T_o	T_a
10.	15	30.10	0	50	0.089	32.1	21.3	49.83	36.63	20.45
					0.077	32.1	22.2			
					0.084	24.0	22.9			
					0.077	27.5	23.9			
					0.085	30.4	21.0			
					0.086	22.1	20.5			
					0.090	27.0	18.8			
10..	15	30.83	0	60	0.074	38.2	30.5	50.45	36.22	20.23
					0.068	23.3	32.5			
					0.066	31.9	31.7			
					0.072	30.5	31.7			
					0.071	35.9	30.9			
					0.072	32.1	28.4			
10.	15	36.94	0.048	10	0.406	6.0	2.7	56.75	32.83	16.76
					0.408	4.8	2.8			
					0.415	3.9	2.7			
					0.418	4.6	2.9			
10.	15	34.12	0.050	20	0.209	6.0	4.9	53.30	33.18	16.66
					0.220	6.3	5.0			
					0.201	6.4	4.7			
					0.220	7.3	4.8			
					0.213	6.4	4.6			
					0.208	6.4	5.6			
10..	15	32.41	0.057	30	0.141	9.4	7.3	52.83	34.26	16.66
					0.147	8.7	6.9			
					0.148	8.5	6.7			
					0.142	9.0	7.2			
10.	15	35.46	0.047	40	0.098	11.9	8.7	57.80	34.23	16.60
					0.095	9.3	10.1			
					0.099	10.5	8.8			
					0.107	11.3	9.5			
					0.098	13.6	8.9			
					0.098	10.8	8.9			
10.	15	29.47	0.057	50	0.089	13.2	10.8	47.30	33.78	16.51
					0.084	14.2	10.3			
					0.079	15.0	9.4			
					0.080	12.4	9.7			
10.	15	36.24	0.053	60	0.067	11.9	9.6	54.44	32.10	16.41
					0.071	15.5	10.3			
					0.071	14.4	11.0			
					0.071	17.4	11.9			

APPENDIX A (continued). TABULATED DATA

L/D	θ	F	R	X/D	$\Delta T_c/\Delta T_o$	W/D	Y/D	V_o	T_o	T_a
10.	15	29.59	0.107	10	0.309	5.2	2.9	45.52	31.25	13.34
					0.333	4.4	2.1			
					0.349	5.2	2.0			
					0.331	4.6	2.7			
					0.346	4.8	2.1			
					0.373	4.1	2.3			
10.	15	32.56	0.098	20	0.195	7.7	3.9	49.97	30.39	11.34
					0.200	6.2	4.5			
					0.186	7.2	3.6			
					0.184	6.9	3.3			
10.	15	29.67	0.103	20	0.178	6.3	4.1	47.50	31.56	11.44
					0.223	6.5	4.2			
					0.184	6.8	3.7			
					0.191	7.4	3.9			
					0.195	5.9	4.7			
					0.203	6.7	3.7			
10.	15	29.06	0.106	20	0.202	6.9	3.7	46.50	31.59	11.58
					0.214	5.9	3.6			
					0.207	7.8	3.7			
					0.202	6.7	4.3			
10.	15	33.32	0.105	30	0.125	9.8	4.8	48.75	29.07	11.06
					0.138	9.7	5.4			
					0.127	9.6	5.5			
					0.130	9.6	5.5			
10..	15	32.2	0.104	30	0.122	7.8	5.2	47.40	29.29	11.22
					0.135	9.4	5.9			
					0.124	8.7	5.9			
					0.136	7.3	5.2			
10.	15	33.81	0.098	40	0.099	8.9	6.0	51.20	29.81	10.70
					0.105	9.2	6.3			
					0.095	9.5	7.6			
10.	15	34.11	0.099	40	0.104	11.2	7.3	51.35	29.71	10.85
					0.104	10.6	6.6			
					0.092	9.1	7.3			
					0.083	12.5	6.7			
10.	15	32.61	0.104	40	0.101	11.9	7.6	49.20	29.81	10.97
					0.096	10.0	6.6			
					0.096	9.8	7.3			
10..	15	32.83	0.095	50	0.079	10.8	8.0	50.50	30.04	10.20
					0.077	10.7	7.2			

APPENDIX A (continued). TABULATED DATA

L/D	θ	F	R	X/D	$\Delta T_c/\Delta T_o$	W/D	Y/D	V_o	T_o	T_a
10.	15	35.45	0.096	50	0.072	10.6	6.0	51.05	28.49	10.57
					0.074	11.4	6.7			
					0.068	13.4	6.1			
10.	15	33.64	0.091	60	0.061	11.9	10.1	52.80	30.53	10.04
					0.060	12.5	10.5			
					0.066	13.6	10.6			
10.	15	30.07	0.252	10	0.277	5.0	3.0	42.05	29.36	14.22
					0.275	4.0	3.1			
10.	15	29.98	0.250	10	0.284	4.2	2.3	41.60	29.21	14.27
					0.281	3.7	2.0			
10.	15	30.20	0.251	10	0.349	3.4	2.5	41.66	29.08	14.27
					0.331	4.0	2.5			
					0.325	4.0	3.8			
10.	15	31.13	0.239	20	0.218	5.9	3.1	43.88	29.52	14.20
					0.206	5.5	3.4			
					0.209	5.5	2.8			
					0.219	6.3	3.4			
10.	15	28.85	0.256	30	0.132	6.5	4.0	41.12	29.76	14.16
					0.127	6.0	4.1			
10.	15	31.84	0.250	30	0.138	7.0	4.0	41.92	27.97	14.05
					0.136	7.3	3.4			
10.	15	30.10	0.251	40	0.109	9.0	4.7	41.66	29.08	14.10
					0.109	7.7	3.4			
					0.106	7.2	5.6			
10.	15	30.08	0.249	40	0.101	7.9	5.7	42.11	29.33	14.11
					0.102	8.5	4.3			
					0.103	8.6	3.8			
10.	15	31.94	0.231	50	0.107	8.7	5.1	43.03	28.48	14.10
					0.099	8.7	5.0			
					0.097	8.3	4.2			
10.	15	34.21	0.262	50	0.077	10.4	4.8	48.98	29.71	13.81
					0.079	8.4	4.2			
10.	15	32.83	0.253	60	0.071	10.7	3.6	49.20	30.77	13.74
					0.068	9.8	5.2			
					0.069	9.4	5.5			

APPENDIX A (continued). TABULATED DATA

L/D	θ	F	R	X/D	$\Delta T_c/\Delta T_o$	W/D	Y/D	V_o	T_o	T_o
10.	15	33.05	0.259	60	0.065	12.6	5.0	49.10	30.52	13.65
					0.072	10.3	4.0			
10.	15	31.00	0.254	10	0.343	4.1	3.8	49.80	36.61	21.70
					0.340	4.8	3.3			
10.	15	31.49	0.252	10	0.349	3.7	3.4	49.80	36.33	21.85
10.	15	31.43	0.252	20	0.174	6.2	4.6	50.72	36.84	21.91
					0.180	5.9	4.5			
10.	15	31.20	0.248	20	0.188	5.4	4.0	50.50	36.96	22.00
					0.190	7.0	3.8			
10.	15	31.61	0.246	20	0.157	7.5	4.7	51.14	37.02	22.10
10.	15	31.39	0.242	30	0.115	8.5	5.2	51.23	36.24	20.39
					0.116	7.2	5.3			
10.	15	30.81	0.246	30	0.126	8.3	4.7	51.00	36.64	20.46
					0.129	7.8	5.4			
10.	15	30.48	0.247	30	0.124	7.8	5.3	50.83	36.86	20.53
					0.124	10.8	5.0			
10.	15	30.74	0.244	40	0.080	7.6	7.2	51.06	36.82	20.63
					0.080	7.4	6.8			
10.	15	31.05	0.244	40	0.101	9.8	5.6	51.75	37.07	20.92
					0.096	8.4	5.9			
10.	15	31.17	0.244	40	0.101	7.1	6.0	51.67	37.05	21.13
10.	15	30.07	0.259	50	0.077	12.4	7.2	48.64	36.61	21.42
					0.067	10.1	6.2			
10.	15	30.62	0.252	50	0.079	9.1	7.0	49.88	36.82	21.48
					0.075	7.9	6.8			
10.	15	31.53	0.251	50	0.064	9.7	6.8	50.18	36.34	21.62
					0.069	10.7	5.3			
10.	15	30.91	0.248	30	0.117	7.3	5.7	51.23	37.39	21.73
					0.110	8.2	4.2			
10.	15	29.79	0.252	10	0.315	5.4	3.6	49.80	37.67	21.85
					0.304	4.0	3.7			

APPENDIX A (continued). TABULATED DATA

L/D	θ	F	R	X/D	$\Delta T_c/\Delta T_o$	W/D	Y/D	V_o	T_o	T_a
10.	15	30.35	0.497	10	0.273	3.2	1.3	41.48	28.88	14.28
10.	15	30.18	0.502	10	0.334	3.6	1.6	41.10	28.82	14.32
10.	15	30.89	0.496	10	0.353	3.3	1.6	41.79	28.69	14.32
					0.335	3.8	0.8			
10.	15	29.69	0.506	20	0.173	5.0	1.6	40.78	29.03	14.36
10.	15	28.61	0.505	20	0.176	6.1	1.9	40.30	29.59	14.35
					0.184	5.0	2.1			
10.	15	29.00	0.506	20	0.170	6.3	2.1	40.78	29.57	14.40
					0.168	5.3	2.1			
10.	15	30.91	0.506	30	0.123	5.6	3.3	50.01	33.50	15.47
					0.122	4.9	3.1			
10.	15	30.24	0.512	30	0.149	5.3	2.4	49.28	33.68	15.44
					0.137	5.8	2.9			
10.	15	30.25	0.511	30	0.120	6.9	3.2	49.21	33.61	15.38
					0.127	6.1	2.0			
10.	15	30.80	0.500	30	0.119	5.8	2.0	50.34	33.71	15.33
					0.136	5.6	2.5			
10.	15	31.29	0.492	40	0.141	6.7	3.0	51.44	33.83	15.26
					0.125	4.8	3.2			
10.	15	30.75	0.504	40	0.098	6.2	2.2	49.94	33.48	15.19
					0.104	7.5	2.1			
10.	15	30.99	0.496	40	0.096	8.4	3.2	50.75	33.71	15.23
					0.091	6.9	2.1			
10.	15	30.30	0.506	40	0.097	6.0	3.1	49.72	33.71	15.11
					0.095	5.7	3.0			
10.	15	30.41	0.499	50	0.085	9.3	2.5	50.09	33.78	15.04
					0.078	6.9	2.4			
10.	15	30.64	0.490	50	0.083	7.1	2.7	50.67	33.83	14.89
					0.077	6.0	3.7			
10.	15	30.54	0.487	60	0.067	8.0	2.4	50.92	34.05	14.98
					0.064	8.7	2.9			
10.	15	31.28	0.493	60	0.083	7.8	3.7	50.75	33.27	14.79

APPENDIX A (continued). TABULATED DATA

L/D	θ	F	R	X/D	$\Delta T_c/\Delta T_o$	W/D	Y/D	V_o	T_o	T_a
10.	15	55.73	0.051	10	0.438	5.0	3.6	79.00	30.58	16.05
					0.459	5.7	3.7			
					0.451	4.5	3.6			
					0.470	6.0	4.0			
					0.435	4.9	3.4			
					0.427	5.0	3.7			
					0.436	5.7	3.6			
10	15.	56.73	0.050	20	0.218	6.5	5.4	80.40	30.52	15.94
					0.224	6.8	5.1			
					0.216	8.3	5.2			
					0.212	8.1	6.1			
					0.207	8.1	6.2			
10..	15	56.26	0.049	30	0.148	10.5	8.5	80.56	30.67	15.78
					0.148	11.2	9.1			
					0.156	10.5	8.4			
					0.153	9.9	9.1			
					0.155	8.2	7.8			
					0.153	8.5	9.3			
					0.164	9.6	8.2			
10.	15	55.62	0.050	30	0.147	9.7	7.8	80.50	30.97	15.89
					0.147	10.8	8.4			
					0.150	8.5	7.9			
					0.150	12.1	8.8			
10..	15	56.30	0.056	40	0.103	9.2	9.7	75.25	29.20	15.80
					0.110	12.1	9.1			
					0.113	12.2	10.4			
					0.109	11.3	10.6			
					0.113	12.4	10.3			
					0.116	10.8	10.6			
10.	15	62.01	0.049	50	0.083	12.2	11.4	84.09	20.40	15.62
					0.091	10.6	10.4			
					0.086	13.4	1169			
					0.083	15.8	11.8			
					0.083	12.6	11.1			
					0.086	14.2	11.0			
10..	15	62.13	0.049	60	0.071	14.4	12.6	84.09	29.34	15.58
					0.076	12.8	12.8			
					0.081	12.6	12.4			
					0.074	13.1	11.9			
					0.075	13.8	11.7			

APPENDIX A (continued). TABULATED DATA

L/D	θ	F	R	X/D	$\Delta T_c/\Delta T_o$	W/D	Y/D	V_o	T_o	T_a
10..	15	55.84	0.103	10	0.423	4.6	4.2	77.68	30.22	16.15
					0.405	4.3	4.1			
					0.462	4.8	4.2			
					0.389	4.6	4.5			
					0.396	4.6	3.5			
10..	15	56.81	0.098	10	0.435	4.8	3.6	78.34	30.06	14.18
					0.438	4.8	3.9			
					0.425	4.2	3.4			
10.	15	56.34	0.099	20	0.223	6.7	6.0	77.74	30.10	16.24
					0.226	6.8	5.6			
					0.207	7.3	6.0			
					0.217	7.8	5.6			
10..	15	57.90	0.099	20	0.208	6.9	5.2	76.65	26.86	11.40
					0.197	7.3	5.4			
					0.195	8.0	5.7			
					0.192	8.2	5.5			
					0.179	6.4	5.4			
10.	15	58.38	0.100	30	0.142	8.9	6.0	77.99	27.10	11.49
					0.135	8.8	5.7			
					0.118	8.8	6.0			
					0.111	10.3	5.0			
					0.112	9.8	5.5			
10.	15	56.95	0.103	30	0.129	8.4	6.3	76.24	27.19	11.58
					0.132	8.2	5.4			
					0.131	7.4	6.8			
					0.119	10.5	4.9			
10.	15	58.59	0.100	40	0.110	10.4	6.8	77.68	27.01	11.67
					0.123	10.7	7.3			
					0.116	9.2	8.1			
					0.102	10.9	6.4			
					0.113	9.4	7.9			
10.	15	58.22	0.101	40	0.092	10.9	7.0	77.18	27.06	11.79
					0.104	12.4	7.8			
					0.111	10.8	6.9			
					0.111	9.2	7.1			
10..	15	56.30	0.103	50	0.084	8.1	7.1	74.62	27.07	11.89
					0.093	11.4	6.7			
					0.090	13.0	7.7			
10..	15	58.47	0.100	50	0.076	9.7	8.3	76.00	26.74	12.04
					0.086	13.5	6.9			
					0.081	12.5	8.5			
					0.074	12.1	6.6			

APPENDIX A (continued). TABULATED DATA

L/D	θ	F	R	X/D	$\Delta T_c/\Delta T_o$	W/D	Y/D	V_o	T_o	T_a
10.	15	57.38	0.102	60	0.069	12.0	7.7	74.64	26.81	12.15
					0.070	12.4	7.2			
					0.070	11.1	7.8			
					0.072	9.4	7.4			
					0.069	13.9	8.5			
10.	15	57.38	0.102	60	0.062	10.5	7.3	74.78	26.90	12.25
					0.073	13.1	8.7			
					0.072	14.6	6.3			
					0.075	10.9	9.9			
10.	15	57.46	0.249	10	0.421	3.9	2.3	76.25	29.16	16.01
10.	15	57.12	0.249	10	0.356	4.2	2.3	76.13	29.22	15.96
					0.380	4.9	2.4			
10.	15	55.57	0.257	10	0.422	4.1	2.6	74.28	29.24	15.88
					0.425	4.9	2.6			
10.	15	55.17	0.259	20	0.209	5.4	3.7	74.04	29.29	15.83
					0.205	6.4	3.5			
10.	15	57.04	0.251	20	0.223	5.9	4.5	76.68	29.31	15.80
					0.231	5.1	4.0			
					0.210	5.1	4.0			
10.	15	55.05	0.254	20	0.187	5.8	4.2	74.86	29.34	15.72
					0.212	5.2	3.9			
					0.195	5.9	3.6			
10.	15	53.79	0.258	30	0.142	7.1	4.5	74.02	29.75	15.69
					0.144	7.0	4.2			
					0.143	7.5	4.1			
10.	15	54.72	0.252	40	0.093	9.5	5.3	75.72	29.77	15.50
					0.096	9.6	4.7			
10.	15	60.39	0.244	40	0.101	0.5	5.5	77.64	26.94	12.99
					0.098	9.7	4.8			
					0.102	8.8	5.3			
10.	15	57.35	0.256	50	0.078	9.6	5.1	74.18	26.98	12.78
					0.083	7.7	5.2			
					0.080	9.4	4.4			
10.	15	58.09	0.252	50	0.089	10.1	5.8	75.18	26.97	12.73
					0.091	9.8	4.6			

APPENDIX A (continued). TABULATED DATA

L/D	θ	F	R	X/D	$\Delta T_c/\Delta T_o$	W/D	Y/D	V_o	T_o	T_a
10.	15	58.44	0.250	50	0.083	10.7	5.6	75.82	26.98	12.63
					0.085	9.9	5.4			
10.	15	57.21	0.258	60	0.078	10.0	4.8	73.97	26.82	12.46
					0.073	10.3	5.1			
10.	15	57.98	0.251	60	0.075	8.9	6.2	74.98	26.79	12.38
					0.083	9.3	5.4			
					0.076	8.8	5.4			
10.	15	58.88	0.250	60	0.074	10.6	7.0	75.82	26.77	12.52
					0.073	9.4	5.4			
10.	15	56.96	0.489	10	0.266	5.5	2.7	76.52	29.44	16.07
10.	15	54.45	0.510	10	0.263	4.0	1.9	73.62	29.59	16.10
10.	15	55.90	0.499	10	0.251	4.0	2.4	75.38	29.58	16.18
10.	15	56.82	0.504	10	0.300	5.1	2.3	74.24	28.98	16.24
10.	15	57.34	0.494	10	0.274	4.0	2.2	75.62	29.20	16.31
10.	15	56.52	0.502	20	0.175	6.0	2.1	73.80	29.03	16.37
10.	15	55.78	0.504	10	0.166	7.1	2.7	74.22	29.44	16.41
10.	15	54.48	0.510	20	0.172	5.2	2.4	72.84	29.57	16.48
10.	15	56.08	0.502	20	0.134	4.4	1.9	74.64	29.51	16.53
10.	15	56.42	0.505	30	0.130	7.2	2.3	74.64	29.41	16.57
10.	15	54.35	0.523	30	0.123	6.6	3.5	71.74	29.40	16.63
10.	15	55.43	0.516	30	0.112	5.7	3.8	73.09	29.44	16.74
10.	15	55.30	0.502	40	0.104	7.1	3.4	74.67	29.93	16.76
10.	15	55.81	0.499	40	0.089	8.3	4.5	75.30	29.96	16.85
10.	15	54.63	0.509	40	0.096	8.2	3.0	73.80	30.02	16.90
10.	15	55.02	0.498	40	0.083	8.0	3.8	73.99	29.94	16.93
10.	15	55.68	0.498	50	0.080	6.4	3.4	74.52	29.87	16.97
10.	15	55.33	0.500	50	0.083	8.8	3.6	74.07	29.92	17.04

APPENDIX A (continued). TABULATED DATA

L/D	θ	F	R	X/D	$\Delta T_c/\Delta T_o$	W/D	Y/D	V_o	T_o	T_a
10.	15	54.76	0.509	50	0.090	6.6	4.0	73.15	29.90	17.08
10.	15	57.94	.0.497	60	0.051	7.8	3.5	75.98	28.95	16.06
10.	15	55.98	0.508	60	0.054	8.6	2.5	73.4	28.99	16.13
10.	15	57.46	0.485	60	0.052	10.0	3.9	77.07	29.48	16.18
10.	15	55.58	0.497	60	0.060	9.0	4.0	75.38	29.71	16.21
10.	30	32.50	0	10	0.348	8.8	8.1	50.13	34.67	20.00
					0.358	6.7	7.3			
					0.381	7.6	7.1			
					0.358	8.1	7.1			
					0.378	6.9	7.1			
					0.382	5.9	7.2			
					0.381	8.5	7.3			
					0.379	7.6	7.2			
					0.381	6.8	7.2			
					0.374	6.4	7.2			
					0.378	7.2	7.1			
10..	30	30.77	0	20	0.163	10.6	17.1	50.42	36.20	20.13
					0.152	13.6	18.0			
					0.166	17.3	17.8			
					0.167	16.4	17.0			
					0.175	11.1	16.7			
					0.171	9.5	16.8			
					0.167	11.8	17.1			
					0.170	13.6	16.7			
					0.178	14.0	16.7			
					0.184	11.5	15.5			
					0.179	12.0	15.3			
10.	30	30.61	0	30	0.109	19.9	16.7	50.51	36.45	20.26
					0.108	15.9	27.8			
					0.102	12.7	26.5			
					0.105	23.7	25.7			
					0.117	21.1	27.8			
					0.103	27.1	26.1			
					0.110	19.5	26.3			
					0.116	21.6	25.7			
10.	30	30.32	0	40	0.072	33.9	52.1	50.99	37.14	20.64
					0.072	39.5	57.5			
					0.069	32.5	50.7			

APPENDIX A (continued). TABULATED DATA

L/D	θ	F	R	X/D	$\Delta T_c/\Delta T_o$	W/D	Y/D	V_o	T_o	T_a
10.	30	30.12	0	50	0.071	32.5	50.2	49.32	36.53	20.75
10..	30	32.59	0	40	0.069	27.2	33.6	51.78	35.94	21.01
					0.073	26.4	31.0			
					0.062	25.5	31.9			
					0.068	22.9	35.3			
					0.064	28.9	32.3			
					0.072	27.2	32.7			
10.	30	30.49	0	60	0.057	33.8	54.8	49.63	36.63	21.18
					0.066	35.5	54.8			
					0.057	30.4	53.1			
					0.055	38.9	56.9			
					0.056	41.4	53.1			
10.	30	31.54	0.255	50	0.062	11.0	8.8	49.87	36.02	21.33
					0.061	10.8	8.6			
10.	30	32.30	0.250	50	0.057	9.0	8.3	51.02	36.05	21.43
					0.059	10.7	7.9			
10.	30	32.60	0.248	40	0.063	9.1	8.7	51.32	36.00	21.48
					0.061	9.4	6.8			
10.	30	32.37	0.249	40	0.070	10.0	8.9	50.63	35.91	21.57
					0.070	9.2	8.3			
10.	30	32.93	0.252	30	0.087	7.6	7.3	50.63	35.54	21.61
					0.082	7.4	7.9			
10.	30	33.89	0.241	30	0.097	8.6	9.0	51.20	35.19	21.66
					0.094	7.6	7.3			
10.	30	32.07	0.244	30	0.089	7.3	7.7	50.70	36.24	21.71
					0.091	718	7.7			
10..	30	31.53	0.239	20	0.151	8.0	6.9	51.42	37.01	21.77
					0.151	8.2	6.3			
10..	30	31.02	0.249	20	0.137	8.0	6.3	50.72	37.10	21.80
					0.134	6.1	6.4			
10.	30	30.82	0.245	10	0.263	5.0	4.9	50.48	37.16	21.83
					0.259	5.1	4.6			
10.	30	30.68	0.245	10	0.265	4.6	5.3	50.38	37.24	21.87
					0.264	3.7	4.5			
					0.279	6.7	5.0			

APPENDIX A (continued). TABULATED DATA

L/D	θ	F	R	X/D	$\Delta T_c/\Delta T_o$	W/D	Y/D	V_o	T_o	T_a
10.	30	30.52	0.256	10	0.259	5.1	4.7	50.28	37.26	21.77
10.	30	30.59	0.245	20	0.136	7.0	7.0	50.32	37.33	21.95
					0.136	7.3	6.6			
10..	30	29.38	0.251	40	0.083	8.7	10.2	49.14	37.80	22.05
					0.083	7.2	8.1			
10.	30	29.96	0.248	50	0.069	9.4	9.6	50.33	37.91	22.14
					0.069	9.3	9.2			
10..	45	11.18	0.101	10	0.196	8.5	10.0	25.28	45.00	17.33
					0.208	7.6	10.0			
					0.202	6.9	9.0			
					0.195	6.2	10.5			
					0.214	7.8	10.0			
					0.194	7.1	10.0			
					0.101	8.4	9.1			
10.	45	10.61	0.104	20	0.112	6.3	12.8	24.70	45.54	15.68
					0.106	9.4	13.3			
					0.103	9.4	13.5			
					0.109	9.1	12.3			
					0.111	10.7	13.3			
10.	45	11.50	0.098	20	0.099	8.8	12.7	25.82	44.65	17.16
					0.097	8.8	12.1			
					0.107	10.4	14.0			
					0.103	8.1	13.4			
					0.098	7.6	14.3			
10..	45	10.13	0.107	30	0.070	11.2	14.7	23.89	46.04	15.54
					0.072	7.1	15.0			
					0.072	7.0	14.9			
10.	45	10.34	0.102	30	0.076	12.8	16.2	24.73	46.60	15.50
					0.076	12.6	16.6			
					0.073	11.9	15.6			
					0.072	10.6	15.5			
10.	45	9.96	0.105	40	0.050	17.1	15.1	23.90	46.63	15.32
					0.049	16.4	16.6			
					0.052	11.9	17.1			
					0.053	12.5	15.9			
10.	45	10.40	0.102	40	0.053	12.2	17.5	24.57	45.98	15.18
					0.048	11.4	16.9			
					0.045	11.3	17.7			

APPENDIX A (continued). TABULATED DATA

L/D	θ	F	R	X/D	$\Delta T_c/\Delta T_o$	W/D	Y/D	V_o	T_o	T_a
10.	45	10.22	0.104	50	0.043	18.3	19.0	24.24	46.08	15.02
					0.044	16.9	18.3			
10.	45	11.53	0.101	50	0.041	15.6	17.0	24.62	41.93	14.82
					0.036	13.9	18.1			
10.	45	10.64	0.496	10	0.151	4.1	4.1	25.20	46.85	17.40
					0.161	3.9	3.6			
					0.160	4.8	4.0			
10.	45	10.63	0.506	10	0.190	4.2	3.9	24.79	46.27	17.51
10.	45	11.08	0.489	10	0.202	5.2	4.1	25.49	45.75	17.56
10.	45	10.67	0.511	20	0.102	5.1	4.3	24.14	45.13	17.56
					0.108	5.6	4.2			
10.	45	11.10	0.502	20	0.188	6.6	4.7	25.14	45.20	17.68
					0.182	6.2	4.4			
10.	45	11.00	0.501	20	0.109	5.9	5.1	24.96	45.29	17.74
					0.112	6.6	5.1			
10.	45	11.2	0.506	30	0.092	6.5	5.4	24.86	44.52	17.80
					0.082	6.2	5.1			
10.	45	10.88	0.486	30	0.079	8.1	5.3	25.46	46.05	16.57
					0.081	5.7	5.5			
10.	45	10.96	0.493	30	0.083	6.9	5.2	25.28	45.53	16.68
					0.086	7.8	5.1			
10.	45	10.88	0.502	40	0.078	7.9	5.6	24.90	45.25	16.75
					0.073	7.6	5.5			
10.	45	10.62	0.513	40	0.067	9.1	4.8	24.27	45.22	16.83
					0.068	8.8	4.8			
10.	45	10.78	0.494	40	0.072	7.5	5.7	25.21	46.16	16.88
					0.080	5.8	5.8			
10.	45	11.17	0.499	50	0.073	7.8	6.5	24.98	44.43	17.00
					0.074	6.9	6.5			
10.	45	10.75	0.509	50	0.065	8.8	6.5	24.57	45.33	17.13
					0.067	9.1	5.5			
10.	45	11.15	0.502	50	0.060	9.4	5.8	24.66	44.11	17.22
					0.064	7.6	5.5			

APPENDIX A (continued). TABULATED DATA

L/D	θ	F	R	X/D	$\Delta T_c/\Delta T_o$	W/D	Y/D	V_o	T_o	T_a
10.	45	32.41	0	40	0.078	37.1	45.5	50.63	32.80	15.90
					0.079	40.5	49.7			
					0.076	24.0	45.5			
10.	45	30.84	0	40	0.085	36.0	44.6	51.10	34.70	16.70
					0.074	34.7	47.4			
10.	45	31.34	0	40	0.086	35.7	47.3	50.63	34.10	16.85
					0.075	32.5	47.4			
					0.075	32.9	47.3			
10..	45	31.60	0	50	0.068	26.2	64.5	51.10	34.18	16.93
					0.057	27.9	76.1			
10.	45	31.72	0	50	0.075	22.8	61.1	50.93	34.04	17.02
					0.076	26.3	56.3			
					0.070	20.3	66.2			
					0.072	27.9	59.0			
10.	45	32.31	0	30	0.096	16.4	34.3	50.43	33.42	17.18
					0.099	18.8	34.5			
					0.095	22.2	35.9			
10.	45	31.44	0	30	0.081	15.6	32.0	50.97	34.46	17.35
					0.086	22.4	32.8			
					0.087	20.1	30.9			
10..	45	32.20	0	20	0.146	9.8	20.9	50.71	33.74	17.39
					0.144	10.2	19.8			
					0.138	12.4	21.3			
					0.136	11.0	21.4			
					0.148	14.5	21.8			
10.	45	32.19	0	10	0.274	8.5	11.8	50.30	33.64	17.56
					0.301	10.2	10.1			
					0.310	10.2	10.4			
					0.293	10.4	10.6			
					0.294	12.3	9.5			
					0.299	11.1	9.7			
					0.290	9.9	10.6			
					0.294	10.2	10.3			
					0.294	11.1	10.1			

APPENDIX A (continued). TABULATED DATA

L/D	θ	F	R	X/D	$\Delta T_c/\Delta T_o$	W/D	Y/D	V_o	T_o	T_a
10.	45	32.71	0.052	10	0.316	6.3	8.5	49.71	31.96	15.50
					0.291	7.5	7.8			
					0.295	7.1	8.6			
					0.327	7.1	8.4			
					0.316	7.3	7.8			
					0.311	7.6	8.3			
					0.315	7.3	8.9			
					0.310	5.8	8.3			
					0.331	6.8	8.0			
					0.318	7.6	7.8			
					0.317	6.7	8.6			
10.	45	33.35	0.048	20	0.148	11.7	14.9	50.47	31.82	15.49
					0.156	12.8	16.8			
					0.159	11.5	15.1			
					0.138	10.9	13.8			
					0.139	14.9	15.5			
					0.136	12.3	14.4			
					0.133	11.5	15.6			
					0.127	10.3	15.0			
					0.125	12.4	13.2			
					0.143	9.6	15.1			
					0.144	9.9	15.6			
10.	45	34.82	0.049	30	0.091	10.7	18.9	50.47	30.78	15.44
					0.095	13.4	17.5			
					0.089	12.6	20.4			
					0.091	13.0	20.9			
					0.093	14.9	20.3			
					0.095	12.3	19.1			
					0.092	18.1	19.2			
					0.094	11.5	12.2			
					0.093	9.6	17.9			
10.	45	34.55	0.050	40	0.063	16.1	23.7	50.60	30.98	15.36
					0.063	15.4	24.2			
					0.065	18.9	24.1			
					0.067	15.3	24.1			
10.	45	34.47	0.049	50	0.065	15.7	23.5	50.56	30.98	15.28
					0.063	16.9	22.5			
					0.063	17.5	26.0			
					0.065	17.1	27.6			
					0.070	18.0	25.6			
					0.073	20.8	25.6			
					0.063	19.0	27.2			
					0.062	18.6	20.0			

APPENDIX A (continued). TABULATED DATA

L/D	θ	F	R	X/D	$\Delta T_c/\Delta T_o$	W/D	Y/D	V_o	T_o	T_a
10.	45	35.49	0.051	60	0.051	10.3	26.6	50.25	30.11	15.18
					0.055	18.0	26.5			
					0.050	24.7	27.5			
					0.056	24.2	28.7			
					0.054	19.7	26.9			
					0.061	17.5	26.9			
					0.061	21.0	26.9			
10.	45	34.67	0.096	10	0.280	6.4	7.9	52.37	31.84	15.62
					0.270	7.8	8.0			
					0.264	9.7	7.6			
					0.269	6.8	8.3			
					0.241	7.0	7.8			
					0.276	5.8	7.7			
10.	45	33.22	0.099	20	0.139	10.2	13.3	50.03	31.79	15.66
					0.123	9.8	13.8			
					0.125	9.7	13.2			
					0.128	9.8	13.7			
					0.132	9.8	12.0			
10.	45	33.79	0.099	30	0.083	13.4	14.8	50.50	31.63	15.70
					0.084	14.6	14.2			
					0.085	13.1	15.1			
					0.079	12.8	14.2			
					0.080	10.0	13.8			
					0.086	9.5	14.8			
10.	45	34.35	0.098	40	0.070	9.3	16.3	50.69	31.35	15.74
					0.067	5.8	15.8			
					0.060	9.7	15.7			
					0.068	10.6	18.6			
					0.069	10.7	15.5			
10.	45	32.95	0.100	50	0.059	12.0	16.6	49.46	31.77	15.78
					0.062	12.4	18.0			
					0.059	14.8	18.7			
					0.062	14.1	18.7			
10.	45	32.65	0.103	60	0.047	12.2	22.7	49.00	31.77	15.81
					0.050	11.7	21.3			
					0.045	15.4	24.1			
10.	45	32.33	0.248	10	0.202	6.9	5.5	50.13	33.54	17.72
					0.175	6.1	4.6			
					0.185	5.6	5.7			

APPENDIX A (continued). TABULATED DATA

L/D	θ	F	R	X/D	$\Delta T_c/\Delta T_o$	W/D	Y/D	V_o	T_o	T_a
10.	45	32.61	0.245	10	0.191	6.5	6.5	50.72	33.68	17.85
					0.193	5.5	5.5			
10..	45	32.37	0.246	10	0.217	5.3	6.5	50.19	33.66	17.95
					0.228	5.5	5.6			
10.	45	32.46	0.246	20	0.109	6.8	6.9	50.69	34.31	18.84
					0.114	7.9	6.7			
					0.118	7.2	6.9			
10.	45	32.27	0.241	20	0.102	7.0	7.6	51.32	34.82	18.98
					0.104	7.0	6.8			
					0.102	6.9	7.0			
10.	45	31.69	0.248	30	0.090	9.0	9.1	50.80	35.06	19.05
					0.096	7.6	8.1			
10.	45	31.45	0.246	30	0.079	8.3	7.9	50.56	35.15	19.08
					0.085	7.3	8.3			
10.	45	32.48	0.242	40	0.072	9.1	9.5	51.93	35.05	19.15
					0.067	10.1	9.7			
10..	45	32.23	0.250	40	0.063	11.1	10.0	51.49	35.06	19.21
					0.064	9.6	7.5			
10..	45	31.92	0.243	50	0.059	11.9	11.3	50.58	34.88	19.25
					0.056	11.5	9.8			
10.	45	29.97	0.245	50	0.058	11.0	10.9	49.88	36.16	19.33
					0.054	9.2	8.1			
10.	45	31.35	0.244	50	0.067	10.4	9.6	51.56	35.95	19.51
					0.059	9.2	9.0			
10.	45	31.10	0.248	40	0.078	8.8	10.0	50.97	35.93	19.64
					0.073	7.9	8.3			
10.	45	31.16	0.249	30	0.082	9.0	8.9	50.71	35.81	19.74
					0.085	8.0	8.7			
10..	45	31.40	0.249	20	0.123	8.6	8.4	51.02	35.83	19.84
					0.127	7.7	7.7			

APPENDIX A (continued). TABULATED DATA

L/D	θ	F	R	X/D	$\Delta T_c/\Delta T_o$	W/D	Y/D	V_o	T_o	T_a
10.	45	55.29	0.050	10	0.309	8.6	8.9	75.61	27.85	12.02
					0.310	9.2	8.9			
					0.330	8.7	9.4			
					0.320	9.1	9.5			
					0.267	9.1	8.6			
					0.300	8.8	8.9			
					0.276	8.5	8.9			
					0.305	8.5	8.7			
10.	45	54.28	0.051	20	0.136	12.6	13.9	74.42	27.85	11.89
					0.139	11.2	16.4			
					0.138	12.1	14.2			
					0.144	11.9	15.1			
					0.149	11.2	15.1			
					0.144	11.2	14.6			
10.	45	55.07	0.050	30	0.101	14.8	18.9	75.50	27.81	11.78
					0.101	13.4	18.3			
					0.105	12.5	18.6			
					0.111	12.5	18.8			
					0.098	13.2	19.0			
					0.104	14.8	18.5			
					0.107	14.1	18.5			
10.	45	53.50	0.051	40	0.072	17.1	24.3	73.92	27.94	11.66
					0.070	18.6	23.0			
					0.072	22.5	21.4			
					0.071	18.8	23.0			
10.	45	54.15	0.051	50	0.049	20.4	25.8	75.13	27.96	11.49
					0.055	20.9	25.8			
					0.055	20.9	25.9			
					0.039	20.1	27.1			
					0.051	19.3	24.6			
10.	45	54.57	0.052	60	0.055	22.2	26.9	74.52	27.52	11.30
					0.045	18.9	26.3			
					0.043	19.6	26.3			
					0.048	19.6	27.6			
10.	45	54.59	0.101	10	0.256	7.3	8.5	73.92	27.71	12.22
					0.251	8.1	7.9			
					0.289	7.7	8.2			
					0.257	6.7	8.4			
					0.263	7.1	8.1			
10..	45	54.20	0.100	20	0.132	11.6	11.9	74.59	28.13	12.30
					0.124	10.9	12.5			
					0.122	10.7	11.8			
					0.116	12.0	11.2			

APPENDIX A (continued). TABULATED DATA

L/D	θ	F	R	X/D	$\Delta T_c/\Delta T_o$	W/D	Y/D	V_o	T_o	T_a
10.	45	53.65	0.101	30	0.091	10.9	15.9	74.30	28.29	12.37
					0.090	10.9	15.2			
					0.080	9.9	16.0			
					0.082	11.8	15.2			
					0.083	10.2	14.6			
					0.080	9.7	14.6			
10.	45	57.80	0.105	40	0.070	13.0	15.3	72.74	27.53	14.95
					0.065	11.0	15.0			
					0.064	13.0	15.9			
10.	45	55.06	0.105	50	0.057	15.0	16.0	72.00	28.35	15.07
					0.055	14.8	18.1			
					0.048	14.6	16.3			
					0.052	14.5	16.7			
10.	45	57.46	0.100	60	0.050	16.2	18.6	75.13	28.40	15.15
					0.048	15.7	18.5			
					0.051	14.8	19.3			
					0.047	13.5	18.7			
10.	60	29.72	0	6.6	0.404		10.3	49.86	38.52	23.14
				8.5	0.297		14.4			
				12.8	0.186		22.6			
				18.1	0.123		35.6			
				20.3	0.084		43.3			
				29.8	0.060		58.1			
				35.0	0.047		68.0			
10.	60	30.68	0	5.0	0.394		10.1	48.84	36.60	22.04
				6.3	0.360		11.8			
				7.6	0.261		15.1			
				10.8	0.219		19.6			
				13.9	0.164		26.0			
				16.4	0.129		33.7			
				23.9	0.082		48.3			
				27.6	0.060		58.1			
				34.9	0.054		73.2			
10.	60	30.69	0.252	10	0.172	6.0	7.0	49.74	37.74	23.23
					0.157	6.5	6.6			
10.	60	30.70	0.250	10	0.156	6.3	6.7	50.40	38.10	23.33
					0.154	6.8	6.5			
10.	60	30.70	0.248	20	0.080	7.4	7.8	50.48	38.15	23.34
					0.084	6.8	8.4			

APPENDIX A (continued). TABULATED DATA

L/D	θ	F	R	X/D	$\Delta T_c/\Delta T_o$	W/D	Y/D	V_o	T_o	T_a
10.	60	31.04	0.247	30	0.057	8.3	10.7	50.99	38.15	23.38
					0.064	7.7	9.0			
					0.058	9.4	8.5			
10.	60	29.70	0.257	40	0.046	11.7	9.8	49.64	38.74	23.66
					0.050	11.0	8.9			
10.	60	30.50	0.244	50	0.036	10.2	12.9	50.97	38.79	23.75
					0.040	11.6	13.5			
10.	60	30.19	0.246	50	0.047	7.5	11.5	50.47	38.84	23.82
					0.049	8.4	9.9			
10.	60	30.70	0.245	50	0.057	8.7	11.6	50.89	38.71	23.93
					0.056	9.4	10.5			
10.	60	30.82	0.253	40	0.051	8.9	10.7	49.64	38.09	24.03
10.	60	31.30	0.251	30	0.063	9.3	9.4	50.05	37.99	24.13
					0.068	8.5	9.3			
10.	60	30.98	0.251	30	0.048	9.3	9.4	50.13	38.64	24.72
					0.050	8.3	9.6			
10.	60	30.37	0.254	20	0.099	6.9	9.2	49.64	38.59	24.28
					0.094	7.7	8.0			
10.	60	30.43	0.254	20	0.083	7.9	9.4	49.64	38.60	24.36
					0.074	7.0	8.9			
10.	60	31.17	0.243	10	0.156	5.6	6.6	50.84	38.64	24.43
10.	90	10.06	0.092	40	0.038	19.9	21.4	25.20	49.85	19.25
					0.037	18.8	26.0			
					0.044	13.6	22.3			
					0.039	30.4	24.1			
					0.046	26.6	22.2			
10.	90	10.57	0.091	40	0.047	12.3	19.7	25.79	48.79	19.35
					0.044	26.2	21.2			
					0.048	23.3	20.1			
					0.053	22.6	19.7			
					0.041	18.6	26.3			
					0.040	20.9	23.7			
10.	90	10.59	0.099	30	0.056	10.9	17.4	25.30	48.00	19.45
					0.057	12.6	14.8			
					0.052	14.0	17.5			
					0.048	21.6	18.9			

APPENDIX A (continued). TABULATED DATA

L/D	θ	F	R	X/D	$\Delta T_o/\Delta T_o$	W/D	Y/D	V_o	T_o	T_a
10.	90	10.37	0.101	20	0.050	12.3	16.6	24.66	47.84	19.54
					0.046	16.0	17.2			
					0.050	13.0	21.9			
					0.049	13.8	22.4			
					0.048	11.6	22.1			
10..	90	9.84	0.102	10	0.066	7.0	15.9	24.53	49.80	19.60
					0.067	8.4	15.7			
					0.072	12.2	15.8			
					0.069	9.1	16.9			
					0.081	7.6	17.4			
					0.079	11.2	16.3			
10.	90	9.60	0.106	5	0.106	11.8	12.0	24.10	50.15	19.70
					0.097	8.5	10.9			
					0.124	10.1	13.4			
					0.118	9.8	13.4			
					0.111	10.5	12.8			
10.	90	11.03	0.259	20	0.069	6.3	9.7	25.25	46.02	18.78
					0.074	7.2	7.8			
10.	90	11.59	0.249	20	0.079	5.0	9.9	26.30	45.76	18.88
					0.077	8.8	8.9			
10.	90	10.90	0.257	10	0.109	6.0	9.1	24.63	45.62	18.94
					0.128	6.4	8.3			
10.	90	10.97	0.238	10	0.120	6.7	9.3	24.90	45.83	19.02
					0.113	7.3	6.8			
10.	90	11.19	0.246	10	0.136	7.1	7.2	25.11	45.42	19.12
10.	90	11.24	0.244	5	0.148	5.4	6.7	24.86	44.92	19.19
					0.165	7.2	5.9			
10.	90	8.88	0.266	30	0.068	6.8	12.1	22.53	50.04	18.30
					0.061	9.8	9.5			
					0.061	7.9	12.1			
10.	90	11.06	0.257	30	0.064	8.5	10.9	24.74	45.09	18.59
					0.065	9.4	11.3			
10.	90	10.98	0.256	30	0.058	8.6	10.6	24.82	45.52	18.70
					0.059	6.6	11.1			
10.	90	10.87	0.246	5	0.169	5.1	6.6	25.21	46.01	17.36
					0.178	4.8	7.0			

APPENDIX A (continued). TABULATED DATA

L/D	θ	F	R	X/D	$\Delta T_c/\Delta T_0$	W/D	Y/D	V_o	T_o	T_a
10.	90	10.66	0.246	5	0.172	5.0	7.2	25.21	46.83	17.50
					0.177	4.9	6.5			
10.	90	10.30	0.262	10	0.115	7.7	7.7	24.57	47.22	17.61
					0.122	6.2	8.1			
10.	90	11.06	0.248	10	0.125	6.8	7.5	26.04	46.70	17.69
					0.132	6.4	6.4			
10.	90	10.61	0.246	20	0.074	6.9	10.6	24.80	46.50	17.90
					0.076	8.0	10.2			
10.	90	10.14	0.253	20	0.080	7.7	9.0	23.64	46.46	18.04
					0.081	6.8	9.0			
10.	90	10.45	0.248	30	0.056	10.9	6.4	24.60	46.87	18.08
					0.055	6.4	9.8			
10.	90	10.61	0.237	30	0.047	7.8	11.6	25.4	47.46	18.15
					0.050	7.2	10.4			
10.	90	11.06	0.499	40	0.061	9.3	5.8	24.61	44.74	18.22
					0.059	8.0	5.8			
10.	90	11.06	0.485	40	0.057	6.6	5.4	25.04	45.40	18.27
					0.058	5.9	5.4			
					0.068	8.4	6.2			
10.	90	11.10	0.489	30	0.070	6.9	3.8	25.32	45.74	18.34
10.	90	11.51	0.496	30	0.086	4.3	3.5	24.90	43.80	18.41
10.	90	11.23	0.494	20	0.108	6.0	6.2	24.92	44.74	18.48
					0.102	4.7	4.5			
10.	90	10.91	0.509	10	0.142	5.1	5.6	24.65	45.48	18.67
10.	90	10.97	0.507	10	0.137	5.1	5.6	24.73	45.52	18.73
10.	90	11.24	0.490	10	0.136	4.8	4.0	25.50	45.63	18.61
					0.151	4.2	4.4			
10.	90	11.24	0.493	10	0.147	4.2	4.4	25.54	45.67	18.70
10.	90	10.98	0.504	20	0.101	7.7	5.8	24.90	45.59	18.53
					0.104	6.4	4.7			
10.	90	10.99	0.502	20	0.099	8.0	4.8	24.97	45.48	18.50

APPENDIX A (continued). TABULATED DATA

L/D	θ	F	R	X/D	$\Delta T_c/\Delta T_o$	W/D	Y/D	V_o	T_o	T_a
10	90	10.24	0.498	5	0.262	4.2	3.9	24.43	47.63	18.72
					0.257	4.9	2.8			
10.	90	10.51	0.495	5	0.246	4.3	4.3	24.50	46.73	18.77
					0.269	3.8	3.1			
10..	90	10.66	0.476	5	0.212	5.0	3.9	25.39	47.63	18.83
					0.223	5.0	1.6			
10.	90	10.29	0.491	5	0.257	4.5	3.9	24.44	47.55	18.92
10.	90	10.09	0.510	5	0.243	4.1	4.1	24.11	47.80	18.97
					0.216	3.6	2.7			
10..	90	10.40	0.462	10	0.159	5.5	4.8	25.60	49.01	18.92
					0.158	6.1	4.0			
10..	90	9.85	0.511	10	0.139	4.4	4.7	24.30	49.10	18.99
					0.146	6.2	2.6			
10.	90	9.70	0.513	10	0.151	5.4	4.5	24.30	49.80	19.05
					0.130	4.7	3.8			
10.	90	10.24	0.507	20	0.108	5.6	6.3	24.73	48.27	19.06
					0.110	5.6	4.0			
10.	90	10.02	0.509	20	0.089	6.8	4.9	24.86	49.42	19.15
					0.098	6.0	4.1			
10.	90	9.98	0.510	30	0.081	7.9	7.0	24.37	48.80	19.21
10.	90	10.58	0.483	30	0.090	5.5	6.6	26.00	49.07	19.27
					0.088	7.4	4.8			
10..	90	10.19	0.489	40	0.060	8.2	6.2	25.11	49.20	19.34
					0.057	7.8	6.0			
10.	90	29.63	0.050	40	0.054	28.3	49.4	50.08	39.40	24.30
					0.054	25.4	46.0			
					0.046	32.2	42.9			
					0.049	28.5	45.4			
10..	90	31.79	0.0486	30	0.057	24.7	33.8	51.65	38.33	24.08
					0.070	36.8	40.7			
					0.056	37.2	38.2			
					0.065	29.8	37.6			
					0.063	24.5	36.5			

APPENDIX A (continued). TABULATED DATA

L/D	θ	F	R	X/D	$\Delta T_c/\Delta T_o$	W/D	Y/D	V_o	T_o	T_a
10.	90	30.97	0.050	20	0.057	28.5	32.6	50.63	38.47	24.08
					0.056	29.7	34.1			
					0.061	29.3	32.6			
					0.056	27.6	32.6			
					0.057	29.7	34.8			
					0.055	26.8	34.1			
10.	90	30.98	0.049	10	0.107	22.2	27.2	50.80	38.57	24.12
					0.099	26.9	24.9			
					0.095	16.7	26.6			
					0.098	25.2	26.5			
					0.094	24.2	27.0			
					0.100	26.8	27.7			
					0.103	26.1	28.3			
10.	90	30.99	0.050	5	0.124	29.5	22.9	50.45	38.39	24.12
					0.110	18.9	20.2			
					0.111	28.2	19.7			
					0.120	21.9	20.6			
					0.119	18.6	21.6			
10.	90	30.94	0.095	5	0.140	10.0	12.2	50.80	34.23	16.21
					0.137	10.4	13.4			
					0.138	9.4	13.5			
10.	90	30.66	0.099	5	0.157	10.1	12.9	49.52	33.85	16.30
					0.148	9.7	11.6			
					0.159	11.4	12.1			
10.	90	32.26	0.099	10	0.093	9.0	15.0	51.10	33.40	16.40
					0.103	8.9	14.0			
					0.098	9.7	14.7			
10.	90	32.77	0.096	10	0.095	11.7	16.8	51.49	33.22	16.46
					0.085	10.4	14.3			
					0.086	10.1	14.9			
10.	90	31.68	0.096	20	0.062	17.7	18.3	51.67	34.39	16.90
					0.056	15.5	18.9			
					0.057	16.0	16.6			
10.	90	31.63	0.097	30	0.064	18.6	14.8	51.93	34.75	17.27
					0.061	17.5	14.4			
10.	90	30.75	0.101	30	0.052	16.8	18.4	50.38	34.76	17.40
					0.052	19.3	15.1			
					0.051	17.1	15.5			

APPENDIX A (continued). TABULATED DATA

L/D	θ	F	R	X/D	$\Delta T_c/\Delta T_o$	W/D	Y/D	V_o	T_o	T_a
10.	90	32.62	0.095	40	0.050	18.6	10.7	51.75	34.03	17.60
					0.049	22.0	10.3			
10.	90	31.78	0.099	40	0.048	20.6	14.1	50.80	34.30	17.74
					0.052	22.3	15.0			
					0.051	15.0	16.5			
10.	90	33.68	0.238	40	0.048	10.9	10.5	52.58	34.64	19.45
					0.047	8.3	9.9			
10.	90	33.47	0.237	40	0.049	11.9	11.1	52.93	34.97	19.50
					0.051	8.5	10.0			
10.	90	31.77	0.245	30	0.065	9.7	9.3	51.06	35.46	19.67
					0.069	6.7	9.0			
10.	90	33.23	0.242	30	0.056	9.9	11.0	52.38	34.97	19.63
					0.059	6.8	9.3			
10.	90	32.22	0.244	20	0.097	8.0	8.9	51.75	35.47	19.72
					0.093	9.4	7.3			
10.	90	31.83	0.247	20	0.083	9.4	9.6	51.18	35.54	19.78
					0.085	7.9	8.6			
10.	90	31.89	0.244	10	0.103	7.3	7.1	51.75	35.81	19.86
10.	90	30.52	0.245	10	0.126	6.7	8.5	51.50	36.81	19.89
10.	90	30.42	0.249	5	0.183	5.4	6.3	51.23	36.83	20.00
					0.194	5.7	4.4			
10.	90	30.20	0.250	5	0.185	6.8	6.7	50.80	36.82	20.06
					0.187	5.7	5.4			
10.	90	30.39	0.244	5	0.163	4.8	6.9	51.14	36.87	20.12
					0.173	5.9	5.4			
10.	90	30.02	0.248	5	0.166	4.8	6.6	50.47	36.88	20.17
					0.160	6.9	5.1			
10.	90	29.43	0.257	5	0.163	6.0	8.5	49.48	36.91	20.23
					0.168	7.0	6.6			
10.	90	29.73	0.245	10	0.107	5.8	7.9	49.89	36.90	20.31
					0.105	4.3	6.3			
10.	90	33.13	0.255	20	0.088	8.6	9.2	49.68	34.45	20.70
					0.085	8.3	7.2			

APPENDIX A (continued). TABULATED DATA

L/D	θ	F	R	X/D	$\Delta T_a/\Delta T_o$	W/D	Y/D	V_o	T_o	T_a
10.	90	32.22	0.252	20	0.078	6.5	9.3	50.05	35.26	20.74
					0.089	7.5	6.9			
10.	90	31.04	0.253	30	0.059	8.7	9.7	49.48	35.89	20.77
					0.059	9.2	8.9			
10.	90	30.59	0.256	30	0.059	8.4	9.7	48.00	35.53	20.80
					0.058	9.1	9.5			
10.	90	31.98	0.245	40	0.064	9.0	11.4	50.55	35.72	20.82
					0.056	8.8	8.7			
10.	90	32.30	0.244	40	0.065	9.6	9.3	50.78	35.59	20.82
					0.073	6.3	10.1			
10.	90	32.04	0.494	50	0.043	12.2	11.7	50.63	35.70	20.80
					0.042	7.7	12.6			
					0.039	9.7	11.6			
10.	90	32.15	0.496	50	0.046	5.9	3.5	50.53	35.57	20.81
					0.054	6.3	5.4			
					0.048	7.2	5.7			
10.	90	31.80	0.494	40	0.064	6.6	7.5	50.80	35.97	20.83
					0.069	6.3	5.7			
10.	90	31.49	0.497	40	0.053	9.1	7.6	50.47	36.05	20.84
					0.053	7.6	5.9			
10.	90	31.49	0.497	30	0.054	7.5	6.4	50.24	35.95	20.85
					0.054	6.1	4.4			
10.	90	32.18	0.509	30	0.065	7.9	5.5	50.05	35.36	20.86
					0.068	5.7	4.6			
10.	90	30.76	0.515	20	0.090	5.9	4.7	49.56	36.20	20.88
10.	90	30.57	0.496	20	0.093	7.8	5.0	50.55	36.86	20.92
					0.104	6.2	4.2			
10.	90	30.60	0.503	10	0.132	4.6	4.7	50.38	36.78	20.95
10.	90	30.16	0.507	10	0.181	5.1	4.5	49.73	36.83	21.00
					0.181	5.0	3.6			
10.	90	31.02	0.503	5	0.193	4.2	4.4	49.97	36.27	21.02
					0.204	4.2	3.8			

APPENDIX A (continued). TABULATED DATA

L/D	θ	F	R	X/D	$\Delta T_c/\Delta T_o$	W/D	Y/D	V_o	T_o	T_a
10.	90	31.05	0.501	5	0.233	4.2	3.3	50.05	36.32	21.06
					0.245	3.7	3.5			
10.	90	30.79	0.504	5	0.179	2.9	1.7	49.40	36.22	21.08
10.	90	31.66	0.496	5	0.200	4.9	4.0	50.21	35.97	21.14
					0.205	5.8	3.7			
10.	90	31.35	0.489	5	0.188	4.6	4.3	51.33	36.75	21.14
					0.183	5.7	3.8			
10.	90	31.55	0.494	10	0.140	5.4	3.5	51.01	36.47	21.19
					0.137	5.2	3.4			
10.	90	31.51	0.490	10	0.129	5.3	3.7	51.23	36.63	21.24
					0.142	5.5	4.4			
10.	90	30.23	0.503	20	0.097	6.0	5.4	49.56	36.85	21.27
					0.101	4.4	4.8			
10.	90	31.15	0.492	20	0.106	6.7	4.7	50.80	36.74	21.30
					0.098	5.0	4.4			
10.	90	30.90	0.499	30	0.076	6.7	4.9	50.30	36.72	21.34
					0.069	6.3	4.4			
10.	90	31.44	0.490	30	0.079	6.8	5.6	51.02	36.67	21.39
					0.081	5.9	5.0			
10.	90	33.31	0.502	40	0.056	6.3	6.2	49.80	31.37	15.17
10.	90	31.21	0.494	40	0.061	7.2	5.7	50.47	33.41	15.30
					0.061	8.9	5.1			
10.	90	31.05	0.497	40	0.073	8.5	5.5	50.89	33.80	15.37
					0.073	5.1	4.8			
10.	90	29.94	0.516	50	0.063	9.7	6.3	49.16	33.88	15.43
					0.061	8.4	5.5			
10.	90	59.70	0.050	40	0.058	32.7	41.5	80.37	31.74	19.92
					0.053	30.1	39.1			
10.	90	55.55	0.049	40	0.051	35.9	38.1	78.00	32.60	19.95
					0.050	29.3	38.9			
					0.049	34.3	47.0			

APPENDIX A (continued). TABULATED DATA

L/D	θ	F	R	X/D	$\Delta T_c/\Delta T_o$	W/D	Y/D	V_o	T_o	T_a
10.	90	56.33	0.048	30	0.069	30.7	30.1	77.79	32.29	20.00
					0.070	27.4	36.5			
					0.070	30.9	36.6			
10.	90	56.77	0.051	30	0.064	34.4	38.6	78.70	32.45	20.13
					0.064	36.3	35.1			
					0.060	31.9	36.9			
10.	90	56.54	0.049	20	0.066	27.7	31.5	78.50	32.52	20.19
					0.063	25.9	30.6			
					0.068	27.5	32.7			
10.	90	57.68	0.050	20	0.063	22.6	29.8	78.40	32.17	20.30
					0.065	26.3	30.4			
					0.066	24.8	29.8			
					0.064	25.4	33.1			
10.	90	60.18	0.052	10	0.090	21.5	23.8	78.98	31.54	20.35
					0.087	19.3	21.5			
					0.083	19.0	23.7			
					0.078	21.1	23.4			
10.	90	58.05	0.053	10	0.097	19.8	24.0	77.11	31.82	20.44
					0.089	20.4	24.3			
					0.093	21.6	26.7			
10.	90	59.89	0.047	5	0.147	24.5	21.3	79.00	31.73	20.50
					0.146	23.2	21.9			
					0.148	22.5	19.7			
10.	90	58.27	0.051	5	0.141	20.1	19.3	76.72	31.73	20.56
					0.141	23.2	17.0			
					0.141	18.5	18.7			
					0.138	20.6	16.9			
10.	90	58.72	0.052	2.5	0.214	19.8	14.0	77.70	31.84	10.58
					0.200	17.6	13.8			
					0.195	19.0	14.0			
					0.190	17.1	12.4			
					0.121	17.9	12.9			
					0.200	16.2	13.0			
10.	90	60.09	0.105	50	0.044	15.1	15.9	77.63	30.06	18.47
					0.053	14.2	15.7			
10.	90	52.36	0.113	50	0.047	17.1	18.4	68.80	30.44	18.55
					0.045	19.2	14.1			

APPENDIX A (continued). TABULATED DATA

L/D	θ	F	R	X/D	$\Delta T_c/\Delta T_o$	W/D	Y/D	V_o	T_o	T_a
10..	90	58.42	0.103	50	0.050	16.9	15.9	77.24	30.59	18.61
					0.049	21.9	13.4			
10.	90	57.83	0.104	40	0.048	18.1	13.1	76.07	30.53	18.67
					0.055	16.7	15.3			
10.	90	57.77	0.102	40	0.045	15.3	16.0	77.36	30.94	18.78
					0.039	19.5	19.9			
10.	90	57.71	0.101	30	0.056	19.8	14.3	77.38	30.98	18.81
					0.050	15.9	16.8			
10.	90	58.31	0.103	30	0.049	16.8	13.4	78.04	30.98	18.86
					0.048	15.9	14.3			
10.	90	56.60	0.103	30	0.064	15.0	15.1	75.74	31.02	18.93
					0.057	15.1	14.3			
10.	90	56.50	0.096	20	0.067	14.1	20.5	77.76	31.71	19.16
					0.065	14.4	14.7			
10.	90	53.65	0.101	20	0.073	12.7	16.3	74.70	32.02	19.28
					0.075	10.4	18.2			
10.	90	54.41	0.099	20	0.093	10.1	14.8	76.20	32.19	19.36
					0.086	8.3	5.7			
10.	90	53.52	0.099	10	0.081	11.0	15.6	75.20	32.30	19.43
					0.082	10.9	15.6			
10.	90	58.79	0.103	5	0.146	8.7	11.2	74.85	30.38	19.40
					0.152	10.6	10.9			
10.	90	55.90	0.105	5	0.158	9.5	13.1	74.50	31.29	19.50
					0.165	10.3	13.3			
10.	90	55.41	0.108	5	0.140	9.7	11.9	74.10	31.40	19.58
					0.139	8.3	11.4			
10.	90	55.08	0.106	5	0.139	8.5	11.9	74.46	31.66	19.65
					0.136	9.9	12.1			
10.	90	55.57	0.105	5	0.153	13.5	12.1	74.70	31.60	19.73
					0.147	9.3	11.2			
10.	90	56.67	0.103	10	0.085	11.6	14.1	74.70	31.24	19.76
					0.091	10.9	15.9			
10.	90	55.40	0.104	10	0.085	11.5	15.1	74.33	31.62	19.82
					0.087	10.6	15.6			

APPENDIX A (continued). TABULATED DATA

L/D	θ	F	R	X/D	$\Delta T_c/\Delta T_o$	W/D	Y/D	V_o	T_o	T_a
10.	90	54.09	0.107	20	0.063 0.065	12.2 11.2	13.3 15.9	72.56	31.63	19.85
10.	90	54.62	0.107	20	0.053 0.051	15.7 11.9	15.4 17.2	73.38	31.70	19.91
10.	90	58.04	0.101	30	0.059 0.060	16.8 14.3	14.7 15.9	78.8	31.73	19.62
10.	90	58.08	0.100	30	0.058 0.053	16.6 15.1	13.4 12.8	79.94	32.05	19.72
10.	90	56.23	0.099	40	0.054 0.054	27.1 20.0	13.6 16.9	77.89	32.22	19.78
10.	90	56.36	0.098	40	0.057 0.054	21.8 19.3	18.0 16.3	78.16	32.28	19.85
10.	90	56.57	0.266	40	0.060	8.4	9.1	76.29	30.75	18.23
10.	90	58.93	0.274	40	0.061	9.6	9.1	77.44	30.19	18.15
10.	90	57.88	0.254	30	0.067	8.4	8.4	75.82	30.32	18.35
10.	90	58.54	0.257	40	0.059	9.7	10.3	78.82	29.98	18.25
10.	90	57.24	0.254	40	0.063	13.3	9.4	76.23	30.52	18.26
10.	90	57.59	0.256	20	0.097	7.5	8.0	75.95	30.50	18.55
10.	90	59.26	0.248	10	0.096	8.3	9.2	77.90	30.48	18.60
10.	90	59.01	0.247	10	0.112	7.3	8.7	77.24	30.46	18.70
10.	90	59.74	0.243	5	0.179	6.1	6.3	78.70	30.57	18.70
10.	90	57.87	0.253	5	0.196	6.2	6.9	76.46	30.67	18.77
10.	90	60.00	0.244	5	0.173	8.4	6.8	78.16	28.20	14.92
10.	90	58.39	0.249	5	0.190	7.0	6.6	76.46	28.40	15.10
10.	90	59.09	0.250	5	0.184	4.8	6.1	77.53	29.85	17.62
10.	90	58.01	0.249	5	0.213	5.8	5.4	77.90	30.38	17.74
10.	90	59.86	0.243	10	0.108	6.3	5.8	79.95	30.33	17.84
10.	90	58.90	0.248	10	0.117	6.7	7.3	78.57	30.33	17.89

APPENDIX A (continued). TABULATED DATA

L/D	θ	F	R	X/D	$\Delta T_c/\Delta T_o$	W/D	Y/D	V_o	T_o	T_a
10.	90	58.87	0.247	20	0.076	9.3	7.4	78.60	30.36	17.91
10.	90	59.04	0.241	20	0.095	7.1	8.1	80.16	30.71	17.93
10.	90	59.99	0.237	30	0.064	9.8	7.3	82.10	30.92	18.01
10.	90	60.48	0.238	30	0.063	11.2	9.0	82.70	30.96	18.12
10.	90	55.57	0.259	40	0.066	9.2	10.2	75.32	30.90	18.30
10.	90	54.30	0.266	50	0.050	11.8	9.4	73.50	30.89	18.34
10.	90	56.69	0.255	50	0.058	10.7	11.0	76.24	30.79	18.39
10.	90	57.12	0.273	40	0.070	10.0	9.3	76.20	30.53	18.22
10.	90	58.84	0.251	20	0.091	8.5	8.4	77.50	30.45	18.50
10.	90	61.58	0.482	50	0.051	6.7	5.8	77.63	28.15	16.02
10.	90	59.60	0.501	50	0.051	6.6	5.4	76.33	28.49	16.10
10.	90	60.72	0.490	50	0.053	11.2	5.6	78.47	28.72	16.17
10.	90	61.97	0.494	50	0.056	8.0	5.1	77.50	28.19	16.34
10.	90	60.59	0.490	40	0.055	6.9	4.8	76.85	28.50	16.42
10.	90	64.07	0.507	40	0.067	6.3	3.5	76.72	27.48	16.47
10.	90	63.15	0.496	40	0.058	8.3	5.1	78.03	28.13	16.63
10.	90	60.42	0.499	30	0.072	7.2	5.2	76.33	28.96	17.33
10.	90	59.19	0.487	30	0.085	7.6	5.3	78.15	29.85	17.41
10.	90	56.97	0.499	20	0.095	7.5	4.8	75.85	30.05	17.47
10.	90	56.90	0.511	20	0.110	6.6	5.5	75.70	30.07	17.53
10.	90	59.06	0.494	10	0.159	6.9	3.5	78.33	30.05	17.60
10.	90	59.74	0.490	10	0.164	6.0	4.2	78.43	29.88	17.64
10.	90	58.80	0.507	5	0.228	5.4	4.0	76.72	29.70	17.55
10.	90	55.97	0.503	5	0.221	6.1	3.7	77.37	30.93	17.67

APPENDIX A (continued). TABULATED DATA

L/D	θ	F	R	X/D	$\Delta T_c/\Delta T_o$	W/D	Y/D	V_o	T_o	T_a
10.	90	54.83	0.514	5	0.214	5.2	3.3	75.25	30.81	17.73
10.	90	55.70	0.489	5	0.218	5.9	3.5	78.65	31.48	17.84
10.	90	53.89	0.501	5	0.214	4.7	3.7	76.71	31.67	17.88
10.	90	53.71	0.505	5	0.192	5.6	3.2	76.20	31.64	17.95
10.	90	57.46	0.501	10	0.114	5.1	3.8	76.74	30.41	17.98
10.	90	59.82	0.487	10	0.122	6.1	4.3	78.60	30.10	18.00
10.	90	59.61	0.497	20	0.104	6.8	4.5	77.36	29.86	29.86
10.	90	62.32	0.489	20	0.109	8.4	4.5	78.30	29.26	18.00
10.	90	60.44	0.494	20	0.104	9.3	3.6	77.90	29.75	18.03
10.	90	60.57	0.497	30	0.089	8.2	3.8	77.76	29.69	18.04
10.	90	60.34	0.497	30	0.099	6.0	5.0	77.34	29.67	18.07
10.	90	63.36	0.512	40	0.077	8.0	4.7	77.57	28.61	17.70
10.	90	60.74	0.514	40	0.062	7.5	5.4	77.76	29.50	17.82
10.	90	59.97	0.511	40	0.055	7.3	4.3	77.43	29.71	17.90
10.	90	59.62	0.503	50	0.046	6.2	5.7	77.24	29.81	17.96
10.	90	59.62	0.506	50	0.057	8.0	5.3	77.24	29.84	18.02

APPENDIX A (continued). TABULATED DATA

L/D	θ	F	R	X/D	$\Delta T_c/\Delta T_o$	W/D	Y/D	V_o	T_o	T_a
5.	45	9.62	0.105	10	0.193	7.3	8.9	24.03	46.85	9.41
					0.215	8.5	9.2			
					0.198	8.2	8.2			
					0.217	6.0	8.2			
					0.208	5.8	7.9			
					0.209	7.7	8.2			
					0.203	6.8	8.6			
5.	45	9.65	0.101	20	0.126	8.6	11.9	23.88	46.40	9.19
					0.123	8.8	11.7			
					0.132	10.4	10.2			
					0.126	8.6	11.0			
					0.121	8.8	10.4			
					0.121	11.1	11.0			
					0.123	12.0	9.8			
					0.126	10.6	11.4			
5.	45	11.40	0.097	30	0.093	13.4	15.1	24.83	41.02	8.96
					0.113	10.1	11.7			
					0.119	11.7	10.3			
					0.115	11.9	10.5			
					0.111	12.6	10.5			
					0.115	13.7	10.8			
5.	45	10.10	0.106	40	0.088	14.3	12.2	24.29	44.83	8.60
					0.089	17.9	12.0			
					0.084	13.3	11.4			
					0.072	13.2	10.5			
5.	45	10.19	0.104	60	0.077	16.3	11.2	24.22	44.47	8.35
					0.076	14.9	15.9			
					0.066	9.6	14.7			
5.	45	52.81	0.049	10	0.259	8.0	9.4	62.86	23.91	9.66
					0.290	7.8	9.5			
					0.279	7.1	8.8			
					0.244	8.4	9.4			
					0.263	8.5	9.4			
5.	45	54.13	0.050	20	0.153	10.0	11.8	60.97	22.94	9.91
					0.148	10.4	13.7			
					0.155	11.6	13.3			
					0.144	13.8	13.2			
					0.146	12.1	14.0			
					0.146	11.1	13.6			

L/D	θ	F	R	X/D	$\Delta T_c/\Delta T_o$	W/D	Y/D	V_o	T_o	T_a
5.	45	54.19	0.051	30	0.128	12.7	17.2	59.87	22.67	10.09
					0.127	16.2	18.9			
					0.135	14.7	17.6			
					0.130	12.2	16.5			
5.	45	57.51	0.051	40	0.094	16.3	19.9	60.89	21.98	10.23
					0.109	14.2	20.1			
					0.118	18.5	18.7			
					0.102	16.5	20.3			
					0.102	18.4	18.1			
5.	45	57.48	0.053	60	0.080	16.5	23.4	60.29	21.90	10.40
					0.097	23.2	20.6			
					0.095	17.2	22.1			
					0.094	19.4	20.8			
5.	45	58.18	0.101	10	0.225	8.2	8.1	59.78	23.71	14.36
					0.217	7.2	7.6			
					0.225	6.7	7.9			
					0.234	6.1	7.4			
					0.233	6.1	7.3			
5.	45	57.71	0.100	20	0.121	10.1	9.9	59.39	23.71	14.32
					0.129	9.5	10.6			
					0.120	10.2	11.5			
					0.130	10.7	10.6			
5.	45	56.91	0.101	30	0.110	12.0	12.0	59.77	23.98	14.25
					0.118	13.6	12.6			
5.	45	57.13	0.103	40	0.099	14.7	12.0	59.23	23.74	14.18
					0.099	12.3	11.6			
					0.092	16.4	13.1			
5.	45	58.45	0.097	60	0.072	14.3	14.0	61.69	23.99	14.13
					0.088	17.7	15.5			
					0.075	21.3	14.6			
5.	90	10.69	0.099	10	0.117	13.4	11.4	25.20	46.47	16.93
					0.121	13.0	12.2			
					0.109	11.7	13.3			
					0.125	14.0	12.7			
5.	90	9.90	0.095	20	0.116	16.8	16.4	25.03	49.49	17.15
					0.099	18.2	12.7			
					0.099	9.9	10.2			
					0.105	15.9	12.1			
					0.117	16.9	15.3			
					0.103	19.6	11.3			

APPENDIX A (continued). TABULATED DATA

L/D	θ	F	R	X/D	$\Delta T_c/\Delta T_o$	W/D	Y/D	V_o	T_o	T_a
5.	90	9.68	0.101	30	0.090	14.6	19.2	24.82	50.13	17.25
					0.076	17.5	16.7			
					0.074	18.9	18.2			
					0.072	20.7	16.1			
5.	90	9.55	0.104	40	0.071	17.0	20.4	24.17	49.61	17.37
					0.069	18.8	19.5			
					0.077	17.5	17.1			
					0.064	20.1	16.5			
5.	90	9.51	0.107	60	0.052	13.9	22.4	24.06	49.63	17.49
					0.050	15.9	26.3			
					0.051	16.7	24.4			
					0.052	22.1	18.5			
5.	90	10.03	0.504	10	0.156	6.4	3.9	24.71	48.27	16.83
					0.155	5.5	4.6			
5.	90	10.07	0.503	10	0.164	5.7	4.2	24.91	48.41	16.75
					0.148	3.9	3.8			
5.	90	10.42	0.499	10	0.158	6.8	3.9	25.07	47.21	16.66
					0.140	5.5	4.5			
5.	90	10.77	0.493	20	0.087	5.6	4.1	25.07	45.87	16.58
					0.091	7.3	4.1			
5.	90	11.33	0.503	20	0.095	6.3	4.3	24.92	43.66	16.55
					0.091	6.9	4.7			
5.	90	12.01	0.482	30	0.083	8.0	5.0	25.76	42.72	16.51
5.	90	10.40	0.512	30	0.094	7.7	4.3	24.66	46.53	16.44
					0.080	5.8	5.7			
5.	90	10.50	0.503	30	0.085	8.8	4.8	24.87	46.48	16.38
					0.081	8.5	4.2			
5.	90	10.61	0.500	40	0.067	8.5	4.8	24.85	46.00	16.28
					0.071	9.6	4.8			
5.	90	10.40	0.504	40	0.063	7.1	5.0	24.94	46.92	16.16
					0.067	9.0	4.3			
5.	90	10.91	0.503	40	0.064	9.1	4.9	24.56	44.34	16.03
5.	90	11.07	0.495	50	0.058	10.5	4.1	24.89	44.29	15.97
					0.064	10.1	4.9			

APPENDIX A (continued). TABULATED DATA

L/D	θ	F	R	X/D	$\Delta T_c/\Delta T_o$	W/D	Y/D	V_o	T_o	T_a
5.	90	10.51	0.521	50	0.065	7.7	5.4	23.78	44.51	15.89
					0.071	6.6	4.7			
					0.066	6.5	5.0			
5.	90	10.96	0.508	60	0.061	10.1	4.4	24.64	44.22	15.79
5.	90	10.92	0.510	60	0.054	8.7	4.2	24.52	44.15	15.71
					0.055	8.5	3.5			
5.	90	10.79	0.540	60	0.050	8.3	3.1	23.20	42.46	15.61
					0.048	10.2	3.0			
5.	90	55.45	0.051	10	0.128	17.1	21.1	59.10	24.40	14.54
					0.115	16.0	22.0			
					0.120	21.7	19.8			
5.	90	55.80	0.050	20	0.132	21.2	27.7	60.20	24.61	14.60
					0.100	21.9	25.4			
					0.105	16.6	31.0			
					0.095	19.4	28.9			
5.	90	55.26	0.049	30	0.098	19.6	34.3	59.57	24.65	14.68
					0.104	23.3	33.8			
					0.092	24.9	36.8			
					0.111	24.5	37.9			
5.	90	55.25	0.052	40	0.086	14.3	33.6	59.57	24.70	14.76
					0.078	25.0	30.9			
					0.086	24.9	33.6			
					0.099	20.8	34.8			
5.	90	55.47	0.051	60	0.055	17.6	44.7	59.60	24.67	14.81
					0.075	31.9	45.1			
					0.071	17.3	43.7			
					0.071	23.6	45.7			
5.	90	59.84	0.098	10	0.129	11.9	10.9	60.49	24.15	15.45
					0.150	13.0	12.1			
					0.132	15.3	4.7			
5.	90	59.92	0.100	10	0.128	13.7	11.4	60.78	24.17	15.39
					0.137	12.9	11.0			
					0.133	12.9	10.9			
5.	90	59.19	0.100	20	0.101	13.5	14.0	60.27	24.19	15.35
					0.110	14.2	13.9			
					0.103	19.2	15.3			

APPENDIX A (continued). TABULATED DATA

L/D	θ	F	R	X/D	$\Delta T_c/\Delta T_o$	W/D	Y/D	V_o	T_o	T_a
5.	90	59.65	0.098	20	0.152	15.9	14.0	60.9	24.21	15.29
					0.145	16.4	15.8			
5.	90	58.84	0.098	30	0.135	16.5	15.6	60.49	24.26	15.24
					0.135	15.6	17.5			
5.	90	56.32	0.106	30	0.109	17.8	15.9	58.83	24.46	15.17
					0.109	15.7	15.0			
5.	90	51.65	0.106	40	0.119	16.0	16.8	56.10	25.02	15.12
					0.115	16.6	15.5			
5.	90	52.58	0.105	40	0.098	18.3	16.3	57.25	25.03	15.05
					0.103	19.8	16.9			
5.	90	55.08	0.100	50	0.082	16.1	17.0	59.68	24.94	15.02
					0.086	15.7	18.2			
5.	90	56.59	0.097	60	0.093	20.1	19.8	60.83	24.73	14.89
					0.078	22.6	17.9			
					0.077	20.8	20.6			
5.	90	56.64	0.102	60	0.073	20.0	17.0	59.90	24.44	14.84
					0.080	22.7	16.3			
5.	90	57.81	0.503	10	0.134	6.3	4.0	59.70	24.22	15.06
5.	90	57.57	0.503	10	0.144	6.3	3.5	59.59	24.23	15.01
					0.131	4.1	3.4			
5.	90	59.90	0.478	20	0.097	6.1	5.3	62.21	24.25	14.98
					0.092	4.6	4.9			
5.	90	56.98	0.508	20	0.086	7.0	4.8	59.22	24.23	14.93
5.	90	58.46	0.498	20	0.119	7.3	4.8	60.00	24.03	14.90
					0.084	3.7	4.8			
5.	90	57.51	0.486	30	0.083	8.7	5.0	61.51	26.11	17.21
5.	90	58.50	0.476	30	0.067	6.9	4.9	62.64	26.08	17.13
					0.059	8.0	4.5			
5.	90	54.29	0.522	40	0.066	8.4	3.4	57.97	26.00	17.08
					0.050	7.9	3.9			

APPENDIX A (continued). TABULATED DATA

L/D	θ	F	R	X/D	$\Delta T_c/\Delta T_o$	W/D	Y/D	V_o	T_o	T_a
2.5	45	11.46	0.098	10	0.280	4.9	4.8	27.03	44.40	9.67
					0.265	7.0	5.3			
					0.282	5.7	5.8			
					0.286	6.7	4.9			
					0.279	6.5	5.7			
					0.305	6.6	6.1			
2.5	45	11.45	0.095	20	0.198	7.4	12.6	27.03	44.50	9.91
					0.195	8.1	13.3			
					0.219	11.4	12.7			
					0.200	10.6	13.2			
					0.187	9.9	10.4			
					0.191	10.3	13.0			
2.5	45	11.28	0.097	30	0.171	9.8	16.4	26.53	44.40	10.17
					0.171	11.6	15.0			
					0.169	12.4	13.8			
					0.156	12.1	14.5			
					0.156	11.6	13.6			
					0.167	12.1	15.5			
2.5	45	11.59	0.100	40	0.123	8.4	19.1	25.93	42.39	10.41
					0.125	14.6	19.1			
					0.133	14.9	19.1			
					0.132	13.8	16.9			
					0.132	13.8	16.9			
					0.130	12.9	17.4			
2.5	45	10.93	0.108	60	0.105	16.3	23.1	23.84	41.46	10.63
					0.104	10.4	22.6			
					0.100	15.8	22.6			
					0.112	11.5	20.4			
2.5	90	10.70	0.101	10	0.221	11.3	18.9	25.15	45.51	14.38
					0.180	13.9	18.6			
					0.189	12.8	18.4			
2.5	90	10.29	0.099	20	0.140	12.8	24.6	25.10	47.02	14.21
					0.149	14.1	22.7			
					0.134	12.2	24.6			
					0.128	16.3	22.4			
					0.120	11.4	24.4			
					0.138	12.4	23.7			
2.5	90	10.19	0.976	30	0.098	21.5	29.4	25.10	47.30	14.04
					0.102	22.6	28.2			
					0.096	19.5	27.6			
					0.108	23.3	30.2			

APPENDIX A (continued). TABULATED DATA

L/D	θ	F	R	X/D	$\Delta T_o/\Delta T_o$	W/D	Y/D	V_o	T_o	T_a
2.5	90	10.92	0.097	40	0.092	28.5	33.1	25.04	43.43	10.54
					0.081	27.3	37.2			
					0.064	27.7	35.3			
					0.080	36.5	30.2			
					0.096	25.3	31.9			
2.5	90	10.75	0.105	60	0.080	55.9	36.9	24.62	43.31	10.25
					0.087	53.1	30.3			
					0.057	46.3	43.4			
					0.065	40.1	35.8			
					0.066	37.6	42.9			
2.5	90	10.24	0.499	10	0.179	5.1	5.8	24.91	47.00	14.56
					0.178	4.7	5.3			
2.5	90	9.33	0.491	10	0.162	6.0	5.5	25.24	51.82	14.69
					0.147	6.2	5.6			
2.5	90	10.42	0.496	20	0.141	6.8	7.5	25.21	46.85	14.77
					0.129	7.0	7.0			
2.5	90	11.79	0.498	20	0.135	7.4	7.8	25.16	41.82	14.58
					0.140	5.9	7.8			
2.5	90	13.00	0.487	30	0.119	8.3	8.6	25.50	39.11	15.07
					0.113	8.4	8.7			
2.5	90	12.11	0.490	30	0.118	9.9	9.4	25.27	41.07	14.72
					0.118	10.3	9.3			
2.5	90	11.85	0.504	40	0.096	10.8	8.8	24.82	41.23	14.85
					0.103	7.3	7.7			
2.5	90	12.12	0.493	40	0.112	10.1	9.1	25.27	41.06	14.79
					0.116	10.7	9.1			
2.5	90	12.26	0.504	60	0.086	11.7	8.5	24.9	40.29	14.99
					0.075	11.2	9.7			
2.5	90	12.11	0.499	60	0.100	10.0	8.6	25.00	40.73	14.92
					0.101	12.1	8.4			
2.5	90	51.70	0.050	10	0.168	23.6	31.9	49.12	23.02	15.02
					0.158	23.1	33.8			
					0.169	29.5	29.9			
					0.140	22.8	38.5			
					0.147	30.1	33.9			

APPENDIX A (continued). TABULATED DATA

L/D	θ	F	R	X/D	$\Delta T_c/\Delta T_o$	W/D	Y/D	V_o	T_o	T_a
2.5	90	48.51	0.049	20	0.128	34.4	40.8	50.20	24.17	14.93
					0.112	34.5	43.9			
					0.091	33.5	53.5			
2.5	90	47.71	0.049	30	0.143	45.2*	74.9*	49.86	24.30	14.85
2.5	90	52.31	0.096	10	0.229	12.0	16.0	50.60	23.32	15.11
					0.252	13.6	18.7			
					0.233	11.9	18.7			
					0.235	14.6	18.2			
2.5	90	50.95	0.104	20	0.209	11.4	21.3	48.88	23.26	15.19
					0.197	13.9	20.4			
2.5	90	51.80	0.102	30	0.134	14.3	21.8	49.41	23.21	15.23
					0.137	17.9	22.1			
					0.101	15.9	21.8			
					0.120	15.5	25.4			
2.5	90	51.33	0.102	40	0.129	17.8	25.2	48.96	23.26	15.30
					0.131	21.3	31.1			
2.5	90	55.02	0.504	10	0.170	6.7	4.0	49.58	23.55	16.76
2.5	90	56.70	0.491	10	0.200	6.0	5.0	50.89	23.48	16.72
2.5	90	56.91	0.496	10	0.180	5.4	4.0	50.40	23.29	16.68
					0.196	6.7	4.0			
2.5	90	53.52	0.492	20	0.122	9.4	8.2	51.22	23.24	15.20
2.5	90	57.66	0.494	20	0.129	8.1	5.6	50.65	23.15	16.61
					0.146	7.3	5.7			
2.5	90	56.61	0.503	20	0.145	9.1	6.2	49.55	23.05	16.52
2.5	90	63.96	0.493	30	0.116	9.5	10.2	50.18	21.21	15.57
2.5	90	62.95	0.499	30	0.126	10.7	6.3	49.81	21.28	15.55
2.5	90	61.02	0.497	30	0.118	7.8	6.1	49.98	21.61	15.52
2.5	90	61.22	0.499	40	0.106	10.8	5.8	49.98	21.56	15.49
2.5	90	61.34	0.501	40	0.107	12.1	7.0	49.90	21.50	15.46
2.5	90	60.34	0.509	40	0.113	13.5	3.9	48.85	21.43	15.43

APPENDIX A (continued). TABULATED DATA

L/D	θ	F	R	X/D	$\Delta T_c/\Delta T_o$	W/D	Y/D	V_o	T_o	T_a
2.5	90	60.14	0.509	60	0.087	12.2	5.7	49.08	21.68	15.67
2.5	90	59.32	0.518	60	0.110	11.2	7.7	48.27	21.70	15.74
2.5	90	59.77	0.512	60	0.086	10.4	7.4	48.86	21.79	15.79
2.5	90	61.43	0.499	60	0.110	9.8	6.8	50.37	21.85	15.83

TECHNICAL REPORT DATA *(Please read Instructions on the reverse before completing)*		
1. REPORT NO. EPA-600/3-76-101	2.	3. RECIPIENT'S ACCESSION NO.
4. TITLE AND SUBTITLE An Experimental/Analytical Investigation of Deep Submerged Multiple Buoyant Jets		5. REPORT DATE September 1976 6. PERFORMING ORGANIZATION CODE
7. AUTHOR(S) L. D. Kannberg and L. R. Davis		8. PERFORMING ORGANIZATION REPORT NO.
9. PERFORMING ORGANIZATION NAME AND ADDRESS Oregon State University Corvallis, Oregon 97330		10. PROGRAM ELEMENT NO. 1BA032 11. CONTRACT/GRANT NO. Grant No. R-800818
12. SPONSORING AGENCY NAME AND ADDRESS U.S. Environmental Protection Agency Office of Research and Development Corvallis, Environmental Research Laboratory Corvallis, Oregon 97330		13. TYPE OF REPORT AND PERIOD COVERED Final 14. SPONSORING AGENCY CODE EPA-ORD
15. SUPPLEMENTARY NOTES		

16. ABSTRACT The results of an experimental and analytical study of deep submerged multiple-port thermal discharges are presented. The experimental results include the measured downstream thermal dilution, width, and centerline trajectory of the buoyant thermal plume from multiple port discharges consisting of a row of equally spaced discharge ports. Independent parameters for which measurements were obtained include port spacing, discharge Froude Number, discharge angle, and discharge to ambient velocity ratio. Results indicate that decreasing port spacing greatly decreases thermal dilution.

The analytical portion of this report presents a modified version of the Hirst lumped differential plume model. It has been extensively modified to include multiple plume effects including gradual transition of the plume profiles from simple axisymmetric profiles to merging profiles and finally to fully merged profiles and entrainment based on the variable available entrainment surface of merging plumes. The results of the tuned model agree well with abailable experimental data.

17. KEY WORDS AND DOCUMENT ANALYSIS		
a. DESCRIPTORS	b. IDENTIFIERS/OPEN ENDED TERMS	c. COSATI Field/Group
Thermal Pollution*, Jet Flow	Submerged Multiple Jets	20D
18. DISTRIBUTION STATEMENT Release to Public	19. SECURITY CLASS *(This Report)* Unclassified 20. SECURITY CLASS *(This page)* Unclassified	21. NO. OF PAGES 266 22. PRICE

EPA Form 2220-1 (9-73)

* U. S. GOVERNMENT PRINTING OFFICE: 1976—796-314/ 12 REGION 10